GASEOUS DIFFUSION

IN MOLECULAR SIEVES

A thesis submitted for

the Degree of Doctor of Philosophy

in the Faculty of Engineering of the University of London

by

Christopher John Whitford, B.Sc., A.C.G.I.

Department of Chemical Engineering
and Chemical Technology,
Imperial College of Science and Technology,
London, S.W.7.

September, 1969.

ABSTRACT

The diffusion of carbon dioxide is studied in a Linde type 5A molecular sieve pellet over a range of temperatures and pressures about ambient. The work consists of two complementary parts.

1. Theoretical calculations of molecular potentials are used to estimate equilibrium adsorption isotherms, heats of adsorption and crystal diffusivities from 573°K to 173°K for dilute systems, and the results are compared with published data.

2. A practical apparatus has been designed and used to measure breakthrough curves for the dynamic self diffusion of carbon dioxide in a 'one dimensional' sieve pellet bed from - 25°C to 25°C, at atmospheric pressure. The diffusion process is modelled by considering both pore and crystal diffusion processes and estimates of diffusivities are obtained by fitting the model to the practical results. The resulting practical crystal diffusivities are compared with the theoretical values obtained and the practical pore diffusivities are compared with bulk gas diffusivities for carbon dioxide.

ACKNOWLEDGMENTS

The author wishes to express his gratitude to Professor R.W.H. Sargent for his encouragement, and sustained interest in this work, also to the Science Research Council, the Courtaulds Fund, and the I.B.M. Support Fund for financial support during the course of this work.

Thanks are due to the departmental glassblowers who were always willing to repair broken glassware at short notice and the departmental workshop staff, in particular Bert Lucas, who took great care in building parts of the apparatus. The author also wishes to thank his fellow postgraduates in the computing section for their help and advice.

CONTENTS

CHAPTER 1 - INTRODUCTION

The diffusion of gases in molecular sieves has been of interest for many years and the use of molecular sieves in industrial adsorption processes is now widespread. Traditional design methods for adsorbers have tended to be 'rule of thumb' but with the advent of fairly cheap high speed digital computers more sophisticated approaches to the design problem can be made.

A great deal of work has been done on the basic structure and sorption properties of many commercial and naturally occurring sieves which gives some insight into the distinctive adsorption processes which characterise them. Recently work has been proceeding along two lines: model determination for fixed beds of sieves, and prediction of isotherm and heats of adsorption data in highly idealised systems using basic molecular data and statistical mechanical theory.

Chandrasekharan[1] tested several of the models reviewed by Vermeulen[19] for predicting fixed bed behaviour, using experimental data on removing carbon dioxide from air in a fixed bed of Linde 4A molecular sieve. He found that none of the models predicted breakthrough curves over a wide range of data but that Rosen's model[20], which takes account of diffusion through the crystal matrix gave the best fit.

Wilson[3] did further work over a wider range of variables and described a model for a fixed bed adsorber which was fitted to data for carbon dioxide removal from air in a fixed bed of Linde 5A sieve. He obtained estimates of crystal and pore diffusivities using several different isotherm approximations. Dworjanyn[2] also calculated pore and crystal diffusivities using Rosen's model on data for carbon dioxide self diffusion in Linde 4A sieves at ambient temperature and pressure, and outlined a method for calculating molecular potentials from basic molecular data. He was unable to calculate theoretical crystal diffusivities from the molecular potentials due to the blocking effect of the exchangeable cations in the 4A sieve, which tend to prevent intercage translation.

The above work indicated that crystal diffusion played a role in the adsorption processes in molecular sieves and it was postulated that diffusion in the crystal matrix would become the controlling process at sub-ambient temperatures.

The work presented here was evolved to study this problem by making measurements of breakthrough curves in a practical diffusion system over a range of temperatures, and fitting a mathematical model describing the diffusion process to these results to obtain estimates of diffusivities. A theoretical approach was then used extending Dworjanyn's[2] work

on molecular potentials to obtain crystal diffusivities, isotherms and heats of adsorption which can be compared with the practical diffusivities obtained here, and published practical data for isotherms and heats of adsorption. This permits an assessment of the role of 'crystal diffusion' in molecular sieves and investigates the feasibility of predicting adsorption data and diffusivities by a purely theoretical method based only on the molecular properties of the adsorbate and the sieve.

The system studied in this work is the self diffusion of carbon dioxide in a Linde 5A molecular sieve. The 5A sieve was chosen since it is known that the exchangeable cations do not block all of the interconnecting windows between cages and hence theoretical diffusivities can be calculated. Carbon dioxide was chosen as adsorbate as it is involved in many industrial adsorption processes and is readily available as $C^{14}O_2$. Hence tracer studies can be used in the practical measurement of breakthrough curves. Carbon dioxide also exhibits a large quadrupole moment and so the relative importance of the various potential interactions of the adsorbate with the sieve can be assessed by including repulsion, dispersion, induction and electrostatic effects in the potential model developed. A statistical mechanical approach is used to derive expressions for diffusivities, isotherms and heats of

adsorption from the molecular potentials.

A mathematical model is developed which describes the diffusion processes in the pores and crystals of a commercial sieve pellet. It was intended at the outset that this model should be kept as simple as possible by reducing the diffusion problem to a one dimensional diffusion process with a step change in concentration at the exchange surface at zero time. Also a self diffusion process excludes thermal effects and ensures there are no concentration changes as such occurring during the diffusion process. This excludes variable diffusion coefficients and permits the use of a single point on the adsorption isotherm to describe the equilibrium state.

An apparatus was built to measure breakthrough curves for a single 5A pellet at ambient and sub-ambient temperatures under conditions compatible with the model, so that the diffusion processes occurring in a single pellet rather than a bed of pellets could be studied.

CHAPTER 2 - THEORY

2.1 The Structure of Type 5A Molecular Sieve

Broussard and Shoemaker[7] describe the Linde 5A sieve structure based on the cubo-octahedral structural unit $2Na_2O.4CaO.6Al_2O_3.12SiO_2.xH_2O$.

This unit has a characteristic dimension $a_o = 12.31 \pm 0.01$ Å and the following table gives the ion coordinate positions based on fractions of this parameter.

TABLE 2.1

Numbers and type of ion	Distance from centre of large cage			Distance from centre of small cage		
12 OI	0	0.272O	0.5	0	0.228O	0.5
12 OII	0.2122	0.2122	0.5	0	0.2878	0.2878
24 OIII	0.1518	0.3882	0.3882	0.1118	0.1118	0.3482
24 Al, Si (AS)	0.1273	0.3028	0.5	0	0.1972	0.3727
8 Na, Ca	0.3050	0.3050	0.3050	0.1950	0.1950	0.1950

It is convenient to refer only to oxygen ions when discussing the spatial arrangement of this sieve as these are fairly large compared with the other ions. Later it will be shown that the 48 oxygen ions in the unit cell

together with the exchangeable cations contribute the most significant part to the potential structure of the system.

The spatial array of synthetic molecular sieves of the Linde 'A' type have been described by several workers.[4,5,6,9,27] It is well known that these sieves form regular three dimensional arrays of cages interconnected by windows formed by oxygen ions. In the Linde 5A sieve these cages are of two distinct types, differing both in size and mode of interconnection. The large cages are almost spherical and have a free diameter of about 11.4 Å. They are inscribed in the unit cube, side 12.31 Å. The six faces of the cube contain the main oxygen windows which are formed by a ring of eight oxygen ions. These rings are about 4.3 Å free diameter. Thus the main system of cages consists of a regular three dimensional array in which each cage is linked to six others along rectangular axes by O8 windows. The small cages have a free diameter of about 7 Å and form the secondary system. They occur in the space formed when eight of the basic large cages are taken together as a composite cube. The geometric centre of this cube includes eight rings of oxygen ions, one from each of the eight large cage structures. These rings have a free diameter of about 2.6 Å and are formed by six oxygen ions. These ions lie on two slightly displaced planes perpendicular to a (111) axis referred to the large cages. The small cages also form a regular three

FIGURE 2.1

OXYGEN ION POSITIONS IN THE LINDE 5A SIEVE

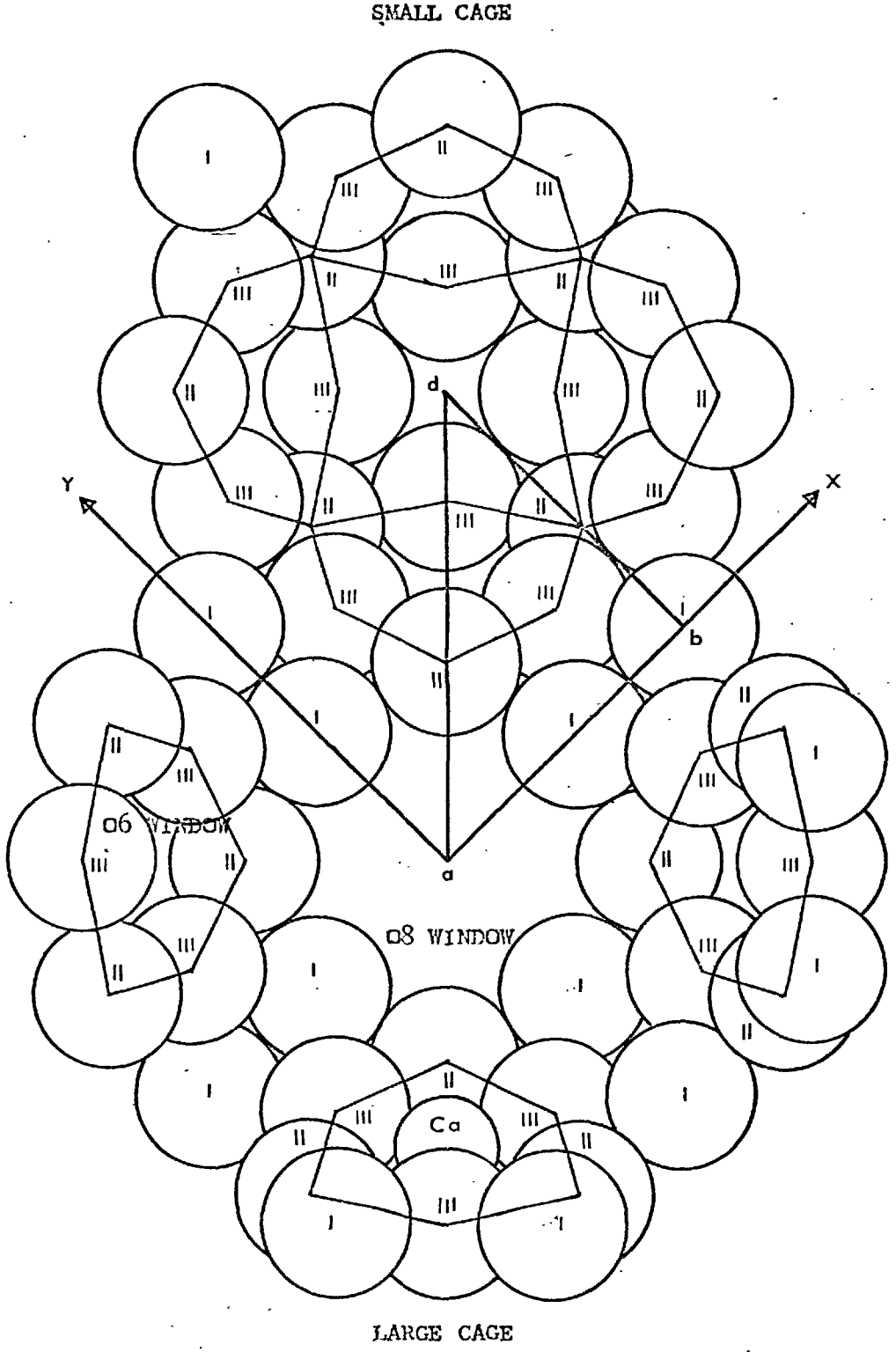

dimensional array and are interstitially located with respect to the large cages.

The small cages are each linked to eight large cages via O6 windows in (111) directions but have no direct connection one to another. It can be seen that the large cages offer the greater number of choices of translation to an adsorbed gas molecule. It can jump to any of six large cages via an O8 window or any of eight small cages via an O6 window. Jumps from a small cage can be to any of eight large cages via an O6 window but it should be noted that the exchangeable cations lie in (111) directions and block the O6 windows, so tending to present translation between large and small cages.

The oxygen ions in table 2.1 are referred to as types I, II and III. In figure 2.1 which shows the positions of the oxygen ions in part of a large and small cage, it can be seen that O8 windows are formed by types I and II only and O6 windows and small cages by types II and III only.

2.2 Contributions to the Intermolecular Forces in the Carbon Dioxide-Linde 5A Sieve System

The following assumptions are made to help to decide which of the many intermolecular forces arising from molecule-molecule interactions are of importance in the CO_2/5A system. These assumptions are modified in later chapters where the results obtained show them to be incorrect, but are

necessary at this stage to define a potential function for the system.

1) Initially only one carbon dioxide molecule is considered, it being situated in one particular large cage of a hypothetical molecular sieve crystal defined by (2), (3) and (4).

2) The empty sieve cages surrounding the one of importance extend to a sufficiently large distance in three dimensions such that the distant cages have a negligible potential effect on the carbon dioxide molecule.

3) The molecules forming the crystal structure are all present in their fully ionised states as O^{2-}, Si^{4+}, Al^{3+}, Ca^{2+}, Na^{+}.

4) The lattice positions of these ions are as given by Broussard and Shoemaker.[7]

5) The ions are rigidly fixed in these positions.

6) No water of crystallisation is present in the sieve cages.

7) The carbon dioxide molecule is considered as being spherically symmetric.

Also use is made of the fact that the carbon dioxide molecule has a large polarisability and quadrupole moment and a negligible permanent dipole.

The following intermolecular force contributions are based on the above statements for a single carbon dioxide molecule free to move within the

free space of a large cage and interacting with the ions forming the sieve structure. When the interaction does not involve the charge on the ion, the ion is referred to as a molecule.in the following sections.

2.2.1 Dispersion Force

When two molecules interact, long range forces are set up. These have been evaluated quantum-mechanically to give what is known as the London dispersion force between a pair of molecules (a) and (b).
The potential is represented by:

$$\phi_{ab}^{DIS} = - \frac{B_{ab}}{r_{ab}^{6}} \quad (= \phi_D) \qquad 2.1$$

Here r_{ab} is the separation between an ion (a) and the carbon dioxide molecule (b).

The constant B_{ab} is given by:[10]

$$B_{ab} = - \frac{3}{2} \left(\frac{\gamma_a \gamma_b}{\gamma_a + \gamma_b}\right) \alpha_a \alpha_b \qquad \text{(London)}$$

$$B_{ab} = -6mc^2(\alpha_a \chi_a + \alpha_b \chi_b) \qquad \text{(Lennard-Jones)}$$

$$B_{ab} = -\frac{3}{2} e^2 \sqrt{a^o} \left(\frac{a_a a_b}{\sqrt{(a_a/n_a^o)} + \sqrt{(a_b/n_b^o)}} \right) \quad \text{(Slater-Kirkwood)}$$

$$B_{ab} = -6\, mc^2 \frac{a_a a_b}{a_a/\chi_a + a_b/\chi_b} \quad \text{(Kirkwood-Müller)} \qquad 2.2$$

Barrer[8] has pointed out that these various expressions for B_{ab} are mainly empirical. Sample calculations show that the Kirkwood-Müller expression gives a value almost twice that for the London expression. The others give intermediate results. However, the Kirkwood-Müller expression is used since data for it is readily available, but it must be noted that it may over-estimate the dispersion force.

When considering a carbon dioxide molecule interacting with many ions, it is assumed that the total dispersion potential is the scalar sum of the individual pair potentials. Thus:

$$\sum \phi_D = \sum_r \frac{B_{ab}}{r^2} \qquad 2.3$$

2.2.2 Induction Force

When an ion interacts with a neutral molecule the ion induces a dipole in the molecule. This sets up an induced dipole moment $C_a a_b / r_{ab}^2$ in molecule (b). The potential can be represented by:

$$\phi_{ab}^{IND} = -\frac{C_a^2 \alpha_b}{2r_{ab}^4} \quad (= \phi_p) \qquad 2.4$$

This expression has the form,

$$\phi_p = -\frac{\alpha_b}{2}(F)^2$$

where the vector F represents the field at (b) due to the ion at (a). When many ions are interacting with the carbon dioxide molecule at (b) the total potential will be the vector sum of the individual pair interactions. If the field at (b) is resolved into its component parts in the three co-ordinate directions this summation becomes:

$$\sum \phi_p = -\frac{\alpha_b}{2}\left(\left(\sum_r \frac{C_a}{r^2} \cdot \frac{x}{r}\right)^2 + \left(\sum_r \frac{C_a}{r^2} \cdot \frac{y}{r}\right)^2 + \left(\sum_r \frac{C_a}{r^2} \cdot \frac{z}{r}\right)^2 \right) \qquad 2.5$$

where

$$r^2 = x^2 + y^2 + z^2$$

and (x,y,z) is the position of ion (a) with respect to molecule (b).

It is known that the interaction force is directional since a molecule will align its induced charge distribution so that it has maximum interaction with the field. A carbon dioxide molecule is essentially cylindrical in shape and will align but for simplicity it has been assumed spherical.

2.2.3 Electrostatic Force

Only since 1960 has much practical work been done in the field of multipole interactions. The interaction of a carbon dioxide molecule and an ion comes under this heading since carbon dioxide has a large permanent quadrupole moment. It is known that the interaction is directional and of the form:

$$\phi_{ab}^{ELEC} = \frac{C_a Q_b}{4 r_{ab}^3} (3 \cos^2 \Theta_b - 1)$$

This function can be averaged over all orientation angles Θ_b, of the carbon dioxide molecule by the function[10]:

$$\bar{\phi}_{ab}^{ELEC} = \frac{\iint \phi_{ab} \exp(-\frac{\phi_{ab}}{kT}) dw_a dw_b}{\iint \exp(-\frac{\phi_{ab}}{kT}) dw_a dw_b}$$

where $dw = \sin \Theta d\Theta d\phi$

FIGURE 2.2

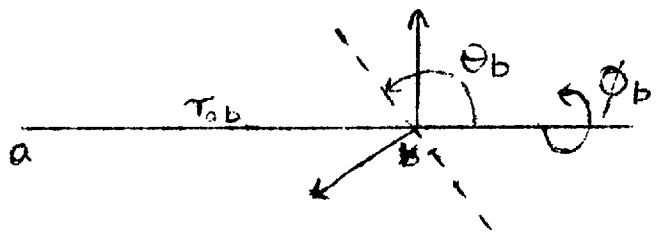

This integration represents a transformation to a spherically symmetric potential function with the use of a Boltzmann weighting factor, and allows for the fact that the interacting molecule spends most of its time in the orientation that gives the maximum interaction. Physically the function assumes r_{ab} is constant whilst the molecule rotates.

The result of the integration is[10]:

$$\bar{\phi}_{ab}^{ELEC} = -\frac{C_a^2 Q_b^2}{2O\ kT} \cdot \frac{1}{r_{ab}^6} \quad (= \phi_Q) \qquad 2.6$$

It should be noted that the potential is now attractive and temperature dependent. It is assumed that when one carbon dioxide molecule interacts with many ions the resultant potential is the scalar sum of the individual pair interactions, i.e.

$$\sum \phi_Q = -\sum_r \frac{C_a^2 Q_b^2}{2OkT} \cdot \frac{1}{r^6} \qquad 2.7$$

2.2.4 Repulsion Force

At small molecular separations approaching collision distances, a highly repulsive, short range force is set up. Little is known about the true nature of this force and it is customary to represent it by an inverse twelfth power term of the form:

$$\phi_{ab}^{REP} = \frac{A}{r_{ab}^{12}} \qquad (= \phi_R) \qquad 2.8$$

The constant A is chosen to give the correct equilibrium separation and is therefore a function of the other potential contributions; it is evaluated later, by a similar procedure to that used in formulating the Lennard-Jones 12:6 potential function.

Again it is assumed that the total repulsion potential for many ions is the scalar sum of the individual pair interactions. Thus:

$$\sum \phi_R = \sum_r \frac{A}{r^{12}} \qquad 2.8a$$

2.2.5 Final Potential Function for one CO_2 Molecule

The above contributions may be combined to obtain the total potential for a single carbon dioxide molecule at a particular point in space inside a large sieve cage. Thus the total potential can be written as:

$$\phi = \sum_r f(B,D,E,\rho_e) \cdot \frac{1}{r^{12}} - \sum_r B \cdot \frac{1}{r^6}$$

$$- D\left(\sum_r C_a \cdot \frac{1}{r^2}\right)^2 - \sum_r E \cdot \frac{1}{r^6} \qquad 2.9$$

where:

$$B = -\frac{6mc^2 a_a a_b}{\frac{a_a}{\chi_a} + \frac{a_b}{\chi_b}} \qquad D = \frac{a_b}{2} \qquad E = \frac{C_a^2 Q_b^2}{20kT}$$

The constants $f(B,D,E,\rho_e)$ are obtained using the relation

$$\left(\frac{d\phi}{dr}\right)_{r=\rho_e} = 0$$

Thus $$f(B,D,E,\rho_e) = \frac{B\rho_e^6}{2}\left(1 + \frac{a_b C_a^2 \rho_e^2}{3B} + \frac{C_a^2 Q_b^2}{20kTB}\right) \qquad 2.9a$$

It is convenient to replace r using the dimensionless transformation $r = a_o R$ where a_o is the unit cell characteristic dimension. The final expression used then becomes:

$$\phi = \sum_R \frac{B\rho_e^6}{2a_o^{12}}\left(1 + \frac{a_b e^2 C_a^2 \rho_e^2}{3B} + \frac{e^2 C_a^2 Q_b^2}{20kTB}\right) \cdot \frac{1}{R^{12}}$$

$$- \sum_R \frac{B}{a_o^6}\frac{1}{R^6} - \sum_R \frac{e^2 a_b}{2a_o^4}\left(\frac{C_a}{R^2}\right)^2 - \sum_R \frac{e^2 Q_b^2}{20kTa_o^6} \cdot \frac{C_a^2}{R^6} \qquad 2.10$$

The summation $\sum_R$ is for all ions having a significant potential effect on the CO_2 molecule, and the charge on an ion is separated into the charge on an electron and a multiple C_a. It should be noted that

B, ρ_e and C_a vary according to the particular ion being considered in the summation, and χ_b, α_b and Q_b are fixed constants for the carbon dioxide molecule.

2.2.6 Interactions of Two Carbon Dioxide Molecules in the Linde 5A Sieve System

The preceding section is easily extended to cover the case where two carbon dioxide molecules are free to move within the free space of a large cage. Here the two molecules interact with each other as well as with the ions forming the sieve crystal.

The carbon dioxide-carbon dioxide interaction consists of the following terms:

Dispersion Potential, $$E_D = + 3mc^2 \alpha_b \chi_b \cdot \frac{1}{r^6} = - \frac{B'}{r^6} \qquad 2.11$$

Induction Potential, $$E_P = 0 \qquad 2.12$$

Electrostatic Potential, $$E_Q = - \frac{7}{40} \frac{Q_b^4}{kT} \cdot \frac{1}{r^{10}} = - \frac{D'}{r^{10}} \qquad 2.13$$

Repulsion Potential, $$E_R = f'(B', D', \rho_e') \frac{1}{r^{12}} \qquad 2.14$$

In equation 2.11 the Kirkwood Müller term for B' is used as before. The induction potential is zero as there is no permanent charge on the carbon

dioxide molecule. Equation 2.13 is obtained after using a Boltzmann weighting factor as in section 2.2.3

The constant f' is evaluated using the condition

$$\left(\frac{dE}{dr}\right)_{r=\rho_e'} = 0 \quad \text{where} \quad E = E_R + E_D + E_Q$$

and it is convenient to replace r by the dimensionless separation R' where $R' = r/b_o$ and $b_o = a_o/20$, the unit grid size (see section 3.2). Thus the interaction potential between two carbon dioxide molecules is given by:

$$E = \frac{B' \rho_e'^{6}}{2b_o^{12}} \left(1 + \frac{5}{3} \frac{D'}{B' \rho_e'^{4}}\right) \frac{1}{R'^{12}} - \frac{B'}{b_o^{6}} \cdot \frac{1}{R'^{6}} - \frac{D'}{b_o^{10}} \cdot \frac{1}{R'^{10}} \qquad 2.15$$

It is assumed that the carbon dioxide-ion interaction is unaffected by the presence of the second carbon dioxide molecule so that equations 2.10 and 2.15 completely describe the interactions in the system.

2.3 The Configuration Integral

The configuration integral Q_N for N molecules is defined by:

$$Q_N = \frac{1}{N!} \int_V \cdots \int \exp(-\phi_T/kT) d\underline{r}_1 \cdots d\underline{r}_N \qquad 2.16$$

where $\underline{r}_i$ is the position vector of the molecule i, V is the geometric volume containing the molecules and ϕ_T the total potential energy, which for a gas in a solid adsorbent is given by:

$$\phi_T = \sum_{i=1}^{N} \phi(\underline{r}_i) + \sum_{i=1}^{N} \sum_{j>i} E(\underline{r}_i, \underline{r}_j) \qquad 2.17$$

Here E represents the gas-gas interaction and ϕ the gas-adsorbent interaction given by equations 2.15 and 2.10.

Write: $$f_{ij} = \exp(-E(\underline{r}_i, \underline{r}_j)) - 1 \qquad 2.18$$

and using the fact that: $\exp(-\sum_i a_i) = \prod_i \exp(-a_i)$, it follows from equations 2.16, 2.17 and 2.18 that:

$$Q_N = \frac{1}{N!\Gamma^N} \int_V \cdots \int \prod_{i=1}^{N} \exp(-\phi(\underline{r}_i)/kT)$$

$$\times \prod_{i=1}^{N} \prod_{j>i} (f_{ij} + 1)\, d\underline{r}_1 \cdots d\underline{r}_N \qquad 2.19$$

Now f_{ij} is significantly different from zero only if molecules i and j are close together (i.e. $\| \underline{r}_i - \underline{r}_j \|$ is small). Thus if the gas density is such that the probability of three or more molecules being close together is negligible then all the products of the f_{ij} are approximately zero. Thus

expanding the integral in equation 2.19 and neglecting all such products gives:

$$Q_N = \frac{1}{N!} \int_V \cdots \int \prod_{i=1}^{N} \exp\left(-\phi(\underline{r}_i)/kT\right) d\underline{r}_1 \cdots d\underline{r}_N$$

$$+ \frac{1}{N!} \int_V \cdots \int \sum_{i=1}^{N} \sum_{j>i} f_{ij} \cdot \prod_{i=1}^{N} \exp\left(-\phi(\underline{r}_i)/kT\right) d\underline{r}_1 \cdots d\underline{r}_N \qquad 2.20$$

Now the first integral factorises into a product of N integrals, which are all identical since the molecules are identical, and are given by:

$$V_o = \int_V \exp\left(-\phi(\underline{r})/kT\right) \cdot d\underline{r} \qquad 2.21$$

The second integral factorises similarly so that we may write:

$$\frac{1}{N!} \int_V \cdots \int \sum_{i=1}^{N} \sum_{j>i} f_{ij} \prod_{i=1}^{N} \exp\left(-\frac{\phi(\underline{r}_i)}{kT}\right) d\underline{r}_1 \cdots d\underline{r}_N$$

$$= \frac{1}{N!} V_o^{N-2} \frac{N^2}{2} \iint_V f_{ij} \exp \frac{\left(-\phi(\underline{r}_1) - \phi(\underline{r}_2)\right)}{kT} d\underline{r}_1 \, d\underline{r}_2$$

This is obtained by integrating over all the molecules except for the two of interest. In the summations $\sum_{i=1}^{N} \sum_{j>i} f_{ij}$ there are $\frac{1}{2}N(N+1)$ terms, i.e. approximately $\frac{N^2}{2}$ terms, and for each f_{ij} the integration is over all other (N-2) identical molecules giving V_o^{N-2} for the value of

$$\int_V \cdots \int \prod_{i=1}^{N-2} \exp\left(-\frac{\phi(\underline{r}_i)}{kT}\right) d\underline{r}_1 \cdots d\underline{r}_{N-2}$$

Finally combining the factorised expressions for the two terms in equation 2.20 gives:

$$Q_N = \frac{V_o^N}{N!}\left(1 - \frac{N^2 B}{V_o}\right) \qquad 2.22$$

where:

$$B = -\frac{1}{2V_o} \iint_V f_{12} \exp\left(-\frac{\phi(\underline{r}_1) + \phi(\underline{r}_2)}{kT}\right) d\underline{r}_1 d\underline{r}_2 \qquad 2.23$$

2.4 The Partition Function and Equilibrium Isotherm

The partition function Z_N for N molecules is defined by:

$$Z_N = Q_N/\gamma^{3N} \qquad 2.24$$

where $\gamma = h/\sqrt{2\pi mkT}$.

Using the theory of imperfect gases, the Helmholtz free energy F of the system is given by:

$$F = -kT \log Z_N = -kT \log Q_N + 3NkT \log \gamma \qquad 2.25$$

From equations 2.22 and 2.25:

$$F = -NkT \log V_o + kT \log N! - kT \log\left(1 - \frac{N^2 B}{V_o}\right) + 3NkT \log \gamma \qquad 2.26$$

For large N we may use Stirling's approximation,

$$\text{Log } N! = N \log N - N$$

and if N^2B/V_o is small, equation 2.26 approximates to

$$F = - NkT \log \frac{V_o}{N} - NkT(1-3 \log \gamma) + \frac{N^2 kTB}{V_o} \qquad 2.27$$

Write: $N = n\overline{N}$, $R = k\overline{N}$, $B' = B\overline{N}$

then: $$F = - nRT \log \frac{V_o}{n\overline{N}} - nRT(1-3 \log \gamma) + \frac{n^2 RTB'}{V_o} \qquad 2.28$$

hence: $$\mu = \frac{\partial F}{\partial n} = - RT \log \frac{V_o}{n\overline{N}} + 3RT \log \gamma + \frac{2nRTB'}{V_o} \qquad 2.29$$

For the gas phase with no adsorbent, the same equations hold with $E(\underline{r}_i) = O$ everywhere, since the development is quite general. Equation 2.21 then gives simply the geometric volume V, whilst equation 2.23 is replaced by:

$$B_g = - \frac{1}{2V_g} \int_{V_g}\int f_{12} \, d\underline{r}_1 d\underline{r}_2 \qquad 2.30$$

The analogues of equations 2.28 and 2.29 are:

$$F_g = - n_g RT \log \frac{V_g}{n_g \overline{N}} - n_g RT(1-3 \log \gamma) + \frac{n_g^2 RTB' g}{V_g} \qquad 2.31$$

$$\text{and } \mu_g = -RT \log \frac{V_g}{n_g \overline{N}} + 3RT \log \gamma + \frac{2n_g RTB'_g}{V_g} \qquad 2.32$$

Also the gas bulk pressure p is related to the bulk Helmholtz free energy by:

$$p = -\frac{\partial F_g}{\partial V_g} = \frac{n_g RT}{V_g} + \frac{n_g^2 RTB'_g}{V_g^2} \qquad 2.33$$

For equilibrium between the adsorbed and the gas phase $\mu_g = \mu$, so from equations 2.32 and 2.29 :

$$RT \log \frac{V_g}{n_g} \cdot \frac{n}{V_o} = 2RT\left(B'_g \cdot \frac{n_g}{V_g} - B' \cdot \frac{n}{V_o}\right) \qquad 2.34$$

$$\text{i.e. } \frac{n}{V_o} \simeq \frac{n_g}{V_g}\left(1 + 2\left(B'_g \cdot \frac{n_g}{V_g} - B' \cdot \frac{n}{V_o}\right)\right) \qquad 2.35$$

Eliminating n_g between equations 2.33 and 2.35 and neglecting higher powers of p and n_g gives:

$$n \simeq \frac{pV_o}{RT}\left(1 + \frac{p}{RT}(B'_g - 2B')\right) \qquad 2.36$$

Equation 2.36 relates the number of moles n of gas adsorbed in volume V of the sieve, in this case the volume of the unit cube side a_o, to the bulk gas pressure p at temperature T in terms of the molecular potentials

of the system as contained in the terms V_o and B'. Thus an equilibrium isotherm may be obtained for the system under conditions sufficiently dilute for only two body interactions to be of importance which corresponds at most to two to three carbon dioxide molecules per cage.

For the hypothetical case of a single adsorbed carbon dioxide molecule, $E(\underline{r}_i,\underline{r}_j) = 0$ and equation 2.36 reduces to,

$$n = \frac{pV_o}{RT} \qquad 2.37$$

and V_o may be approximated by

$$V_o = \sum_v \exp(-\frac{\phi(\underline{r})}{kT})\delta V \qquad 2.38$$

where δV is an element of cage volume per point.

For two adsorbed carbon dioxide molecules in the sieve cage $E(\underline{r}_i,\underline{r}_j) \neq 0$ and B' may be approximated by:

$$B' = -\frac{N}{2V_o} \sum_v \sum_v \left(\exp(-\frac{E(\underline{r}_1,\underline{r}_2)}{kT}) - 1 \right) \cdot \left(\exp(-\frac{\phi(\underline{r}_1)+\phi(\underline{r}_2)}{kT}) \right) \delta V^2 \qquad 2.39$$

2.5 Theoretical Heats of Adsorption

Theoretical heats of adsorption for carbon dioxide adsorbed in a Linde 5A sieve as a function of temperature and pressure can be obtained from values of V_o, B' and B'_g over the range of validity of the theoretical

isotherm (equation 2.36). The heat of adsorption per mole of gas at bulk pressure p and temperature T is:

$$-\delta H = \delta U + p\delta V \qquad 2.40$$

where δU is the difference in internal energy per mole between gas in the bulk and sieve phases and $p\delta V$ is the work done per mole in transferring the gas from one phase to the other.

The internal energy of the gas in the sieve phase is related to the partition function Z_N by :

$$U = kT^2 \frac{\partial}{\partial T} (\log Z_N)$$

where $$F = -kT \log Z_N \quad (10)$$

Hence $$U = F - T \left(\frac{\partial F}{\partial T}\right)_V \qquad 2.41$$

Now $$F \simeq nRT \log \frac{V_o}{n\bar{N}} - nRT(1-3 \log \gamma) + \frac{n^2 RTB'}{V_o}$$

(equation 2.28) where F is the Helmholtz free energy per cage. From equations 2.41 and 2.28 the internal energy per mole of gas in the sieve phase for n moles of gas adsorbed per cage is

$$\frac{U}{n} = \frac{RT^2}{V_o}\frac{dV_o}{dT} + \frac{nRT^2}{V_o^2}\left(B' \frac{dV_o}{dT} - V_o \frac{dB'}{dT}\right) \qquad 2.42$$

The analogue of equation 2.42 for the bulk phase can be written in terms of V_g/n_g giving:

$$\frac{U_g}{n_g} = \frac{n_g}{V_g} RT^2 \frac{\partial}{\partial T}\left(\frac{V_g}{n_g}\right) + \frac{n_g}{V_g} RT^2 \left(B'_g \frac{n_g}{V_g} \frac{\partial}{\partial T}\left(\frac{V_g}{n_g}\right) - \frac{dB'_g}{dT}\right) \qquad 2.43$$

where V_g/n_g is the volume per mole that n moles of gas per cage in the sieve phase would occupy at temperature T and pressure p in the bulk phase.

At some temperature T, and given a value of the bulk pressure p, then n for these conditions is fixed by equation 2.36 and V_g/n_g by equation 2.33. Since V_o, B' and B'_g are functions of temperature only then U/n and U_g/n_g can be obtained from equations 2.42 and 2.43. The value of $\frac{\partial}{\partial T}\frac{V_g}{n_g}$ is obtained from equation 2.33 giving:

$$p \frac{\partial}{\partial T}\left(\frac{V_g}{n_g}\right) = R + \frac{n_g}{V_g} RB'_g + \frac{n_g}{V_g} RT \frac{dB_g}{dT} \qquad 2.44$$

The corresponding value to V_g/n_g in the sieve phase is a_o^3/n where a_o^3 is the volume of a sieve cage. Hence from equation 2.40 the heat of adsorption per mole at temperature T and pressure p is:

$$-\delta H = \frac{U_g}{n_g} - \frac{U}{n} + p\left(\frac{V_g}{n_g} - \frac{a_o^3}{n}\right) \qquad 2.45$$

2.6 Theoretical Crystal Diffusivities

The crystal diffusivity D_c can be related to the transition probabilities for a gas molecule translating from one large cage to the next through an O8 window by a similar method to that used by Vineyard.[11]

The transition probability per unit time, G, can be written as:

$$G = \sqrt{\frac{RT}{2\pi M}} \times \frac{\int_s \exp(-\phi_T/kT)dS}{\int_v \exp(-\phi_T/kT)dV} \qquad 2.46$$

and D_c is related to G by:

$$D_c = \delta^2 G \qquad 2.47$$

δ is the transition jump distance, and in the case for transition through an O8 window δ may be replaced by a_o. Combining equations 2.46 and 2.47 gives:

$$D_c = a_o^2 \sqrt{\frac{RT}{2\pi M}} \times \frac{\int_s \exp(-\phi_T/kT)dS}{\int_v \exp(-\phi_T/kT)dV} \qquad 2.48$$

where the volume for the integral in the denominator is the volume of the

cage of origin and the surface for the integral in the numerator is the area of the window through which the transition occurs.

In the case where the cage of origin contains a single carbon dioxide molecule, the total potential for the system ϕ_T reduces to ϕ (see equation 2.17) and equation 2.48 can be approximated by:

$$D_c = a_o^2 \sqrt{\frac{RT}{2\pi M}} \times \frac{\sum_s \exp(-\phi/kT)\delta S}{\sum_v \exp(-\phi/kT)\delta V} \qquad 2.49$$

2.7 Mathematical Model of the Diffusion Process

2.7.1 Description of Model

The model describes the one dimensional diffusion of carbon dioxide in a cylindrical molecular sieve pellet, initially saturated with carbon dioxide labelled with carbon 14, which undergoes a dynamic self diffusion process with unlabelled carbon dioxide at constant temperature and pressure. The practical apparatus is arranged such that diffusion takes place only along the long axis of the pellet, and the exchange surface is at one of the flat ends of the pellet.

A simple approximation to the interior of the pellet is used in which it is assumed there is a uniform distribution of single sized spherical crystals

FIGURE 2.3

SCHEMATIC CONCENTRATION PROFILES IN PORES AND CRYSTALS

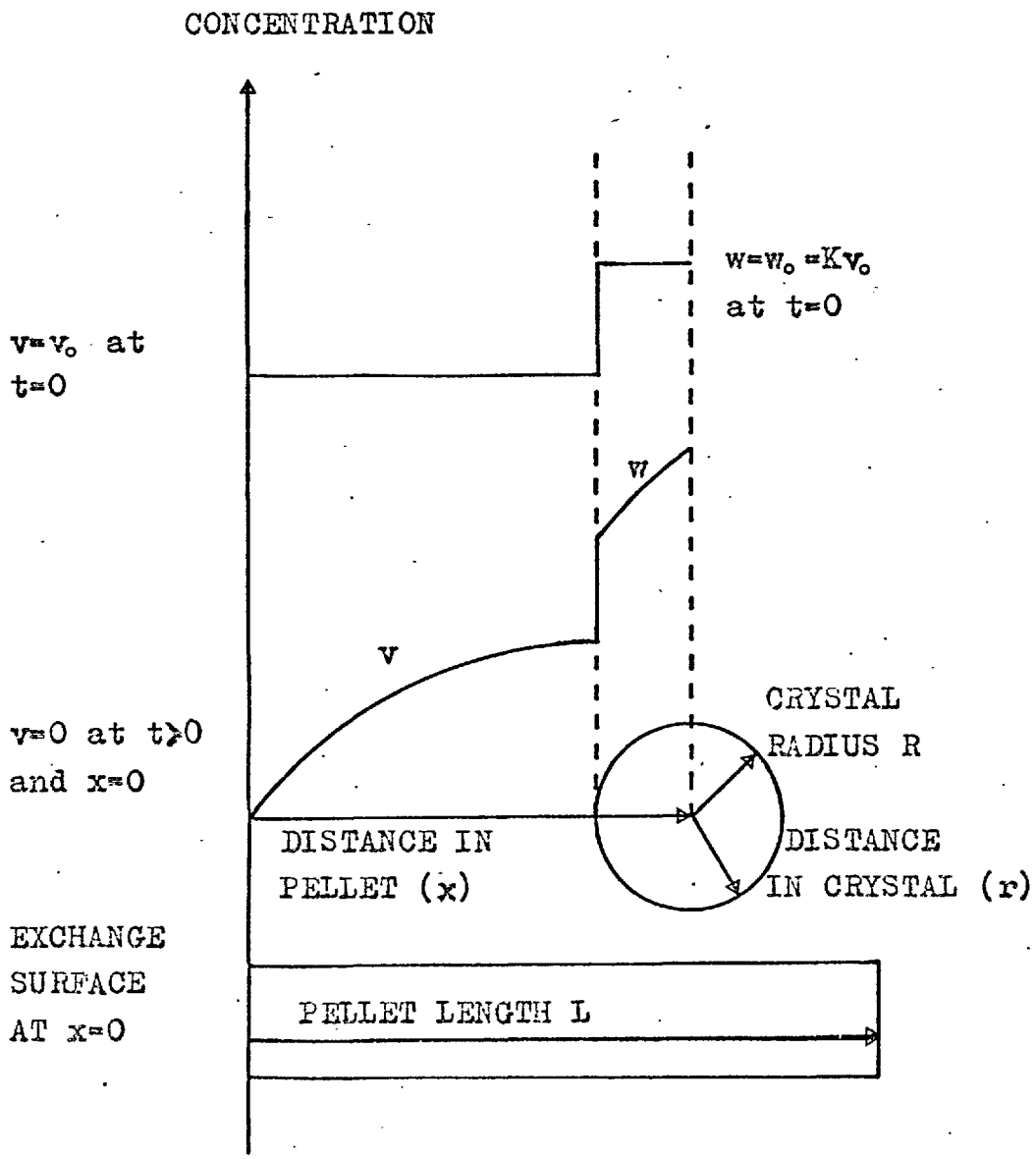

without any significant contact between one another. Each crystal is surrounded by a gas of uniform composition and the gas just inside the crystal is in thermodynamic equilibrium with the gas just outside. The diffusion processes inside the crystal and in the pore structure of the pellet are governed by Fick's law. Since the exchange process is between labelled and unlabelled carbon dioxide there is no concentration change as such as diffusion proceeds and so a single point on the equilibrium isotherm establishes the equilibrium relationship between gas in the crystal and gas in the pore. At zero time the labelled carbon dioxide concentration at the exchange surface is reduced to zero and maintained at this till the diffusion process is complete. (see figure 2.3).

2.7.2 Crystal Equations

The assumptions that the crystals are single sized, spherical and surrounded by gas of uniform composition gives spherical symmetry. Thus:

$$\frac{\partial w}{\partial t} = D_c \nabla^2 w = D_c\left(\frac{\partial^2 w}{\partial r^2} + \frac{2}{r}\frac{\partial w}{\partial r}\right) \qquad 2.50$$

describes the intra-crystalline diffusion.

The rate of accumulation of adsorbate Q_c per unit volume of crystal is given by:

$$V_c Q_c = \int_{\underline{S}} (N_c)_{r=R} \, d\underline{S} = \int_{\underline{S}} D_c \left(\frac{\partial w}{\partial r}\right)_{r=R} \cdot d\underline{S} \qquad 2.51$$

Hence, $$Q_c = \frac{3}{R} D_c \left(\frac{\partial w}{\partial r}\right)_{r=R} \qquad 2.52$$

The thermodynamic equilibrium at the surface of the crystal is represented by:

$$(w)_{r=R} = Kv \qquad 2.53$$

2.7.3 Pellet Equations

A material balance over an arbitrary volume V in the pellet enclosed by some boundary $\underline{s}$ gives:

$$-\int_{\underline{s}} \underline{N}_p \cdot d\underline{S} = \int_v \left(E_p \frac{\partial v}{\partial t} + (1-E_p)Q_c\right)dV \qquad 2.54$$

where $\underline{N}_p$ is the mass flux in the pores given by $\underline{N}_p = - D_p \, \partial v/\partial x$. By Green's Theorem,

$$\int_{\underline{s}} \underline{N}_p \cdot d\underline{S} = \int \nabla \cdot \underline{N}_p \, dV \qquad 2.55$$

Now since the material balance is over an arbitrary volume of pellet the integrands may be equated. 'A posteriori' calculation shows that the pore accumulation $E_p \, \partial v/\partial t$ can be neglected. Thus:

$$D_p \frac{\partial^2 v}{\partial x^2} = (1 - E_p)Q_c \qquad 2.56$$

The boundary conditions for these equations are:

At $t = O$, $O \leq x \leq L$; $v = v_o$

$O \leq r \leq R$; $w = w_o = Kv_o$

For $t > O$, at $x = L$; $\partial v/\partial x = O$ 2.57

at $x = O$; $v = O$

at $r = O$, $O \leq x \leq L$; $\partial w/\partial r = O$

It is convenient to express these equations in dimensionless form by defining the dimensionless variables:

$$x' = \frac{x}{L} \qquad r' = \frac{r}{R} \qquad v' = \frac{v}{v_o}$$

$$w' = \frac{w}{v_o} \qquad t' = \frac{t\,D_p}{L^2}$$

Hence from equations 2.52 and 2.56

$$\frac{\partial^2 v'}{\partial x'^2} = 3(1-E_p)\,\frac{D_c L^2}{R^2 D_p}\left(\frac{\partial w'}{\partial r'}\right)_{r'=1} \qquad 2.58$$

and write $P = D_p R^2 / D_c L^2$ 2.58a

From equation 2.50

$$P\,\frac{\partial w'}{\partial t} = \frac{\partial^2 w'}{\partial r'^2} + \frac{2}{r'}\,\frac{\partial w'}{\partial r'} \qquad 2.59$$

From equation 2.57 :

At $t' = 0$, $0 \leq r' \leq 1$; $v' = 1$ and $w' = K$

$0 \leq x' \leq 1$;

For $t' > 0$, at $x' = 1$; $\partial v'/\partial x' = 0$

at $x' = 0$; $v' = 0$ 2.60

at $r' = 0$; $0 \leq x' \leq 1$; $\partial w'/\partial r' = 0$

and from equation 2.53

at $r' = 1$, $0 \leq x' \leq 1$; $w' = Kv'$ 2.60a

Equations 2.58, 2.59 and 2.60 now define the model with $w' = w'(x', r', t')$ and $v' = v'(x', t')$.

2.7.4 Finite Difference Solution

Equations 2.58 and 2.59 are solved by an implicit method to obviate stability problems,[12] using the following finite difference approximations.

Time increment,	$t' = i\delta t'$	$i = 0,1,2.....$
Space increment in pellet,	$x' = j\delta x'$	$j = 0,1,2...m$; $m\delta x' = 1$
Space increment in crystal,	$r' = k\delta r'$	$k = 0,1,2...n$; $n\delta r' = 1$

In the crystal, since time is explicitly involved, six values of w' will

be needed to write an approximation to equation 2.59, and in the pellet since time is implicit, three values of v' will be needed to write an approximation to equation 2.58 . The approximations used for say space dimension r' are:

$$\frac{\partial w'}{\partial r'} = \frac{w'_{k+1} - w'_{k-1}}{2\delta r'}$$

$$\frac{\partial^2 w'}{\partial r'^2} = \frac{w'_{k+1} - 2w'_k + w'_{k-1}}{(\delta r')^2}$$

and for time : $$\left(\frac{\partial w'}{\partial t'}\right)_{i+\frac{1}{2}} = \frac{w'_{i+1} - w_i}{\delta t'}$$

To keep consistency with an implicit solution, in the crystal the LHS of equation 2.59 is evaluated at time $i + \frac{1}{2}$ and the RHS at the average of the values at times i and i + 1. The pellet equation (2.58) is evaluated at time i.

Thus from equation 2.58 :

$$\left(\frac{\partial w'}{\partial r'}\right)_{r'=1} = G_{i,j} = Q(v'_{i,j-1} - 2v'_{i,j} + v'_{i,j+1})$$

$$\text{with} \quad 1 \leq j \leq (m-1) \qquad 2.61$$

and using equation 2.61 :

$$G_{i,m} = 2Q(v'_{i,m-1} - v'_{i,m}) \qquad 2.61a$$

where $Q = P/3(1-E_p)(\delta x')^2 = Pm^2/3(1-E_p)$

and $v'_{i,o} = O$

From equation 2.59 :

$$-\frac{k+1}{k} w'_{i+1,j,k+1} + (\beta + 2)w'_{i+1,j,k} - \frac{k-1}{k} w'_{i+1,j,k-1} =$$

$$= \frac{k+1}{k} w'_{i,j,k+1} + (\beta - 2)\, w'_{i,j,k} + \frac{k-1}{k} w'_{i,j,k-1}$$

$$\text{with} \quad 1 \leq k \leq n \qquad 2.62$$

where $\beta = 2P(\delta r')^2/\delta t' = 2P/n^2\delta t'$.

Note that values of w' for $k = O$ do not appear in the equation; values for $k = n+1$ are given by :

$$w'_{i,j,n+1} = w'_{i,j,n-1} + \frac{2}{n} \cdot G_{i,j} \qquad 2.62a$$

Equation 2.62 may be written in the form :

$$a_{k,k-1}\, w'_{i+1,j,k-1} + a_{k,k} w'_{i+1,j,k} + a_{k,k+1} w'_{i+1,j,k+1} = b_k$$

$$\text{with} \quad 1 \leq k \leq n \qquad 2.63$$

where $a_{k,k-1} = -\frac{k-1}{k}$

$a_{k,k} = \beta + 2$

$a_{k,k+1} = -\frac{k+1}{k}$

$$b_k = -a_{k,k-1} w^t_{i,j,k-1} + (\beta-2) w^t_{i,j,k} - a_{k,k+1} w^t_{i,j,k+1}$$

with $1 \leq k < n$ 2.64

and for $k = n$:

$a_{n,n-1} = -2$; $a_{n,n} = \beta+2$; $a_{n,n+1} = 0$

$$b_n = 2w^t_{i,j,n-1} + (\beta-2) w^t_{i,j,n} + \frac{2(n+1)}{n^2} (G_{i+1,j} + G_{i,j}) \qquad 2.64a$$

The algorithm used to solve the equations 2.61, 2.61a, 2.63, 2.64 and 2.64a is:

For one time step, given all $v^t_{i,j}$, $w^t_{i,j,k}$, $G_{i,j}$

1) Estimate $v^t_{i+1,j}$ for $1 \leq j \leq m$

2) Compute $G_{i+1,j}$ for $1 \leq j \leq m$ using equations 2.61 and 2.61a .

3) Compute $a_{k,k-1}$, $a_{k,k}$, $a_{k,k+1}$, b_k for

$1 \leq k \leq n$ using equations 2.63 and 2.63a .

4) Solve the resulting set of linear equations for the $w^{i}_{i+1,j,k}$ for $1 \leq k \leq n$.

5) Compute $v^{ii}_{i+1,j} = w^{i}_{i+1,j,n}/K$

6) If the change in any $v^{i}_{i+1,j}$ over the step exceeds the permitted error, repeat from step 2 with new estimates for $v^{i}_{i+1,j}$ where :

$$\text{New } v^{i}_{i+1,j} = (1-\beta^{i})v^{i}_{i+1,j} + \beta^{i} v^{ii}_{i+1,j}$$

where β^{i} is a given relaxation parameter $0 < \beta^{i} < 2$.

For the case where $P = 0$ (i.e. D_c is infinite) and thus pure diffusion is the controlling process the pellet equation is:

$$\frac{\partial^2 v^{i}}{\partial x^{i2}} = \frac{\partial}{\partial t^{i}} (E_p v^{i} + (1-E_p)Kv^{i}) \qquad 2.65$$

with the boundary conditions:

$$\begin{aligned} &\text{At } t^{i} = 0, \quad 0 \leq x^{i} \leq 1 ; \quad v^{i} = 1 \\ &\text{For } t^{i} > 0, \quad x^{i} = 0 ; \quad v^{i} = 0 \qquad 2.65a \\ &\qquad\qquad x^{i} = 1 ; \quad \partial v^{i}/\partial x^{i} = 0 \end{aligned}$$

whence $v^{i}_{i,o} = 0$ for all $i > 0$.

The finite difference approximation is :

$$- v^{1}_{i+1,j-1} + (\chi + 2)v^{1}_{i+1,j} - v^{1}_{i+1,j+1} =$$

$$= v^{1}_{i,j-1} + (\chi - 2)v^{1}_{i,j} + v^{1}_{i,j+1}$$

$$\text{with} \quad 1 \leq j \leq (m-1) \qquad 2.66$$

and for $j = m$

$$-2v^{1}_{i+1,m-1} + (\chi + 2)v^{1}_{i+1,m} = 2v^{1}_{i,m-1} + (\chi - 2)v^{1}_{i,m} \qquad 2.66a$$

where $\chi = 2(E_p + (1 - E_p)K)/m^2 \partial t^1$.

The algorithm used in this case is for each time step the $v^{1}_{i+1,j}$ with $1 \leq j \leq m$ are obtained from the $v^{1}_{i,j}$ with $1 \leq j \leq m$ by solving the set of linear equations 2.66 and 2.66a .

CHAPTER 3 - COMPUTATIONAL METHODS

3.1 Generation of a Sieve Structure

Equation 2.10 describes the interaction between a single carbon dioxide molecule and the ionic framework of the Linde 5A sieve. Before this equation can be used a sieve structure must be generated using the ion positions given in table 2.1. This table can be expanded in terms of the Oxygen, Sodium and Calcium ion positions to give table 3.1, which fully describes the positions of the ions in the positive quadrant (X, Y, Z). The Aluminium and Silicon ions have been omitted as it is shown in Chapter 6 that their potential effect is negligible.

3.1.1 Full Ion Reflection

The ions in table 3.1 have to be reflected out to generate a three dimensional network of sieve cages, each cage formed by a unit cell, which itself is formed by 56 ions (48 oxygen and 8 NaCa ions). There are two separate ways in which the data ions can be reflected. One maintains 56 ions per cage throughout the generated structure and as a result of this leaves the resulting composite cube devoid of ions on

three faces. The other fills these faces with oxygen ions, forming O8 windows, and maintains a symmetric structure.

TABLE 3.1

ION	X	Y	Z
OI	O	O.272O	O.5
OI	O	O.5	O.272O
OI	O.272O	O	O.5
OI	O.272O	O.5	O
OI	O.5	O	O.272O
OI	O.5	O.272O	O
OII	O.2122	O.2122	O.5
OII	O.2122	O.5	O.2122
OII	O.5	O.2122	O.2122
OIII	O.1518	O.3882	O.3882
OIII	O.3882	O.1518	O.3882
OIII	O.3882	O.3882	O.1518
NaCa	O.3O5O	O.3O5O	O.3O5O

In a composite cube formed by $(2n - 1)^3$ unit cells, n = 1,2,3..... there will be $56 \times (2n - 1)^3$ ions in the first structure and $56 \times (2n - 1)^3 + 8 \times 3 \times (2n - 1)^2$ ions in the second structure.

The term $8 \times 3 \times (2n - 1)^2$ represents the surface oxygen ions in the three faces that were unfilled in the first case. Each unfilled face includes $(2n - 1)^2$ faces of unit cells, each of which includes eight oxygen ions. The number of ions expected to be generated for composite cubes of increasing size is given in table 3.2.

If the six AS ions are included in the data table there will be $80 \times (2n - 1)^3 + 3 \times 16 \times (2n - 1)^2$ ions in a composite cube containing $(2n - 1)^3$ unit cells. The number of ions expected to be generated for various values of n is given in table 3.3.

TABLE 3.2

n	RMAX = (2n-1)/2	$56 \times (2n - 1)^3$	$24 \times (2n-1)^2$	TOTAL NO. OF IONS	NO. OF UNIT CELLS = $(2n-1)^3$
1	0.5	56	24	80	1
2	1.5	1512	216	1728	27
3	2.5	7000	600	7600	125
4	3.5	19208	1176	20384	343
5	4.5	40824	1944	42768	729
6	5.5	74536	2904	77440	1331

TABLE 3.3

n	1	2	3	4	5	6
TOTAL NUMBER OF IONS	128	2592	11200	29792	62208	112288
NUMBER OF UNIT CELLS	1	27	125	343	729	1331

The method by which the ions in table 3.1 are reflected to give the number of ions in table 3.2 is best seen by analysing the procedure for a single cage. Six OI ions, three OII ions, three OIII ions and a single NaCa ion form the data table. Designating the co-ordinates of these ions as AI, BI, CI ; I = O, 1, 2.....12, then these co-ordinates have to be reflected to form all combinations of $\pm$AI, $\pm$BI, $\pm$CI. In general any co-ordinate can have two values, i.e. $\pm$ GI, so there will be 2^3 positions generated per line of data. To avoid repeating ion positions, the procedure is subject to the condition that if any co-ordinate GI = O then GI $\cong$ -GI. This only occurs in data for OI ions so only 2^2 positions are generated for the first six lines of data. This is summarised in table 3.4.

TABLE 3.4

I	NO. OF VALUES FOR CO-ORDINATE			LINES OF DATA OF THIS TYPE	POINTS GENERATED
	AI	BI	CI		
0-5	1	2	2	6	24
6-8	2	2	2	3	24
9-11	2	2	2	3	24
12	2	2	2	1	8
					$\sum$=80

The procedure is readily extended to n = 2, etc. The ion co-ordinates are in units of a_o, the unit cell characteristic dimension, so the data ions have only to be expanded in the form $\pm(m \pm GI)$ m = 0, 1, 2....m' to simulate ions in all regions outside the range of the data table. The value assigned to m' is such that $\pm(m' \pm GI) < RMAX$ for the value of n being considered, i.e. m' = n - 1.

For n = 2 the general co-ordinate GI can take six values. These are $\pm GI$, $\pm(1 - GI)$ and $\pm(1 + GI)$. To avoid repetition of points, if GI = 0 then GI $\equiv$ -GI, 1+GI $\equiv$ 1 - GI and -1+GI $\equiv$ -1-GI giving three values only. Also if GI = 0.5 then GI $\equiv$ 1-GI and -1+GI $\equiv$ -GI giving four values only. This will then generate the following numbers of ions.

TABLE 3.5

I	NO. OF VALUES FOR CO-ORDINATE			LINES OF DATA OF THIS TYPE	POINTS GENERATED
	AI	BI	CI		
0-5	3	6	4	6	27 x 16
6-8	6	6	4	3	27 x 16
9-11	6	6	6	3	27 x 24
12	6	6	6	1	27 x 8
					$\sum$ = 1728

3.1.2 Half Plane Reflection

The preceding ion projection method maps out the positions of all ions in a cubic space which contains as many unit cells as required. For computation purposes it is more convenient to use a method which maps out all ions in the region $X \geq 0$ and to generate the ions in the region $X < 0$ later in the program.

TABLE 3.6

I	NO. OF VALUES OF CO-ORDINATE			LINES OF DATE OF THIS TYPE	LATER REFLEC-TION	POINTS GENER-ATED
	AI	BI	CI			
O-1 (AI=O)	1	6	4	2	1	16 x 3
O-1 (AI≠O	1	6	4	2	2	16 x 6
2-3	3	3	4	2	2	16 x 9
4-5	2	3	6	2	2	16 x 9
6-7	3	6	4	2	2	16 x 18
8	2	6	6	1	2	16 x 9
9-12	3	6	6	4	2	16 x 54
						$\sum$ = 1728

For n = 2 in this method, the co-ordinate AI will now take three values. These are AI, 1+AI and 1-AI, i.e. those co-ordinates which lie between O and RMAX for n = 2. The co-ordinates BI and CI can take six values as before. To avoid repetition of points, if AI = O there is only this one value and the point is not reflected later in the program. Also 1+AI ≡ 1-AI giving one other value which will be reflected later. If BI or CI = O there will be three values of this co-ordinate and if BI or CI = O.5 there will

be four values, all of which will be reflected later. This procedure, in the main analogous to the preceding one, will generate the number of ions given in table 3.6 .

3.2 Carbon Dioxide-Ion Interaction

Having outlined the method by which the data ions are projected, a procedure is required that will evaluate the interaction between a carbon dioxide molecule situated inside a large cage and these ions. If a model of a perfect crystal of the Linde 5A molecular sieve is examined, it can be seen that the region bounded by a cube side a_o centred on a large cage contains four points of structural symmetry. These are the centre of a large cage, the centre of a small cage, the centre of an O8 window and the centre of an O4 bridge.[9] If these four points, all of which are included in the unit cell structure, are joined, one obtains a tetrahedron. Because of the existing symmetry this tetrahedron is the smallest region of space within the unit cell from which the whole structure can be generated both spatially and potentially by appropriate reflections and rotations.

Figure 3.1

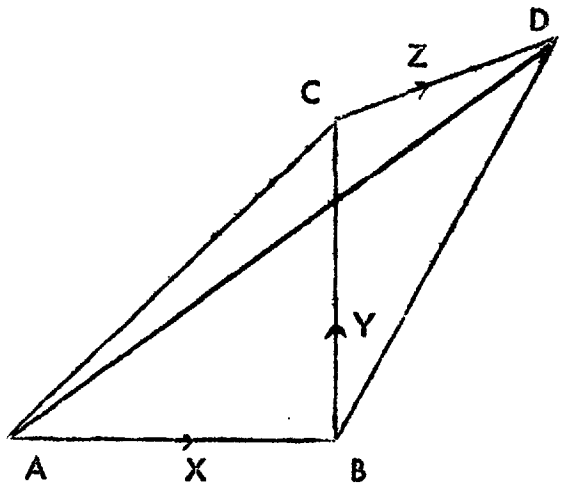

A set of rectangular co-ordinate axes as shown in figure 3.1 are used to contain the tetrahedron, with the origin at the centre of the large cage of interest.

A is the centre of the large cage

B is the centre of the O8 window

C is the centre of the O4 bridge

D is the centre of the small cage

Here 2AB is the unit cell dimension a_o = 12.31Å . The ion positions given by Broussard and Shoemaker and quoted in table 3.1 are also in units of a_o and all lie in the quadrant (X,Y,Z), bounded by the tetrahedron. This shape represents 1/48th. of the total volume of the unit

cube, and suitable reflection of the ion positions in (X,Y,Z) will create for computation purposes as many interconnected cages in three dimensions as necessary. When the potentials have been determined in (X,Y,Z), suitable reflection of the values will give the potentials throughout the region of the unit cube.

To simplify computation further the Si^{4+} and Al^{3+} ions are considered as a hypothetical $AS^{3\frac{1}{2}+}$ ion. The properties of this are obtained from the geometric mean polarisability and arithmetic mean susceptibility and ionic radius of the separate aluminium and silicon ions. Similarly a hypothetical $NaCa^{1\frac{1}{2}+}$ or $Ca^{1\frac{1}{2}+}$ ion is used. This permits one of these ions to be located in each of the eight O6 windows bordering the large cage, which fits in better with the basic symmetry.

For computation within the tetrahedron it was decided to use a three dimensional grid with a grid line separation of $a_o/20$. This gives a convenient labelling system to locate the particular point of computation which will lie in the range $10 \geq X \geq Y \geq Z \geq 0$ and also a maximum of 286 points at which the potential can be evaluated.

3.3 Point Reflections and Point Multiples within the Tetrahedral Grid

When the interaction potential has been computed inside the tetrahedron using equation 2.10, the results obtained can be reflected to fill the

whole of the region inside the large cage. As far as equation 2.37 is concerned, all that is required at this stage is to be able to evaluate the point multiple for these results since equation 2.38 depends only on the value of the potential. However, a complete potential map will be required later and so the reflected positions are given in full, together with the point multiple.

The points inside the tetrahedron fall into eight groups, which can be recognised by the algebraic relationship between the co-ordinates of each grid point.

3.3.1 Point (a)

$$X = Y = Z = O \qquad 3.1$$

This is a unique point.

3.3.2 Line (ab)

$X = J$ and $Y = Z = O$ with $O < J \leq 10$

These points can be reflected six times onto the points represented by:-

$X = \pm J$ and $Y = Z = O$

$Y = \pm J$ and $Z = X = O$

$Z = \pm J$ and $X = Y = O$

with $O < J \leq 10$ 3.2

LINES OF SYMMETRY IN THE UNIT CUBE

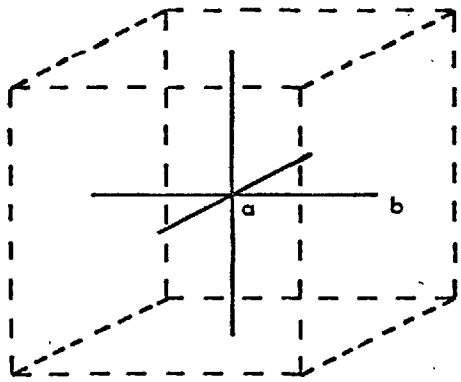

FIGURE 3.2

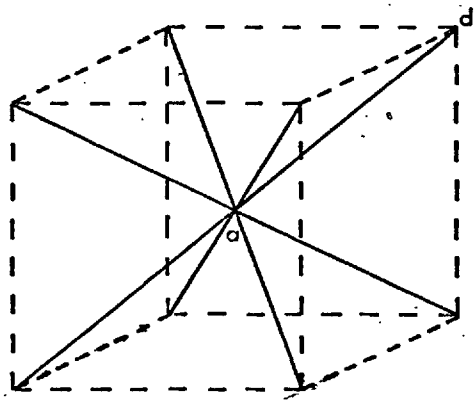

FIGURE 3.3

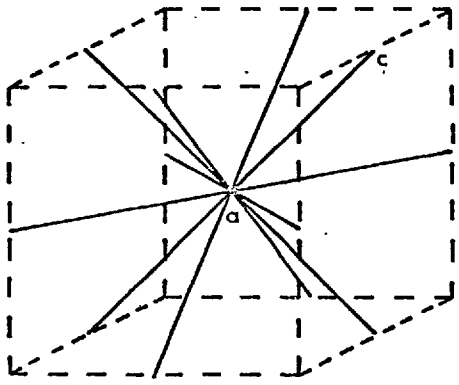

FIGURE 3.4

These are lines that join the mid points of the six faces of the unit cube to its centre. (See figure 3.2).

3.3.3 Line (ad)

$$X = Y = Z = J \quad \text{with} \quad 0 < J \leq 10$$

These points can be reflected eight times onto the points given by

$$X = Y = Z = \pm J \quad \text{with} \quad 0 < J \leq 10 \qquad 3.3$$

These are lines joining the corners of the unit cube to its centre. (See figure 3.3).

3.3.4 Line (ac)

$$X = Y = J \quad \text{and} \quad Z = 0 \quad \text{with} \quad 0 < J \leq 10$$

These points can be reflected twelve times onto the points given by:

$$X = Y = \pm J \quad \text{and} \quad Z = 0$$

$$X = Z = \pm J \quad \text{and} \quad Y = 0$$

$$Y = Z = \pm J \quad \text{and} \quad X = 0$$

$$\text{with} \quad 0 < J \leq 10 \qquad 3.4$$

These are lines that join the mid points of the edges of the unit cube to its centre. (See figure 3.4).

3.3.5 Plane (abc)

$$Z = 0 \quad \text{and} \quad X = J, \quad Y = K \quad \text{with} \quad 0 < J \leq 10$$

$$\text{and} \quad 0 < K < 10$$

These points can be reflected twenty-four times onto the points given by:

$$Z = O, \quad X = \pm J, \quad Y = \pm K$$

$$Z = O, \quad X = \pm K, \quad Y = \pm J$$

$$Y = O, \quad Z = \pm J, \quad X = \pm K$$

$$Y = O, \quad Z = \pm K, \quad X = \pm J$$

$$X = O, \quad Y = \pm J, \quad Z = \pm K$$

$$X = O, \quad Y = \pm K, \quad Z = \pm J$$

$$\text{with } O < J \leq 10 \quad \text{and} \quad O < K < 10 \qquad 3.5$$

These points lie on three planes in the direction of the co-ordinate axes. (See figure 3.5).

3.3.6 Plane (acd)

$$X = Y = J \quad \text{and } Z = K \quad \text{with } O < J < 10$$

$$\text{and } O < K \leq 10$$

These points can be reflected twenty-four times onto the points given by:

$$X = Y = \pm J \quad \text{and} \quad Z = \pm K$$

$$X = Z = \pm J \quad \text{and} \quad Y = \pm K$$

$$Y = Z = \pm J \quad \text{and} \quad X = \pm K$$

$$\text{with } O < J < 10 \quad \text{and} \quad O < K \leq 10 \qquad 3.6$$

PLANES OF SYMMETRY IN THE UNIT CUBE

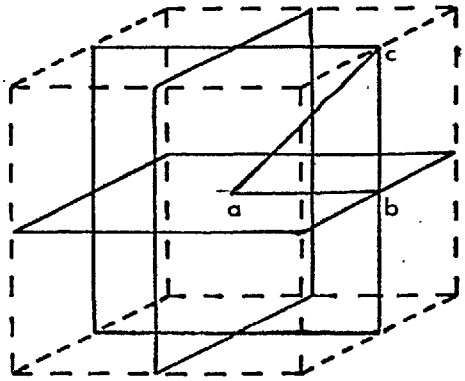

FIGURE 3.5

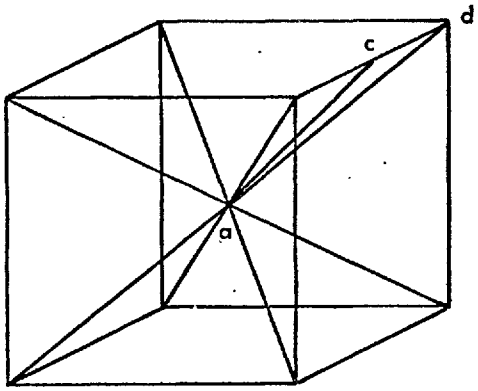

FIGURE 3.6

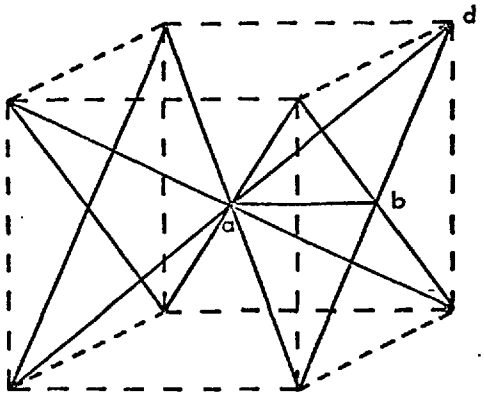

FIGURE 3.7

(Only two planes shown for the sake of clarity)

These points lie on six planes formed by the six pairs of diagonally opposite edges of the cube and the diagonals joining their ends through the centre of the cube. (See figure 3.6).

3.3.7 Plane (abd)

$X = J$ and $Y = Z = K$ with $0 < J < 10$

and $0 < K < 10$

These points can be reflected twenty-four times onto the points given by:

$X = \pm J$ and $Y = Z = \pm K$

$Y = \pm J$ and $Z = X = \pm K$

$Z = \pm J$ and $X = Y = \pm K$

with $0 < J < 10$ and $0 < K < 10$ 3.7

These points lie on six planes formed by the six pairs of diagonally opposite edges of the cube and the diagonals joining their ends through the mid points of the faces of the cube. (See figure 3.7).

3.3.8 All other points

$X = J$, $Y = K$, $Z = L$ with $0 < J \leq 10$,

$0 < K < 10$ and $0 < L < 10$

These points can be reflected forty-eight times onto the points given by:

$$X = \pm J, \quad Y = \pm K, \quad Z = \pm L$$

$$X = \pm J, \quad Y = \pm L, \quad Z = \pm K$$

$$X = \pm K, \quad Y = \pm J, \quad Z = \pm L$$

$$X = \pm K, \quad Y = \pm L, \quad Z = \pm J$$

$$X = \pm L, \quad Y = \pm J, \quad Z = \pm K$$

$$X = \pm L, \quad Y = \pm K, \quad Z = \pm J$$

with $0 < J \leq 10$, $0 < K < 10$ and $0 < L < 10$ 3.8

These eight types of reflection contain all the information required to map out the potentials obtained for the 286 points within the tetrahedron onto the 9261 points within the unit cube.

TABLE 3.7

REGION	INCLUDES	POINTS IN REGION	POINT MULTIPLE	REFLECTION TYPE
Point a	-	1	1	1
Line ab	Point b	10	6	2
ad	d	10	8	3
ac	c	10	12	4
Plane abc	Line bc	45	24	5
acd	cd	45	24	6
abd	bd	45	24	7
Tetrahedron abcd	Plane bcd	120	48	8

It may be noted that Σ(points x point multiple) = 9261 = $(21)^3$ which checks that all points have been reflected correctly.

3.3.9 Point Multiple Recognition

Sections 3.3.1 - 8 contain the algebraic relationships between the co-ordinates of any grid point (J,K,L) for it to have some particular point multiple. The flow diagram in figure 3.8 shows the procedure used to recognise these multiples.

3.3.10 The Carbon Dioxide-Ion Interaction Program

A program was written in EXCHLF Autocode which evaluated the carbon dioxide-ion potentials using the theoretical relationships outlined in section 2.2 and the preceding computational methods. The flow diagrams are given in figures 3.9 and 3.10 . A listing of the program is given in Appendix C .

3.4. The Equilibrium Isotherm

Equation 2.39 is programmed as follows. Having obtained a set of potentials in the region $10 \geq X \geq Y \geq Z \geq 0$, it is convenient to redefine the origin of these as a corner of the cube containing the unit cell. Using the same grid separation, the potentials will then lie in the region $20 \geq X \geq Y \geq Z \geq 10$.

FIGURE 3.8 GRID POINT REFLECTION FLOW DIAGRAM

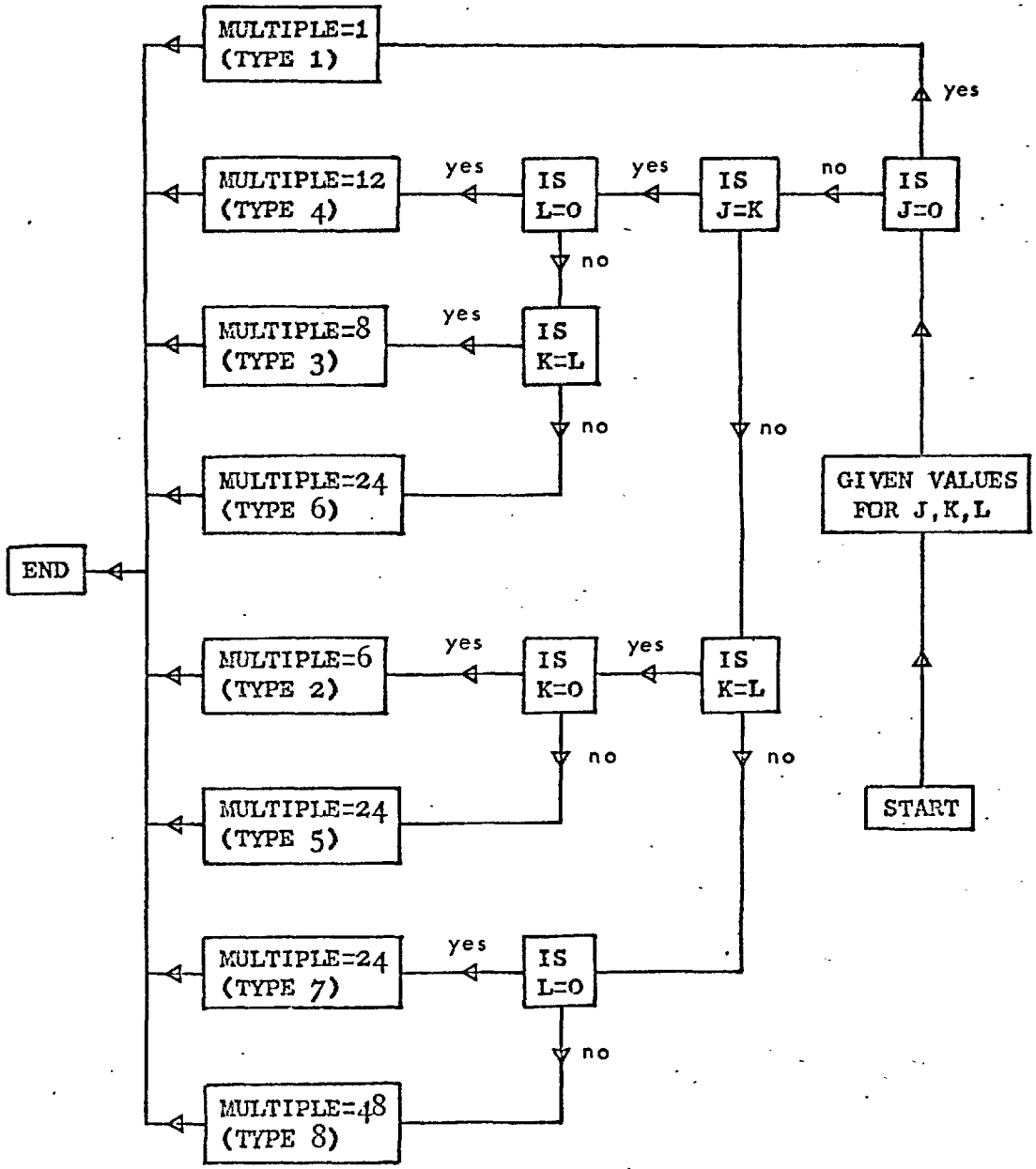

FIGURE 3.9 SIEVE POTENTIAL FLOW DIAGRAM

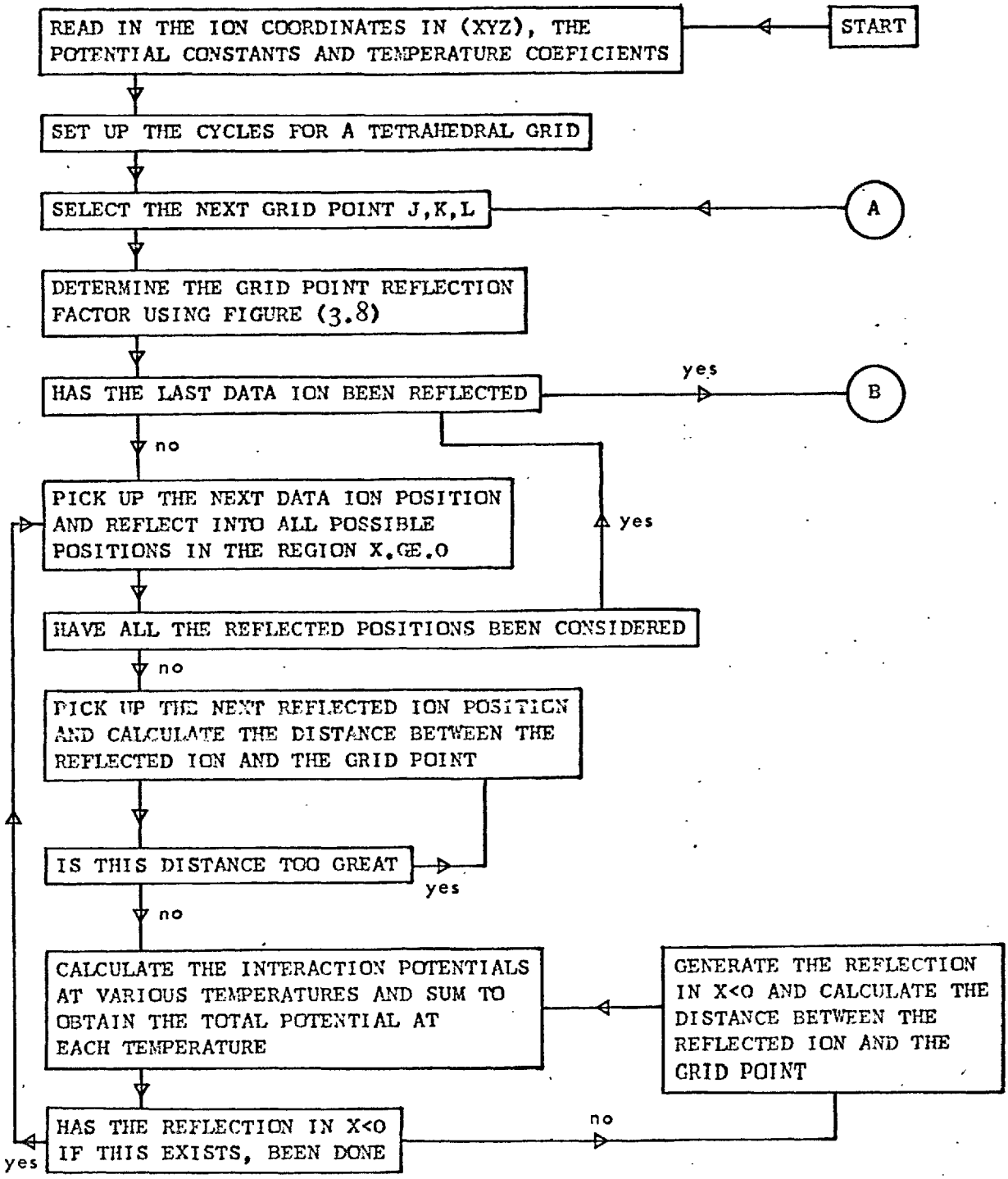

FIGURE 3.10 SIEVE POTENTIAL FLOW DIAGRAM

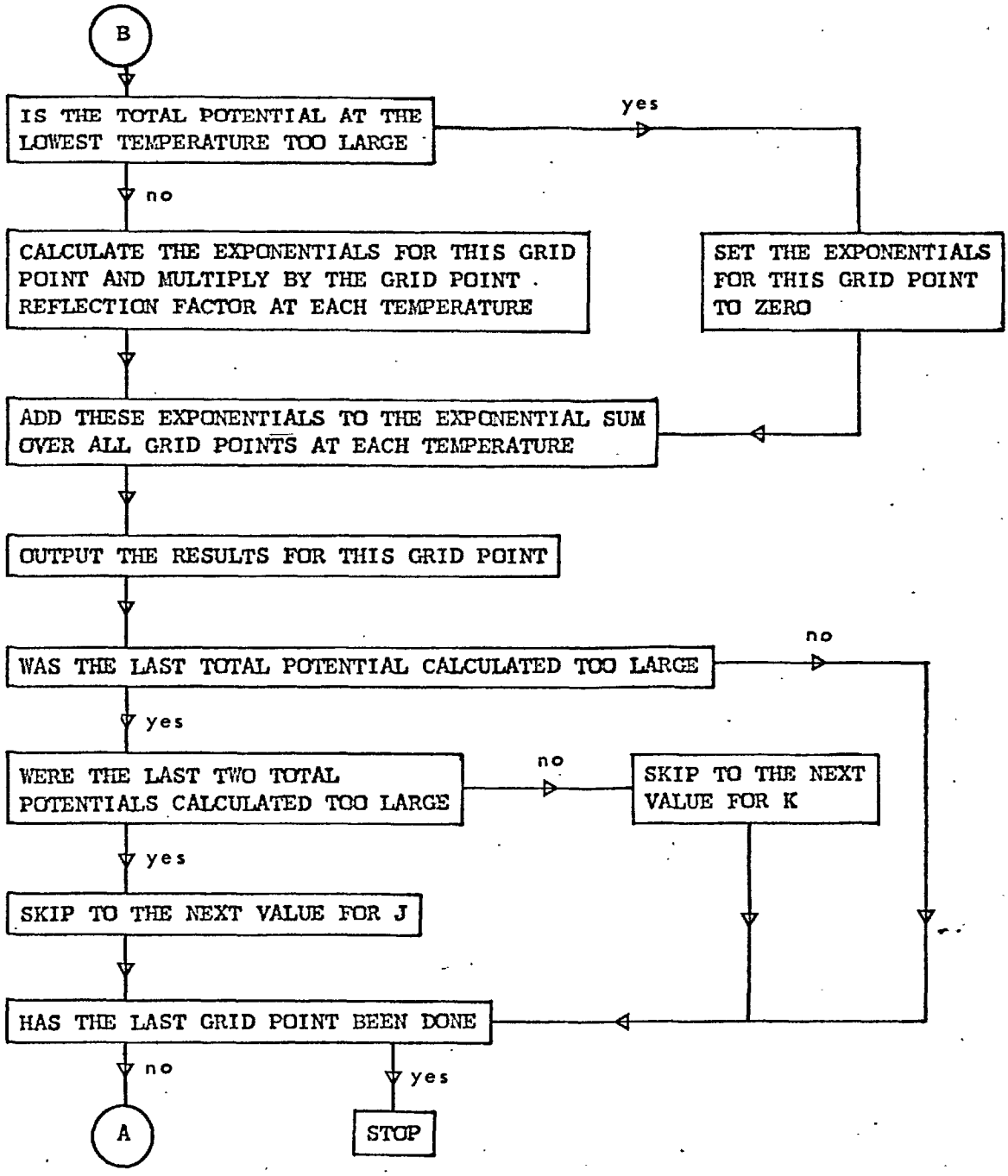

Equations 3.1 to 3.8 are in terms of the old grid co-ordinates (J,K,L). With the new origin, for example, the first line in equation 3.8 becomes:

$$X = J, \quad Y = K, \quad Z = L$$

$$X = 20-J, \quad Y = 20-K, \quad Z = 20-L$$

with $10 < J \leq 20$, $10 < K < 20$ and $10 < L < 20$ 3.9

i.e. the points are now reflected about (10,10,10) instead of (0,0,0).

If the forty-eight points in equation 3.8 are reordered and written in the form of equation 3.9 , the procedure for reflecting any particular value in the set of potentials is greatly simplified. Firstly the value has to be recognised as belonging to a particular reflection type. (These are numbered 1 to 8 in table 3.7) Then all the reflected positions of this value can be found using table 3.8. This table shows how the forty-eight possible reflected values are ordered, and the sequence in which the program generates each according to the reflection type.

In the unit cube containing 9261 grid points it would be possible to compute 9260 + 9259 + ... + 2 + 1 = 42,878,430 different pair interactions between two carbon dioxide molecules free to be placed at any of the grid points except the one occupied by the other.

TABLE 3.8 REFLECTIONS OF GRID POINT (J,K,L)

LABEL	X=J	Y=K	Z=L	REFLECTION TYPE 2	3	4	5	6	7	8
1	J	K	L	1	1	1	1	1	1	1
2	J	K	20-L		2			2	2	2
3	J	20-K	L		3		2	3	3	3
4	J	20-K	20-L		4	5		4	4	4
5	J	L	K				3	5		5
6	J	20-L	K					6		6
7	J	L	20-K				4	7		7
8	J	20-L	20-K					8		8
9	K	L	J	2		2	5		5	9
10	K	20-L	J						6	10
11	K	20-L	20-J				6		7	11
12	K	20-L	20-J			6			8	12
13	K	J	L				7			13
14	K	J	20-L							14
15	K	20-J	L				8			15
16	K	20-J	20-L							16
17	20-J	K	L	3	5	3	9	9	9	17
18	20-J	K	20-L		6			10	10	18
19	20-J	20-K	L		7		10	11	11	19
20	20-J	20-K	20-L		8	7		12	12	20
21	20-J	L	K				11	13		21
22	20-J	20-L	K					14		22
23	20-J	L	20-K				12	15		23
24	20-J	20-L	20-K					16		24
25	20-K	L	J			4	13		13	25
26	20-K	20-L	J						14	26
27	20-K	L	20-J	4			14		15	27
28	20-K	20-L	20-J			8			16	28
29	20-K	J	L				15			29
30	20-K	J	20-L							30
31	20-K	20-J	L				16			31
32	20-K	20-J	20-L							32
33	L	J	K			9	17	17	17	33
34	L	20-J	K				18	18	18	34
35	20-L	J	20-K	5			19	19	19	35
36	20-L	20-J	20-K				20	20	20	36
37	L	K	J				21			37
38	20-L	K	20-J			10	22			38
39	L	20-K	J				23			39
40	20-L	20-K	20-J				24			40
41	20-L	J	K					21	21	41
42	L	J	20-K					22	22	42
43	20-L	20-J	K	6		11		23	23	43
44	L	20-J	20-K					24	24	44
45	20-L	K	J							45
46	L	K	20-J							46
47	20-L	20-K	J							47
48	L	20-K	20-J			12				48

Using the basic symmetry of the system it is not necessary to compute all these interactions, and many of them can be inferred using the reflection table 3.8 and the point multiple values. The way this is done can be seen by analysing a simple two dimensional case using a square grid containing 25 points.

Figure 3.11

04	14	24	34	44
03	13	23	33	43
02	12	22	32	42
01	11	21	31	41
00	10	20	30	40

The grid points lie at the centre of the small squares, labelled as shown in figure 3.11. The shaded region is treated as the input points and these are used to generate all the other grid positions using table 3.9.

TABLE 3.9

POINT	POINT MULTIPLE	REFLECTED POINTS
22	1	
32	4	23, 12, 21
33	4	13, 11, 31
42	4	24, 02, 20
43	8	34, 14, 03, 01, 10, 30, 41
44	4	04, 00, 40

The first carbon dioxide molecule is placed at (22) and the second successively at (22), (32), (33), (42), (43) and (44). If the pair interaction is calculated between these six second points and the first point, then multiplying each value in turn by the point multiples in table (3.9), will give the total interaction for all the twenty-four possible pairs. When the second molecule is at (22) it is coincident with the first so the interaction is neglected.

The first carbon dioxide molecule is next placed at (32) and the second successively at (32), (33) ..... (44). The pair interaction must now be calculated for all possible reflections of both points. The second molecule is constrained such that it cannot be at (22) as this interaction has already been included in the first set as (22 - 32).

When both molecules are at (32) the interaction is neglected as the molecules are coincident. However, the first molecule at (32) has three reflected positions and all interactions of these reflected first molecules with all second and reflected second molecules must be included. The way these interactions can be systematically generated is as follows.

The first molecule is at (32) which has a point multiple of 4. Thus all summations of interactions with the second molecule and its reflections will be multiplied by 4 except when the second molecule is at (32). In

this case the first point multiple must be reduced as the coincidence at (32) will also occur in three other reflected positions, eliminating some interactions. There will be only 6 possible different interactions obtainable after reflection of both molecules at (32). These are (32 - 23), (32 - 12), (32 - 21), (23 - 12), (23 - 21) and (12 - 21).

When the second molecule is at (33) which has a point multiple of 4, there will be 4 x 4 interactions generated, of which 4 must actually be calculated. The second molecule then moves to the remaining points which in turn generates a further 4 x 4 + 4 x 8 + 4 x 4 interactions, of which only the 4 + 8 + 4 different interactions are calculated. Having moved the second molecule through its range of positions, the first is moved to (33) and the process repeated. Finally, both molecules arrive at (44) which has a point multiple of 4. Both molecules can be reflected onto (O4), (OO) and (4O) so the following interactions are possible: (44 - O4), (44 - OO), (44 - 4O), (O4 - OO), (O4 - 4O) and (OO - 4O).

Table 3.10 summarises the foregoing interactions.

TABLE 3.10

FIRST POINT	MULTIPLE	SECOND POINT AND MULTIPLE						NUMBER OF POINTS GENERATED	SUM
		1	4	4	4	8	4		
22	1	22	32	33	42	43	44	(4+4+4+8+4)	24
32	4		32	33	42	43	44	2x(3)+4x(4+4+8+4)	86
33	4			33	42	43	44	2x(3)+4x(4+8+4)	70
42	4				42	43	44	2x(3) +4x(8+4)	54
43	8					43	44	4x(7) +8x(4)	60
44	4						44	2x(3)	6

In table 3.10 the bracketed terms represent the number of pair calculations that must be done, and the summations the total number of interactions inferred from these by suitable multiplication. The table generates 300 pairs as is expected since 24 * 23 + ... 3 + 2 + 1 = 300.

The general rule deduced from table 3.10 is to move both molecules systematically through all their possible positions such that if the positions were numbered 1, ...i, ...k^1 for the first and 1,....j,....m^1 for the second, then the second molecule must take all possible values of j before i is increased with $j \geq i$. If the point multiple associated with position i is k and with j is m then when i = j, $(m-1)xk/2$ pairs are generated and (m - 1) are calculated. When j > i then m x k pairs are generated but only m are calculated.

This procedure is readily applied to the case when the grid points are distributed throughout a tetrahedron. The ordering of the grid points is immaterial so long as the list is exhausted systematically. The above general rule gives the method of calculating all possible pair interactions where the carbon dioxide molecules are constrained to be at grid points at which the carbon dioxide ion potential gives a value of $K\exp(-\phi/kT) > 1$, where K is the point multiple for the grid point. This means that about 200 of the 286 possible grid points are automatically discarded when evaluating equation 2.39.

When each molecule-molecule interaction is calculated the molecule-ion term

$$\exp(-(\phi(\underline{r}_1) + \phi(\underline{r}_2))/kT)$$

is generated by assigning the value of the potential at the first point to $\phi(\underline{r}_1)$ and that at the second point to $\phi(\underline{r}_2)$ irrespective of the actual reflected positions of the molecules.

3.4.1 The CO_2-CO_2 Interaction Program

A program was written in EXCHLF Autocode which evaluated equation 2.39 given the results for the carbon dioxide-ion potentials at some temperature using the computational methods described above. The flow diagram for this program is given in figure 3.12 and a listing in Appendix C.

FIGURE 3.12 CRYSTAL SECOND VIRIAL COEFFICIENT FLOW DIAGRAM

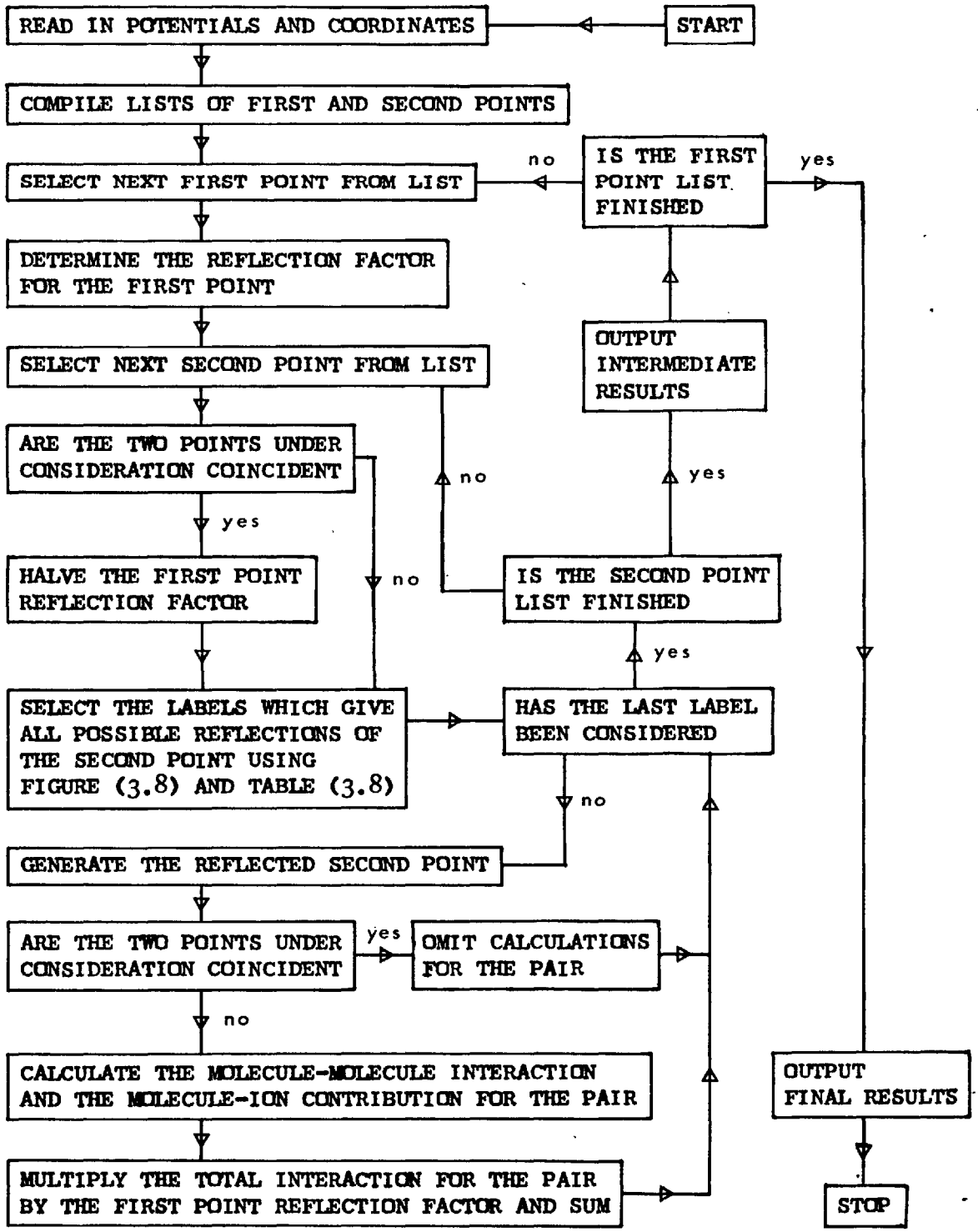

3.5 The Diffusion Model

3.5.1 The Fraction of Carbon Dioxide Desorbed from the Pellet

The two algorithms in section 2.7.4 result in sets of crystal and pore concentrations at each time interval for which the finite difference approximations are solved. These concentrations need to be converted into pellet accumulations so that the model gives the fraction of carbon dioxide desorbed from the pellet at time t.

Using the same notation as in sections 2.7.2 and 2.7.3 the accumulation in the pellet at time t is given by

$$ACCU = A\int_0^L \left(E_p v + \frac{(1-E_p)}{\frac{4\pi R^3}{3}} \int_0^R 4\pi r^2 w dr\right)dx \qquad 3.10$$

This equation can be written in dimensionless form using the substitutions:

$$ACCU' = \frac{ACCU}{A.L.v_o} \qquad x' = \frac{x}{L} \qquad r' = \frac{r}{R}$$

$$v' = \frac{v}{v_o} \qquad w' = \frac{w}{v_o} \qquad 3.11$$

Hence from equations 3.10 and 3.11

$$ACCU' = \int_0^1 (E_p v' + 3(1-E_p) \int_0^1 r'^2 w' dr')dx' \qquad 3.12$$

For the initial accumulation ($t' = 0$) we have $v' = 1$ and $w' = K$ for $0 \leq x' \leq 1$ and $0 \leq r' \leq 1$.

Hence:

$$ACCO = \int_0^1 (E_p + 3(1-E_p) \int_0^1 Kr'^2 dr')dx'$$

$$= E_p + (1-E_p)K \qquad 3.13$$

ACCO is the dimensionless zero time accumulation in the pellet and so the fraction of carbon dioxide desorbed at time t ($t > 0$) is given by:

$$FRAC = 1 - \frac{ACCU'}{ACCO} \qquad 3.14$$

3.5.2 Finite Difference Increments

The time and space intervals chosen were $\delta t = 1$ second for $t \leq 100$ and $\delta t = 10$ seconds for $100 < t \leq 10{,}000$; $\delta r = R/6$ and $\delta x = L/6$.

The practical values for the fraction of carbon dioxide desorbed from the pellet were measured at unit increments of $\sqrt{t}$ in the range

$0 \leq \sqrt{t} \leq 10$, and increments of 5 units in the range $10 \leq \sqrt{t} \leq 100$. The computed values of FRAC need to be evaluated at values of $\sqrt{t}$ which correspond as closely as possible to these values so that a direct comparison of results can be made. The model time increments were chosen using this criterion since the stability of the finite difference solution permits a wide choice in the time increment values. The end time of 10,000 secs. was chosen since the practical runs terminated at this time.

The space intervals chosen give a reasonably refined model of the pore and crystal structure without having a large number of iterations at each time step to get convergence of the pore concentration to within the specified limit. This limit was such that the error in dimensionless pore concentration was less than 0.01% at each time step.

A value of the relaxation parameter BETA' was chosen which gave the most rapid convergence of the error in pore concentration at each time step. Table 3.11 shows the results obtained for this error at three times for various values of BETA'. The value of 0.88 was chosen as the best.

TABLE 3.11

CHOICE OF RELAXATION PARAMETER BETA'

BETA'	ERROR IN PORE CONCENTRATION		
	TIME=10 SEC.	TIME=20 SEC.	TIME=30 SEC.
0.85	2.531,-5	7.280,-5	6.741,-5
0.86	1.793,-5	5.837,-5	5.315,-5
0.87	1.301,-5	4.870,-5	4.268,-5
0.88	1.067,-5	4.385,-5	3.620,-5
0.89	1.096,-5	4.393,-5	3.360,-5
0.90	1.401,-5	4.913,-5	3.473,-5
0.91	1.991,-5	5.943,-5	3.980,-5

NOTE: In this and many subsequent tables, numbers normally written with an exponent in powers of ten have been written with a 'comma' to denote the use of an exponent.

i.e. 1.234×10^{-3} is written 1.234,-3 etc.

3.5.3 Least Squares Fitting of the Diffusion Model to the Practical Results

A program was written in FORTRAN IV based on the flow diagram shown in figures 3.13, 3.14 and 3.15. This program computes the fraction of carbon dioxide desorbed from the pellet (FRAC) at values of $\sqrt{t}$ given values for the pore and crystal diffusivities, pellet porosity and other parameters defining the system (see table 6.21). The program was controlled by a minimisation routine due to Powell[13] which finds the minimum of a function of several variables without using derivatives. The function used was:

$$F = \sum_i (f_{T_i}(D_p, D_c) - f_{P_i}(D_p, D_c))^2 \qquad 3.15$$

where f_{T_i} and f_{P_i} are the theoretical and practical values of FRAC at time t. The summation is over all values of time for which FRAC is computed for $100 \leq t \leq 10{,}000$ secs.

3.5.4 Discretization Error

In a pore diffusion process governed by Fick's law diffusion, the analytical solution for the fraction of gas desorbed from a slab initially at concentration C_o with the surface concentration maintained

FIGURE 3.13 DIFFUSION MODEL FLOW DIAGRAM

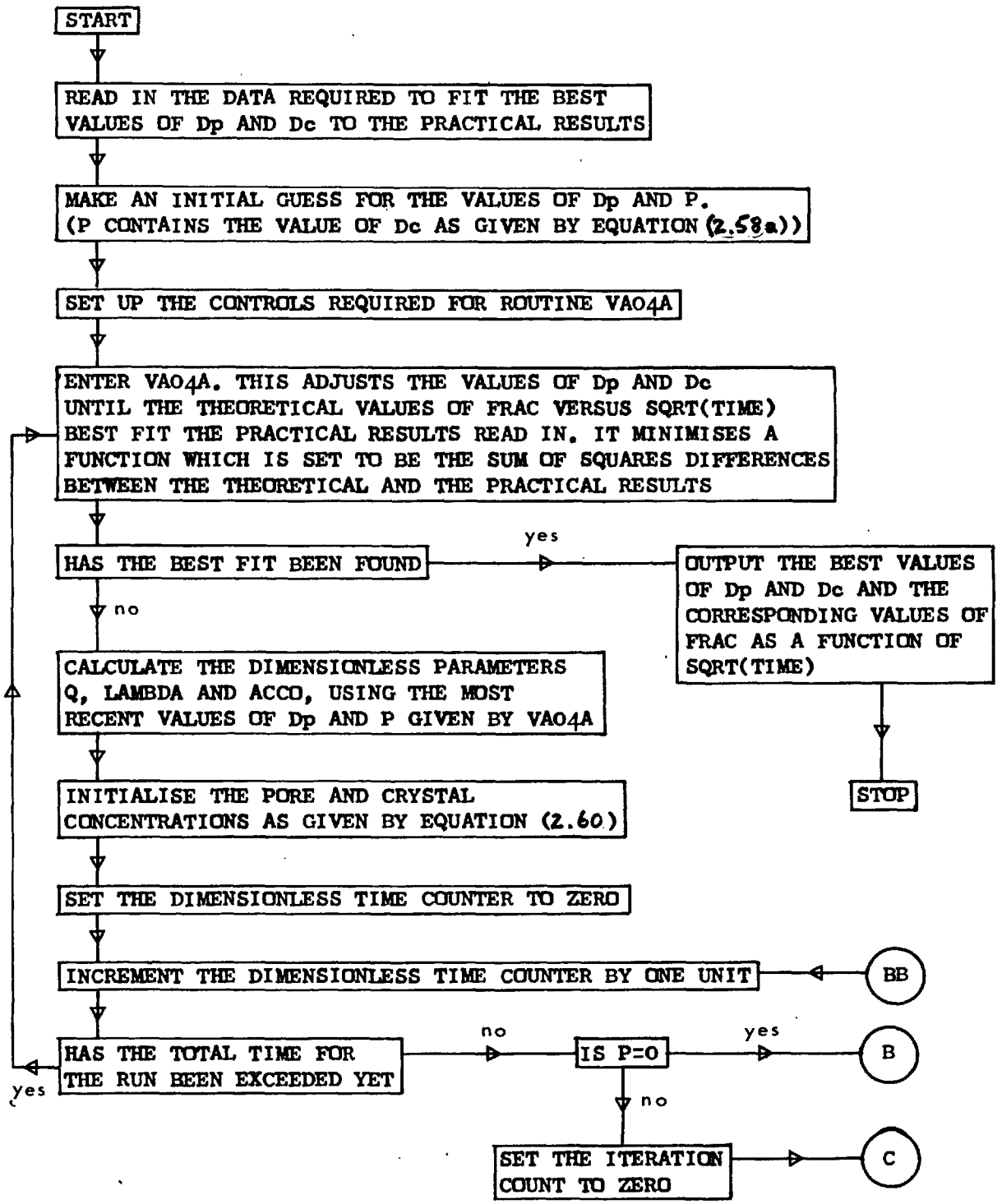

FIGURE 3.14 DIFFUSION MODEL FLOW DIAGRAM

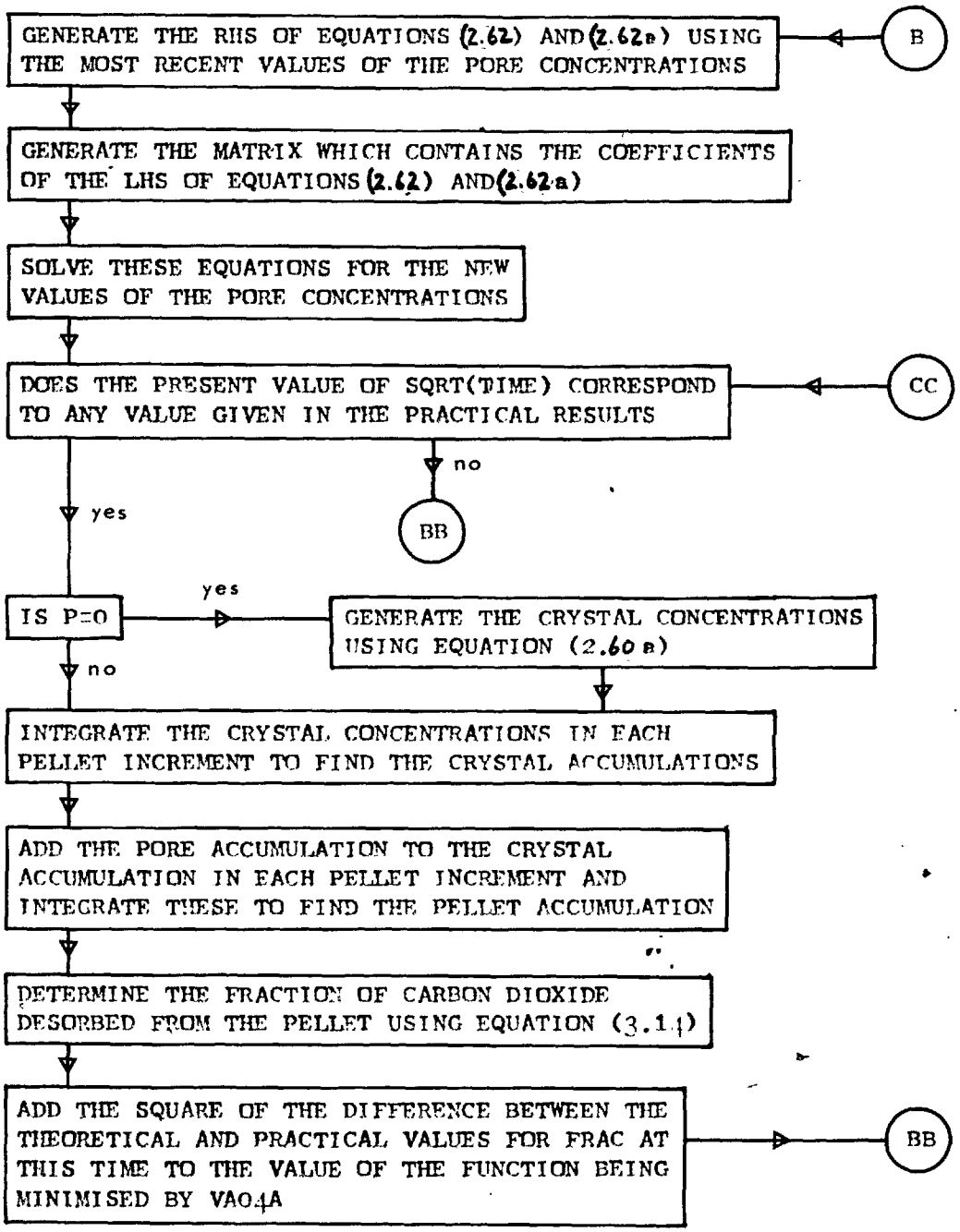

FIGURE 3.15 DIFFUSION MODEL FLOW DIAGRAM

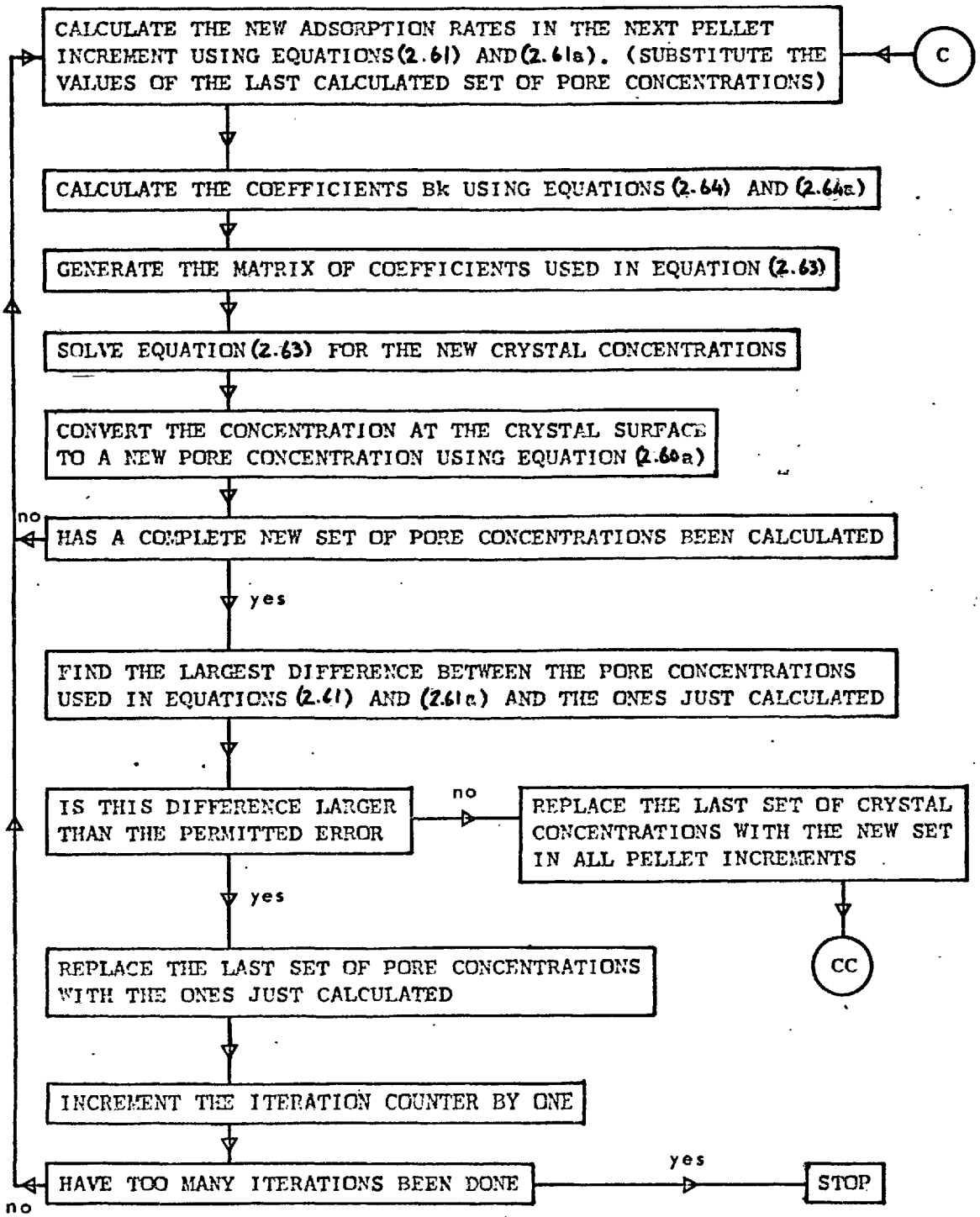

at zero for $t > 0$ is[14]:

$$FRAC = \frac{C_t}{C_o} = 1 - \frac{8}{\pi^2} \sum_{n=o}^{\infty} \frac{1}{(2n+1)^2} \exp \frac{(-D_p(2n+1)^2\pi^2 t)}{4L^2} \qquad 3.16$$

This expression gives a straight line plot for FRAC versus initial values of $\sqrt{t}$ which passes through the origin and characterises pore diffusion processes.

It was found that the present model with P set to zero, which means pore diffusion is controlling, gave initial values for FRAC that were significantly greater than the expected values for a straight line plot through the origin. However, this difference decreased at later times and became negligible for $t > 100$ sec.

A test case was investigated without using the minimisation routine and values of FRAC were computed for an initial time step which was repeatedly reduced in value. When $\delta t = 0.001$ seconds was reached, the initial value of FRAC obtained was 0.0556. Further reduction of δt did not reduce this value whereas it was to be expected that FRAC would tend to zero as δt tended to zero.

The value of FRAC is obtained by a Simpson integration over the six increments into which the pellet is divided. As δt tends to zero

the results for the first set of pore concentrations will not change significantly from their initial values of unity. Since $P = O$, (or $D_c = \infty$) the crystal concentrations in the six crystal increments used will all be identical and equal to the local crystal surface concentration. This is given by equation 2.60a, and as $v' = 1$ then all $w' = K$ in the crystals.

The second integral in equation 3.12 represents the crystal accumulation. When this is numerically integrated the following result is obtained:

$$K \int_0^1 r'^2 dr' =$$

$$= \frac{K}{3 \times 6}\left(1 \times O + 4 \times \left(\frac{1}{6}\right)^2 + 2 \times \left(\frac{2}{6}\right)^2 + 4 \times \left(\frac{3}{6}\right)^2 + 2 \times \left(\frac{4}{6}\right)^2 + 4 \times \left(\frac{5}{6}\right)^2 + 1\right)$$

$$= K/3 \text{ as expected.}$$

The first integral becomes:

$$\int_0^1 (E_p + (1-E_p)K)dx' =$$

$$= \frac{E_p + (1-E_p)K}{3 \times 6} \times (1 + 4 + 2 + 4 + 2 + 4 + 1)$$

$$= (E_p + (1 - E_p)K) \times \frac{18}{18}$$

which is equal to the zero time accumulation as given by equation 3.13. However, one of the boundary conditions for the pellet is for $t' > 0$ and $x' = 0$ then $v' = 0$. This means that the leading term in the summation for the first integral is forced to zero giving a pore accumulation of $(E_p + (1 - E_p)K) \times 17/18$. Thus this boundary condition means that the integration method used to find ACCU' always gives a value of 1/18 for FRAC, instead of zero, for the initial time step, no matter how small this is made. At later times the pore concentrations in the increments closest to the exchange surface of the pellet are tending towards zero and so this source of error reduces and becomes insignificant.

It requires at least 34 space increments in the pellet to reduce the value of FRAC to less than 1% of ACCO in the first time step. Such a refined model for the pore structure is unwarranted so the model was used without modification to the integration method, and values of FRAC up to $t = 100$ secs. were discarded. After this time the rest of the curve of FRAC versus $\sqrt{t}$ could be extrapolated back through the origin

with P = O which showed the model was giving correct results at later times. The computed values of FRAC were compared with the practical values in the range $100 \leq t \leq 10{,}000$ using equation 3.15.

CHAPTER 4 - EXPERIMENTAL APPARATUS

The apparatus was designed to study the diffusion of carbon dioxide in a one dimensional molecular sieve pellet bed at temperatures ranging from ambient down to -100°C. It was housed in a flame proof laboratory suitable for radio active work in class S of the Imperial College Regulations on Radiation Hazards, and consisted of three main parts.

a) A vacuum system. This incorporated units for vacuum production and measurement; active carbon dioxide production, storage, and volumetric measurement; and a carbon dioxide storage and flow system.

b) A cryostat. This housed the diffusion cell in which the diffusion process occurred.

c) A scintillation flow counter and counting set.

General views of the vacuum system, the cryostat and the counting set are given in plates 4.1 and 4.2 and figure 5.1.

PLATE 4.1

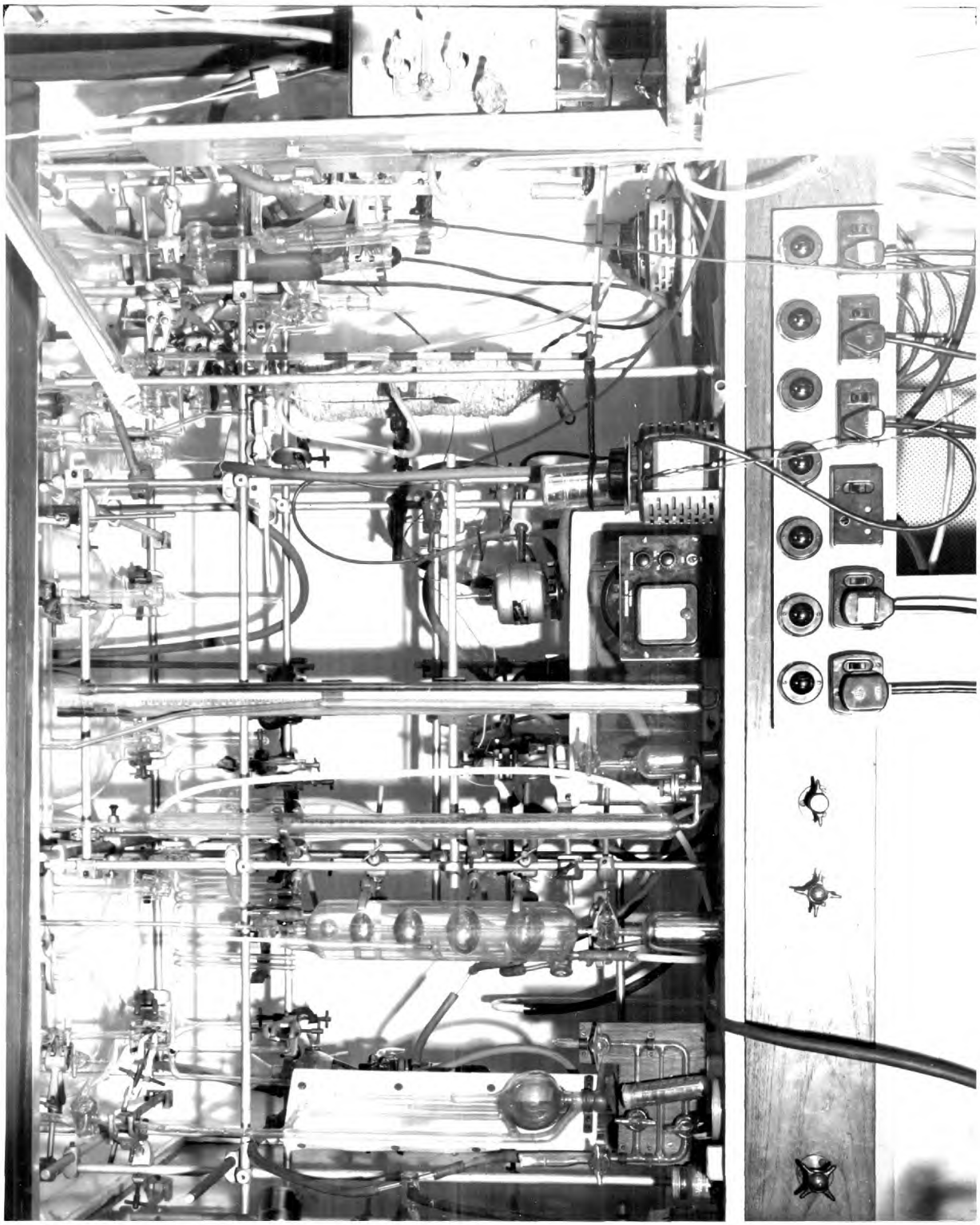

PLATE 4.2

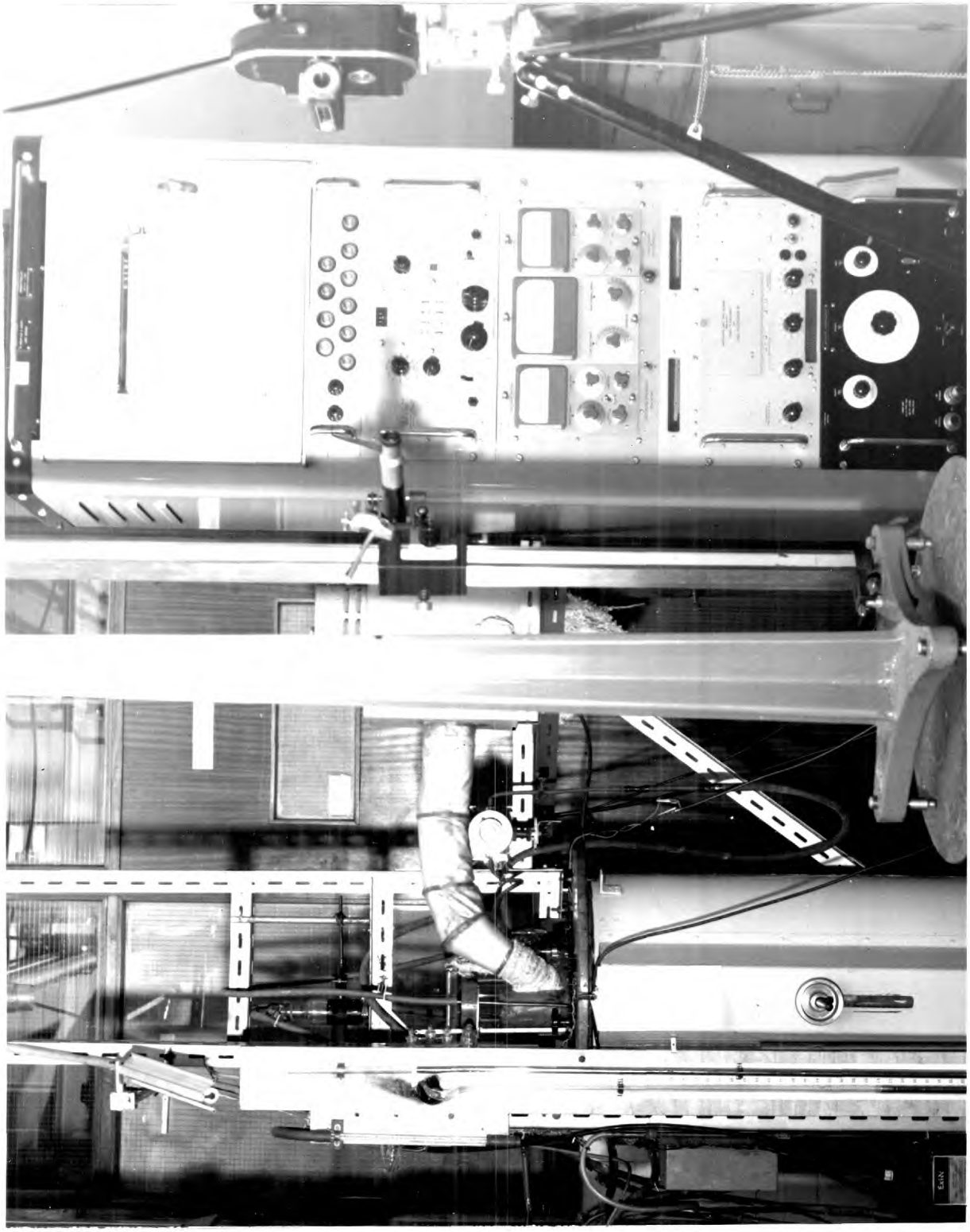

4.1 The Vacuum System

This was housed in a fume cupboard and constructed mainly from pyrex glass.

4.1.1 Vacuum Production and Measurement

A vacuum ring main was made from three centimetre bore tubing. One side was connected to a two stage oil diffusion pump and the other to a McLeod gauge. The diffusion pump, backed by a rotary vacuum pump and a liquid nitrogen trap produced vacua down to 2×10^{-5} mm. mercury absolute. Vacua down to 10^{-3} mm. mercury absolute were measured by a Pirani gauge and gauge head, and down to 10^{-5} mm. mercury absolute by a McLeod gauge.

4.1.2 Active Carbon Dioxide Storage and Volumetric Measurement

The vacuum ring main was isolated into two sections by stop cocks, one side being used for active carbon dioxide transfer and the other for vacuum application. Five storage flasks and cold traps for active gas storage were connected to the active side of the ring main. The other side was provided with a vacuum link to the active metering section. This incorporated two gas burettes with a total calibrated volume of 257 c.c. at 25°C. enclosed in thermostatically controlled

water jackets. A mercury manometer made from one centimetre bore Viridia tubing, and two cold legs to facilitate gas transfer completed the system. One of these legs was located on the line between the burettes and the active side of the ring main. The other was attached close to the gas manifold. This permitted active carbon dioxide transfer as required from the storage flasks to the burettes, and subsequent transfer to and from the cryostat. All connection lines in this part of the system were one millimetre bore capillary tubing to improve the accuracy of volumetric measurement.

4.1.3 Active Carbon Dioxide Production

This section comprised of a generating bottle and several cooling coils connected to the active side of the ring main. Active carbon dioxide was prepared by the action of concentrated sulphuric acid in vacuo on solid labelled Barium Carbonate in one milli-curie lots. The active carbon dioxide generated could be dried and separated from any acid mist by alternate transfer between cooling coils immersed in acetone - solid CO_2 and liquid nitrogen baths, before transfer to the storage flasks.

4.1.4 Carbon Dioxide Storage and Flow System

Commercial carbon dioxide in 28 lb. cylinders was used throughout as Orsat gas analysis could not detect any significant contaminants.

FIGURE 4.1 CARRIER CO2 FLOW LINES

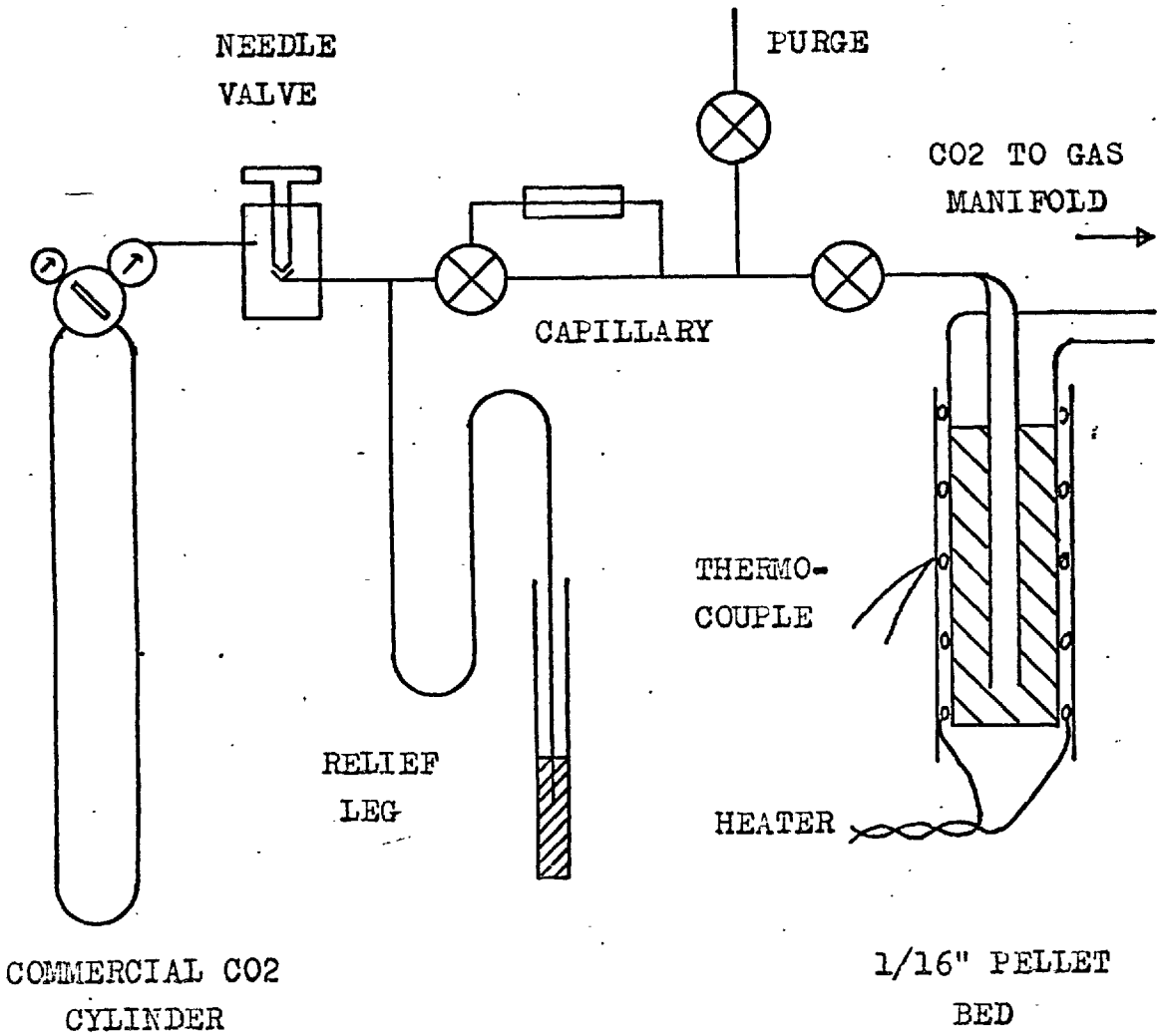

This gas was passed once through a bed of 1/16 inch diameter type 5A molecular sieve pellets to remove any traces of water before it reached the gas manifold. The bed was wound with a heater to enable it to be regenerated from time to time, and a thermocouple was used to measure the regeneration temperature.

A constant flow rate of carbon dioxide carrier gas was essential whilst counting. A needle valve used as an orifice, and in conjunction with a gas relief bubbling leg, provided the necessary degree of control. This arrangement enabled constant flow rates of carrier gas to be maintained indefinitely whilst counting.(see figure 4.1)

4.1.5 The Gas Manifold

The gas manifold was an assembly of lines and stop cocks whereby several successive operations could be carried out via a single line connecting the vacuum system to the cryostat. These operations were the evacuation of the molecular sieve bed in the cryostat, the passage and return of active carbon dioxide to the molecular sieve bed and finally the passage of carrier carbon dioxide.(see figure 4.2)

4.1.6 Ancillary Equipment

The thermostats which maintained the sieve regeneration temperature used 5%-20% Rhodium-Platinum thermocouples, connected by screened

FIGURE 4.2 THE GAS MANIFOLD

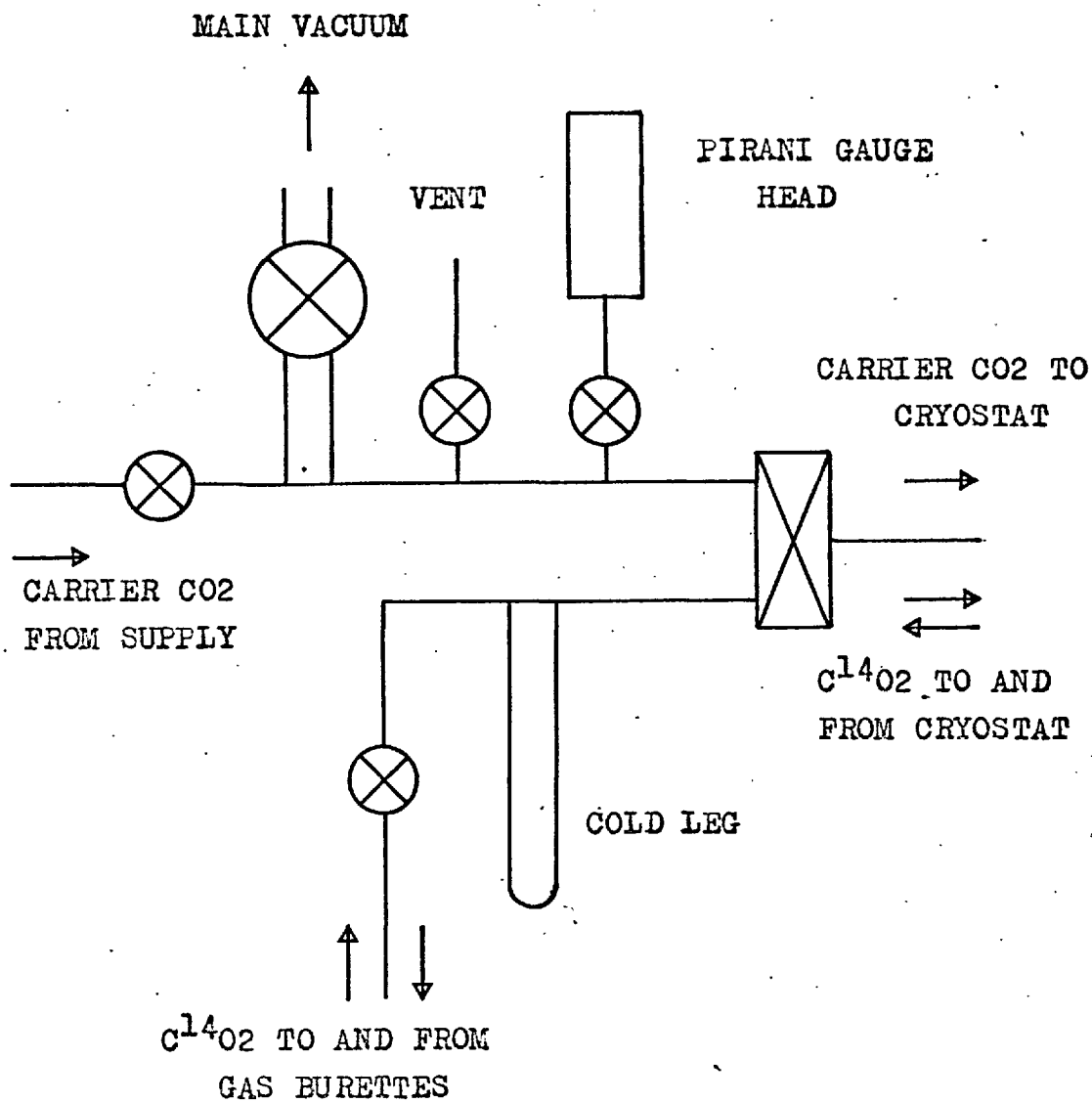

leads to a Philips Recorder. This had a controlling mode and was used to limit the heater temperatures. Mains A.C. power was used through a Variac controller.

The water jacketed burettes were maintained at 25°C using a Sunvic controller and a toluene switch. The water was circulated by a centrifugal pump.

The mercury levels in the gas burettes were raised and lowered by compressed nitrogen and low grade vacuum respectively, supplied to the mercury reservoirs. The low grade vacuum was produced by a small rotary pump separate from the main vacuum backing pump.

4.2 The Cryostat

The cryostat shown in figure 4.3 and plate 4.2 was encased in an air-tight steel drum, fitted with a stout wooden lid bolted to the top of the drum and sealed with a rubber gasket. A second drum was mounted inside the first and suspended on wires, passing over pulleys, which were attached to counter balance weights outside the main drum. The inner drum could be raised or lowered six inches by handles fitted to the counter balance weights. The pulleys mounted in the outer drum were housed inside air-tight metal boxes and the wires leading from these

FIGURE 4.3

SCHEMATIC ARRANGEMENT OF THE CRYOSTAT

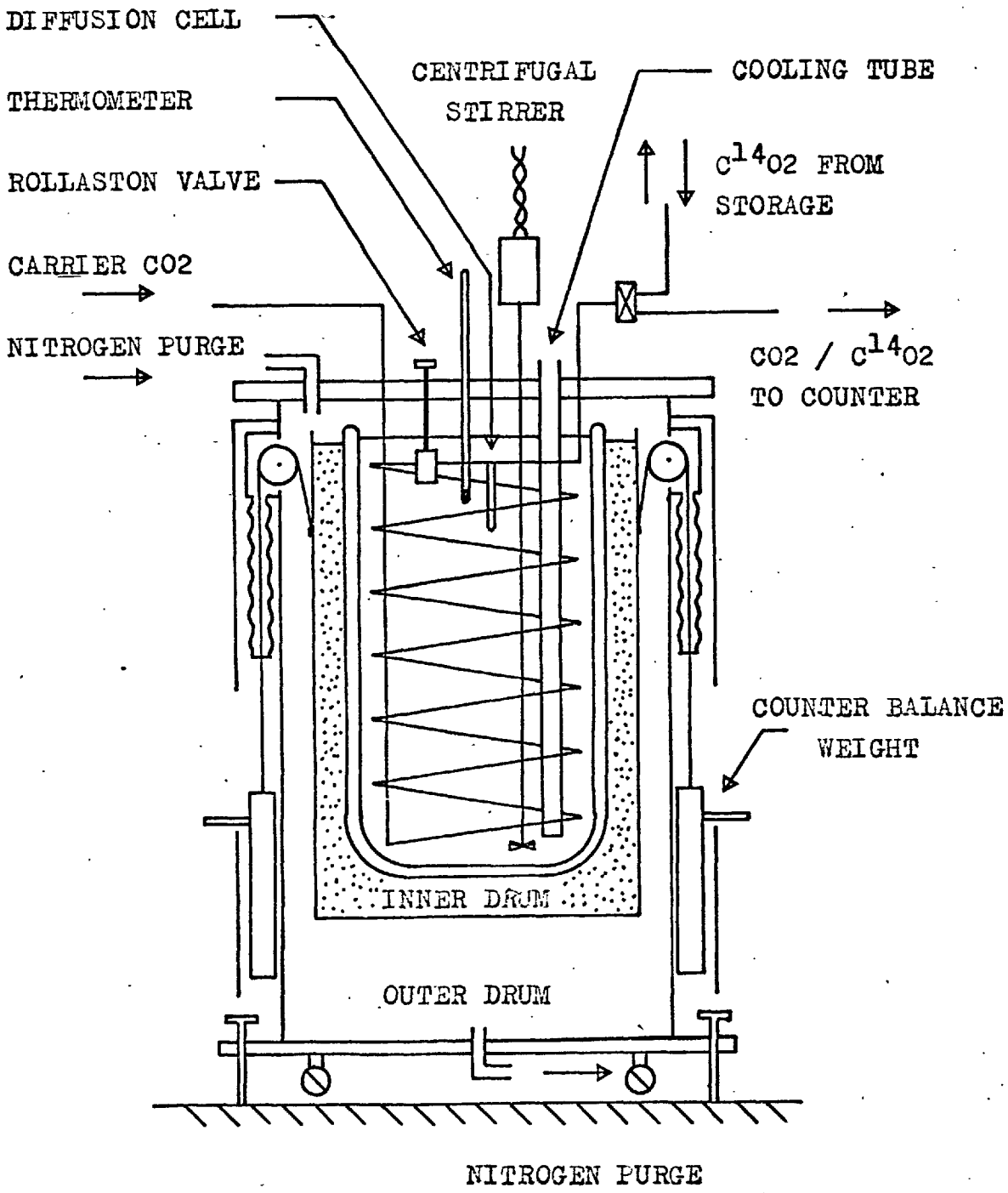

to the weights were encased in expanding rubber hoses to keep the cryostat container air-tight.

A twenty centimetre diameter dewar flask was placed inside the inner drum and insulated from it by granular cork. This dewar housed all the ancillary equipment associated with the diffusion cell, and was filled with acetone which acted as the cryostatic liquid. Carbon dioxide carrier gas was passed in through the wooden lid via a copper line wound into a six inch diameter spiral which was mounted inside the dewar. This coil terminated at a Rollaston vacuum valve fitted with a special neoprene rubber diaphragm and seat so that it would operate at temperatures down to -100°C. The diffusion cell was attached to the Rollaston valve by a glass to metal seal and the carrier carbon dioxide line continued back through the cryostat lid to a two-way stop cock.

The acetone was stirred by a high speed centrifugal pump. The stirrer motor was housed on top of the lid and encased in an air-tight polythene cover. The acetone was cooled by manually pouring liquid nitrogen into a massive copper tube sealed at its lower end and projecting well into the cryostat. An alcohol in glass thermometer encased in a glass thimble filled with acetone, and projecting into the cryostatic liquid, allowed the temperature of the diffusion cell to be measured.

FIGURE 4.4

SCHEMATIC ARRANGEMENT OF THE CRYOSTAT FLOW LINES

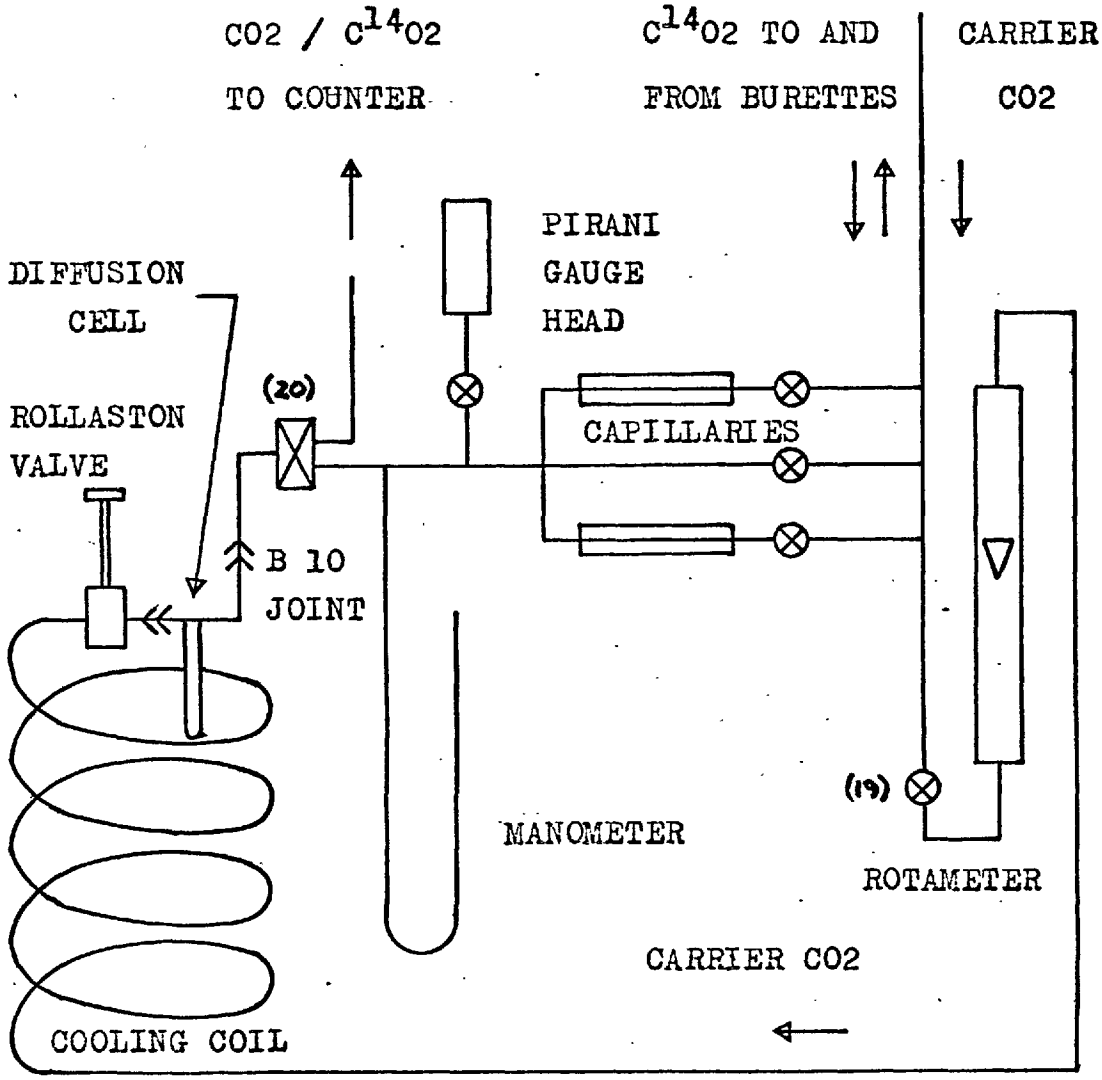

The thimble permitted the thermometer bulb to be positioned at the same level as the molecular sieve pellets in the diffusion cell, yet easily removable when the molecular sieve was regenerated. Access to the diffusion cell was via a perspex inspection hatch let into the cryostat lid. This hatch was made easily removable to facilitate replacement of the diffusion cell when necessary.

A rotameter was used to measure the carrier carbon dioxide gas flow rate, and was connected between the link line from the vacuum equipment and the copper cooling coil, using a glass to metal seal. A mercury manometer constructed from one centimetre bore Viridia tubing and a Pirani gauge head were used to measure the pressure inside the diffusion cell. These and a system of capillaries, used to limit the pumping rate when evacuating the diffusion cell, were connected between the link line and the two-way stopcock (20), as shown in figure 4.4.

This arrangement allowed the copper cooling coil to be filled with carrier carbon dioxide so that the carbon dioxide in it was brought to the same temperature as the diffusion cell before the start of a run. It also allowed the diffusion cell to be evacuated and charged with active carbon dioxide without disturbing the carrier gas in the cooling coil, since this could be isolated between the Rollaston valve and cock (19).

The cryostat was fitted with a nitrogen purge to flush out all traces of atmospheric oxygen before the diffusion cell heater was switched on. The exit purge gas was bubbled through an oil trap which ensured that the outer cryostat drum was pressurised slightly above ambient. It also provided a simple visual check that the purge was on, to minimise explosion risk.

The whole apparatus was mounted on a stout base fitted with four screw jacks so that it could be raised off the castors fitted, and on which it was normally moved. Thus the cryostat could be rigidly positioned in relation to the vacuum apparatus and this gave some protection to the fragile link line. The length of this line was kept to a minimum as the dead space between the gas burettes and the diffusion cell, when this was being charged with active carbon dioxide, had to be kept well under the total burette volume.

4.2.1 The Diffusion Cell

The outer jacket of this was made from H26X glass which will withstand heating up to 400°C under high vacuum without deforming. 0.120 inch bore Viridia tube was chosen such that it was a close sliding fit inside the H26X glass, together with glass rod of the same

FIGURE 4.5

SCHEMATIC ARRANGEMENT OF THE DIFFUSION CELL

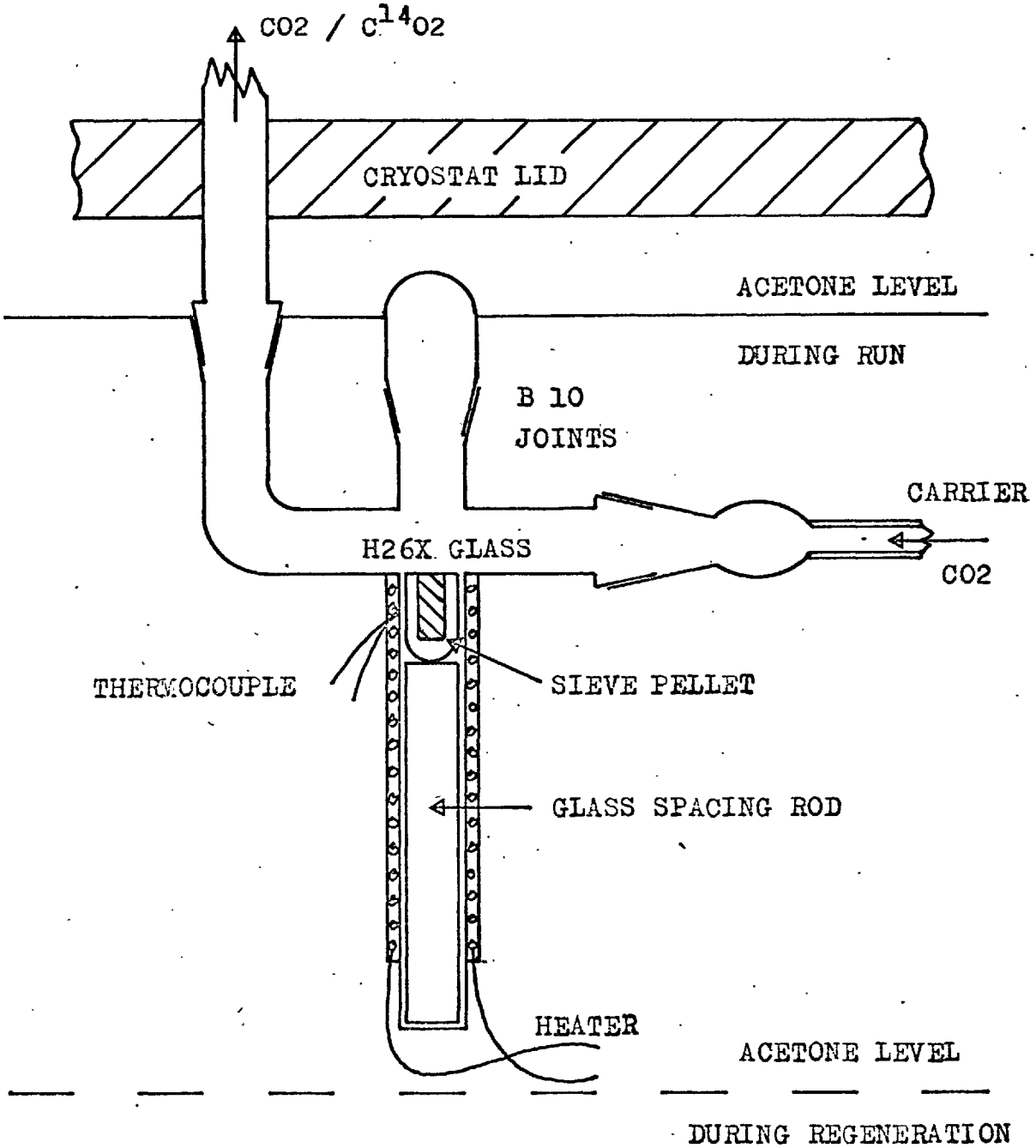

diameter. The H26X glass was made up into the shape illustrated in Figure 4.5. The nominal size of the molecular sieve pellets used was 1/8 inch and several pellets were selectively chosen, from a batch, that were a tight push fit in the Viridia bore. A one centimetre long, one dimensional pellet bed was assembled by squaring off the ends of the chosen pellets and pushing them into a one centimetre length of the Viridia tubing sealed at one end. This bed was positioned on top of the glass rod cut to length so that the open end of the bed was just inside the cross tube carrying the carrier carbon dioxide. The cell was fitted with a removable cap so that the bed could be replaced by a similar piece of glass rod to permit trial runs to be made.

The H26X glass jacket was wound with a heater incorporating a 5%-20% Rhodium-Platinum thermocouple. The cell was attached to the carrier carbon dioxide flow line in the cryostat by B10 cone and socket joints, and a standard union to the Rollaston valve.

4.2 The Counting Apparatus

Flowing carbon dioxide labelled with C^{14} may be counted using three types of detectors. Geiger Müller counters are not very satisfactory since the detected count rate needs correcting for the long dead time

(about 200 micro seconds) of the tubes. Proportional counters have a faster response with a dead time of about 2 micro seconds. However, both systems when counting $C^{14}O_2$ have limited count lives of up to 10^9 counts as the tubes are halogen quenched.

Scintillation detectors provide simple counting systems. An investigation of the scintillating materials used for detecting labelled carbon dioxide (weak beta radiation, about 0.15 MeV peak energy) showed that the most suitable were plastic sheets and tubing incorporating anthracene crystals in the plastic matrix, and pure anthracene crystals mounted on suitable holders. These scintillation materials have a response time of 1.3 nano seconds. During a series of experiments using anthracene crystals embedded in plastic as a detector, it was found that the plastic absorbed active carbon dioxide and this completely masked the decay rate that was being investigated. It was found that pure anthracene crystals mounted on glass discs did not absorb carbon dioxide and so gave a true indication of the decay rate in the diffusion cell.

When counting in flow systems with rapidly changing rates of activity Dworjanyn[2] suggested that it was advantageous to use two counters. One has a small counting volume to detect high decay rates, and the other a large counting volume to detect low decay rates.

FIGURE 4.6

SCINTILLATION COUNTER

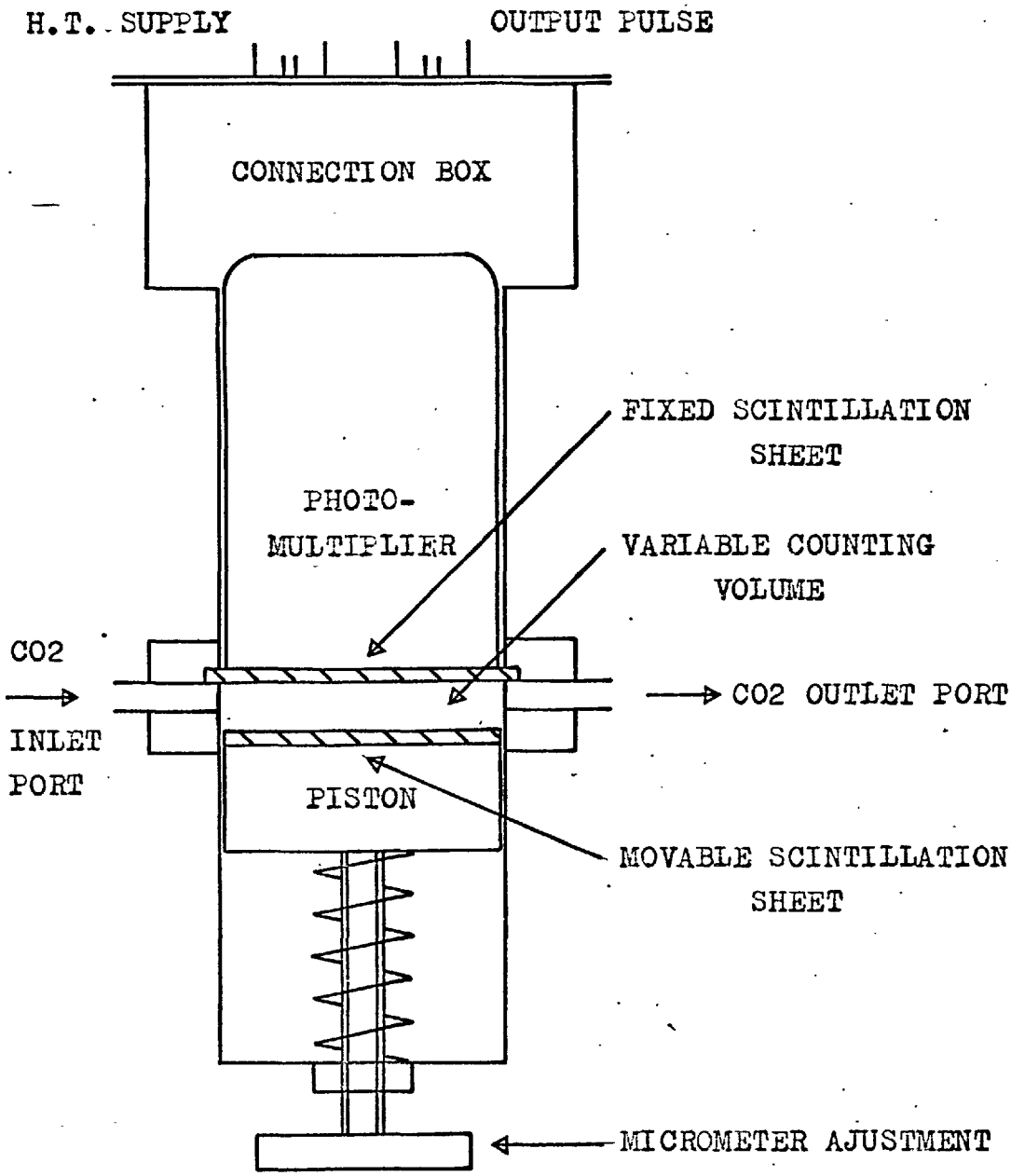

This idea was incorporated into a single counter with a variable counting volume, using a piston and cylinder arrangement, as shown in figure 4.6. A two inch diameter nylon piston was mounted in a brass cylinder and provided with a micrometer adjustment which gave it about half an inch of travel. The piston was backed by a spring to eliminate backlash in the adjustment. A second brass cylinder housed a photomultiplier and was bolted to the first. Two sheets of scintillation material were used. One was attached to the piston facing the photomultiplier and the other to the window of the photomultiplier. The two sheets of scintillation material thus bounded a variable counting volume given by the micrometer reading, which ranged from zero to fifteen cubic centimetres in just over a quarter of an inch of piston travel. Carbon dioxide inlet and outlet ports were provided in the plane of the fixed scintillation sheet.

A suitable photomultiplier tube was obtained to detect the low intensity light emitted by the anthracene crystals activated by beta radiation. Final selection was made by the manufacturers who provided a tube with low noise and high amplification characteristics.

The photomultiplier output pulses were passed to a pulse counting set shown in figure 4.7. The scaler-timer gave a continuous record of

FIGURE 4.7

THE COUNTING SET

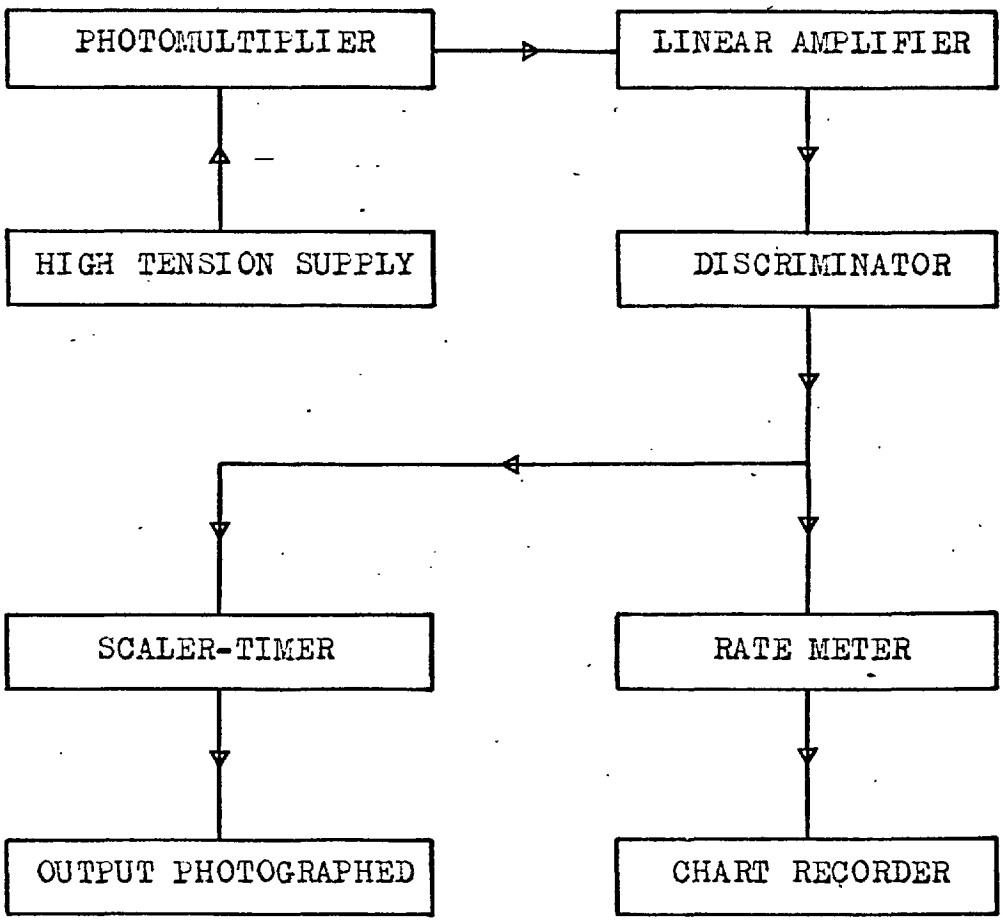

counts against a time base in multiples of 0.1 seconds. A permanent record of this output was obtained by photographing the scaler-timer using a sixteen millimetre cine-camera running at sixteen frames per second. A Philips chart and pen recorder gave a continuous output of the count rate versus time. This was used to check that the start and end count rates for each series of runs were matching, together with the maximum count rate attained just after the start of each run.

CHAPTER 5 - EXPERIMENTAL PROCEDURE

5.1 Preliminary Bed Regeneration

Firstly the one sixteenth inch pellet bed had to be regenerated to remove moisture and other gases. This was done by slow evacuation and heating to three hundred degrees centigrade. After a period of ten hours the best vacuum obtained was 10^{-3}mm. mercury absolute compared with 2×10^{-5}mm. mercury absolute on outgassing the glassware. All subsequent regenerations of this bed were taken as being complete after this pressure had been maintained for three hours at three hundred degrees centigrade. On allowing the bed to cool under constant pumping the pressure naturally fell to the lowest measurable with the McLeod gauge. (10^{-5}mm. mercury absolute).

The carbon dioxide line from the supply cylinder was purged during this regeneration. Carbon dioxide was admitted through the capillary bypass after isolating the bed from the vacuum pumps. This prevented the pressure wave formed from expelling the sieve pellets into the vacuum lines. Finally carbon dioxide was passed freely through the bed to allow the system to settle.

5.2 Active CO_2 Preparation

Active carbon dioxide labelled with C^{14} was prepared in vacuo by the action of concentrated sulphuric acid on a one milli-curie lot of labelled Barium Carbonate. The reaction flask was gently warmed to liberate all the gas formed. The evolved gas was transferred to the drying tubes using a liquid nitrogen bath, and freed from any traces of acid mist and water by alternate transfer between cooling sections immersed in liquid nitrogen and acetone-solid CO_2 baths. The active carbon dioxide was then transferred to a storage flask which had been previously evacuated.

The burette system was evacuated and then filled with carrier carbon dioxide. An amount of this was added to the active carbon dioxide sufficient to dilute it to an activity of about 20,000 counts per cubic centimetre per second. The burettes were then evacuated again and the mixture of active and carrier carbon dioxide passed back and forth between them and the storage flask by liquid nitrogen transfer to aid mixing. The system was left for several days to allow diffusion to complete the mixing process.

5.3 Run Procedure

The cryostat was cooled to the required temperature using liquid nitrogen and maintained at this throughout the run. Because of the large thermal capacity of the system, temperatures down to -25°C could be maintained with little effort to better than $\pm$ 0.5°C. The nitrogen purge was turned on to sweep out all traces of atmospheric oxygen from inside the cryostat. The carrier carbon dioxide flow was started and the flow rate set to 100 c.c./min. This was best done by presetting the low pressure stage of the carbon dioxide cylinder valve to 1 psig. and the relief leg to two inches of water pressure above ambient. Then the needle valve was adjusted, in conjunction with a pinch clip positioned close to the counter on the upstream flow side, till the flow rate was 100 c.c./min., with the excess carbon dioxide bubbling through the relief leg at a reasonable rate. A reference datum for the pressure inside the diffusion cell was made by locating the cross hair in a cathetometer telescope on the mercury meniscus in the cryostat manometer. The pressure inside the cell was measured using the same manometer.

After the flow system had settled, the carrier carbon dioxide flow was stopped successively at cock (20), the Rollaston valve and cocks

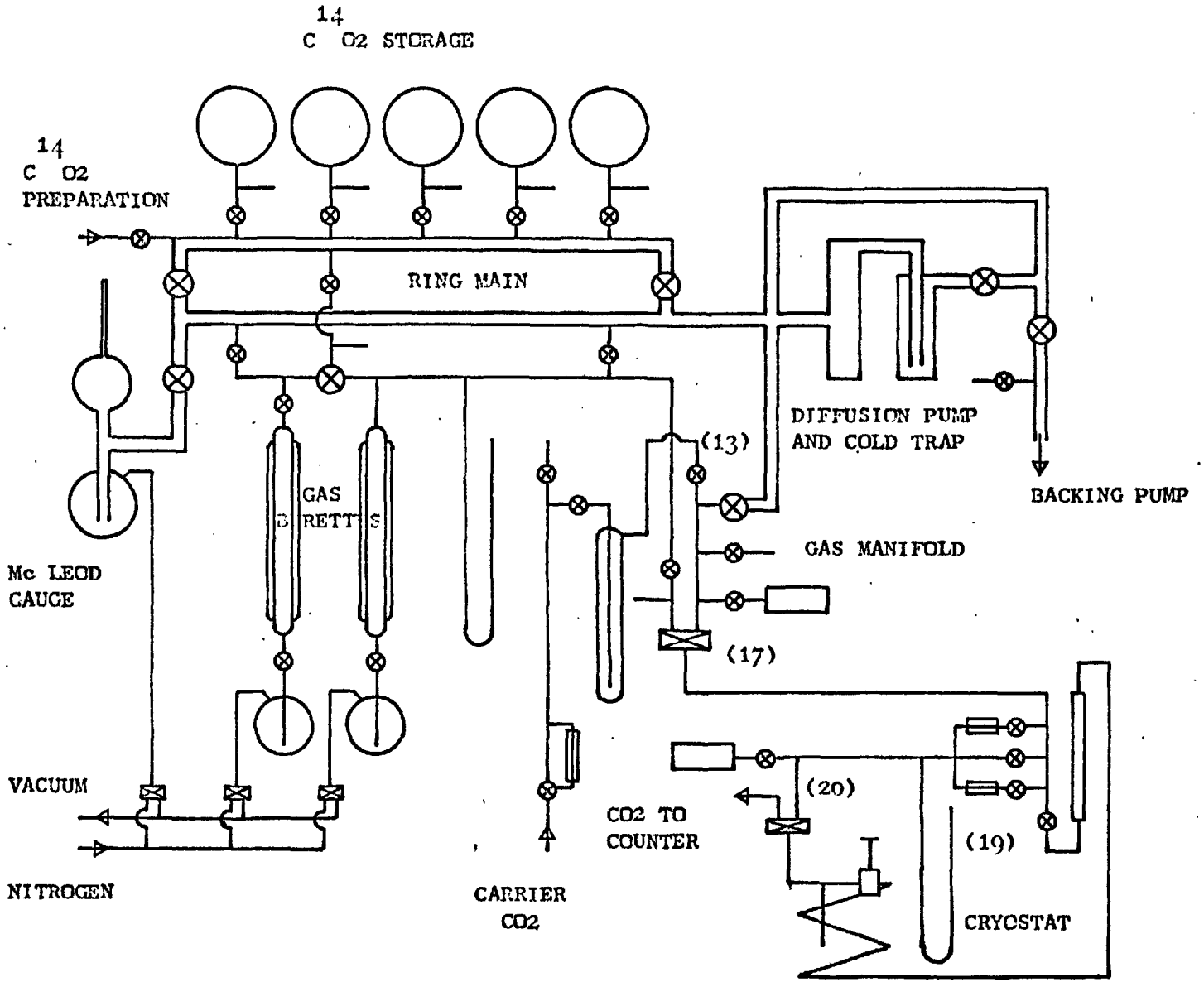

FIGURE 5.1

OVERALL ARRANGEMENT OF FLOW LINES

(19), (17) and (13). (Refer to figure 5.1) The carbon dioxide was allowed to stream freely from the relief leg. Thus at any later time the flow could be restarted and it would immediately rise to its present value. This procedure also ensured that the carrier gas precooling coil in the cryostat contained carbon dioxide at a known temperature and pressure.

The cryostat inner drum was fully lowered so that the acetone level dropped below the level of the diffusion cell heater and the thermometer was removed from its thimble. The diffusion cell was slowly heated so that the temperature rise was not greater than $10^{\circ}C$ per minute. When the cell had reached about $140^{\circ}C$ it was slowly evacuated using the capillaries to limit the pumping rate so that the pressure change was not greater than two centimetres of mercury per minute. These conditions ensured that the pellets in the one centimetre bed were outgassed slowly so as to prevent them from being expelled from the Viridia tube. It usually took thirty minutes to reach conditions of $300^{\circ}C$ and 10^{-3}mm. mercury absolute in the diffusion cell and these conditions were maintained for one hour as a standard diffusion cell regeneration procedure.

The system was then isolated at cock (20) and active carbon

dioxide admitted from the burettes by reversing the two-way cock (17). The pressure was allowed to rise till it was one millimetre of mercury above the carrier carbon dioxide pressure datum. The burette readings were noted and active carbon dioxide was carefully admitted to the diffusion cell via cock (20). The cell was allowed to cool to the run temperature, after switching the heater off, by raising the inner drum in the cryostat so that the diffusion cell was re-immersed in the acetone. The gas pressure was adjusted as necessary to keep it up to the new datum level as the cell cooled and the bed became saturated with active carbon dioxide. Saturation was assumed to be reached when the pressure remained constant for a period of at least thirty minutes.

At this stage the new burette readings gave the amount of active carbon dioxide admitted to the diffusion cell at ambient pressure and the run temperature. The cell was isolated at cock (20) and the excess active carbon dioxide in the transfer lines was returned to the burettes by liquid nitrogen transfer. The link line was evacuated to remove the last traces of active gas. The manifold was isolated from the vacuum pumps and carrier carbon dioxide readmitted. When the pressure had reached its datum level cock (19) was opened.

During this procedure the counting set was switched on and the counter background level measured. The scaler-timer was reset to zero and on opening the Rollaston valve and cock (20) carrier gas flow commenced and counting started. The excess pressure of one millimetre of mercury between the active gas in the diffusion cell and the carrier gas in the precooling coil ensured that the former was not diluted by carrier gas during the short period elapsing between opening the Rollaston valve and cock (20). Thus the initial concentration level measured in the diffusion cell was the same as that in the burettes.

The output of the scaler-timer was photographed continuously until the initial step change in concentration had passed through the counter. Then batches of fifty frames were taken at subsequent time intervals chosen such that the square root of time measured in seconds increased linearly.

At 25°C it was found that the gas activity in the counter had decayed almost to the background level after 10,000 seconds. This time was taken as the running time for lower temperatures. The total amount of active carbon dioxide adsorbed by the bed was obtained by reheating the diffusion cell to 300°C after 10,000 seconds without flow interruption. This desorbed all the active carbon dioxide in the

bed and the count was continued till the background level was reached.

The dead space gas in the diffusion cell was counted by replacing the one centimetre bed by an identical glass blank and repeating the run, such runs being designated 'trial' runs as distinct from 'pellet' runs. Differencing the accumulated count at any time gave the amount of active carbon dioxide that had diffused out of the bed. The total amount of active gas diffused was obtained from the difference in accumulated count at infinite time, which for the purposes of these runs was any time at which both the pellet run and the trial run had reached background level, as measured by the counter. A comparison of this value with that for any earlier time gave the fraction of active carbon dioxide that had diffused out of the bed up till that time.

5.4 Counter Signal to Noise Ratio

The best signal to noise ratio for counting was obtained by setting the amplifier integration and differentiation time constants to 0.32 micro seconds and comparing the background and a test count rate over a range of photomultiplier voltage and amplifier attenuation settings. This was done by first finding the variation in background over the range of settings and then filling the counter with a batch of active gas and

finding the variation in count rate over the same range. The working conditions chosen from the tests were 20 dB attenuation at the amplifier and 1175 volts supplied to the photomultiplier.

5.5 Choice of Carrier Gas Flow Rate

A separate series of trial runs were done at ambient temperature and pressure in which the integral count was measured over a fixed time interval and at several different flow rates.(see figure 5.2). The amount of active gas counted is proportional to the product of the integral count and the flow rate and this was plotted in figure 5.3. It can be seen that the amount of gas counted becomes constant above a flow rate of 100 c.c./min., indicating essentially zero concentration at the pellet surface. This flow rate was chosen for all subsequent work as it represents the minimum flow rate at which the amount of gas counted becomes independent of flow rate and at the same time minimises the gas mixing in the flow line between the diffusion cell and the counter.

5.6 Choice of Counter Volume

Since the counter volume had been designed to have a variable counting volume it was hoped to find optimum values of this for both the initial high decay rate and the subsequent low decay rate near the end

FIGURE 5.2

VARIATION OF IC AT 2500 SECS WITH CO2 FLOW RATE

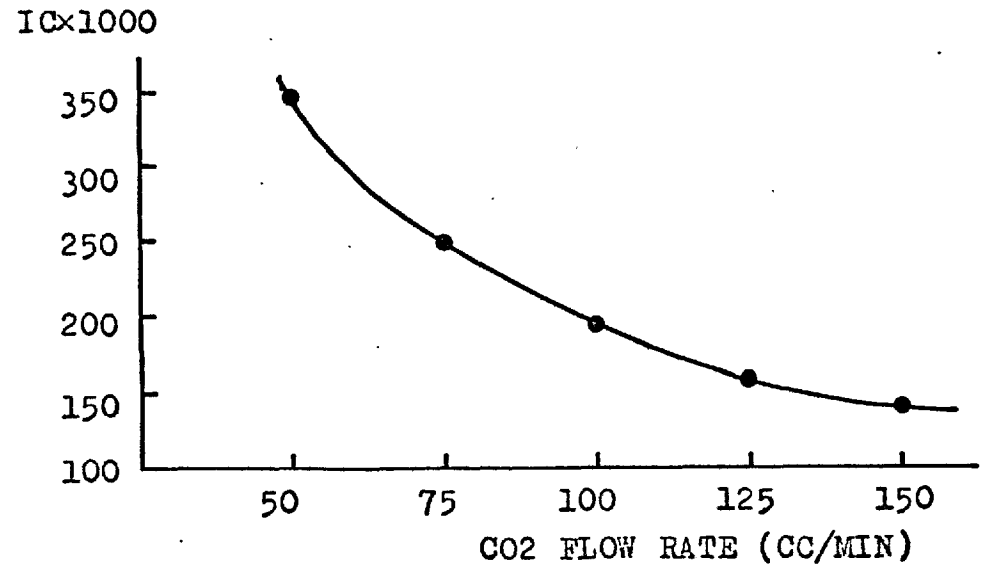

FIGURE 5.3

VARIATION OF IC×FLOW RATE WITH CO2 FLOW RATE

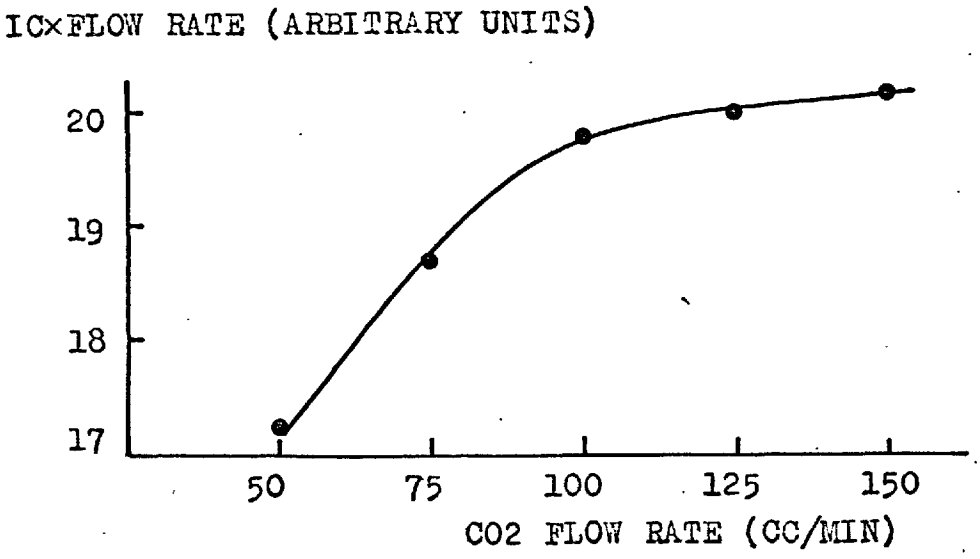

of a run. Static tests showed that the count rate increased almost linearly with counter volume but under flow conditions counting at say 4 c/s no increase in count rate was obtained by increasing the counter volume.

In view of this a fixed counting volume was chosen that was suitable for detecting the initial high decay rate since most counting errors were expected here. A series of trial runs were done at ambient temperature and pressure to determine the maximum count rate at start over a range of counter volumes. No criterion was available to choose a working point on the curve obtained so a value of 2.7 c.c. was arbitrarily selected. This value ensured that the accumulated count at 10,000 seconds was as large as possible compared with the accumulated background count at the same time, and yet still within the range of the maximum count store of the scaler-timer, this being 999,999 counts.

CHAPTER 6 - RESULTS

6.1 Molecular Data for Potential Calculations

The literature data given in Appendix A shows that other workers have based their potential calculations for systems similar to the one studied here on constants which exhibit a wide variation in values according to their source. It will be seen later that the results obtained in this work are sensitive to changes in the data used and as wide as possible choice was made from these to assess the full range of theoretical results.

Theoretical polarisabilities, susceptibilities and equilibrium radii for the structural ions in the sieve were calculated using screening constants (10), and these values were compared with the literature values. It was not possible to calculate these constants for the partially ionised states finally used for the oxygen ions because the relationships used only permit integral degrees of ionisation in units of the charge on an electron.

The theoretical values obtained show that the literature values for sodium, calcium and oxygen are based on fully ionised states, though this is not always explicitly stated. The values finally used are given in table A6 together with the potential constants used in equation 2.10

for the various combinations of the constants for carbon dioxide, oxygen and the exchangeable cations.

6.2 Computed Carbon Dioxide - Linde 5A Sieve Potentials

The first set of programs was run using data taken from Appendix A to test the rate of convergence of the four terms in equation 2.10 as potential contributions from ions at increasing distances from the carbon dioxide molecule were included in the summations. A 12-6 potential function was included in these and subsequent test runs as it was to be expected that equation 2.10 and a 12-6 potential would give approximately comparable results.

Potentials were initially computed along a line between the centre of the large cage containing the carbon dioxide molecule and the centre of an O8 window. The ion positions in the data table were reflected to simulate composite cubes containing from 27 to 1331 unit cages. This permitted contributions from ions at increasing separations to be computed sequentially. A check was made on the data reflection procedure to ensure that the correct total number of ions were being generated in agreement with table 3.3.

The results given in table 6.1 were obtained using the ion projection method described in section 3.1.1 neglecting ions with a greater separation from the carbon dioxide molecule than was specified by the program. (This separation is in terms of the distance squared.)

The repulsion potential for the three grid points quoted in table 6.1 has converged for $RMAX^2 = 2.25$ and the dispersion and quadrupole potentials have almost converged when $RMAX^2 = 6.25$. The polarisation potential varies in a random fashion and including ions at large distances from the carbon dioxide molecule does not improve the convergence. Finally, the quadrupole potential dominates the total potential, which differs greatly from the 12:6 potential.

The convergence of the polarisation potential was improved by modifying the procedure for projecting the data ions as described in section 3.1.2. Instead of generating all the ions and then testing each against a separation criterion, the program was rewritten to generate all ions in the region $X \geq O$ for all Y and Z. Then the interaction for pairs of ions with the carbon dioxide molecule was calculated. The first ion in a pair is at point (X,Y,Z) in the region $X \geq O$ with $R^2 < RMAX^2$ and the second is the ion at the point (X', Y', Z') such

TABLE 6.1 CONVERGENCE OF POTENTIALS FOR NON-SYMMETRIC ION REFLECTION. FULLY IONISED STATES. RUNS 16-20

RMAX SQ.	2.25	6.25	12.25	20.25	30.25
TOTAL NO. OF IONS PROJECTED	2592	11200	29792	62208	112288
GRID POINT (0,0,0)					
IONS IN SUMMATION	1072	5088	14264	30208	55728
PHI R	3.615,-4	3.615,-4	3.615,-4	3.615,-4	3.615,-4
-PHI D	1.469,-3	1.496,-3	1.501,-3	1.502,-3	1.503,-3
-PHI P	9.052,-23	6.309,-24	5.131,-24	1.428,-21	3.772,-21
-PHI Q298	3.589,-2	3.655,-2	3.667,-2	3.671,-2	3.672,-2
-PHI T298	3.699,-2	3.769,-2	3.781,-2	3.785,-2	3.786,-2
-PHI 12-6	1.451,-3	1.478,-3	1.483,-3	1.484,-3	1.485,-3
GRID POINT (5,0,0)					
IONS IN SUMMATION	1088	5116	14276	30408	55532
PHI R	6.644,-3	6.644,-3	6.644,-3	6.644,-3	6.644,-3
-PHI D	3.213,-3	3.240,-3	3.245,-3	3.247,-3	3.247,-3
-PHI P	8.403,-6	8.218,-4	3.536,-4	4.595,-7	2.079,-4
-PHI Q298	7.645,-2	7.714,-2	7.726,-2	7.730,-2	7.731,-2
-PHI T298	7.302,-2	7.456,-2	7.421,-2	7.390,-2	7.412,-2
-PHI 12-6	2.871,-3	2.899,-3	2.903,-3	2,905,-3	2.905,-3
GRID POINT (10,0,0)					
IONS IN SUMMATION	1032	5104	14212	30284	55196
PHI R	1.790,-1	1.790,-1	1.790,-1	1.790,-1	1.790,-1
-PHI D	1.055,-2	1.058,-2	1.058,-2	1.058,-2	1.058,-2
-PHI P	3.733,-4	1.775,-3	8.918,-5	2.034,-4	1.143,-4
-PHI Q298	2.272,-1	2.280,-1	2.281,-1	2.281,-1	2.281,-1
-PHI T298	5.908,-2	6.123,-2	5.973,-2	5.988,-2	5.980,-2
-PHI 12-6	9.547,-4	9.864,-4	9.912,-4	9.927,-4	9.932,-4

that $X' = -X$, $Y' = -Y$ and $Z' = -Z$ irrespective of the value of R^2. This gave a more symmetric summation procedure and improved the convergence of the polarisation potential as more ions were included in the calculation. A check was again made that the same total number of ions was generated as in the previous set of runs.

Referring to table 6.2, at the grid point (5,0,0), the value of the polarisation potential now settles to a reasonably constant value which is not significantly affected by the number of ions included in the summation. The values for the other potentials remain the same as in the previous set of runs, as is to be expected if the ion projection procedure is correct.

Turning to the quadrupole potential contribution, it is obvious that the values obtained are far too large, since it is known that the quadrupole potential is similar in magnitude to the dispersion potential, at least in regions within the sieve cage which are not close to the ionic framework. If equation 2.10 is examined, it is seen that the only parameter that can be adjusted is the apparent charge residing on each ion. Originally it was stated in section 2.2 that all the ions were assumed to be fully ionised, but if partial ionisation is assumed the quadrupole potential and the quadrupole contribution in PHIR2 is reduced.

TABLE 6.2 CONVERGENCE OF POTENTIALS FOR SYMMETRIC ION REFLECTION. FULLY IONISED STATES. RUNS 33-37

RMAX SQ.	2.25	6.25	12.25	20.25	30.25
TOTAL NO. OF IONS PROJECTED	2592	11200	29792	62208	112288
GRID POINT (0,0,0)					
IONS IN SUMMATION	1072	5088	14264	30208	55728
PHI R	3.615,-4	3.615,-4	3.615,-4	3.615,-4	3.615,-4
-PHI D	1.469,-3	1.496,-3	1.501,-3	1.502,-3	1.503,-3
-PHI P	4.096,-24	1.097,-24	1.067,-24	5.019,-24	2.535,-23
-PHI Q298	3.589,-2	3.655,-2	3.667,-2	3.671,-2	3.672,-2
-PHI T298	3.699,-2	3.769,-2	3.781,-2	3.785,-2	3.786,-2
-PHI 12-6	1.451,-3	1.478,-3	1.483,-3	1.484,-3	1.485,-3
GRID POINT (5,0,0)					
IONS IN SUMMATION	1312	5856	15776	32728	59256
PHI R	6.644,-3	6.644,-3	6.644,-3	6.644,-3	6.644,-3
-PHI D	3.217,-3	3.241,-3	3.245,-3	3.247,-3	3.247,-3
-PHI P	5.041,-10	1.266,-4	1.842,-4	1.258,-4	1.963,-4
-PHI Q298	7.654,-2	7.716,-2	7.727,-2	7.730,-2	7.731,-2
-PHI T298	7.312,-2	7.388,-2	7.405,-2	7.403,-2	7.411,-2
-PHI 12-6	2.875,-3	2.899,-3	2.904,-3	2.905,-3	2.905,-3
GRID POINT (10,0,0)					
IONS IN SUMMATION	1496	6488	17080	35056	62456
PHI R	1.790,-1	1.790,-1	1.790,-1	1.790,-1	1.790,-1
-PHI D	1.055,-2	1.058,-2	1.058,-2	1.058,-2	1.059,-2
-PHI P	1.160,-3	5.843,-5	2.455,-5	5.873,-5	5.740,-6
-PHI Q298	2.273,-1	2.280,-1	2.281,-1	2.281,-1	2.281,-1
-PHI T298	6.001,-2	5.959,-2	5.967,-2	5.974,-2	5.970,-2
-PHI 12-6	9.604,-4	9.874,-4	9.916,-4	9.928,-4	9.933,-4

Barrer and Gibbons[15] found that using partially ionised states for a single sieve cage gave results for the relative importance of potential contributions which were comparable with practical values based on heats of adsorption data for the sieve[16].

Partial ionisation was also assumed in the present work but since Na^{+} and Ca^{++} ions are freely exchangeable, it is assumed that these are always present in their fully ionised states. The Al^{3+} and Si^{4+} ions are relatively small and surrounded by tetrahedra of oxygen ions, so as far as the carbon dioxide molecule is concerned it is assumed that their apparent ionic charge is zero. It then remains to allocate a charge of -12e, to balance that residing on the exchangeable cations, amongst the fortyeight oxygen ions constituting the ionic framework of a unit cage. There is no 'a priori' reason to differentiate between the oxygen ions, so the simplest allocation is to assume a charge of -1/4e on each.[17]

This mode of charge allocation will fail at the surface of the generated crystal using the symmetric ion projection method. In effect the crystal will be assigned a net negative charge, caused by overpopulation of the crystal surface, but as the surface ions are distant

TABLE 6.3 CONVERGENCE OF POTENTIALS FOR SYMMETRIC ION REFLECTION. PARTIALLY IONISED STATES. RUNS 40-44

RMAX SQ.	2.25	6.25	12.25	20.25	30.25
TOTAL NO. OF IONS PROJECTED	2592	11200	29792	62208	112288
GRID POINT (0,0,0)					
IONS IN SUMMATION	1072	5088	14264	30208	55728
PHI R	3.789,-5	3.790,-5	3.790,-5	3.790,-5	3.790,-5
-PHI D	1.469,-3	1.496,-3	1.501,-3	1.502,-3	1.503,-3
-PHI P	4.736,-25	5.017,-25	3.380,-25	6.470,-25	1.233,-24
-PHI Q298	1.661,-3	1.696,-3	1.701,-3	1.702,-3	1.703,-3
-PHI T298	3.092,-3	3.154,-3	3.164,-3	3.167,-3	3.168,-3
-PHI 12-6	1.451,-3	1.478,-3	1.483,-3	1.484,-3	1.485,-3
GRID POINT (5,0,0)					
IONS IN SUMMATION	1312	5856	15776	32728	59256
PHI R	5.105,-4	5.105,-4	5.105,-4	5.105,-4	5.105,-4
-PHI D	3.217,-3	3.241,-3	3.245,-3	3.247,-3	3.247,-3
-PHI P	3.711,-4	3.293,-4	2.658,-4	2.625,-4	2.752,-4
-PHI Q298	2.885,-3	2.909,-3	2.913,-3	2.914,-3	2.915,-3
-PHI T298	5.963,-3	5.968,-3	5.914,-3	5.913,-3	5.927,-3
-PHI 12-6	2.875,-3	2.899,-3	2.904,-3	2.905,-3	2.905,-3
GRID POINT (10,0,0)					
IONS IN SUMMATION	1496	6488	17080	35056	62456
PHI R	1.219,-2	1.219,-2	1.219,-2	1.219,-2	1.219,-2
-PHI D	1.055,-2	1.058,-2	1.058,-2	1.058,-2	1.059,-2
-PHI P	2.290,-4	2.298,-5	1.441,-7	9.329,-7	1.284,-6
-PHI Q298	4.116,-3	4.142,-3	4.147,-3	4.148,-3	4.148,-3
-PHI T298	2.711,-3	2.559,-3	2.544,-3	2.548,-3	2.549,-3
-PHI 12-6	9.604,-4	9.874,-4	9.916,-4	9.928,-4	9.933,-4

from the carbon dioxide molecule their potential effect will be small and the error can be neglected. Actually, all surface oxygen ions should be allocated a charge of -1/8e to get an overall charge balance for any generated cubic crystal. Barrer[15] used a similar method, incorporating a charge distribution of 10/48e for internal oxygen ions and 5/48e for surface oxygen ions in a cube containing a single unit cell.

Table 6.3 shows that this modified charge distribution does not affect the results for the dispersion potential. In general the change in the polarisation potential is small, and since this potential is always less than 10% of the dispersion potential the effect of the charge distribution is trivial. At grid point (10,0,0) which is at the centre of an O8 window, the polarisation potential is much reduced. From the point of view of structural symmetry of the sieve the polarisation potential here is expected to be zero, and it would be so if the data ions were referred to an origin at (10,0,0) instead of(0,0,0). The difference in the polarisation potential at these points indicates the slight loss of structural symmetry engendered in moving between the centre of a large cage and the centre of an O8 window, without redefining a new origin for the ion data table. This effect is also encountered in the value for the polarisation potential at (10,10,10) which is the centre of a small cage.

Changing the charge distribution has as expected a large effect on the quadrupole potential, and using the ionisation states $O^{-1/4}$, AS^{o}, $NaCa^{1\frac{1}{2}+}$ gives results of the correct order. Barrer's practical work on Linde X sieves[16] suggested that the ratio of the dispersion to quadrupole potentials was 3:5 at 30°C. The results obtained at this juncture do not bear this out quantitatively but at least they give a similar figure.

The repulsion potential also decreases as a result of the change in charge distribution, the effect being caused by the term designated PHIR2. This term

$$1 + \frac{\alpha_b e^2 C_a^2 \rho_e^2}{3B} + \frac{e^2 Ca^2 Q_b^2}{20kTB}$$

adjusts the repulsion constant to maintain the minimum $(d\phi/dr) = 0$ at $r = \rho_e$ as other types of potential interactions are included in the total potential. (For a 12:6 potential PHIR2 = 1, and including a polarisation interaction results in $PHIR2 = 1 + \frac{\alpha_b e^2 Ca^2 \rho_e^2}{3B}$, etc. The repulsion constant is then given by the product PHIR1.PHIR2 where $PHIR1 = \frac{B\rho_e^6}{2}$). Although the overall polarisation contribution is small, the factor $\alpha_b e^2 Ca^2 \rho_e^2/3B$ must be included for the oxygen and

sodium-calcium ions (see Appendix A, table A6). The charge on the AS ion is taken as zero and as the contribution to the repulsion term from these ions is less than 1% of that for the other ions, this can be neglected in the summation. This can be seen by comparing the values of the repulsion constant for the various ions in table 6.4.

TABLE 6.4

Repulsion Constants PHIR1.PHIR2 for Various Ionisation States

PHIR1 X PHIR2	O^{2-}	$O^{1/4-}$	$AS^{3\frac{1}{2}+}$	AS^{o}	$NaCa^{1\frac{1}{2}+}$
10^{-10} ergs	38.4	2.26	4.24	0.0175	4.18

A fourth set of programs was run based on a reduced set of data ions which neglected the AS^{o} ions. Table 6.5 shows that neglecting these ions results in only a small reduction in the repulsion and polarisation potentials and has the added effect of reducing the computation time as can be seen by the figures for both the total number of projected ions and the ions included in each summation.

In view of these results, production programs were run based on runs 50-54 (see table 6.6) which evaluated the repulsion potential for

TABLE 6.5 CONVERGENCE OF POTENTIALS FOR SYMMETRIC ION REFLECTION. PARTIALLY IONISED STATES. RUNS 50-54

RMAX SQ.	2.25	6.25	12.25	20.25	30.25
TOTAL NO. OF IONS PROJECTED	1728	7600	20384	42768	77440
GRID POINT (0,0,0)					
IONS IN SUMMATION	736	3600	9992	21184	39024
PHI R	3.783,-5	3.783,-5	3.783,-5	3.783,-5	3.783,-5
-PHI D	1.439,-3	1.466,-3	1.471,-3	1.472,-3	1.473,-3
-PHI P	4.736,-25	5.017,-25	3.380,-25	6.470,-25	1.233,-24
-PHI Q298	1.661,-3	1.696,-3	1.701,-3	1.702,-3	1.703,-3
-PHI T298	3.062,-3	3.124,-3	3.134,-3	3.137,-3	3.138,-3
-PHI 12-6	1.421,-3	1.448,-3	1.453,-3	1.454,-3	1.455,-3
GRID POINT (5,0,0)					
IONS IN SUMMATION	928	4112	11040	22920	41464
PHI R	5.096,-4	5.096,-4	5.096,-4	5.096,-4	5.096,-4
-PHI D	3.155,-3	3.179,-3	3.183,-3	3.184,-3	3.184,-3
-PHI P	3.711,-4	3.293,-4	2.658,-4	2.625,-4	2.752,-4
-PHI Q298	2.885,-3	2.909,-3	2.913,-3	2.914,-3	2.915,-3
-PHI T298	5.902,-3	5.907,-3	5.852,-3	5.851,-3	5.865,-3
-PHI 12-6	2.814,-3	2.838,-3	2.842,-3	2.843,-3	2.844,-3
GRID POINT (10,0,0)					
IONS IN SUMMATION	1048	4536	11928	24528	43704
PHI R	1.217,-2	1.217,-2	1.217,-2	1.217,-2	1.217,-2
-PHI D	1.038,-2	1.040,-2	1.041,-2	1.041,-2	1.041,-2
-PHI P	2.290,-4	2.298,-5	1.441,-7	9.329,-7	1.284,-6
-PHI Q298	4.116,-3	4.142,-3	4.147,-3	4.148,-3	4.148,-3
-PHI T298	2.551,-3	2.398,-3	2.384,-3	2.387,-3	2.388,-3
-PHI 12-6	8.001,-4	8.265,-4	8.306,-4	8.318,-4	8.323,-4

all ions with $RMAX^2 < 2.25$, the dispersion and quadrupole potentials for all ions with $RMAX^2 < 6.25$, and the polarisation potential for all ions with $RMAX^2 < 12.25$. This choice of values for $RMAX^2$ was intended as a good compromise between computing time and the accuracy of the results obtained compared with the possible accuracy with $RMAX^2 = 30.25$.

Barrer[16] has done some potential calculations for carbon dioxide adsorbed in a Linde X sieve, and provides an alternative value for the polarisability of oxygen. This value is smaller than the one normally used but since it is based on measurements of oxygen in a potash felspar it should represent a more realistic value for oxygen present in a sieve structure. (See Appendix A.) It was decided to run eight programmes (runs 60-67) to evaluate equations 2.10 and 2.38 in full throughout the accessible regions of the large and small cages. These programmes represented the four cases where the molecular constants for the carbon dioxide molecule were used in conjunction with the two different oxygen polarisabilities and two types of exchangeable cations, namely all calcium and a combination of sodium and calcium. These four cases were repeated using the kinetic radius for the carbon dioxide molecule.

The results for runs 61 and 63 for a calcium sieve with $\rho_e\ CO_2 = 5.12 \times 10^{-8}$ cm and the high and low values for the oxygen polarisability are analysed in detail in the following sections. Run 63 using

TABLE 6.6

LIST OF COMPUTER RUNS FOR POTENTIAL CALCULATIONS

RUNS	PURPOSE
16-20	CONVERGENCE OF POTENTIALS USING NON-SYMMETRIC ION PROJECTION. FULLY IONISED STATES FOR O, NaCa, AS, AT 298 DEG. K
33-37	CONVERGENCE OF POTENTIALS USING SYMMETRIC ION PROJECTION. FULLY IONISED STATES FOR O, NaCa, AS, AT 298 DEG. K
40-44	CONVERGENCE OF POTENTIALS USING SYMMETRIC ION PROJECTION. PARTIALLY IONISED STATES FOR O, NaCa, AS, AT 298 DEG. K
50-54	CONVERGENCE OF POTENTIALS USING SYMMETRIC ION PROJECTION. PARTIALLY IONISED STATES FOR O, NaCa, (AS NEGLECTED) AT 298 DEG. K
60-67	FULL COMPUTATION OF POTENTIALS IN BOTH LARGE AND SMALL CAGES BASED ON RUNS 50-54, AT TWELVE TEMPERATURES FROM 573 TO 173 DEG. K (DETAILS BELOW)
71-82	COMPUTATION OF B' AT TWELVE TEMPERATURES FROM 573 TO 173 DEG. K USING POTENTIALS TAKEN FROM RUN 63
83-94	COMPUTATION OF B' AT TWELVE TEMPERATURES FROM 573 TO 173 DEG. K USING POTENTIALS TAKEN FROM RUN 61

	SIGMA1 AT 273 K	α CO2 X1.0,-8 CM	POL. O -1/4 X1.0,-25 CM3	EXCHANGABLE CATION
60	3.083,12	5.12	39.0	NaCa 1.5+
61	2.128,11	5.12	39.0	Ca 1.5+
62	3.107,10	5.12	16.5	NaCa 1.5+
63	2.477,9	5.12	16.5	Ca 1.5+
64	2.783,38	3.30	16.5	NaCa 1.5+
65	5.113,32	3.30	16.5	Ca 1.5+
66	9.256,36	3.30	39.0	Ca 1.5+
67	6.417,37	3.30	39.0	NaCa 1.5+

$\alpha O^{-1/4} = 16.5 \times 10^{-25}$ cm^3 gave the lowest potentials whilst runs 64-67 using the kinetic radius for the carbon dioxide molecule gave excessively high values. Sample calculations showed that SIGMA1 = $\sum_{v} \exp(-\phi/kt)$ needed to be less than 10^{11} at 273° K to give theoretical predictions for adsorption isotherms which would be in any way comparable with practical curves. In view of this, results for the programs using the kinetic radius for carbon dioxide given in table 6.6 were not processed further.

Each run was programmed over a range of temperatures from 573°K down to 173°K and the values of the potentials for all grid points in the large and small cages with $\phi < 500 \times 10^{-15}$ ergs are given in full in tables A8 and A9 for runs 61 and 63.

The way in which the potentials vary in the open region of the large cage is shown in figures 6.1-3. The potentials are in units of 10^{-15} ergs per carbon dioxide molecule at 298°K and the surrounding structural ions have been omitted. The contours were obtained from data given in table A9 using linear interpolation between grid points, and summarise the main results for run 63. Figure 6.1 shows the potentials in three of the bounding faces of the tetrahedral grid. The contours are unsmoothed and have been matched along the edges of the grid.

FIGURE 6.1

SIEVE POTENTIALS IN THE FACES OF THE TETRAHEDRAL GRID

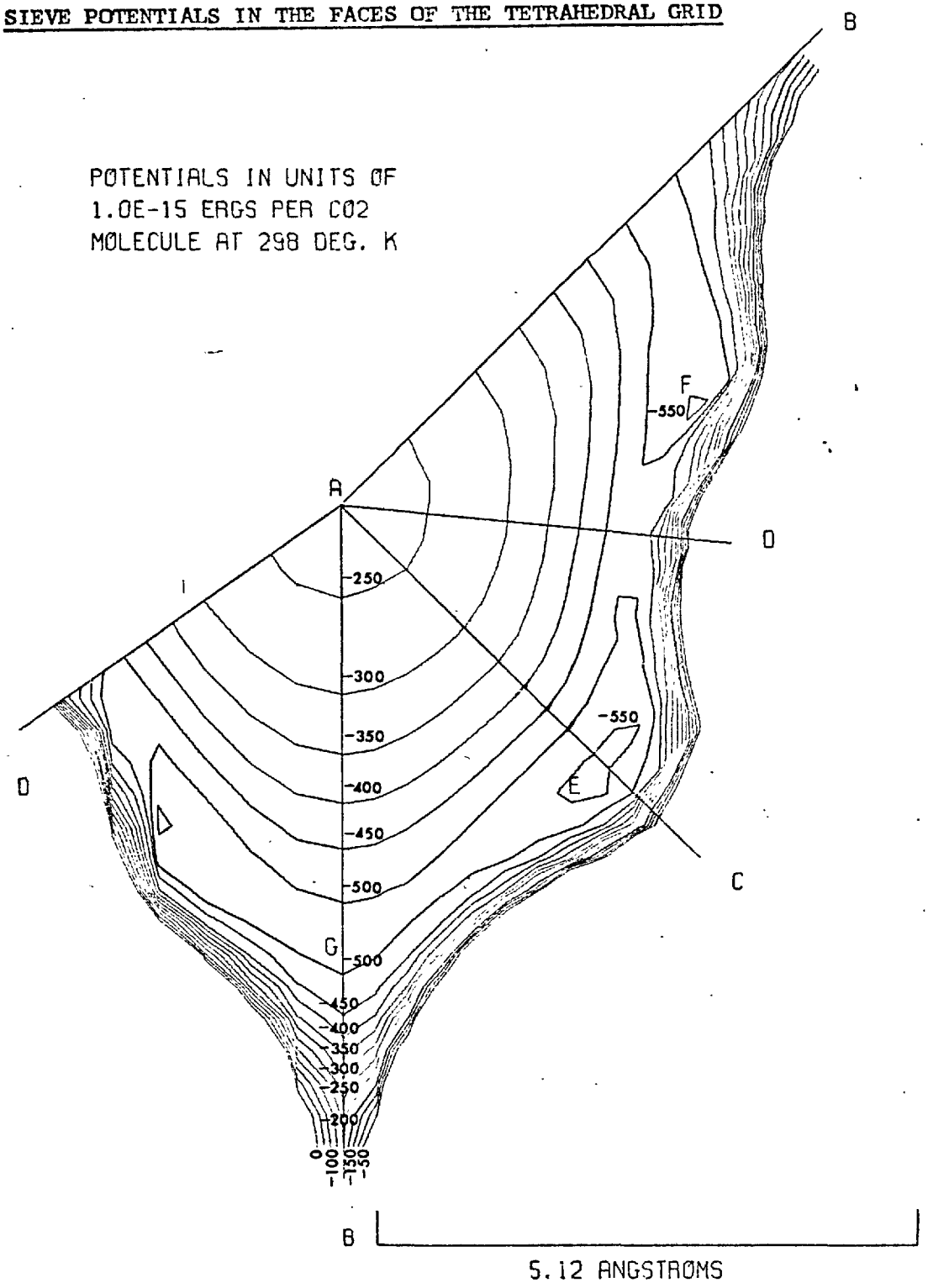

FIGURE 6.2

SIEVE POTENTIALS IN THE Z=0 PLANE

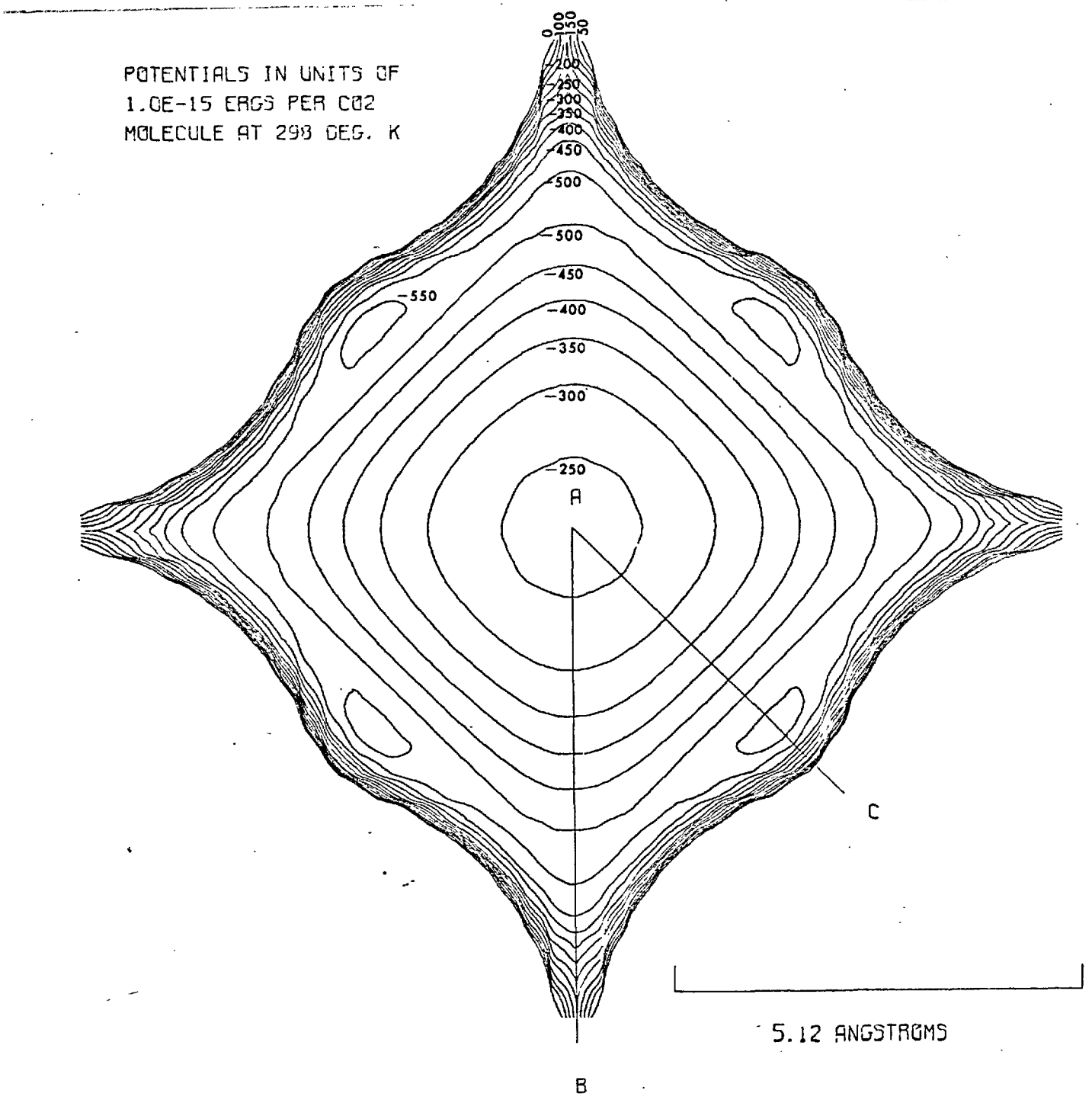

FIGURE 6.3 SIEVE POTENTIALS IN THE Y=Z PLANE

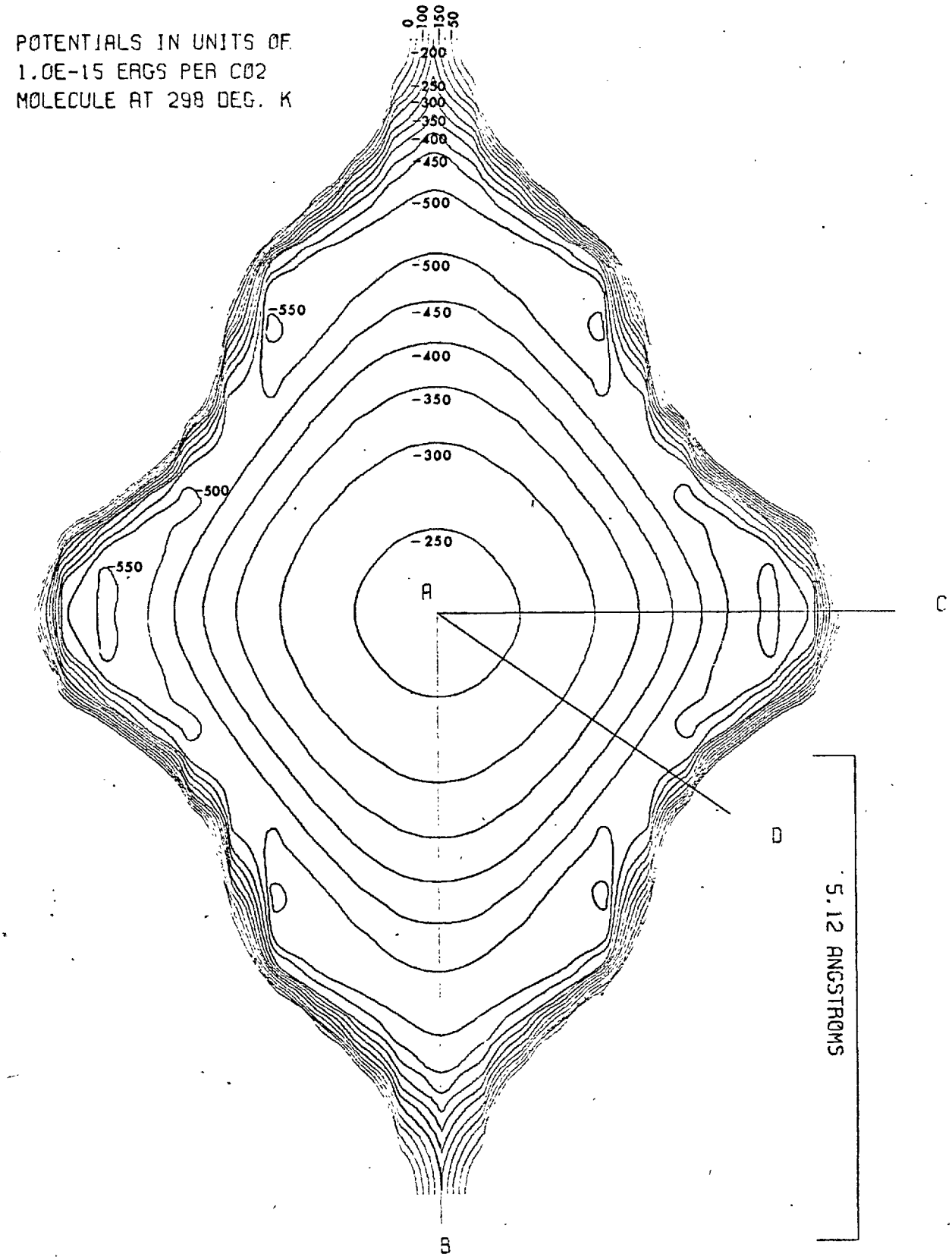

Due to symmetry, the contours in the three planes in the coordinate directions are identical and are obtained from the contours in the face (a b c). These contours are drawn for a complete large cage in figure 6.2 and show how the potentials behave through an O8 window. The potentials in the six planes at $\pm$ 45° to these are obtained from the contours in faces (a c d) and (a b d) and are also identical to one another. The contours are drawn for a complete large cage in figure 6.3 and show how the potentials vary through an O8 window, and also in the (111) direction along which the small cages and O6 windows blocked by exchangeable cations are found. The contours in figures 6.2 and 6.3 have been smoothed and thus differ slightly from those given in the relevant parts of figure 6.1. The contours in the small cages are of little interest and have been omitted.

Figures 6.1-3 show that the region of highest interaction between the carbon dioxide molecule and the ionic framework of the sieve occurs in a spherical shell about 7.5 Å diameter, with major sites of interaction at E and F. At 573°K when the interaction is weaker, these sites are situated in the axial directions at G . The carbon dioxide molecule 5.12 Å diameter is much larger than these regions of high interaction, but it may be noted that if six molecules are located with their centres

approximated at G , i.e. on the coordinate directions of the grid, they completely fill the large cage and lie almost wholly in the region of highest interaction. Also six molecules per cage represent 16 wt% adsorption, compared with the Linde value for saturation of 18.9 wt% at 298°K and 1 atmosphere pressure.

6.3 The Linear Adsorption Isotherm Approximation

Equation 2.38 relates the sieve potentials to the linear isotherm approximation given by equation 2.37. Combining these two equations gives:

$$n = \frac{p}{RT} \sum_{v} \exp(-\frac{\phi(\underline{r})}{kT})\delta V \qquad 6.1$$

In equation 6.1 the summation is over the large cage volume V. The exponential term approximates to zero in all regions where $\phi > 500 \times 10^{-15}$ ergs/molecule for the range of temperatures considered, and all such points lie in the regions shown in figures 6.1-3.

The grid separation used was $a_o/20$ and hence $\delta V = (a_o/20)^3 = 2.32 \times 10^{-28}$ litres. Expressing p in millimetres of mercury, T in °K and using the value for the gas constant R = 62.4 litre.mm Hg/°K.mole enables equation 6.1 to be written as

$$n = 3.72 \times 10^{-30} \cdot \frac{p}{T} \times \sum_{v} \exp(-\phi/kT) \qquad 6.2$$

where n is the number of moles of carbon dioxide adsorbed per cage of the sieve.

It is convenient to express this in terms of the weight percent of carbon dioxide adsorbed as is usual in adsorption isotherm plots. The molecular weight of the Linde 5A calcium sieve is 1668 (neglecting all water) so there are theoretically $\bar{N}$ unit cages in 1668 grams of sieve where $\bar{N}$ is Avogadro's number. The molecular weight of carbon dioxide is 44 so n moles of carbon dioxide is equivalent to

$$q = \frac{n \bar{N} \times 44 \times 100}{1668}$$ grams of carbon dioxide per

100 grams of sieve. Rewriting equation 6.2 in terms of q gives

$$q = 5.9 \times 10^{-6} \times p \times \left(\sum_{v} \exp(-\phi/kT)\right)/T \qquad 6.3$$

Table 6.7 gives the results from runs 61 and 63 for the summation as a function of temperature, and plots of equation 6.3 using this data are given in figures 6.4 and 6.5. Linde data[18] is plotted for comparison.

6.4 The Quadratic Adsorption Isotherm Approximation

Equations 2.36, 2.38 and 2.39 relate the molecule-ion and molecule-molecule interactions to the amount of carbon dioxide adsorbed in the sieve when two molecules are present in a large cage.

Combining these equations and writing n in terms of q, the weight percent of adsorbed carbon dioxide gives:

$$q = 100 \frac{p}{RT} b_o^3 \overline{N} \frac{M_{CO_2}}{M_{sieve}} \sum_1 + 100 \left(\frac{p}{RT}\right)^2 b_o^3 \overline{N} \frac{M_{CO_2}}{M_{sieve}} B'_g \sum_1$$

$$+ 100 \left(\frac{p}{RT}\right)^2 b_o^6 \overline{N}^2 \frac{M_{CO_2}}{M_{sieve}} \sum_2 \qquad 6.4$$

where $$\sum_1 = \sum_v \exp(-\phi/kT)$$

and $$\sum_2 = \sum_v \sum (\exp(-E(\underline{r}_i, \underline{r}_j)/kT) - 1) \times$$

$$\times \exp \frac{(-\phi(\underline{r}_i) - \phi(\underline{r}_j))}{kT}$$

Substituting the values of the constants in equation 6.4 gives q in terms of p mm.Hg and the parameters:

$$\sum_1/T, \quad B'_g, \quad \sum_1/T^2 \quad \text{and} \quad \sum_2/T^2$$

Thus for:

$$R = 62.4 \text{ litre.mm Hg/}^{\circ}\text{K.mole}$$

$$b_o = 6.155 \times 10^{-8} \text{ cm}$$

$$\overline{N} = 6.02 \times 10^{23}$$

$$M_{CO_2} = 44$$

$$M_{sieve} = 1668$$

$$q = 5.93 \times 10^{-6} \, p \frac{\sum 1}{T} + 9.51 \times 10^{-8} \, B'_g \, p^2 \frac{\sum 1}{T^2}$$

$$+ \; 1.33 \times 10^{-11} \, p^2 \frac{\sum 2}{T^2} \qquad 6.5$$

B'_g is the bulk second virial coefficient for carbon dioxide and values of this as a function of temperature were obtained from Lennard-Jones 12-6 potential data.[10] These are given in table 6.8.

The double summation $\sum_2$ discussed in section 3.4 was programmed for twelve temperatures (runs 71-94) using the potentials from runs 61 and 63. The results obtained are given in table 6.7 and a listing of the programme at 323°C in Appendix C.

Figures 6.4 and 6.5 summarise the results in table 6.7 and compare the theoretical linear and quadratic isotherms with Linde

TABLE 6.7

TEMPERATURE VARIATION OF THE SUMMATIONS FOR VO AND B'

USING POTENTIALS FROM RUNS 63 AND 61

TEMP	POTS. FROM RUN 63		POTS. FROM RUN 61	
DEG. K	SIGMA1	-SIGMA2	SIGMA1	-SIGMA2
573	2.897,4	1.588,8	2.146,5	7.843,9
473	1.233,5	2.693,9	1.469,6	3.483,11
423	3.926,5	2.626,10	6.472,6	6.599,12
373	2.136,6	7.488,11	5.312,7	4.385,14
348	6.825,6	7.529,12	2.175,8	7.336,15
323	2.884,7	1.329,14	1.216,9	2.296,17
298	1.969,8	6.092,15	1.154,10	2.069,19
273	2.477,9	9.450,17	2.128,11	6.966,21
248	8.646,10	1.113,21	1.192,13	2.134,25
223	1.314,13	2.461,25	3.287,15	1.544,30
198	2.338,16	7.470,31	1.269,19	2.212,37
173	2.138,21	6.018,41	3.288,24	1.454,48

TABLE 6.8

BULK AND CRYSTAL PHASE SECOND VIRIAL COEFFICIENTS

TEMP	B'g (EQ 2.15)	B'g (PHI L-J)	B' (EQ 2.10) (PHI L-J)	B' (EQ 2.10) (EQ 2.15)
DEG. K	LITRES/MOLE	LITRES/MOLE	LITRES/MOLE	LITRES/MOLE
573	0.0605	-0.012	3.267,-1	3.849,-1
473	0.0580	-0.035	6.991,-1	1.533
423	0.0560	-0.052	3.080	4.965
373	0.0533	-0.074	1.362, 1	2.461, 1
348	0.0515	-0.088	3.824, 1	7.743, 1
323	0.0494	-0.104	1.385, 2	3.234, 2
298	0.0466	-0.124	7.627, 2	2.172, 3
273	0.0435	-0.148	6.869, 3	2.678, 5
248	0.0394	-0.178		
223	0.0343	-0.216		
198	0.0276	-0.266		
173	0.0185	-0.338		

FIGURE 6.4

THEORETICAL EQUILIBRIUM ADSORPTION ISOTHERMS - RUN 63

FIGURE 6.4 THEORETICAL EQUILIBRIUM ADSORPTION ISOTHERMS - RUN 63

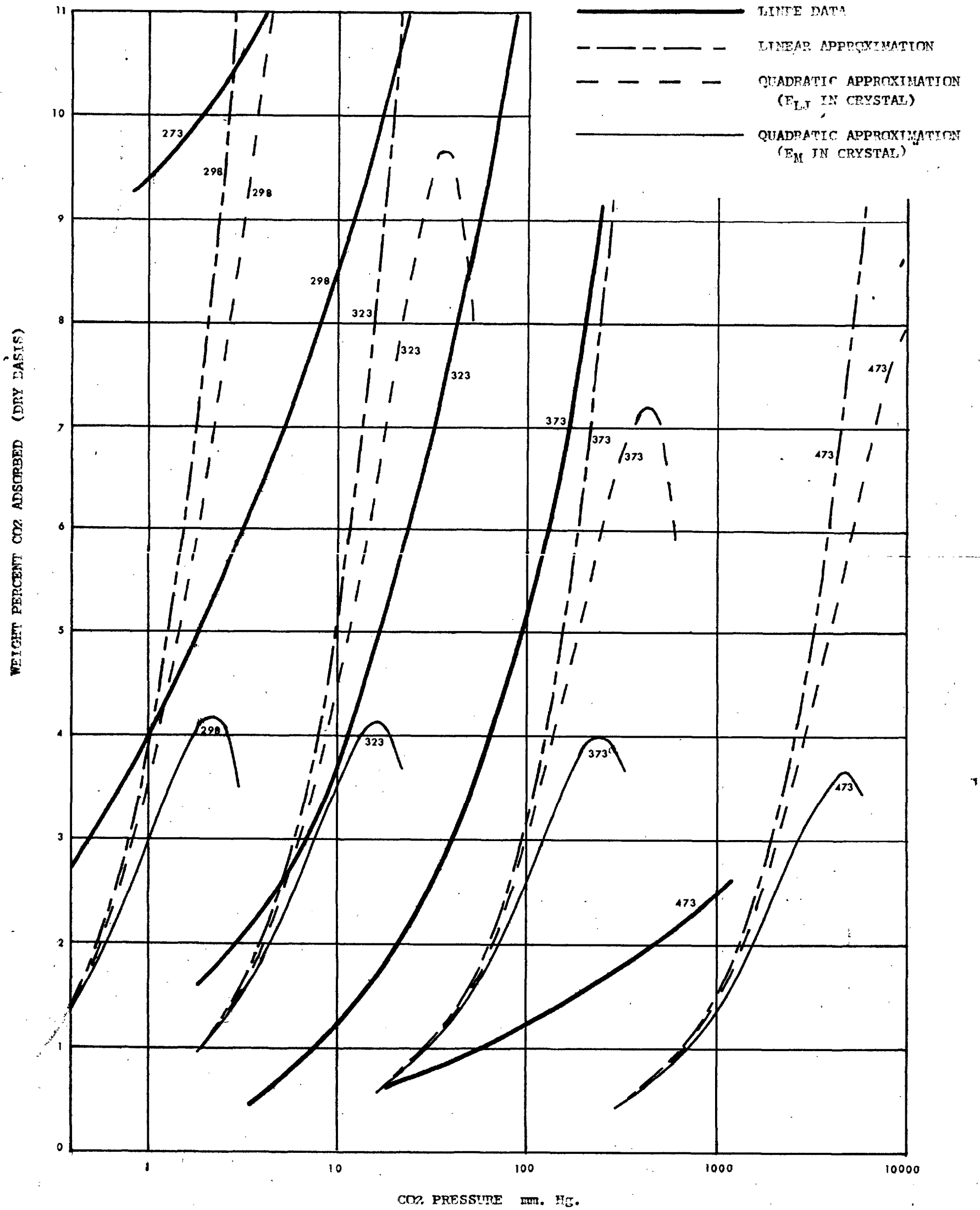

FIGURE 6.5

THEORETICAL EQUILIBRIUM ADSORPTION ISOTHERMS - RUN 61

FIGURE 6.5 THEORETICAL EQUILIBRIUM ADSORPTION ISOTHERMS - RUN 61

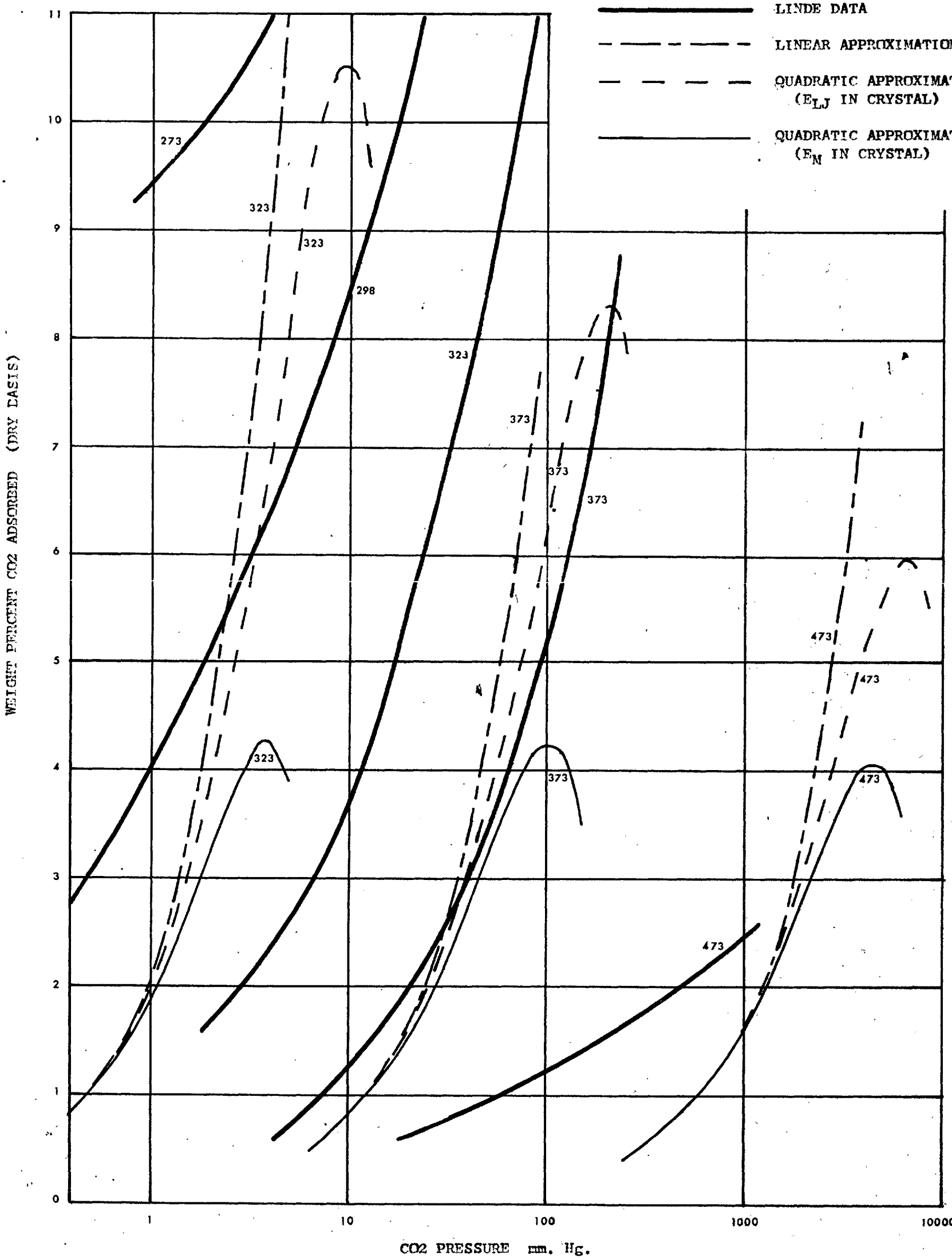

adsorption isotherms for the carbon dioxide - 5A sieve system. The theoretical curves obtained apply to dilute systems so they can only be compared with Linde isotherms at high temperatures. These in general are above the range of temperatures at which practical work was done. No Linde data is available at temperatures below 298°K at pressures sufficiently low to give carbon dioxide concentrations in the sieve comparable with that required for the theoretical analysis.

If it is assumed that the adsorbed carbon dioxide disperses itself evenly throughout the crystals comprising the sieve pellet, then x weight percent adsorption is equivalent to $1668 \times x/44 \times 100$ carbon dioxide molecules per sieve cage, there being $\overline{N}$ cages per mole (1668 grams) of sieve. Thus two molecules in every cage is equivalent to 5.3 wt% adsorption. This value represents an optimistic upper limit for the carbon dioxide concentration in the sieve if the theory is to be applicable. It may be noted that equation 6.5 exhibits a maximum value for q of about 4 wt% adsorption over the twelve temperatures considered.

In general the agreement with the Linde isotherms is poor except over a narrow range of temperatures about 323°K. A review of the basic concepts used in Chopter 2 to define the sieve potentials (equation 2.10) and the quadratic isotherm (equation 2.36) shows that some of the simplifications used are not strictly valid.

As far as the sieve structure is concerned the aluminium and silicon ions have been treated as a single hypothetical AS ion with zero charge and the exchangeable cations shared equally among the O6 windows. The potential contribution from the AS ion has been found to be small so the choice between a single composite ion, or two separate ones, or completely neglecting these ions does not significantly affect the results. Distributing the exchangeable cations equally between the O6 windows is a large departure from reality and for the calcium sieve involves considering 'fractions' of ions. Also the positions of the exchangeable cations are not really known since although they lie in the plane of the O6 windows, in the calcium sieve there are fewer ions than available locations which leaves at least two O6 windows unblocked at any instant in time.

It is necessary to assume partially ionised states for the oxygen ions before realistic values for the quadrupole interaction are obtained. The overall ionisation scheme used for the sieve is somewhat arbitrary although its choice has little or no effect on the three other interactions considered, but the molecular data used is based on fully ionised states as indicated earlier. Also the lower of the two available values for

the polarisability of oxygen gives the only set of theoretical isotherms which are in any way comparable with the Linde data.

The potential function used is based on rigidly fixed ions in the cage structure. It is expected that some degree of relaxation of the structure will occur especially during translation of an adsorbed molecule through an O8 window, since molecules larger than the windows free diameter can pass through it.

Finally all free water normally present in the sieve was neglected, including that associated with structural stability, since nothing is known about the locations of the hydroxyl ions necessary to bind the structure.(21)

A more realistic scheme taking all these factors into consideration would be very complex whereas the present simplifications used permit calculation of the potentials in both large and small cages including the interactions from distant ions.

The way in which the carbon dioxide molecule has been treated also gives rise to sources of error. Throughout this work the carbon dioxide molecule has been assumed to be spherically symmetric, and the potentials obtained from 573°K down to ambient give conditions under which this assumption is substantially valid. The potentials become

unreliable at lower temperatures where the energetics of the system permit molecule alignment, and anisotropy must be considered. Of the possible sizes for the carbon dioxide molecule the value $\rho_e = 5.12$ Å has been strictly adhered to and the molecule assumed to rotate freely with this effective diameter whilst interacting with the sieve matrix. (This value, $\rho_e = 5.12$ Å, is based on the bond length of a carbon monoxide molecule of 1.16 Å and the diameter of an oxygen ion taken as 2.8 Å. Thus O = C = O has the rod length 1.4 + 1.16 + 1.16 + 1.4 = 5.12 Å.) Thus the potentials obtained are not strictly valid when the adsorbed molecule is in regions close to the structural ions.

A simplified approach has been used to define the various potential interactions, and of these only the polarisation potential is not compatible with a freely rotating molecule, though the results obtained show that ϕ_p is small everywhere compared with the total potential. Barrer[16] suggests that in similar systems the polarisation potential can contribute up to 10% of the total potential and hence it may be underestimated here.

Quadratic expressions were fitted to the available Linde adsorption isotherm data over the range 0-4 wt% CO_2 adsorption using a least squares criterion. This showed it was necessary to use an expression of

the form:

$$q = A + Bp + Cp^2 \qquad \text{rather than}$$

$$q = Bp + Cp^2$$

as predicted theoretically. Linde data for the 5A/CO_2 system exists mainly above 273°K and at pressures above 4 mm.Hg. in the range 0-4 wt% adsorption. Without lower pressure data it is difficult to decide if the theoretical expression really fits Linde data. With the available information it can only be stated that if the Linde data plotted in figures 6.4 and 6.5 is represented by a quadratic expression, this expression is different from the one developed theoretically and that if the Linde data is accepted, the theoretical expression is incorrectly formulated.

6.4.1 Bulk and Crystal Phase Second Virial Coefficients

A check was made to see if the potential constants for carbon dioxide given in Appendix A, and using its bond length size, would predict bulk gas second virial coefficients using equations 2.15, 2.18 and 2.30. The results obtained, given in table 6.8, are quite different from the values of B^*_g obtained from equation 2.30 using the Lennard Jones potential and constants for CO_2 to evaluate f_{12}. If equations 2.15, 2.18 and 2.30 are fitted to Lennard Jones $B^*_g(T)$ data[10] by adjusting the size of the CO_2 molecule, good agreement is obtained over the

range 573°K to 173°K using a CO_2 diameter ρ = 3.63 Å. However, this value as shown earlier, being close to the kinetic diameter of CO_2 gives unrealistically high potentials in the sieve and hence high values for B'.

The problem arises that in the crystal both CO_2-CO_2 and CO_2-ion interactions have to be considered together (equation 2.39). The Lennard Jones potential[10] using 4.12 Å for the diameter of CO_2 and a potential well depth of E/k = 189°K accurately describes the CO_2-CO_2 interaction, but cannot describe the CO_2-ion interaction. This needs to be described by equation 2.10, but the analogue of this equation in gas phase (equation 2.15) fails to describe the CO_2-CO_2 interaction unless it is assumed that the CO_2 diameter is 3.63 Å. The use of this value in equation 2.10 then fails to predict the CO_2-ion interaction.

Crystal phase second virial coefficients were recalculated from the potentials from runs 63 and 61 using the Lennard Jones expression and CO_2 parameters for the CO_2-CO_2 interaction. The results are given in table 6.8 and are compared with the original values for B'. Adsorption isotherms were recalculated from equation 2.36 using both available expressions for the CO_2-CO_2 interaction in the bulk phase and the

two different values for B' in the crystal phase. The four resulting isotherms utilising the interactions

Bulk Phase B'_g	Crystal Phase B'	
CO_2-CO_2	CO_2-CO_2	CO_2-ION
$E_{(LJ)}$	$E_{(LJ)}$	ϕ (eqn. 2.10)
	E_M(eqn. 2.15)	ϕ (eqn. 2.10)
E_M(eqn. 2.15)	$E_{(LJ)}$	ϕ (eqn. 2.10)
	E_M(eqn. 2.15)	ϕ (eqn. 2.10)

showed that the choice of models for the bulk phase contribution to the adsorption isotherm was of no importance as this contribution is very small compared with the crystal phase contribution. However, the crystal phase contribution B' has a large effect on the resulting isotherms. These isotherms are plotted for comparison in figures 6.4 and 6.5. This shows that the use of the Lennard Jones potential for the CO_2-CO_2 interaction in the crystal phase causes a deterioration in the agreement first obtained with the Linde data, and the turning points for the theoretical curves are widely scattered compared with the average of 4 wt% CO_2 previously found. This indicates that equation 2.15 represents the CO_2-CO_2 interaction in the crystal phase, better than the Lennard Jones expression.

6.5 Theoretical Heats of Adsorption

Heats of adsorption can be calculated over the upper end of the range of temperatures for which potentials are available. The data required to evaluate equations 2.42 and 2.43 are given in tables 6.9 and 6.10 below. These give the values of V_o and B' taken from runs 63 and 61 respectively. The values of B' in equation 2.39 are based on equation 2.15 whereas B'_g is based on the Lennard-Jones potential. Using this potential for the CO_2-CO_2 interaction in the sieve to evaluate B' reduces the values as shown in table 6.8 but has no discernible effect on the final heats of adsorption obtained.

V_o and B' both exhibit large temperature variations so the gradients dV_o/dT, dB'/dT and dB'_g/dT were obtained by fitting the data to the relationship

$$\ln Y = A + B \ln T$$

and obtaining the gradients using $dY/dT = BY/T$. The range of temperatures chosen were those over which the theoretical isotherms were known to be in approximate agreement with Linde data. Heats of adsorption were evaluated at each temperature over a range of pressures for which the quadratic isotherm was applicable. The results at 298°K are given in full in table 6.11 for data taken from run 63 based on

TABLE 6.9

HEATS OF ADSORPTION DATA DERIVED FROM RUN 63

TEMP DEG. K	VO LITRES	B' LITRES/MOLE	$-\frac{dVO}{dT}$	$-\frac{dB'}{dT}$	$\frac{dB'g}{dT}$
573	6.755,-24	3.849,-1	1.768,-25	9.890,-3	6.775,-5
473	2.876,-23	1.533	9.119,-25	4.772,-2	2.394,-4
423	9.156,-23	4.695	3.247,-24	1.634,-1	3.977,-4
373	4.980,-22	2.461, 1	2.003,-23	9.716,-1	6.418,-4
348	1.592,-21	7.743, 1	6.860,-23	3.276	8.181,-4
323	6.725,-21	3.234, 2	3.123,-22	1.474, 1	1.042,-3
298	4.592,-20	2.172, 3	2.311,-21	1.073, 2	1.346,-3
273	5.777,-19	2.678, 5	3.174,-20	1.444, 3	1.754,-3

TABLE 6.10

HEATS OF ADSORPTION DATA DERIVED FROM RUN 61

TEMP DEG. K	VO LITRES	B' LITRES/MOLE	$-\frac{dVO}{dT}$	$-\frac{dB'}{dT}$	$\frac{dB'g}{dT}$
573	5.005,-23	2.565	1.598,-24	8.140,-2	6.775,-5
473	3.427,-22	1.644, 1	1.350,-23	6.396,-1	2.394,-4
423	1.509,-22	7.157, 1	6.529,-23	3.077	3.977,-4
373	1.239,-20	5.794, 2	6.078,-22	2.825, 1	6.418,-4
348	5.071,-20	2.368, 3	2.667,-21	1.237, 2	8.181,-4
323	2.836,-19	1.325, 4	1.607,-20	7.461, 2	1.042,-3
298	2.692,-18	1.258, 5	1.653,-19	7.677, 3	1.346,-3
273	4.963,-17	2.298, 6	3.326,-18	1.531, 5	1.754,-3

Lennard-Jones potentials in the gas phase, and values for $-\delta H$ over the full temperature range for both runs are given in table 6.12.

The results for $-\delta H$ at each temperature follow the same pattern as that given in table 6.11 in which the heat of adsorption is independent of the pressure over the range studied. Values of n/V_o and n_g/V_g are included as a check. These two terms, both being a function of pressure, should always be equal, since if $n = n_g$ then $V_o = V_g$, as V_o can be interpreted as the volume that n moles of gas in the sieve phase would occupy if present in the bulk phase at the same temperature and pressure. The differences at higher pressures are reduced when B'_g is calculated using equation 2.15 to describe the CO_2-CO_2 interaction in the bulk phase..

The results obtained for the heats of adsorption agree well with practical values given in the literature[23,17] for CO_2/5A adsorption at 25°C. These workers found that $-\delta H$ was a function of pressure when studied over a wider range of pressures than was possible in this work. Their values ranged from 12 to 10 kcal/mole for concentrations from zero up to 2 mmole CO_2/gram adsorbent. These values may be compared with the theoretical values of 12.03 and 10.08 kcal/mole at 25°C given in table 6.12. These values are constant over the

TABLE 6.11

CONTRIBUTIONS TO THE HEAT OF ADSORPTION AT 298 DEG. K

(DATA TAKEN FROM RUN 63)

p mm.Hg.	n MOLES/CAGE	n/VO MOLES/LITRE	ng/Vg MOLES/LITRE	δU KCAL/MOLE	pδV KCAL/MOLE	-δH KCAL/MOLE
0.01	2.463,-26	5.365,-7	5.378,-7	9.48	0.59	10.07
0.02	4.915,-26	1.071,-6	1.076,-6	9.48	0.59	10.07
0.04	9.785,-26	2.131,-6	2.151,-6	9.48	0.59	10.07
0.06	1.461,-25	3.181,-6	3.227,-6	9.48	0.59	10.07
0.08	1.938,-25	4.222,-6	4.302,-6	9.48	0.59	10.07
0.1	2.412,-25	5.252,-6	5.378,-6	9.48	0.59	10.07
0.2	4.708,-25	1.025,-5	1.076,-5	9.49	0.59	10.08
0.4	8.954,-25	1.950,-5	2.151,-5	9.49	0.59	10.08
0.6	1.274,-24	2.774,-5	3.227,-5	9.49	0.59	10.08
0.8	1.606,-24	3.498,-5	4.302,-5	9.49	0.59	10.08
1.0	1.892,-24	4.122,-5	5.378,-5	9.49	0.59	10.08
2.0	2.631,-24	5.371,-5	1.076,-4	9.50	0.59	10.09
4.0	6.482,-25	1.412,-5	1.614,-4	9.49	0.59	10.08
5.0	-2.074,-24					

TABLE 6.12

TEMPERATURE VARIATION OF THE HEAT OF ADSORPTION

TEMP	-δH KCAL/MOLE		TEMP	-δH KCAL/MOLE	
DEG. K	RUN 61	RUN 63	DEG. K	RUN 61	RUN 63
573	23.08	19.05	348	14.05	11.77
473	19.42	15.93	323	13.04	10.93
423	17.08	14.29	298	12.03	10.08
373	15.06	12.62	273	11.02	9.24

range 0.05 to 0.5 mmole CO_2/gram adsorbent over which the isotherm is valid at 25°C.

It can be seen from table 6.11 that the $p\delta V$ term in the theoretical expression for $-\delta H$ is small compared with the internal energy term, which in turn is dominated by $RT^2 \frac{d}{dT} \ln V_o$. This indicates that the heat of adsorption is almost entirely derived from the internal energy of the sorbed carbon dioxide molecules, and is hence independent of the bulk pressure at a given temperature which shows why the results are not affected by the formulation of the gas-gas interaction.

6.6 Theoretical Crystal Diffusivities

Equation 2.49 relates the theoretical crystal diffusivity to the ratio of two partition functions when a single carbon dioxide molecule is adsorbed in a sieve cage and translates through an O8 window. Values for the partition functions were taken from runs 60-63. Thus in equation 2.49:

δS is an element of window surface for one point = $(a_o/20)^2$

δV is an element of cage volume for one point = $(a_o/20)^3$

$R = 8.31 \times 10^7$ ergs.deg^{-1}.mole^{-1}

$M = 44$, molecular weight of carbon dioxide.

Using these values gives:

$$D_c = 1.35 \times 10^{-3} \sqrt{T} \times \frac{\sum_3}{\sum_1} \text{ cm}^2/\text{sec.} \qquad 6.6$$

where $\sum_3 = \sum_s \exp(-\phi/kT)$

$\sum_1 = \sum_v \exp(-\phi/kT)$

Values of T, $\sum_1$ and $\sum_3$ and the corresponding values of D_c are given in table 6.13 which covers the full range of variables permitted by the data. Practical work was done on a calcium sieve and the sodium-calcium sieve results are included for comparison.

There is no good agreement between the practical and theoretical diffusivities for the calcium sieve at the three temperatures which they can be compared (see table 6.22). This is not surprising as the theoretical results are based on a very dilute system in which one CO_2 molecule is situated in isolation in a group of sieve cages whereas the practical diffusivities are based on a fully saturated sieve in which up to eight CO_2 molecules can be contained in adjacent cages. Furthermore the comparison is made at temperatures where the molecular potentials are becoming unreliable. The theoretical crystal diffusivities compare better with Wilson's[3] estimate which is of the order of 10^{-8} cm^2/sec

TABLE 6.13

THEORETICAL CRYSTAL DIFFUSIVITIES BASED ON SIEVE POTENTIALS

RUN 60 USES NaCa 1.5+ ION AND OXYGEN POL. = 39.0,-25 CM3.				RUN 62 USES NaCa 1.5+ ION AND OXYGEN POL. = 16.5,-25 CM3.		
TEMP. DEG. K	SIGMA1	SIGMA3	Dc CM2/SEC	SIGMA1	SIGMA3	Dc CM2/SEC
573	3.101,5	9.812	1.025,-6	4.103,4	5.027	4.668,-6
473	2.493,6	2.170,1	2.566,-7	2.044,5	1.184,1	1.701,-6
423	1.284,7	4.307,1	9.314,-8	7.582,5	2.170,1	7.080,-7
373	1.396,8	1.203,2	2.247,-8	5.403,6	5.552,1	2.670,-7
348	7.197,8	2.457,2	8.610,-9	2.147,7	1.072,2	1.257,-7
323	5.557,9	5.943,2	2.595,-9	1.266,8	2.134,2	1.665,-8
298	8.514,10	1.920,3	5.255,-10	1.306,9	7.288,2	1.300,-8
273	3.083,12	8.797,3	6.365,-11	3.107,10	3.059,3	2.106,-9
248	4.539,14	7.042,4	3.208,-12	2.820,12	2.201,4	1.654,-10
223	4.985,17	1.220,6	4.934,-14	1.992,15	3.347,5	3.387,-12
198	1.964,22	7.610,7	7.369,-17	6.299,19	1.775,7	5.353,-15
173	3.965,29	3.380,10	1.514,-21	8.120,26	6.376,9	1.393,-19

RUN 61 USES Ca 1.5+ ION AND OXYGEN POL. = 39.0,-25 CM3.				RUN 63 USES Ca 1.5+ ION AND OXYGEN POL. = 16.5,-25 CM3.		
TEMP. DEG. K	SIGMA1	SIGMA3	Dc CM2/SEC	SIGMA1	SIGMA3	Dc CM2/SEC
573	2.146,5	9.665	1.455,-6	2.897,4	5.837	6.511,-6
473	1.469,6	2.130,1	1.275,-7	1.233,5	1.162,1	2.760,-6
423	6.472,6	4.220,1	1.810,-7	3.026,5	2.135,1	1.560,-6
373	5.312,7	1.175,2	5.767,-8	2.136,6	5.124,1	6.621,-7
348	2.175,8	2.306,2	2.771,-8	6.825,6	1.046,2	3.860,-7
323	1.216,9	5.785,2	1.151,-8	2.881,7	2.369,2	1.093,-7
298	1.154,10	1.865,3	3.766,-9	1.969,8	7.079,2	8.379,-8
273	2.128,11	8.521,3	8.932,-10	2.477,9	2.964,3	2.669,-8
248	1.192,13	6.800,4	1.213,-10	8.646,10	2.125,4	5.225,-9
223	3.287,15	1.173,6	7.194,-12	1.314,13	3.210,5	4.939,-10
198	1.269,19	7.292,7	1.092,-13	2.339,16	1.699,7	1.380,-11
173	3.288,24	3.215,10	1.736,-16	2.138,21	6.064,9	5.036,-14

under similar conditions. As his work is based on the average of a large batch of 5A pellets, the values obtained here based on a single pellet should be more accurate.

It can be seen that the theoretical diffusivities are sensitive to the value of the partition function in the O8 window, since only one grid point has a negative potential here compared with the many in the large cage which give the value of SIGMA 1. Thus any changes in the molecular constants significantly affect the values of the crystal diffusivities. As noted earlier, relaxation of the ion positions is not considered. It seems likely that relaxation of these positions such that the O8 window enlarges during translation would always result in larger values of the window partition function without significantly affecting the large cage partition function. The highest value would be obtained when the ring's free diameter was equal to the value of ρ_e for a carbon dioxide molecule i.e. 5.12 Å. Since the carbon dioxide molecule is larger than the O8 window, which has a free diameter of 3.9 Å between OI oxygen ions and 4.7 Å between OII oxygen ions, relaxation will result in larger values of the crystal diffusivity than those obtained.

6.7 Practical Results

The diffusion of carbon dioxide in a one centimetre Linde 5A molecular sieve bed as described in Chapter 5, was studied at three temperatures. These were ambient, (25°C), 0°C and -25°C. The results obtained were a record of accumulated count (Integral count, IC) over the range of times 0 to 10,000 seconds, together with end point values of the integral count after the pellet had been desorbed by heating.

The runs at each of the three temperatures, designated series 'A', 'B' and 'C' respectively, each consisted of trial runs to measure the amount of deadspace gas in the diffusion cell in the absence of the pellet bed, and then pellet runs to measure the amount of carbon dioxide desorbed from a saturated pellet together with this dead space gas. It was only necessary to do two trial runs at each temperature as the results for these gave good reproducibility. The pellet runs showed more variation, this being up to 4% of the averaged values over several runs given in table 6.18 used for further analysis.

The method of processing the basic practical results to obtain curves of the fraction of carbon dioxide desorbed from the pellet versus square root time is conveniently illustrated by giving the results and derived data in some detail. The following figures and tables are

all for runs series B at $0^{\circ}C$. Corresponding tables at other temperatures are given in Appendix B.

6.7.1 Estimation of the Run Start Time T_o

The times recorded by the camera and at later times by the timer-scaler had to be adjusted to allow for the interval elapsing between starting the timer-scaler and the front of the initial pulse of active gas entering the counter. A run procedure was adopted whereby this time was always about ten seconds. This permitted measurements of the integral count to be made at suitable times such that the recorded values of film time gave deduced values of run time T_r, close to the experimental points required. These as explained in earlier chapters were required at values of T_r such that $\sqrt{T_r}$ increased linearly.

The initial part of each run which was filmed continuously, was plotted as integral count against film time on linear scales (figure 6.6). The straight line obtained represents the pulse of dead space gas at constant activity passing through the counter. This line can be extrapolated back to the time axis, and the intersection gives the value of T_o. This time represents the time the pulse would reach the counter in plug flow. The initial tail to the curve is caused by mixing in the flow line between the diffusion cell and the counter. The gradients of the

FIGURE 6.6

START TIMES FOR RUNS SERIES 'B' AT 0 DEG. C

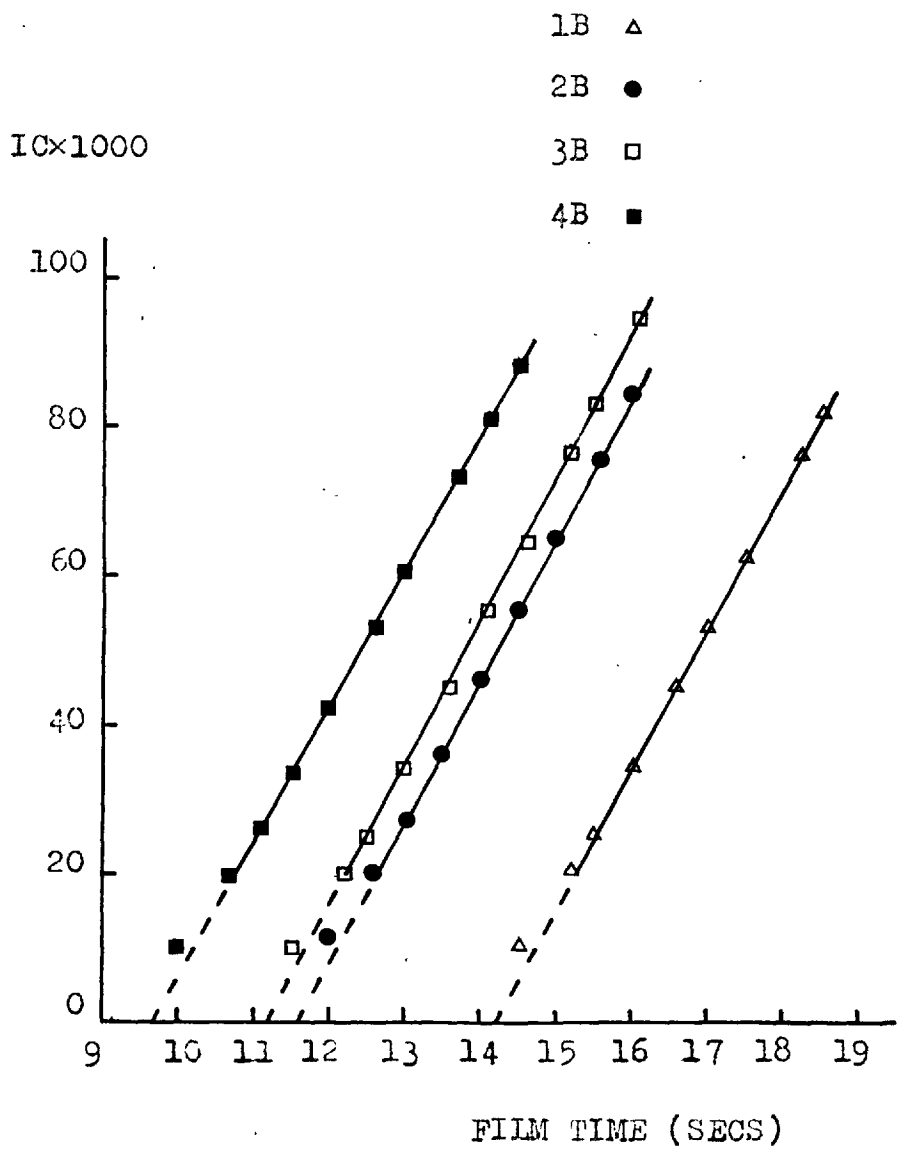

lines should be constant in each series of runs as they represent the initial activity of the gas in the pellet and dead space. The measured values of time T_f can now be converted into run times T_r by subtracting the value T_o from each one.

6.7.2 Background Correction

The background count rate was measured before the start and again at the termination of each run. A check was made that all of the carbon dioxide had been desorbed at the end of a run by comparing the two values obtained, which obviously should not be significantly different. The background count rate was taken to be the average of the two values. The measured values of integral count were corrected for background by subtracting the accumulated background count at time T_f, giving the values IC_r. Tables 6.14-17 give all the measured and deduced results for the four runs reported at $0^{\circ}C$. Plots of IC_r versus $\sqrt{T_r}$ are given in figures 6.7 and 6.8 which clearly show the variation in results from run to run.

The results in tables 6.14-17 and in Appendix B for IC_r in the pellet runs were only reproducible to within 4%. The main reason for this was caused by the carrier gas flow rate failing to rise exactly to

TABLE 6.14

PRACTICAL RESULTS
TRIAL RUN (1B) AT O DEG. C
TO = 14.2 SECS
BACKGROUND = 1.513 c/s

FILM TIME (SECS)	INTEGRAL COUNT	$\sqrt{Tr}$	ICb
14.5	10900		
15.2	20900	1	20876
15.5	25700		
16.0	34600		
16.6	45300		
17.0	53100		
17.5	62900		
18.2	76900	2	76871
18.5	82200		
21.0	123700	2.6	123667
22.0	133000	2.8	132965
23.2	138700	3	138664
24.4	141600	3.2	141562
25.8	143350	3.4	143309
27.2	144237	3.6	144280
28.6	144905	3.8	144860
30.2	145457	4	145409
33.6	146130	4.4	146077
36.2	146477	4.8	146240
46.2	147324	5.7	147249
59.2	147963	6.7	147879
74.2	148532	7.8	148414
91.2	149074	8.8	148930
110.2	149540	9.8	149367
235.2	151723	14.9	151453
410.2	153347	19.9	152702
635.2	154516	25	153516
910.2	155382	30	153950
1235.2	156104	35	154159
1610.2	156770	40	154235
2035.2	157562	45	154362
2510.2	158323	50	154373
3035.2	159190	55	154430
3610.2	160123	60	154443
4235.2	161104	65	154444
4910	162143	70	154413
5635	163290	75	154590
6410	164495	80	154415
7235	165752	85	154372
8110	167094	90	154244
9035	168570	95	154350
10010	170112	100	154362

TABLE 6.15

PRACTICAL RESULTS
TRIAL RUN (2B) AT O DEG. C
TO = 11.6 SECS
BACKGROUND = 1.553 c/s

FILM TIME (SECS)	INTEGRAL COUNT	$\sqrt{Tr}$	ICb
12.0	11900		
12.6	20400	1	20380
13.0	27200		
13.5	36500		
14.0	46200		
14.5	55200		
15.0	65300		
15.6	76700	2	76676
16.0	84700		
18.4	123500	2.6	123471
19.4	132800	2.8	132770
20.6	138500	3	138468
21.8	141400	3.2	141366
23.2	143260	3.4	143224
24.6	144240	3.6	144202
26.1	144940	3.8	144899
27.6	145437	4	145394
31.8	146311	4.5	146262
36.6	146864	5	146807
46.6	147599	5.9	147527
59.6	148250	6.9	148547
74.6	148759	7.9	148643
90.6	149460	9.3	149305
111.6	149764	10	149591
235.6	151875	15	151509
410.6	153542	20	152749
635.6	154732	25	153717
925.6	155585	30.2	154148
1235.6	156246	35	154327
1625.6	156988	40.1	154463
2035.6	157663	45	154502
2510.6	158447	50	154548
3034.6	159316	55	154603
3600.6	160230	60	154623
4235.6	161240	65	154662
4910.6	162307	70	154680
5635.6	163457	75	154704
6410	164656	80	154701
7235	165915	85	154679
8120	167231	90	154620
9035	168654	95	154623
10010	170139	100	154593

TABLE 6.16

PRACTICAL RESULTS
PELLET RUN (3B) AT 0 DEG. C
TO = 11.2 SECS
BACKGROUND = 1.583 c/s

FILM TIME (SECS)	INTEGRAL COUNT	$\sqrt{Tr}$	ICr
11.5	10200		
12.2	20200	1	20181
12.5	24900		
13.0	34100		
13.6	45000		
14.1	55100		
14.6	64400		
15.2	77100	2	77076
15.5	83200		
16.1	94600		
18.0	123100	2.6	123072
19.0	132800	2.8	132770
20.2	139200	3	139168
21.4	142550	3.2	142516
22.8	144480	3.4	144444
24.2	145620	3.6	145582
25.6	146470	3.8	146429
27.2	147130	4	147087
31.4	148380	4.5	148330
36.2	149380	5	149323
46.2	150984	5.9	150911
59.2	152725	6.9	152631
74.2	154510	7.9	154393
91.2	156307	8.9	156163

FILM TIME (SECS)	INTEGRAL COUNT	$\sqrt{Tr}$	ICr
110.2	158057	9.9	157883
235.2	167111	15	166739
410.2	175524	20	174875
635.2	183162	25	182156
910.2	190179	30	188738
1235.2	196896	35	194941
1621.2	201951	40.1	199400
2035.2	209673	45	206451
2530.2	216057	50.1	212052
3051.2	221848	55.1	217018
3610.2	227247	60	221532
4235.2	232391	65	225687
4910.2	237179	70	229406
5635.2	241562	75	232641
6490.2	246020	80.3	235746
7235	249220	85	237767
8110	252436	90	239598
9035	255390	95	241088
10010	258046	100	242200
10510	260000	102.4	243362
11050	264300	105	246808
11570	265419	107.6	247103
12110	266249	110	247079
13210	267965	114.9	247054

TABLE 6.17

PRACTICAL RESULTS
PELLET RUN (4B) AT 0 DEG. C
TO = 9.7 SECS
BACKGROUND = 1.555 c/s

FILM TIME (SECS)	INTEGRAL COUNT	$\sqrt{Tr}$	ICr
10.0	10200		
10.7	20000	1	19983
11.1	26300		
11.5	33200		
12.0	42200		
12.6	53000		
13.0	60500		
13.7	73500	2	73479
14.1	81200		
14.5	88600		
16.5	123900	2.6	123874
17.5	133900	2.8	133873
18.7	140500	3	140471
19.9	143300	3.2	143269
21.3	145000	3.4	144967
22.7	146020	3.6	145985
24.1	146740	3.8	146703
25.7	147300	4	147260
29.9	148600	4.5	148554
34.7	149560	5	149506
45.7	151270	6	151199
59.7	152968	7.1	152875
73.7	154455	8	154340
90.7	156030	9	155889

FILM TIME (SECS)	INTEGRAL COUNT	$\sqrt{Tr}$	ICr
109.7	157640	10	157469
234.7	165684	15	165319
409.7	173421	20	172784
634.7	180648	25	179661
909.7	187324	30	185909
1234.7	193769	35	191849
1609.7	199975	40	197472
2034.7	206332	45	203168
2509.7	212510	50	208607
3204.7	218327	55	213623
3609.7	223796	60	218183
4234.7	228976	65	222391
4909.7	233591	70	225956
5634.7	237808	75	229046
6409.7	241799	80	231832
7235	245387	85	234137
8110	248556	90	235945
9035	251517	95	237468
10010	254130	100	238564
10610	255880	102.5	239537
11010	260170	104.9	243049
11510	261622	107.2	243724
12120	262603	110	243756
13210	264282	114.9	243740

FIGURE 6.7

VARIATION OF ICb AND ICr WITH $\sqrt{Tr}$ AT 0 DEG. C

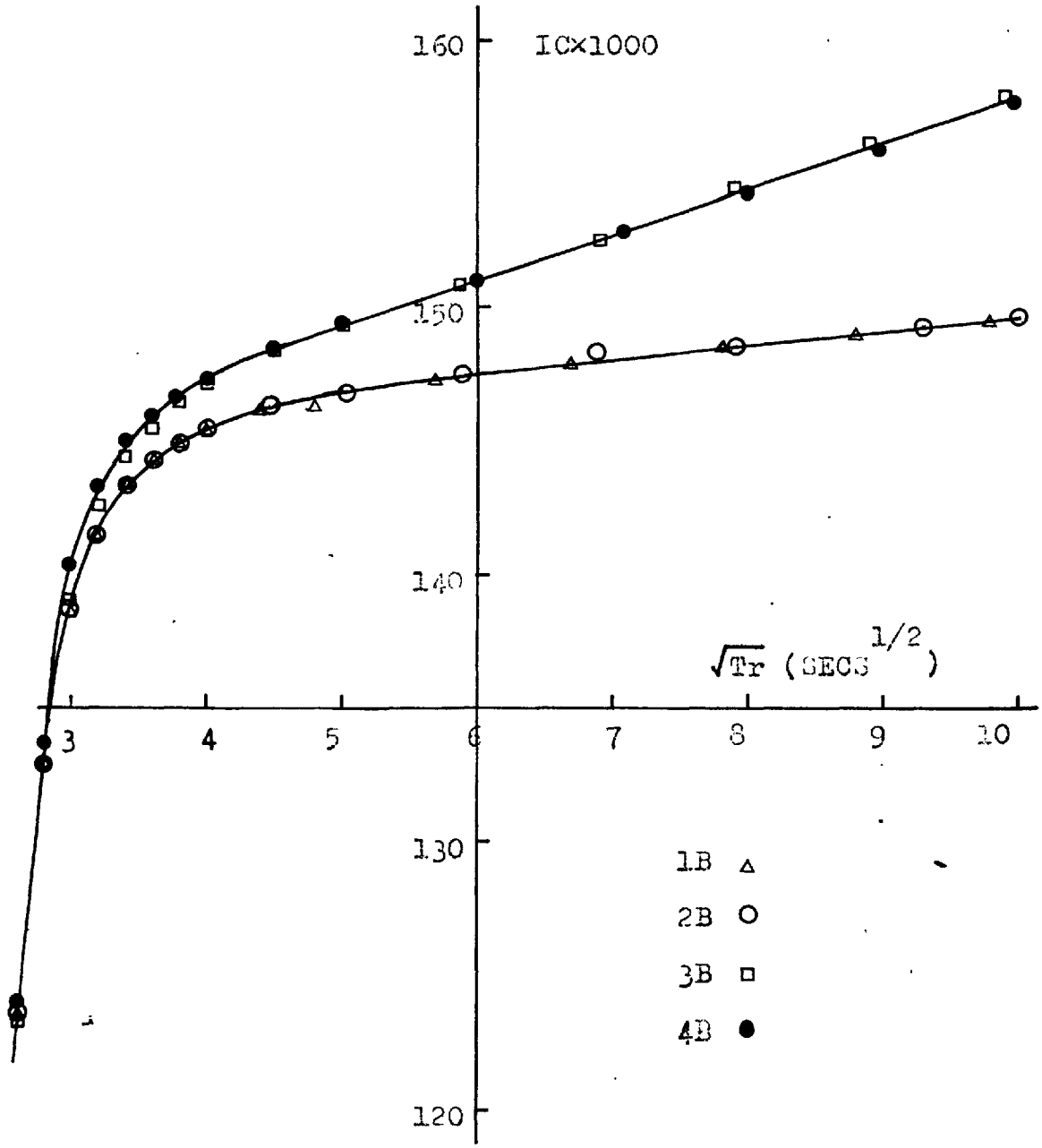

FIGURE 6.8

VARIATION OF ICb AND ICr WITH $\sqrt{Tr}$ AT 0 DEG. C

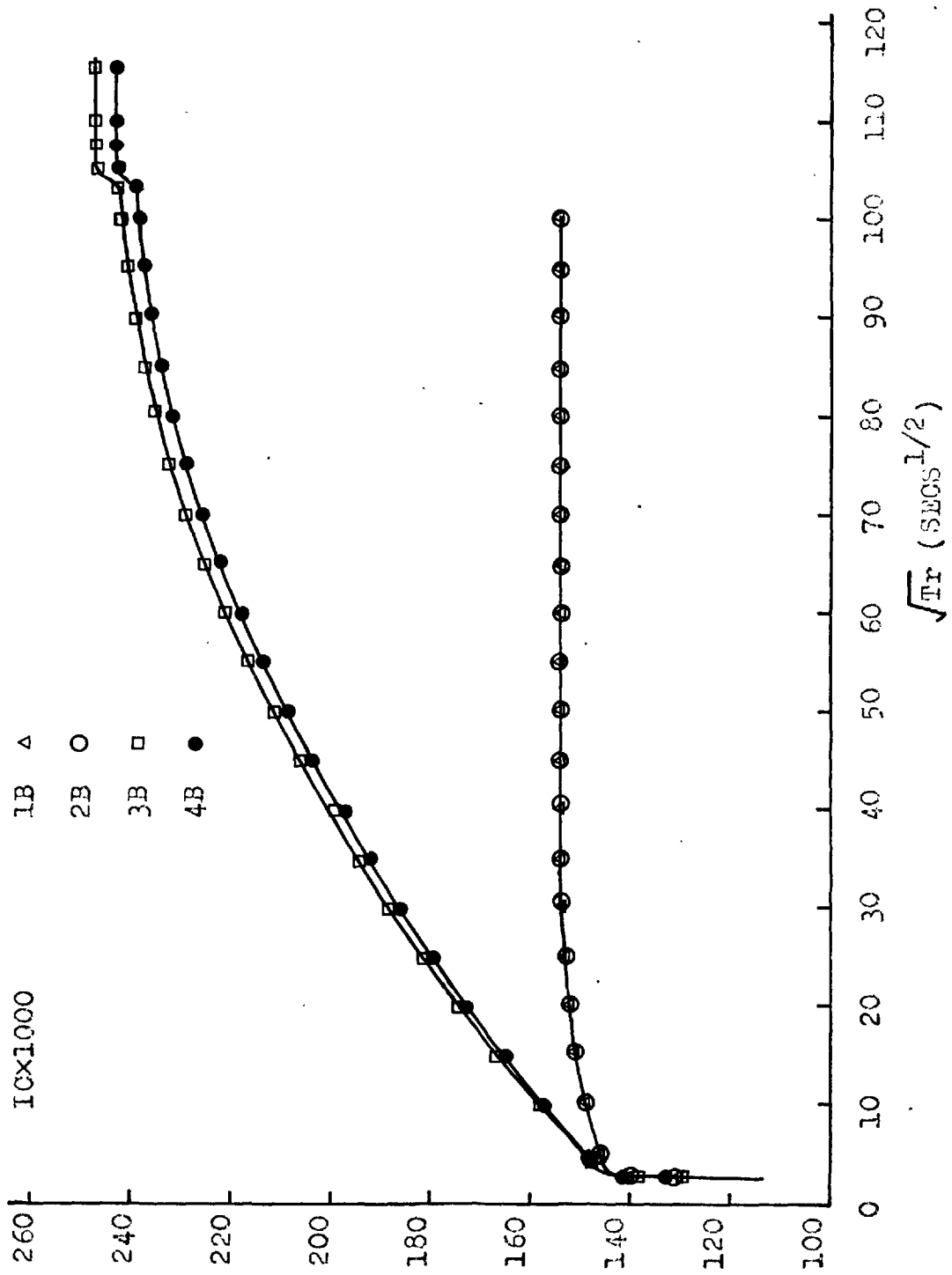

its preset value of 100 cc./min. at the start of counting, and a drift of up to 5% about this value at later times which was corrected when noticed. Pre-mixing of carrier gas in the cooling coil and active gas in the diffusion cell dead space at the start of counting was unpredictable and also affected reproducibility. These two sources of error have opposite effects on the final values of IC_r, the first giving higher values and the second lower values than would be obtained in the absence of these errors. No control could be exercised over the carrier gas flow rate from the time it had been preset, up till the end of the continuous filming stage of the scaler output, and runs were discarded which failed to start with the correct flow rate. This occurred most often in the pellet runs since at least one hour elapsed between presetting the carrier gas flow rate and saturating the pellet with active gas, as compared with about ten minutes in the trial run.

As explained in Chapter 5, every effort was made to reduce carrier gas - active gas premixing in the diffusion cell. When this did occur as shown by a low initial dead space activity, then the runs were discarded. The runs reported may still be subject to this error in a small degree as shown by the variation in the initial gas activity, (figure 6.6), but there is no simple means of quantitatively estimating the

resulting error in IC_r.

The trial runs were reproducible to within 1%. This improvement over the pellet runs was expected because the carrier gas flow rate always tended to rise to its correct preset value on the runs and little pre-mixing of active and carrier gas occurred in the diffusion cell.

6.7.3 The Fraction of Carbon Dioxide Desorbed from the Pellet

The results for IC_r were averaged for each value of $\sqrt{T_r}$ for the trial and pellet runs to give two sets of results at each temperature studied. In cases where the values of $\sqrt{T_r}$ did not coincide with the values required for further analysis, linear interpolation was used to obtain an intermediate result. The average values of IC_r given in table 6.18 were converted to the fraction of carbon dioxide desorbed at time $\sqrt{T_r}$ using the relationship:

$$FRAC = \frac{IC_{rt} - IC_{bt}}{IC_{r\infty} - IC_{b\infty}}$$

where IC_{rt} and IC_{bt} are the values of the integral count at time t for the pellet and trial runs respectively, and $IC_{r\infty}$ and $IC_{b\infty}$ are the corresponding values at the end point. The three unsmoothed curves obtained are given in figure 6.9. The differencing method used to obtain values of FRAC tends to cancel out any systematic errors in each

TABLE 6.18

AVERAGED VALUES OF ICb AND ICr FOR GIVEN VALUES OF $\sqrt{Tr}$

	RUNS SERIES A (25 DEG. C)		RUNS SERIES B (0 DEG. C)		RUNS SERIES C (-25 DEG. C)	
$\sqrt{Tr}$	ICb	ICr	ICb	ICr	ICb	ICr
1	25879	26712	20628	20082	18932	19682
2	100375	99840	76774	75278	74827	72744
3	175267	177232	138566	139820	137669	138286
4	181932	185802	145402	147174	145456	146872
5	183454	189162	146709	149415	146992	149012
6	184311	191831	147526	151124	148061	150488
7	184987	194283	148114	152820	148331	151844
8	185665	196612	148612	154422	148780	153506
9	186252	198744	149120	156124	149225	154277
10	186833	201020	149523	157694	149696	155576
15.2	189358	211088	151500	166236	154533	162325
20	191315	219681	152815	173830	152853	169169
25.1	192298	228496	153600	181038	153874	176502
30	192595	236364	154092	187324	154405	183496
35.1	192803	244330	154305	193456	154657	190633
40	192872	251759	154366	198391	154776	197070
45	192938	259248	154432	204810	154828	203396
50	192968	266272	154461	210230	154849	208941
55	192974	272700	154517	215070	154844	214460
60	192960	278572	154533	219858	154835	219649
65	193073	283767	154553	224039	154856	224274
70	193077	288338	154547	227681	154892	228848
75	193098	292031	154647	230844	154954	232921
80	193120	295178	154558	233735	154944	236107
85	193151	297676	154526	235952	154981	238919
90	193204	299627	154432	237772	154947	241277
95	193203	301171	154487	239278	154924	243232
100	193190	302367	154478	240382	154923	244781
INF	193204	307168	154477	245400	154950	252700

set of runs, so long as the initial part of each curve representing the dead space activity is constant. The runs analysed are those with as similar initial curve shape as possible.

Discrepancies such as the value of IC_r decreasing towards the end of a run were caused by using the average of the background count rates measured before and after each run. Thus it is possible that the mean background rate exceeds the final measured rate. The reason for the differences in measured background rates was not resolved, since the final rate tended to be smaller than the initial rate, not greater as would occur if the pellet had not been completely desorbed. The difference could have been caused by a drift in the counter settings. In any event the difference in background rates was less than 1% and is equivalent to 150 counts accumulated after 10,000 seconds, or 0.06% of the final values of IC_r. This error is less than the variation of count rate during runs which causes the long term fluctuations in the practical breakthrough curves as compared with the smooth theoretical curves given in figures 6.10-14.

6.7.4 . Practical Pellet Porosity

If it is assumed that the Linde 5A sieve comprises 80% crystals by weight, density 1.56 grams/cc., bound together with 20% by weight

FIGURE 6.9

PRACTICAL RESULTS FOR CO2 DIFFUSION IN A ONE DIMENSIONAL LINDE 5A SIEVE PELLET

MEAN RESULTS FOR RUNS AT 25.0 DEGREES CELSIUS ⊕

MEAN RESULTS FOR RUNS AT 0.0 DEGREES CELSIUS △

MEAN RESULTS FOR RUNS AT -25.0 DEGREES CELSIUS +

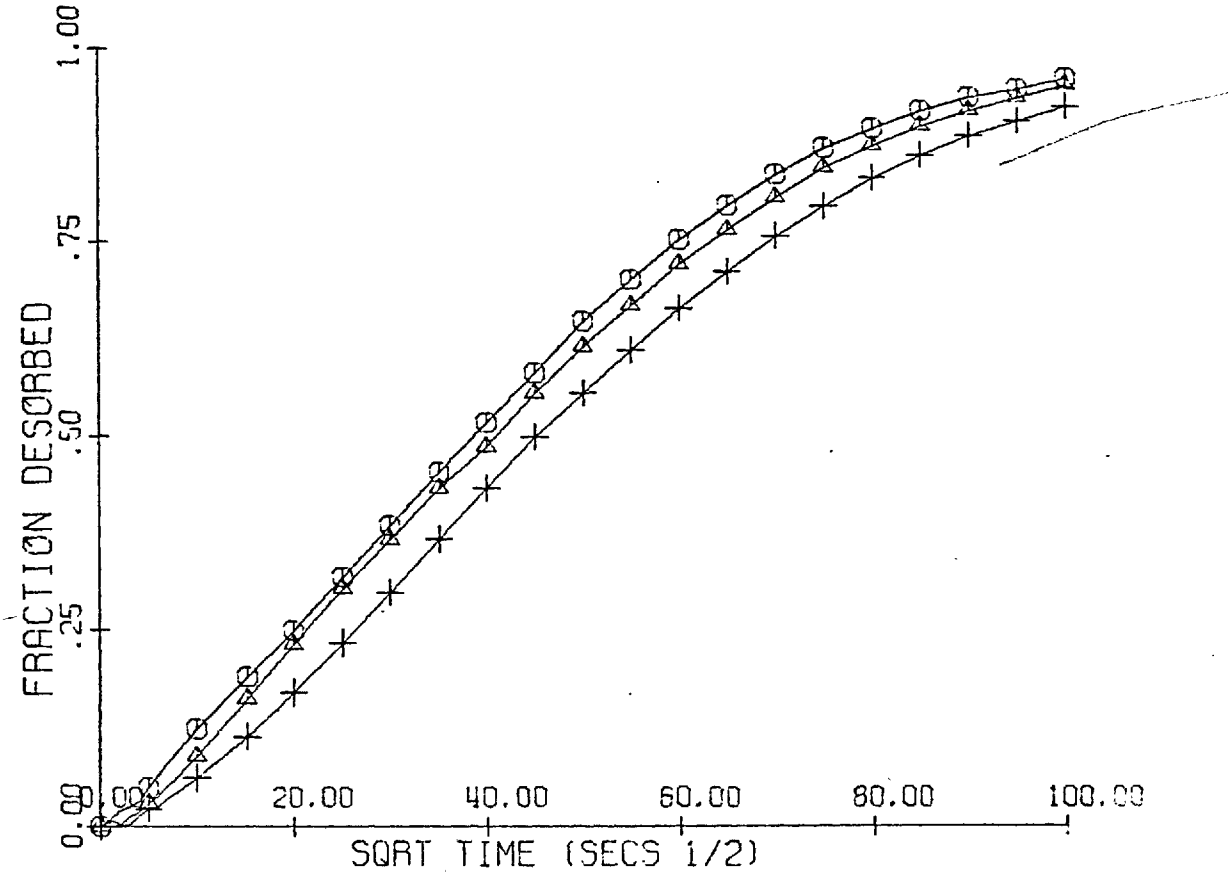

of an inert clay binder, density 2.6 grams/cc.[2] and adsorbs 27.5 weight per cent of water at 25°C and 1 atm.,[18] then it is possible to estimate the pellet porosity from the measured density of the sieve used in the experiment. Using the above figures the theoretical wet density of the sieve assuming zero porosity is 2.07 grams/cc. The measured wet density is 1.29 grams/cc. Thus the apparent porosity of the sieve is:

$$E_p = 1 - \frac{1.29}{2.07} = 0.375$$

6.7.5 Practical K Values

A value for the equilibrium isotherm constant K can be calculated at each of the three temperatures studied from the volume of carbon dioxide in the diffusion cell dead space and the values of IC_∞ for the trial and pellet runs.

Table 6.19 shows the volumes of carbon dioxide at 25°C, 1 atm. admitted to the diffusion cell in each run, together with the corresponding values of IC_∞ and the average values at each temperature.

At 0°C the ratio $IC_{r\infty}/IC_{b\infty}$ is 1.59 (table 6.20). Since the average volume of carbon dioxide admitted in the trial runs was 14.6cc. then the average volume of carbon dioxide adsorbed by the sieve in the pellet runs at 0°C is (1.59 x 14.6) - 14.6 = 8.55 cc. The burette readings indicate that 8.3 cc were admitted which checks with the derived

TABLE 6.19

INTEGRAL COUNTS (IC) AT INFINITE TIME

RUN NUMBER	VOLUME OF CO_2 IN CELL cc AT 25 C. AND 1 ATM.	IC AT INFINITE TIME	AVERAGE VOLUME OF CO_2 IN CELL cc.	AVERAGE IC_∞
1A	13.2	192889	13.2	193204
2A	13.2	193491		
3A	21.5	306901		
4A	20.3	300826	20.9	307168
5A	21.1	313777		
1B	14.5	154362	14.6	154477
2B	14.7	154593		
3B	22.8	247054	22.9	245400
4B	23.1	243740		
1C	16.4	154828	16.2	154950
2C	15.8	155018		
3C	25.3	252772		
4C	25.7	255278	25.4	252700
5C	25.2	250047		

TABLE 6.20

PRACTICAL K VALUES AND COMPARISON WITH LINDE DATA

RUN TEMPERATURE (DEG. C)	25	0	-25
VOLUME OF CO_2 IN CELL (TRIAL RUNS) cc. AT 25 C AND 1 ATM.	13.2	14.6	16.2
ICb_∞ / ICr_∞	1.59	1.59	1.63
VOLUME OF CO_2 ADSORBED BY THE SIEVE PELLET cc. AT 25 C AND 1 ATM.	7.8	8.55	10.2
WEIGHT PERCENT CO_2 ADSORBED	18.5	20.25	23.7
PRACTICAL K VALUES	166.3	167.2	181.8
WEIGHT PERCENT CO_2 ADSORBED (LINDE DATA)	18.9	19.6	

value. The former is taken to be more accurate since the practical method used subjects the burette readings in the pellet runs to more sources of error than in the trial runs.

Now 8.55 cc of carbon dioxide measured at 25°C and 1 atm. is equivalent to

$$\frac{44 \times 8.55 \times 273}{22.4 \times 298} = 15.38 \text{ mg. } CO_2$$

Assuming that the 5A sieve adsorbs 27.5 weight per cent of water at 25°C and 1 atm.,[18] and given the mass of wet sieve used as 97 mg and its volume as 0.075 cc. then the dry sieve mass is 76 mg. Hence 76 mg. of 5A sieve adsorb 15.38 mg of carbon dioxide, or 20.25 weight per cent at 0°C and 1 atm. For comparison, the Linde data sheets give a value of 19.6 wt% adsorption under the same conditions.

The carbon dioxide concentration in the crystals is

$$\frac{8.55 \times 273}{22400 \times 298 \times 0.075 \times 0.625} = 7.46 \times 10^{-3} \text{ gram mole/cc.}$$

which assumes that all of the carbon dioxide resides inside the crystals, whose volume is $0.075 \times (1-E_p)$ cc.

The gas concentration in the pores surrounding the crystals is the same as in the free gas and is

$$\frac{1}{22400} = 4.46 \times 10^{-5} \text{ gram moles/cc.}$$

at $0^{\circ}C$ 1 atm.

Hence the equilibrium isotherm constant K is given by

$$K = \frac{\text{Solid concentration}}{\text{Gas concentration}} = 167.2 \text{ at } 0^{\circ}C \text{ 1 atm.}$$

The results obtained at the three temperatures studied are given in table 6.20 together with Linde adsorption isotherm data for comparison.

Another source of error is shown by the variation in the amount of carbon dioxide adsorbed by the pellet before each run as shown in table 6.19. This could be caused by fluctuations in the cryostat temperature or more likely by a progressive change in the pellet sorption capacity caused by overheating the pellet in the regeneration procedure used to desorb the pellet. If any severe overheating occurs the sieve structure changes, and in any event the initial regeneration of the sieve even at $300^{\circ}C$ as used in this work causes a permanent change in structure which then determines the sorption properties of the sieve.[21] These properties then remain constant so long as the initial regeneration temperature is not exceeded in subsequent regenerations.

6.8 The Diffusion Model

The effect of the pore and crystal diffusivities were investigated before the diffusion model described in section 2.7 was fitted to the practical breakthrough curves. Table 6.21 gives the values of the parameters used in the dimensionless groups and the equations defining the model.

Firstly the model was used to predict curves for a pore diffusion process by setting D_c to infinity; hence from equation 2.58a $P = 0$. The pore diffusivity was varied from 0.02 $cm^2/sec.$ down to 0.005 $cm^2/sec.$ and a set of breakthrough curves obtained, shown in figure 6.10. All the curves are initially straight line plots of the form predicted by equation 3.16 with a suitably chosen diffusivity. It can be seen that the pore diffusivity affects only the slope of each successive curve.

The effect of the crystal diffusion process was then studied by varying P from 0 to 200 with the pore diffusivity held at 0.015 cm^2/sec, and a new set of breakthrough curves obtained, shown in figure 6.11. This shows that increasing the controlling effect of the crystal diffusion process does not significantly affect the slope of the breakthrough curve, but successively displaces it so that the curve becomes more sigmoid as D_c decreases. However, the gaussian elimination used to solve the matrix of crystal concentrations over one time step was subject to large

TABLE 6.21

DATA FOR THE THEORETICAL DIFFUSION MODEL

PELLET LENGTH	L = 1.03 CM.
PELLET POROSITY	Ep = 0.375
MEAN CRYSTAL RADIUS	R = 0.0001 CM.
TIME INCREMENTS	δt = 1 AND 10 SECS.
END TIME FOR RUNS	TIMAX = 10000 SECS.
NUMBER OF PELLET INCREMENTS	= 6
NUMBER OF CRYSTAL INCREMENTS	= 6
RELATIVE ERROR IN PORE CONCENTRATION	= 0.0001
RELAXATION PARAMETER	BETA' = 0.88

TABLE 6.22

PORE AND CRYSTAL DIFFUSIVITIES OBTAINED FROM PRACTICAL WORK

TEMP DEG. C	FITTED Dp CM2/SEC	FITTED Dc CM2/SEC	MEAN SQUARE ERROR
25	0.0148	8.83,-12	2.223,-5
0	0.0138	3.96,-13	5.575,-5
-25	0.0146	8.54,-13	1.814,-4

FIGURE 6.10

THEORETICAL SOLUTION FOR CO2 DIFFUSION IN A ONE DIMENSIONAL LINDE 5A SIEVE PELLET

RESULTS AT 0.0 DEGREES CELSIUS

--INFINITE CRYSTAL DIFFUSIVITY

VARIABLE PORE DIFFUSIVITY

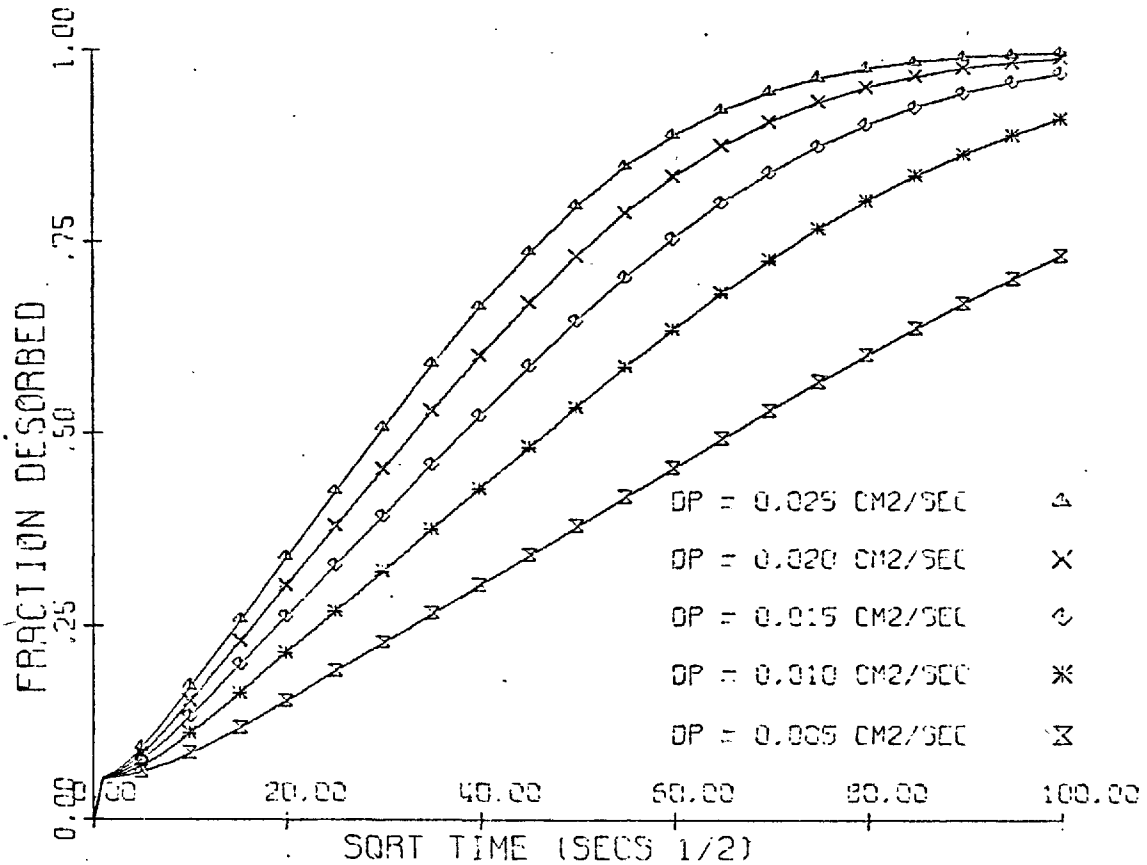

FIGURE 6.11

THEORETICAL SOLUTION FOR CO2 DIFFUSION IN A ONE DIMENSIONAL LINDE 5A SIEVE PELLET

RESULTS AT 0.0 DEGREES CELSIUS

PORE DIFFUSIVITY = 0.015 CM2/SEC

VARIABLE CRYSTAL DIFFUSIVITY

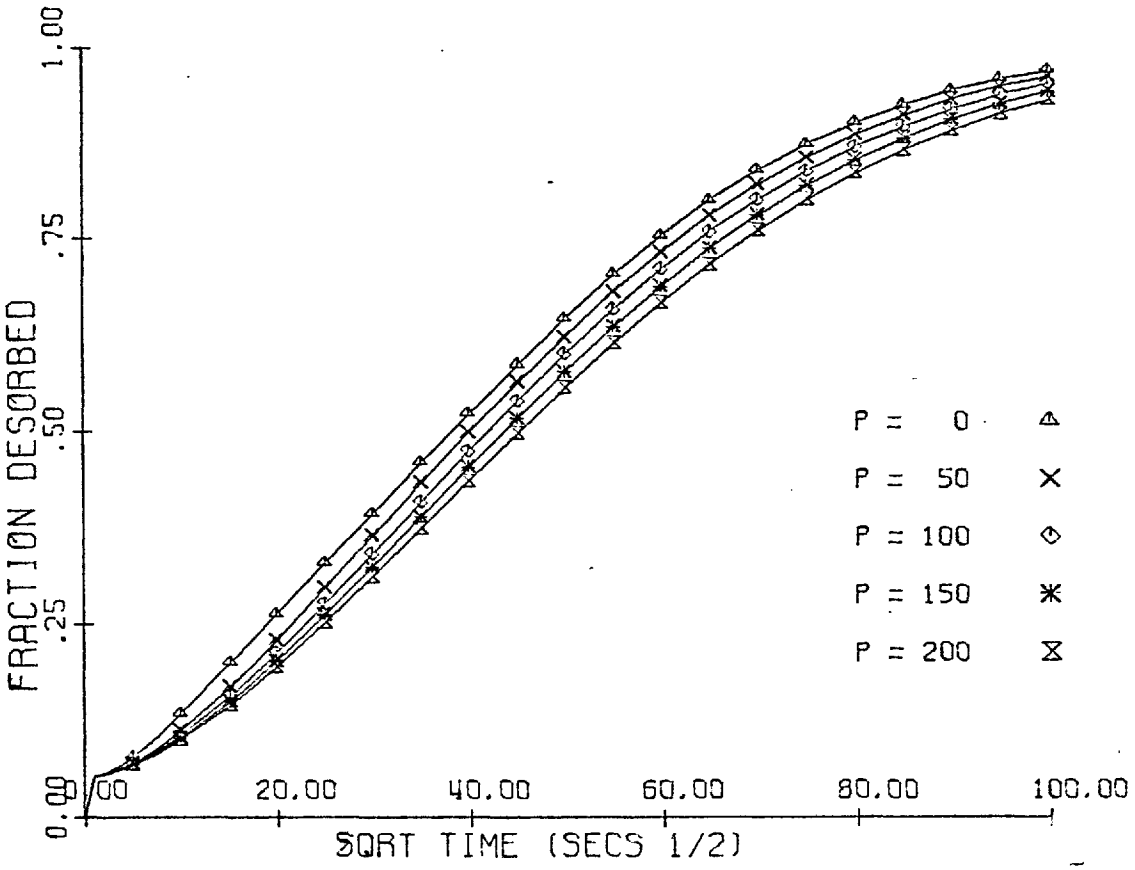

FIGURE 6.12

THEORETICAL SOLUTION FOR C02 DIFFUSION IN A ONE DIMENSIONAL LINDE 5A SIEVE PELLET

PRACTICAL RESULTS AT 25.0 DEGREES CELSIUS ⊙

THEORETICAL-RESULTS AT 25.0 DEGREES CELSIUS ————

WITH PORE DIFFUSIVITY = 0.0148 CM2/SEC.

AND CRYSTAL DIFFUSIVITY = 0.883E-11 CM2/SEC.

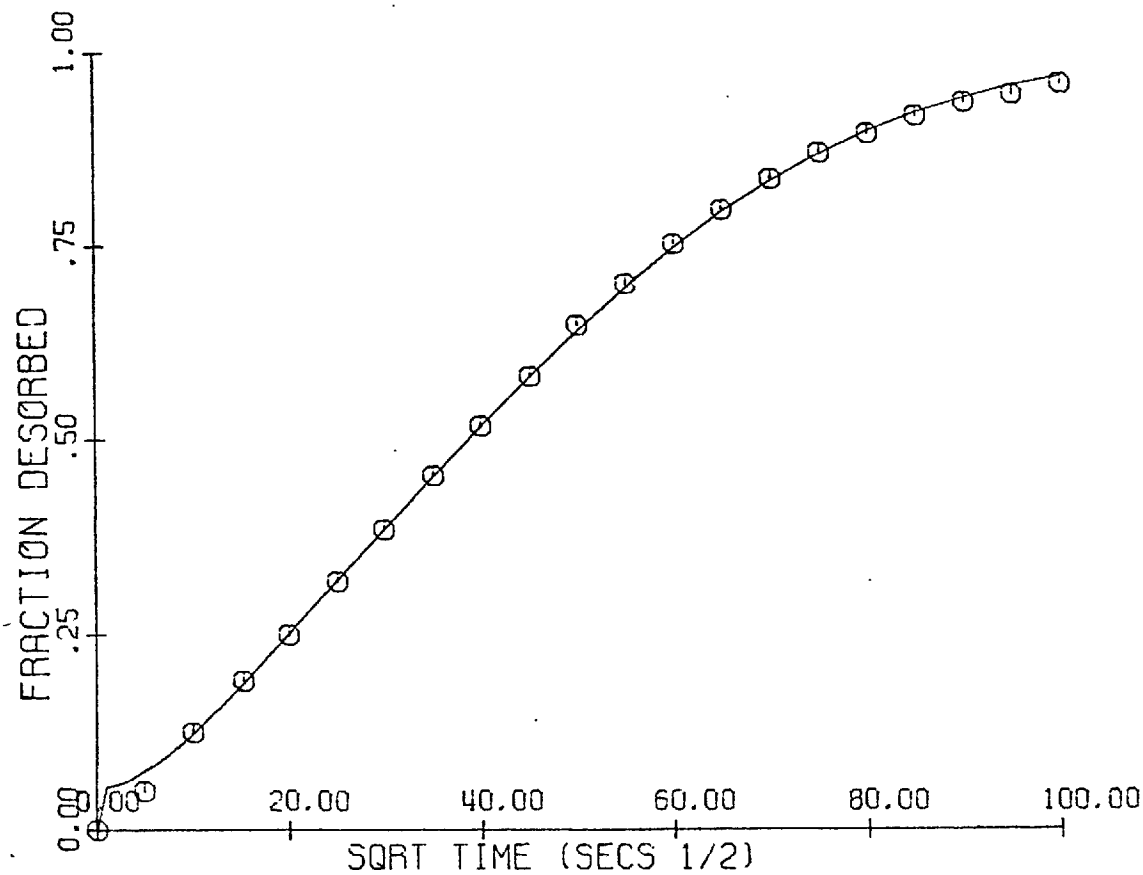

FIGURE 6.13

THEORETICAL SOLUTION FOR CO2 DIFFUSION IN A ONE DIMENSIONAL LINDE 5A SIEVE PELLET

PRACTICAL RESULTS AT 0.0 DEGREES CELSIUS △

THEORETICAL RESULTS AT 0.0 DEGREES CELSIUS ——————

WITH PORE DIFFUSIVITY = 0.0138 CM2/SEC.

AND CRYSTAL DIFFUSIVITY = 0.396E-12 CM2/SEC.

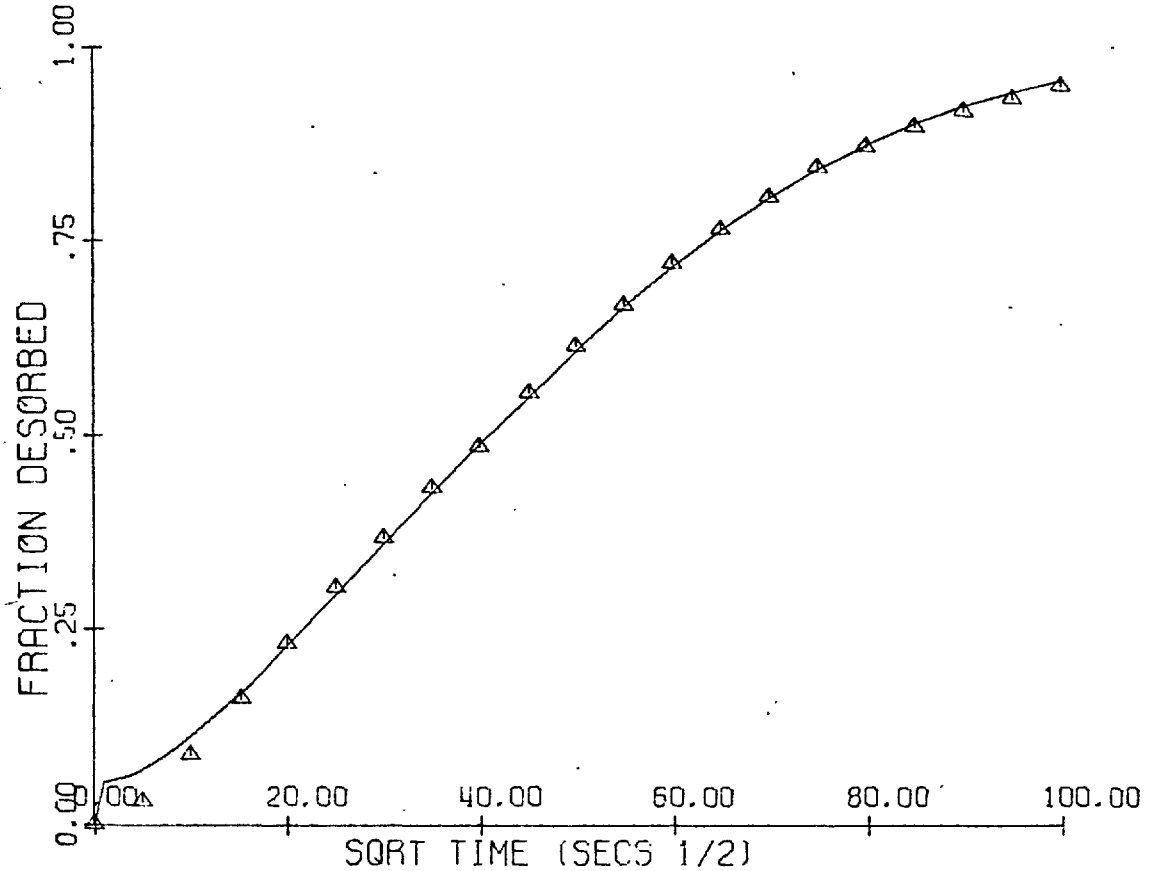

FIGURE 6.14

THEORETICAL SOLUTION FOR CO2 DIFFUSION IN A ONE DIMENSIONAL LINDE 5A SIEVE PELLET

PRACTICAL RESULTS AT -25.0 DEGREES CELSIUS ×

THEORETICAL RESULTS AT -25.0 DEGREES CELSIUS ————

WITH PORE DIFFUSIVITY = 0.0145 CM2/SEC.

AND CRYSTAL DIFFUSIVITY = 0.854E-12 CM2/SEC.

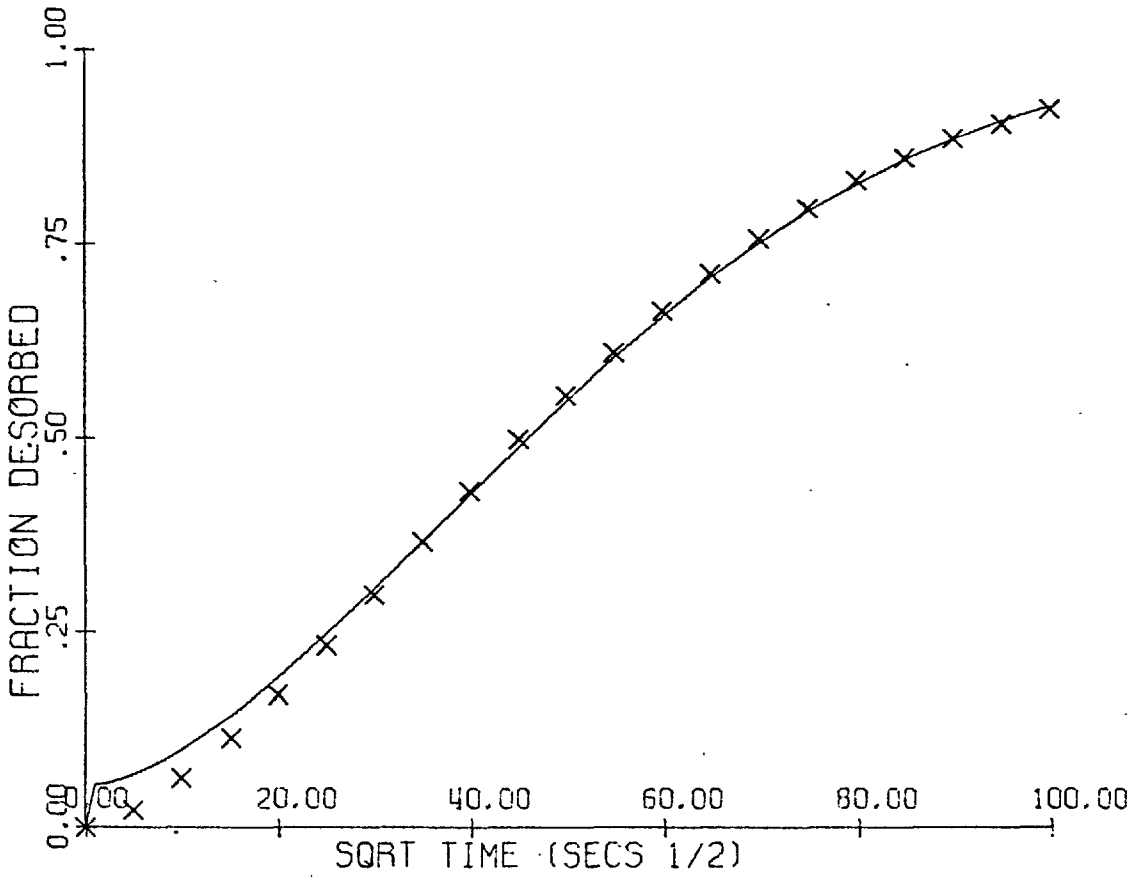

rounding errors when P was close to zero, corresponding to a large but non infinite crystal diffusivity. This rounding error disappeared when P was larger than about 20.

Comparing these results with the shape of the practical curves enabled initial guesses to be made for the diffusivities which would give the approximate slope and displacement required. The model was fitted to the practical results using the techniques described in sections 2.7 and 3.5 and the 'best fitting' diffusivities obtained. These are given in table 6.22 and the practical and theoretical curves at each temperature are compared in figures (6.12-14).

6.8.1 Definition of Pellet Diffusivities and Tortuosity

In a pore diffusion process the diffusion coefficient can be defined in several ways. A pore diffusivity D_p can be defined by:

$$D_p \frac{\partial^2 v}{\partial x^2} = E_p \frac{\partial v}{\partial t} + (1-E_p)K \frac{\partial v}{\partial t} \qquad 6.7$$

An overall diffusivity D_T can be defined by:

$$D_T \frac{\partial^2 v}{\partial x^2} = \frac{\partial v}{\partial t} + \left(\frac{1-E_p}{E_p}\right)K \frac{\partial v}{\partial t} \qquad 6.8$$

and an effective diffusivity by:

$$D_e \frac{\partial^2 v}{\partial x^2} = \frac{\partial v}{\partial t} \qquad 6.9$$

From equations 6.7-9 it follows that :

$$D_e = \frac{D_p}{E_p + (1-E_p)K} = \frac{E_p D_T}{E_p + (1-E_p)K} \qquad 6.10$$

The bulk gas diffusivity D_g is related to D_T by

$$D_g = T\, D_T \qquad 6.11$$

where T is the tortuosity of the system.

6.8.2 Practical Pellet and Crystal Diffusivities

The diffusivities and tortuosities based on equations 6.7-11 given in table 6.23 were calculated from the pore diffusivities in table 6.22.

Equation 3.16 which is a solution of equation 6.9 was also fitted to the practical results to see how well they could be approximated by a pore diffusion process, and also to the theoretical curves at $0^{\circ}C$ for pore diffusion, as a cross check on the model. Tables 6.24 and 6.25 give the diffusivities obtained.

TABLE 6.23

PELLET DIFFUSIVITIES DERIVED FROM PRACTICAL RESULTS

TEMP DEG. C	Dp CM2/SEC	De CM2/SEC	DT CM2/SEC	Dg CM2/SEC	TORTUOSITY T
25	0.0148	1.42,-4	0.0395	0.0729	1.85
0	0.0138	1.32,-4	0.0368	0.0675	1.83
-25	0.0146	1.28,-4	0.0389	0.0617	1.59

TABLE 6.24

EFFECTIVE DIFFUSIVITIES USING A PORE DIFFUSION MODEL FITTED TO PRACTICAL RESULTS

TEMP DEG. C	De (EQ 3.16) CM2/SEC	MEAN SQUARE ERROR
25	1.38,-4	4.15,-5
0	1.24,-4	1.56,-4
-25	1.00,-4	6.33,-4

TABLE 6.25

COMPARISON OF EFFECTIVE DIFFUSIVITIES FOR A PORE DIFFUSION PROCESS FITTED TO FIGURE 6.10

De (MODEL) CM2/SEC	De (EQ 3.16) CM2/SEC	MEAN SQUARE ERROR
2.38,-4	2.38,-4	5.77,-5
1.91,-4	1.91,-4	2.12,-6
1.43,-4	1.43,-4	1.29,-5
9.50,-5	9.60,-5	2.17,-5
4.80,-5	4.80,-5	4.53,-5

The values of the practical diffusivities given in table 6.22 depend to a large extent on the value of the porosity factor used. A value of O.375 was calculated for the pellet used in this work, whereas Dworjanyn[2] calculated a value of O.29 based on a batch of 4A pellets and Wilson[3] used the value of O.35 for 5A pellets. The other 'unknown' which only affects the values of the crystal diffusivity is the mean crystal radius. This was assumed to be one micron, and electron microscope photographs of 5A pellet replicas and pure crystals showed that this was substantially true. These photographs also showed that crystal agglomeration which occurs to a large extent in the pure crystals also appears to occur in the pellets, and may invalidate the assumption that each crystal in the pellet is isolated from its neighbours.

The effective diffusivities given in table 6.23 were calculated using practical K values rather than those inferred from the Linde data sheets. The practical values apply strictly to the pellet bed used rather than to the average value of a batch of pellets, though the differences as indicated by the practical and Linde adsorption figures at one atmosphere given in table 6.2O are not large. The tortuosity factors resulting from the pore diffusivities are reasonably constant and realistic. Dworjanyn[2] also calculated an effective diffusivity for a long pellet bed which was a factor

of ten greater than those given here. His calculation of D_T is in error and reworking the results from his value of D_e gives D_T = 0.48 cm^2/sec.

A check was made to see if the practical breakthrough curves, which do not appear to differ much from curves for a pore diffusion process only, could be fitted using equation 6.9. Table 6.24 clearly shows that they are not adequately fitted by such a simple model because the degree of fit, measured by a sum of squares deviation, deteriorates faster as the temperature decreases than in table 6.22 which is for the two diffusivity model. This shows that intra-crystalline diffusion becomes increasingly significant at sub-ambient temperatures and should be included in a model describing the diffusion processes in a 5A sieve. However, tortuosities based on equations 6.9-11 range from 1.9 at 25°C to 2.0 at -25°C for the pore diffusion model which is less variation than obtained with the more sophisticated model indicating that the tortuosity is not simply geometric as assumed in equation 6.11.

Finally all the theoretical and practical breakthrough curves obtained were plotted on logarithmic probability paper but none of them gave the change in slope reported by Dworjanyn[2] at about 90% CO_2 exchanged. He interpreted the change in slope as an indication that the diffusion mechanism in the crystals had switched from large cage-

large cage transitions to small cage-large cage transitions. If such a change of mechanism does imply a significant change of slope then this further indicates that the small cages in the 5A sieve play little or no part in the crystal diffusion process.

CHAPTER 7 - CONCLUSIONS

This work has demonstrated the possibility that adsorption isotherms, heats of adsorption and intra-crystalline diffusivities in the Linde 5A molecular sieve/CO_2 system can be predicted theoretically using only basic molecular data. In the system studied, pore diffusion is the controlling process at high temperatures, but at sub-ambient temperatures intra-crystalline diffusion becomes significant. Therefore in a mathematical model describing the system both processes must be included. In the intra-crystalline regime it has been inferred that small cage transitions are negligible and the large cage to large cage transitions dominate the diffusion process.

The molecular potentials calculated for an idealised model of a Linde 5A molecular sieve crystal have resulted in reasonable predictions for adsorption isotherms, heats of adsorption and crystal diffusivities for a range of temperatures about ambient and for less than 4 wt.% CO_2 adsorbed by the sieve. Comparison of the range of theoretical results presented here and literature data shows that the former are significantly dependent on the values of the molecular constants used. In particular it has been necessary to assume partially ionised states for the sieve

structural ions, a carbon dioxide molecule size based on bond lengths of carbon monoxide rather than P-V-T data, and an oxygen polarisability based on measurements of oxygen in a potash felspar. Most of these factors have tended to reduce the molecular potentials and their corresponding temperature coefficients. Even so, both the molecular potentials and the temperature coefficients appear to be overestimated especially below 248°K.

The statistical mechanical theory developed in Chapter 2 to predict adsorption isotherms in terms of the large cage potentials is similar to the method described by Barker and Everett.[22] The quadratic expression obtained for the adsorption isotherm should be valid for $p < RT/2B'$ but results in agreement with the Linde adsorption data at about 323°K only. Both the theoretical curve shape and temperature variation differ from the Linde curves when compared over a fairly wide range of temperature and pressure, though fair local agreement has been obtained.

The theoretical heats of adsorption agree well with literature data over a wide range of temperature and are virtually independent of pressure over the range for which they are valid. This suggests that the theoretical isotherms rather than the molecular potentials are incorrectly predicted.

The theoretical crystal diffusivities failed to give close agreement with the crystal diffusivities obtained from the practical work. This was expected because the theoretical expression is only a first order approximation and is used at sub-ambient temperatures where the molecular potentials are least reliable. Also the theoretical expression is based on a single CO_2 molecule in one cage of a large group of empty cages whereas the practical values are for full cages containing up to seven or eight CO_2 molecules.

The practical work has served its purpose in providing reproducible breakthrough curves for the self diffusion of CO_2 in a sieve pellet between 25°C and -25°C at atmospheric pressure. These curves exhibited a significant temperature dependence and permitted pore and crystal diffusivities to be fitted with reasonable reliability. The radio tracing technique used to follow the transfer of labelled CO_2 from the pellet utilising a scintillation counter with an extremely fast response, has provided basic data which gives breakthrough curves which are not subject to large cumulative errors. Unfortunately the apparatus failed to give results at -50°C and below due to insufficient temperature control of the cryostat and subsequent fluctuations in the carrier CO_2 flow rate.

The mathematical model used to describe the diffusion of carbon dioxide in the sieve pellet incorporating transfer in both pore and crystal regimes has provided a relatively simple method of fitting diffusivities to the practical breakthrough curves. The model is not subject to the usual mathematical instabilities encountered in integrating sets of partial differential equations. This enabled a free choice of finite difference parameters to be made and so carbon dioxide accumulations in the pellet could be calculated at chosen times without having to use extremely small space and time increments. Even so rounding error was encountered when the crystal diffusivity was chosen to be large, but not infinite. However, the final crystal diffusivities found to fit the practical curves were small enough to obviate these errors in the numerical techniques used.

This work has answered most of the problems posed by Dworjanyn[2], but further difficulties have arisen. Molecular potentials can be calculated with confidence, but the temperature dependence of derived properties involving the use of the theoretical isotherm are not adequately described by the theory used here. Even with the advent of yet another generation of computers the calculation of properties based on three or more molecules is still lengthy so that predictions cannot be made for large amounts of CO_2 in the crystal. Although theoretical crystal diffusivities

have been obtained, the theory needs to be extended to enable a second order approximation to be made and this is by no means simple. It would be of interest to measure practical breakthrough curves for single spherical pellets of differing sizes now commercially available, and this would also provide a more realistic approach to conditions pertaining in industrial applications of sieves. Any apparatus used to do this would need a more sophisticated temperature and CO_2 flow control than used here. It would benefit from some form of automatic data collection, though it appears that little improvement is necessary in the scintillation counting methods used. The apparatus and techniques described here could be used to make low temperature studies on binary mixtures using counter diffusion techniques in which the sieve is saturated with one species of labelled gas and exchanged with another unlabelled species. It could be expected that simple combination rules would then emerge for the prediction of binary diffusion coefficients from the self diffusion coefficients of the constituents.

APPENDIX A - MOLECULAR DATA AND SIEVE POTENTIALS

The first five tables contain the polarisability, susceptibility and equilibrium radius for sodium, calcium, oxygen, aluminium, silicon and carbon dioxide obtained both from screening constants[10] and the literature. The final entries in these tables are the values used in table A6 which gives the potential constants used in equation 2.10 for the various combinations of the molecular data used in runs 60-67. Table A7 gives the potential constants used in equation 2.15. A detailed breakdown of potential results obtained from runs 61 and 63 are given in tables A8 and A9 at 298°K. Results at other temperatures used in runs 71-94 can be obtained by scaling PHI-Q to allow for its temperature variation. Table A10 gives the values of the summation SIGMAI = $\sum \exp(-\emptyset/kT)$ in the small cages.

TABLE A1

MOLECULAR DATA FOR SODIUM

POLARISABILITY αX1.0,-25 CM3	SUSCEPTIBILITY $-\chi$X1.0,-30 CM3	EQUILIBRIUM RADIUS reX1.0,-8 CM
9.25 (Na)	7.9 (Na)	0.77 (Na)
2.16 (Na+)	3.6 (Na+)	0.70 (Na+)
1.8 (24)	6.95 (24)	0.98 (24)
1.9 (16)	7.0 (16)	0.95 (25)

TABLE A2

MOLECULAR DATA FOR CALCIUM

POLARISABILITY αX1.0,-25 CM3	SUSCEPTIBILITY $-\chi$X1.0,-30 CM3	EQUILIBRIUM RADIUS reX1.0,-8 CM
147 (Ca)	92.6 (Ca)	2.54 (Ca)
14.3 (Ca2+)	18.5 (Ca2+)	0.55 (Ca2+)
4.92 (2)		
4.7 (24)	22.1 (24)	0.99 (24,25)

TABLE A3

MOLECULAR DATA FOR OXYGEN

POLARISABILITY αX1.0,-25 CM3	SUSCEPTIBILITY $-\chi$X1.0,-30 CM3	EQUILIBRIUM RADIUS reX1.0,-8 CM
8.3 (O)	11.6 (O)	0.47 (O)
16.5 (O2-)	16.2 (O2-)	0.55 (O2-)
38.9 (2,16)	20.9 (2,15,	1.4 (2,24,
16.5 (16)	16,24)	25)

TABLE A4

MOLECULAR DATA FOR ALUMINIUM AND SILICON

POLARISABILITY αX1.0,-25 CM3		SUSCEPTIBILITY $-\chi$X1.0,-30 CM3		EQUILIBRIUM RADIUS reX1.0,-8 CM	
210 (Al) 0.77(Al3+)	140 (Si) 0.51 (Si4+)	44.5 (Al) 4.1 (Al3+)	41.5 (Si) 3.3 (Si4+)	1.36 (Al) 0.24 (Al3+)	1.15 (Si) 0.22 (Si4+)
HYPOTHETICAL AS 3.5 +		HYPOTHETICAL AS 3.5 +		HYPOTHETICAL AS 3.5 +	
0.66		3.76		0.48	

TABLE A5

MOLECULAR DATA FOR CARBON DIOXIDE

POLARISABILITY αX1.0,-25 CM3	SUSCEPTIBILITY $-\chi$X1.0,-30 CM3	EQUILIBRIUM RADIUS reX1.0,-8 CM
26.3 (16) 4.1 TO AXIS (16) 19.5 TO AXIS (16) 26.5 AVERAGE (16)	34.5 (2) 30.9 (16)	2.26 (2) 2.56 TO AXIS (16) 1.4 TO AXIS (16) 1.65 KINETIC (16)
ROTATING QUADRUPOLE MOMENT Qb = 4.1,-26 esu. (26)		

TABLE A6

POTENTIAL CONSTANTS AT 298 DEG. K

TERM	UNITS	CO2 (a)	O -1/4 (b)		AS 3.5+ (b)	3/4 Ca 1.5+(b)	NaCa 1.5+(b)
POLARISABILITY α	1.0,-25 CM3	26.5	39.0	16.5	0.66	3.5	2.84
SUSCEPTIBILITY $-\chi$	1.0,-30 CM3	30.9	20.9		3.76	16.6	14.5
EQUILIBRIUM DIAMETER ρe	1.0,-8 CM	5.12 3.30	3.96 3.05		3.04 2.13	3.55 2.64	3.53 2.62
$B=-6mc^2\alpha a\alpha b / \alpha a/\chi a+\alpha b/\chi b$	1.0,-60 ERG.CM6	201	186	80.9	8.3	42.6	35
B/a_0^6	1.0,-10 ERGS	5.77,-7	5.35,-7	2.32,-7	2.38,-8	1.22,-7	1.01,-7
$\rho e^6 / 2B$	1.0, 10 ERGS	4490 321	1036 216	2394 497	4760 562	2350 397	2760 462
$C1=e^2 Ci^2 \alpha b \rho e^2 / 3B$			0.107 0.064	0.246 0.146	277 136	13.5 7.46	16.3 9.0
$C2=e^2 Ci^2 Qb^2 / 20kTB$			0.158	0.363	231	24.8	15.1
PHIR2=1+C1+C2			1.265 1.222	1.609 1.509	509 486	39.3 33.3	32.4 25.1

TABLE A7

POTENTIAL CONSTANTS FOR THE CO2-CO2 INTERACTION

TEMP DEG. K	A' X1.0,-10 ERGS	B' X1.0,-10 ERGS	C' X1.0,-10 ERGS	E X1.0,10 ERGS
573	6.164,6	37	799	1265
473	6.174,6	37	968	1530
423	6.180,6	37	1083	1710
373	6.189,6	37	1228	1940
348	6.194,6	37	1316	2080
323	6.200,6	37	1418	2240
298	6.207,6	37	1537	2430
273	6.215,6	37	1677	2650
248	6.224,6	37	1846	2918
223	6.237,6	37	2053	3245
198	6.251,6	37	2313	3655
173	6.271,6	37	2647	4185

WHERE:

$$A' = \frac{B'\rho_e^6}{2b_o^{12}}\,(1+5C'/3B'\rho_e^4)$$

$$B' = \frac{-3mc^2\alpha_a\chi_a}{b_o^6}$$

$$C' = 7Qb^4/40kTb_o^{10}$$

$$E = 10^{-10}/kT$$

TABLE A8

LARGE CAGE POTENTIALS AT 298 ABSOLUTE - RUN 61

(POTENTIALS IN UNITS OF 1.0,-10 ERGS/CO2 MOLECULE)

GRID POINT	PHI-R	PHI-D	PHI-P	PHI-Q	PHI-TOT
0 0 0	3.783,-5	-1.466,-3	-3.380,-25	-1.696,-3	-3.124,-3
1 0 0	4.478,-5	-1.515,-3	-8.734,-8	-1.759,-3	-3.230,-3
1 1 0	5.371,-5	-1.568,-3	-5.197,-9	-1.830,-3	-3.344,-3
1 1 1	6.550,-5	-1.623,-3	-2.846,-7	-1.913,-3	-3.471,-3
2 0 0	6.880,-5	-1.671,-3	-1.824,-6	-1.940,-3	-3.554,-3
2 1 0	8.483,-5	-1.734,-3	-1.392,-6	-2.038,-3	-3.688,-3
2 1 1	1.072,-4	-1.799,-3	-3.472,-6	-2.157,-3	-3.852,-3
2 2 0	1.421,-4	-1.934,-3	-2.721,-7	-2.327,-3	-4.118,-3
2 2 1	1.895,-4	-2.010,-3	-1.265,-5	-2.513,-3	-4.347,-3
2 2 2	3.759,-4	-2.257,-3	-4.620,-5	-3.091,-3	-5.091,-3
3 0 0	1.219,-4	-1.690,-3	-1.793,-5	-2.217,-3	-4.073,-3
3 1 0	1.547,-4	-2.044,-3	-1.661,-5	-2.359,-3	-4.265,-3
3 1 1	2.020,-4	-2.131,-3	-2.335,-5	-2.539,-3	-4.192,-3
3 2 0	2.755,-4	-2.315,-3	-1.029,-5	-2.784,-3	-4.834,-3
3 2 1	3.846,-4	-2.414,-3	-4.051,-5	-3.091,-3	-5.161,-3
3 2 2	8.560,-4	-2.736,-3	-1.434,-4	-4.086,-3	-6.110,-3
3 3 0	5.712,-4	-2.840,-3	-1.284,-6	-3.474,-3	-5.744,-3
3 3 1	8.507,-4	-2.965,-3	-8.410,-5	-4.025,-3	-6.223,-3
3 3 2	2.249,-3	-3.373,-3	-3.817,-4	-5.937,-3	-7.442,-3
3 3 3	7.447,-3	-4.192,-3	-1.080,-3	-9.960,-3	-7.787,-3
4 0 0	2.375,-4	-2.434,-3	-8.845,-5	-2.556,-3	-4.841,-3
4 1 0	3.103,-4	-2.561,-3	-8.820,-5	-2.753,-3	-5.002,-3
4 1 1	4.121,-4	-2.691,-3	-1.046,-4	-3.012,-3	-5.395,-3
4 2 0	5.904,-4	-2.972,-3	-8.254,-5	-3.354,-3	-5.818,-3
4 2 1	8.260,-4	-3.115,-3	-1.452,-4	-3.827,-3	-6.262,-3
4 2 2	1.940,-3	-3.587,-3	-3.539,-4	-5.431,-3	-7.432,-3
4 3 0	1.314,-3	-3.778,-3	-5.092,-5	-4.357,-3	-6.871,-3
4 3 1	1.972,-3	-3.955,-3	-2.138,-4	-5.267,-3	-7.464,-3
4 3 2	5.754,-3	-4.539,-3	-8.609,-4	-8.665,-3	-8.311,-3
4 3 3	2.378,-2	-5.735,-3	-2.481,-3	-1.684,-2	-1.272,-3
4 4 0	3.219,-3	-5.243,-3	-9.309,-5	-5.680,-3	-7.797,-3
4 4 1	5.021,-3	-5.508,-3	-4.164,-4	-7.285,-3	-8.188,-3
4 4 2	1.721,-2	-6.358,-3	-1.858,-3	-1.393,-2	-4.939,-3
5 0 0	5.096,-4	-3.178,-3	-2.658,-4	-2.908,-3	-5.842,-3
5 1 0	7.014,-4	-3.393,-3	-2.688,-4	-3.163,-3	-6.123,-3
5 1 1	9.399,-4	-3.611,-3	-2.971,-4	-3.503,-3	-6.471,-3
5 2 0	1.509,-3	-4.102,-3	-2.905,-4	-3.951,-3	-6.844,-3
5 2 1	1.974,-3	-4.335,-3	-3.971,-4	-4.594,-3	-7.353,-3
5 2 2	4.341,-3	-5.117,-3	-7.621,-4	-6.850,-3	-8.389,-3

TABLE A8 (CONTINUED)

LARGE CAGE POTENTIALS AT 298 ABSOLUTE - RUN 61

(POTENTIALS IN UNITS OF 1.0,-10 ERGS/CO2 MOLECULE)

GRID POINT	PHI-R	PHI-D	PHI-P	PHI-Q	PHI-TOT
5 3 0	3.815,-3	-5.515,-3	-3.080,-4	-5.301,-3	-7.309,-3
5 3 1	5.066,-3	-5.794,-3	-5.703,-4	-6.592,-3	-7.890,-3
5 3 2	1.322,-2	-6.735,-3	-1.647,-3	-1.170,-3	-6.861,-3
5 4 0	9.956,-3	-8.064,-3	-4.004,-4	-7.140,-3	-5.648,-3
5 4 1	1.428,-2	-8.526,-3	-0.514,-4	-9.526,-3	-4.726,-3
5 5 0	2.921,-2	-1.283,-2	-8.911,-4	-9.250,-3	-6.241,-3
6 0 0	1.190,-3	-4.306,-3	-4.004,-4	-3.239,-3	-6.845,-3
6 1 0	1.828,-3	-4.714,-3	-5.127,-4	-3.547,-3	-6.045,-3
6 1 1	2.510,-3	-5.123,-3	-5.880,-4	-3.952,-3	-7.143,-3
6 2 0	5.172,-3	-6.132,-3	-6.675,-4	-4.519,-3	-6.146,-3
6 2 1	6.062,-3	-6.546,-3	-7.952,-4	-5.270,-3	-6.550,-3
6 2 2	1.182,-2	-8.041,-3	-1.329,-3	-7.952,-3	-5.501,-3
6 3 0	1.798,-2	-9.149,-3	-8.683,-4	-6.251,-3	+1.713,-3
6 3 1	1.868,-2	-9.562,-3	-1.216,-3	-7.753,-3	-1.456,-4
6 3 2	3.334,-2	-1.126,-2	-2.646,-3	-1.388,-2	+5.560,-3
7 0 0	2.816,-3	-5.905,-3	-5.060,-4	-3.541,-3	-7.227,-3
7 1 0	5.179,-3	-6.726,-3	-6.027,-4	-3.909,-3	-6.148,-3
7 1 1	7.536,-3	-7.540,-3	-7.040,-4	-4.365,-3	-5.163,-3
7 2 0	2.311,-2	-9.933,-3	-1.036,-3	-5.142,-3	+6.006,-3
7 2 1	2.431,-2	-1.069,-2	-1.158,-3	-5.909,-3	+6.547,-3
8 0 0	5.993,-3	-7.867,-3	-5.253,-4	-3.821,-3	-6.221,-3
8 1 0	1.374,-2	-9.111,-3	-6.017,-4	-4.282,-3	-5.838,-4
8 1 1	2.111,-2	-1.099,-2	-7.020,-4	-4.800,-3	+4.012,-3
9 0 0	1.010,-2	-9.655,-3	-1.073,-4	-4.049,-3	-3.804,-3
9 1 0	2.805,-2	-1.217,-2	-2.755,-4	-4.631,-3	+1.008,-2
10 0 0	1.217,-2	-1.040,-2	-1.441,-7	-4.142,-3	-2.374,-3
SMALL CAGE POTENTIALS AT 298 ABSOLUTE - RUN 61					
10 10 10	4.463,-3	-6.000,-3	-1.130,-5	-1.765,-2	-2.010,-2
10 10 9	6.596,-3	-7.472,-3	-5.015,-6	-1.947,-2	-2.035,-2
10 10 8	1.464,-2	-9.587,-3	-2.482,-4	-2.422,-2	-1.912,-2
10 10 7	3.943,-2	-1.403,-2	-2.313,-3	-2.070,-2	-7.513,-3
10 9 9	1.060,-2	-8.093,-3	-4.825,-6	-2.202,-2	-1.052,-2
10 9 8	2.601,-2	-1.040,-2	-2.288,-4	-2.891,-2	-1.353,-2
10 9 7	6.954,-2	-1.638,-2	-2.416,-3	-3.713,-2	+1.366,-2
9 9 9	2.031,-2	-8.780,-3	-1.188,-4	-2.599,-2	-1.458,-2
9 9 8	6.317,-2	-1.133,-2	-6.327,-4	-3.746,-2	+1.374,-2

TABLE A9

LARGE CAGE POTENTIALS AT 298 ABSOLUTE - RUN 63

(POTENTIALS IN UNITS OF 1.0,-10 ERGS/CO2 MOLECULE)

GRID POINT	PHI-R	PHI-D	PHI-P	PHI-Q	PHI-TOT
0 0 0	3.585,-5	-6.737,-4	-3.380,-25	-1.696,-3	-2.334,-3
1 0 0	4.263,-5	-6.964,-4	-8.734,-8	-1.759,-3	-2.413,-3
1 1 0	5.169,-5	-7.207,-4	-5.197,-9	-1.830,-3	-2.499,-3
1 1 1	6.436,-5	-7.467,-4	-2.846,-7	-1.913,-3	-2.596,-3
2 0 0	6.499,-5	-7.680,-4	-1.824,-6	-1.940,-3	-2.644,-3
2 1 0	8.189,-5	-7.974,-4	-1.329,-6	-2.038,-3	-2.755,-3
2 1 1	1.076,-4	-8.288,-4	-3.472,-6	-2.157,-3	-2.881,-3
2 2 0	1.405,-4	-8.909,-4	-2.721,-7	-2.327,-3	-3.077,-3
2 2 1	1.005,-4	-9.286,-4	-1.265,-5	-2.513,-3	-3.254,-3
2 2 2	4.371,-4	-1.050,-3	-4.620,-5	-3.001,-3	-3.750,-3
3 0 0	1.092,-4	-8.993,-4	-1.793,-5	-2.217,-3	-3.026,-3
3 1 0	1.430,-4	-9.301,-4	-1.661,-5	-2.359,-3	-3.172,-3
3 1 1	1.977,-4	-9.813,-4	-2.335,-5	-2.539,-3	-3.346,-3
3 2 0	2.648,-4	-1.066,-3	-1.029,-5	-2.784,-3	-3.596,-3
3 2 1	4.075,-4	-1.117,-3	-4.051,-5	-3.001,-3	-3.841,-3
3 2 2	1.034,-3	-1.281,-3	-1.434,-4	-4.086,-3	-4.477,-3
3 3 0	5.398,-4	-1.301,-3	-1.284,-6	-3.474,-3	-4.245,-3
3 3 1	9.215,-4	-1.378,-3	-8.410,-5	-4.025,-3	-4.565,-3
3 3 2	2.887,-3	-1.602,-3	-3.817,-4	-5.037,-3	-5.034,-3
3 3 3	1.033,-2	-2.050,-3	-1.080,-3	-9.060,-3	-2.765,-3
4 0 0	1.916,-4	-1.112,-3	-8.845,-5	-2.556,-3	-3.564,-3
4 1 0	2.586,-4	-1.171,-3	-8.820,-5	-2.753,-3	-3.754,-3
4 1 1	3.672,-4	-1.234,-3	-1.046,-4	-3.012,-3	-3.983,-3
4 2 0	5.190,-4	-1.363,-3	-8.254,-5	-3.354,-3	-4.289,-3
4 2 1	8.106,-4	-1.437,-3	-1.452,-4	-3.827,-3	-4.599,-3
4 2 2	2.268,-3	-1.681,-3	-3.539,-4	-5.431,-3	-5.198,-3
4 3 0	1.123,-3	-1.735,-3	-5.092,-5	-4.357,-3	-5.020,-3
4 3 1	2.009,-3	-1.835,-3	-2.138,-4	-5.267,-3	-5.308,-3
4 3 2	7.349,-3	-2.174,-3	-8.600,-4	-8.665,-3	-4.351,-3
4 4 0	2.527,-3	-2.399,-3	-9.309,-5	-5.680,-3	-5.645,-3
4 4 1	4.852,-3	-2.554,-3	-4.164,-4	-7.285,-3	-5.403,-3
4 4 2	2.210,-2	-3.092,-3	-1.858,-3	-1.393,-2	+3.227,-3
5 0 0	3.584,-4	-1.440,-3	-2.658,-4	-2.908,-3	-4.256,-3
5 1 0	5.022,-4	-1.539,-3	-2.688,-4	-3.163,-3	-4.469,-3
5 1 1	7.121,-4	-1.642,-3	-2.971,-4	-3.503,-3	-4.730,-3
5 2 0	1.090,-3	-1.865,-3	-2.995,-4	-3.951,-3	-5.025,-3
5 2 1	1.621,-3	-1.981,-3	-3.971,-4	-4.594,-3	-5.351,-3

TABLE A9 (CONTINUED)

LARGE CAGE POTENTIALS AT 298 ABSOLUTE - RUN 63

(POTENTIALS IN UNITS OF 1.0,-10 ERGS/CO2 MOLECULE)

GRID POINT	PHI-R	PHI-D	PHI-P	PHI-Q	PHI-TOT
5 2 2	4.416,-3	-2.376,-3	-7.621,-4	-6.850,-3	-5.572,-3
5 3 0	2.687,-3	-2.506,-3	-3.080,-4	-5.301,-3	-5.428,-3
5 3 1	4.294,-3	-2.659,-3	-5.703,-4	-6.592,-3	-5.528,-3
5 3 2	1.534,-2	-3.196,-3	-1.647,-3	-1.170,-2	-1.208,-3
5 4 0	6.643,-3	-3.640,-3	-4.004,-4	-7.140,-3	-4.546,-3
5 4 1	1.155,-2	-3.909,-3	-9.514,-4	-9.526,-3	-2.838,-3
5 5 0	1.793,-2	-5.750,-3	-8.911,-4	-9.250,-3	+2.038,-3
6 0 0	7.416,-4	-1.933,-3	-4.004,-4	-3.239,-3	-4.921,-3
6 1 0	1.137,-3	-2.117,-3	-5.127,-4	-3.547,-3	-5.040,-3
6 1 1	1.609,-3	-2.303,-3	-5.880.-4	-3.952,-3	-5.233,-3
6 2 0	3.144,-3	-2.751,-3	-6.675.-4	-4.519,-3	-4.794,-3
6 2 1	3.996,-3	-2.948,-3	-7.952,-4	-5.270,-3	-5.270,-3
6 2 2	9.006,-3	-3.660,-3	-1.320,-3	-7.952,-3	-3.934,-3
6 3 0	1.058,-2	-4.092,-3	-8.683,-4	-6.251,-3	-6.287,-4
6 3 1	1.211,-2	-4.308,-3	-1.216,-3	-7.753,-3	-1.165,-3
6 3 2	2.887,-2	-5.195,-3	-2.646,-3	-1.288,-2	+7.150,-3
7 0 0	1.633,-3	-2.628,-3	-5.960,-4	-3.541,-3	-5.132,-3
7 1 0	2.975,-3	-2.990,-3	-6.927,-4	-3.909,-3	-4.617,-3
7 1 1	4.356,-3	-3.352,-3	-7.940,-4	-4.365,-3	-4.156,-3
7 2 0	1.299,-2	-4.400,-3	-1.036,-3	-5.142,-3	+2.417,-3
7 2 1	1.395,-2	-4.746,-3	-1.158,-3	-5.909,-3	+2.136,-3
8 0 0	3.371,-3	-3.478,-3	-5.253,-4	-3.821,-3	-4.454,-3
8 1 0	7.666,-3	-6.051,-3	-6.017,-4	-4.282,-3	-1.383,-3
8 1 1	1.178,-2	-4.844,-3	-7.029,-4	-4.809,-3	+1.427,-3
9 0 0	5.617,-3	-4.252,-3	-1.973,-4	-4.049,-3	-2.881,-3
9 1 0	1.552,-2	-5.348,-3	-2.755,-4	-4.631,-3	+5.270,-3
10 0 0	6.755,-3	-4.576,-3	-1.441,-7	-4.142,-3	-1.963,-3
SMALL CAGE POTENTIALS AT 298 ABSOLUTE - RUN 63					
10 10 10	5.624,-3	-3.421,-3	-1.150,-5	-1.765,-2	-1.546,-2
10 10 9	8.351,-3	-3.714,-3	-5.915,-6	-1.947,-2	-1.484,-2
10 10 8	1.745,-2	-4.745,-3	-2.482,-4	-2.422,-2	-1.177,-2
10 10 7	3.718,-2	-7.182,-3	-2.313,-3	-2.070,-2	-2.020,-3
10 9 9	1.379,-2	-4.047,-3	-4.825,-6	-2.202,-2	-1.228,-2
10 9 8	3.323,-2	-5.214,-3	-2.288,-4	-2.891,-2	-1.124,-3
10 9 7	7.371,-2	-7.909,-3	-2.416,-3	-3.713,-2	+2.616,-2
9 9 9	2.770,-2	-4.444,-3	-1.188,-4	-2.590,-2	-2.845,-3

TABLE A10

SMALL CAGE SIGMA1 VALUES

TEMP (DEG. K)	RUN 60	RUN 61	RUN 62	RUN 63
573	4.959,7	4.111,6	9.680,5	8.179,4
473	2.272,10	1.118,9	1.942,8	9.810,6
423	2.776,12	9.325,10	1.351,10	1.685,8
373	2.674,15	5.285,13	6.343,12	1.300,11
348	2.675,17	3.716,15	4.105,14	5.012,12
323	7.192,19	6.479,17	6.748,16	6.254,14
298	1.024,23	5.180,20	5.467,19	2.754,17
273	1.106,27	2.522,24	3.282,23	6.692,20
248	3.682,32	2.257,29	6.254,28	2.549,25
223	2.098,40	1.135,36	1.875,36	4.503,31
198	5.339,51	4.303,45	1.676,47	5.027,40
173	2.969,68	9.586,59	2.118,63	4.562,54

APPENDIX B - PRACTICAL RESULTS

This section contains the practical results obtained at 25°C and - 25°C used to derive table 6.18 and subsequent results. Run start times, To, and the average background counts are included for each run, together with the derived values of $\sqrt{T_r}$, IC_b and IC_r.

TABLE B1

PRACTICAL RESULTS
TRIAL RUN (1A) AT 25 DEG. C
TO = 11.6 SECS
BACKGROUND = 1.528 c/s

FILM TIME (SECS)	INTEGRAL COUNT	$\sqrt{Tr}$	ICb
12.0	14200		
12.6	25700	1	25681
13.0	34400		
13.5	46100		
14.1	60200		
14.5	70300		
15.0	83600		
15.6	99800	2	99776
18.4	158200	2.6	158172
19.4	168500	2.8	168470
20.6	175200	3	175169
21.8	178000	3.2	177967
22.2	179650	3.4	179617
24.6	180860	3.6	180822
26.0	181520	3.8	181840
27.6	182050	4	182008
35.2	183320	4.9	183266
45	184127	5.8	184058
75	185717	8	185602
125	187325	10.6	187134
200	188908	14.1	188692
400	191584	19.7	191973
900	193913	29.8	192538
1250	194654	35.2	192744
1600	195230	39.8	192884
2100	196076	45.7	192867
2500	196653	49.9	192833
3025	197457	54.9	192834
3600	198330	59.9	192838
4225	199319	64.9	192863
4920	200375	70	192857
5750	201608	75.7	192822
8100	205253	89.9	192876
10000	208169	99.9	192889

TABLE B2

PRACTICAL RESULTS
TRIAL RUN (2A) AT 25 DEG. C
TO = 13.4 SECS
BACKGROUND = 1.505 c/s

FILM TIME (SECS)	INTEGRAL COUNT	$\sqrt{Tr}$	ICb
13.5	12300		
14.0	17500		
14.4	26100	1	26078
15.1	44000		
15.5	55900		
16.0	69000		
16.5	82500		
17.4	101000	2	100971
20.2	159900	2.6	159870
21.2	169400	2.8	169368
22.4	175400	3	175366
23.6	178350	3.2	178314
25.0	179960	3.4	179922
27.2	181350	3.7	181309
35.4	183423	4.7	183380
46	184287	5.7	184238
60.1	185033	6.8	184943
75.4	185757	7.9	185644
91.4	186344	8.8	186206
110	186973	9.8	186807
235	189760	14.9	189406
410.4	191837	19.9	191219
635	193165	24.9	192200
960	194165	30.8	192702
1235	194724	35	192865
1610.1	195362	40	192938
2031.1	196077	45	193015
2510	196865	50	193087
3035	197670	55	193102
3610	198520	60	193087
4235	199638	65	193264
4910	200688	70	193208
5635	201849	75	193368
6410	203060	80	193413
7235	204331	85	193442
8110	205663	90	193457
9035	207115	95	193517
10010	208556	100	193491

TABLE B3

PRACTICAL RESULTS
PELLET RUN (3A) AT 25 DEG. C
TO = 12.8 SECS
BACKGROUND = 1.547 c/s

FILM TIME (SECS)	INTEGRAL COUNT	$\sqrt{Tr}$	ICr
13.0	9200		
13.5	19100		
13.8	26100	1	26079
14.0	31400		
14.6	44100		
15.0	53300		
15.5	65500		
16.0	78200		
16.8	99800	2	99774
18.8	157600	2.6	157571
20.6	167800	2.8	167768
21.8	177100	3	177066
23.0	180100	3.2	179964
24.4	182700	3.4	182662
25.8	184030	3.6	183990
27.2	185020	3.8	184978
28.8	185800	4	185755
33.0	187560	4.5	187509
35.8	188440	4.8	188384
43.8	190987	5.7	190910
58.8	193450	6.8	193359
73.8	195710	7.8	195596
92.8	198018	9	197937

FILM TIME (SECS)	INTEGRAL COUNT	$\sqrt{Tr}$	ICr
109.8	199886	9.9	199716
234.8	209989	14.9	209620
409.8	219461	19.9	218827
638.4	228252	25	227270
909.8	236703	30	235296
1234.8	245112	35	243202
1608.8	253240	40	250751
2035	261465	45	258317
2510	269297	50	265414
3035	276688	55	271993
3610	283491	60	277906
4235	289677	67	283125
4910	295325	70	287729
5635	300207	75	291490
6410	304647	80	294731
7235	308484	85	297291
8110	311880	90	299334
9035	314900	95	300923
10010	317710	100	302225
10510	322196	102.5	305937
11010	323764	105	306732
11010	324724	107.2	306918
12010	325480	109.2	306901

TABLE B4

PRACTICAL RESULTS
PELLET RUN (4A) AT 25 DEG. C
TO = 13.5 SECS
BACKGROUND = 1.585 c/s

FILM TIME (SECS)	INTEGRAL COUNT	$\sqrt{Tr}$	ICr
14.0	16000		
14.5	26800	1	26777
15.0	37800		
15.5	50100		
16.1	64700		
16.5	76300		
17.0	89500		
17.5	100500	2	100472
20.3	160700	2.6	160668
21.3	170900	2.8	170866
22.5	177500	3	177464
23.7	181000	3.2	180962
25.1	182750	3.4	182710
26.5	183950	3.6	183908
35.5	188077	4.7	188021
46.5	190900	5.8	190826
65.5	194341	7.2	194237
74.5	195659	7.8	195541
91.5	197857	8.8	197712
110.5	199917	9.9	199741
235.5	209596	14.9	209228

FILM TIME (SECS)	INTEGRAL COUNT	$\sqrt{Tr}$	ICr
410.5	218876	19.9	218225
635.5	227382	25	226375
910.5	235465	30	234022
1235	243246	35	241468
1610	251358	40	248805
2040	259368	45	256134
2510	266729	50	262750
3035	273509	55	268698
3610	279839	60	274116
4235	285781	65	279068
4910	291061	70	283279
5635	295677	75	286746
6410	299913	80	289753
7235	303582	85	292115
8110	306830	90	293976
9035	309744	95	295424
10010	312426	100	296560
10510	316775	102.4	300117
11010	318230	104.9	300779
11510	319080	107.2	300845
12010	319862	109.5	300826

TABLE B5

PRACTICAL RESULTS
PELLET RUN (5A) AT 25 DEG. C
TO = 12.4 SECS
BACKGROUND = 1.584 c/s

FILM TIME (SECS)	INTEGRAL COUNT	$\sqrt{Tr}$	ICr
12.5	9700		
13.1	19400		
13.4	27300	1	27279
14.0	40300		
14.5	51400		
15.0	64100		
15.6	78500		
16.0	88800		
16.4	99300	2	99274
19.2	159400	2.6	159370
20.2	170200	2.8	170168
21.4	177200	3	177166
22.6	180700	3.2	180664
24.0	182700	3.4	182662
25.4	184260	3.6	184220
26.8	185320	3.8	185278
28.4	186265	4	186220
35.4	189176	4.8	189120
46.4	192190	5.8	192127
50.4	195001	6.9	194907
74.4	197465	7.9	197437
91.4	199921	8.9	199726
110.4	202217	9.9	202042

FILM TIME (SECS)	INTEGRAL COUNT	$\sqrt{Tr}$	ICr
235.4	213179	14.9	212806
410.4	223207	20	222557
635.4	232365	25	231359
910.4	241216	30	239774
1235	249819	35	247862
1610	258273	40	255722
2035	266518	45	263294
2510	274627	50	270651
3035	282217	55	277409
3610	289413	60	283694
4235	295816	65	289107
4960	302013	70.2	294156
5635	306783	75	297857
6410	311203	80	301050
7235	315082	85	303622
8110	318426	90	305580
9035	321478	95	307167
10010	324174	100	308318
10510	329262	102.4	312614
11010	331100	104.9	313660
11510	331945	107.2	313713
12010	332757	109.8	313733
12610	333751	112.2	313777

TABLE B6

PRACTICAL RESULTS
TRIAL RUN (1C) AT -25 DEG. C
TO = 11.3 SECS
BACKGROUND = 1.498 c/s

FILM TIME (SECS)	INTEGRAL COUNT	$\sqrt{Tr}$	ICb
12.3	18600	1	18582
12.5	21800		
13.1	32500		
13.5	40900		
14.1	51200		
14.5	58200		
15.0	67900		
15.3	73800	2	73777
15.6	78700		
18.1	119700	2.6	119673
19.1	129700	2.8	129671
20.3	137100	3	137070
21.5	140770	3.2	140738
22.9	143050	3.4	143016
24.3	144180	3.6	144141
25.7	144900	3.8	144962
27.3	145516	4	145475
31.5	146460	4.5	146413
36.3	147071	5	147020
46.3	147841	5.9	147772
59.3	148425	6.9	148336
74.3	148886	7.9	148775
91.3	149321	9	149184
110.3	149735	10	149570
235.3	151722	15	151370
410.3	153301	20	152686
635.3	154567	25	153615
920.3	155526	30.1	154147
1235.3	156258	35	154408
1610.3	156956	40	154543
2035	157653	45	154601
2512	158410	50	154647
3035	159187	55	154640
3620	160031	60	154608
4235	160960	65	154589
4910	162044	70	154688
5635	163191	75	154749
6410	164378	80	154755
7235	165647	85	154809
8110	166972	90	154823
9035	168360	95	154826
10010	169823	100	154828

TABLE B7

PRACTICAL RESULTS
TRIAL RUN (2C) AT -25 DEG. C
TO = 11.2 SECS
BACKGROUND = 1.586 c/s

FILM TIME (SECS)	INTEGRAL COUNT	$\sqrt{Tr}$	ICb
11.5	9200		
12.2	19300	1	19281
12.5	23900		
13.0	34000		
13.5	42700		
14.0	51800		
14.5	62200		
15.2	75900	2	75876
15.5	81500		
18.0	123000	2.6	122971
19.0	132100	2.8	132070
20.2	138300	3	138268
21.4	141250	3.2	141216
22.8	143100	3.4	143064
24.2	144230	3.6	144192
25.6	144910	3.8	144860
27.2	145480	4	145437
31.4	146430	4.5	146380
36.2	147021	5	146964
46.2	147782	5.9	147709
59.2	148355	6.9	148250
74.2	148849	8	148731
91.2	149362	9	149217
110.2	149840	10	149665
235.2	151947	15	151574
410.2	153671	20	153020
636.2	155118	25	154100
910.2	156104	30	154660
1235	156861	35	154902
1610	157563	40	155009
2035	158279	45	155051
2510	159032	50	155051
3120	159997	55.7	155048
3610	160788	60	155062
4235	161839	65	155122
4910	162882	70	155205
5635	164095	75	155158
6420	165294	80	155112
7235	166629	85	155154
8110	167933	90	155020
9035	169352	95	155022
10010	170894	100	155018

TABLE B8

PRACTICAL RESULTS
PELLET RUN (3C) AT -25 DEG. C
TO = 11.5 SECS
BACKGROUND = 1.499 c/s

FILM TIME (SECS)	INTEGRAL COUNT	$\sqrt{Tr}$	ICr
12.5	20100	1	20081
13.1	29300		
13.5	36200		
14.0	45300		
14.5	53800		
15.0	63400		
15.5	71900	2	71877
16.1	83700		
18.3	119600	2.6	119573
19.3	130100	2.8	130071
20.5	137900	3	137869
21.7	141700	3.2	141667
23.1	144150	3.4	144115
24.5	145480	3.6	145443
25.9	146290	3.8	146251
27.5	146950	4	146909
31.7	148280	4.5	148232
36.5	149220	5	149165
46.5	150603	5.9	150533
59.5	151950	7.0	151861
74.5	153215	8	153103
91.5	154555	9	154418
110.5	155857	9.9	155691

FILM TIME (SECS)	INTEGRAL COUNT	$\sqrt{Tr}$	ICr
235.5	162833	15	162479
410.5	170072	20	169457
635.5	177493	25	176541
910.5	184885	30	183525
1235	192204	35	190485
1620	199473	40.1	197043
2035	206108	45	203056
2510	212673	50	208913
3035	218895	55	214345
3613	224996	60	219580
4235	230642	65	224297
4923	236202	70.1	228812
5635	241038	75	232598
6410	245672	80	236662
7255	249828	85	238948
8110	253535	90	241385
9035	256922	95	242922
10010	259967	100	244967
10510	262355	102.4	246605
11110	268521	105	251871
11610	270126	107.8	252726
12110	271930	110	252890
13220	272589	115	252779

TABLE B9

PRACTICAL RESULTS
PELLET RUN (4C) AT -25 DEG. C
TO = 10.2 SECS
BACKGROUND = 1.548 c/s

FILM TIME (SECS)	INTEGRAL COUNT	$\sqrt{Tr}$	ICr
11.2	19900	1	19883
11.5	25100		
12.1	34900		
12.5	43500		
13.0	52800		
13.5	63100		
14.2	74200	2	74178
14.6	82100		
17.0	120100	2.6	120074
18.0	130700	2.8	130672
19.2	138750	3	138720
20.4	141900	3.2	141868
21.8	144360	3.4	144326
23.2	145540	3.6	145504
24.6	146380	3.8	146342
26.2	147010	4	146969
29.6	147950	4.1	147904
35.2	149250	5	149196
46.2	150725	6	150653
59.2	152125	7	152033
74.2	153368	8	153253
91.2	154565	9	154424
110.2	155933	10	155762

FILM TIME (SECS)	INTEGRAL COUNT	$\sqrt{Tr}$	ICr
235.2	162897	15	162533
410.2	170613	20	169978
635.2	178303	25	177320
910.2	186346	30	184937
1235	194080	35	192168
1610	201501	40	199009
2035	208623	45	205473
2510	214871	50	210984
3045	221538	55.1	216824
3610	227479	60	221891
4235	232879	65	226323
4910	238659	70	231058
5635	241500	75	233777
6410	248195	80	238992
7235	252761	85	241561
8110	255999	90	243445
9035	259353	95	245367
10010	262367	100	246872
10510	265855	102.5	249586
11110	271388	105.4	254189
11610	273200	107.7	255228
12110	274035	110	255289
13220	275743	115	255278

TABLE B10

PRACTICAL RESULTS
PELLET RUN (5C) AT -25 DEG. C
TO = 10.8 SECS
BACKGROUND = 1.535 c/s

FILM TIME (SECS)	INTEGRAL COUNT	$\sqrt{Tr}$	ICr
11.0	9100		
11.6	15600		
11.8	19000	1	18982
12.0	22100		
12.5	30100		
13.0	40000		
13.6	51800		
14.0	59100		
14.8	72200	2	72177
15.0	76800		
17.6	121900	2.6	121873
18.6	131500	2.8	131471
19.8	138300	3	138270
21.0	141800	3.2	141768
22.4	144100	3.4	144066
23.8	145350	3.6	145313
25.2	146130	3.8	146039
26.8	146780	4	146739
31.0	147800	4.5	147752
35.8	148730	5	148675
45.8	150080	5.9	150010
58.8	151470	6.9	151380
73.8	152835	7.9	152722
90.8	154058	9	153919

FILM TIME (SECS)	INTEGRAL COUNT	$\sqrt{Tr}$	ICr
109.8	155356	10	155187
234.8	161903	15	161543
400.8	168701	20	168072
634.8	176192	25	175218
909.8	183428	30	182031
1235	190881	35	188986
1610	197748	40	195277
2035	204781	45	201658
2510	210782	50	206929
3035	216071	55	212313
3610	223020	60	217479
4235	228627	65	222127
4921	234365	70.1	226812
5635	239046	75	230397
6410	243827	80	233988
7235	247351	85	236245
8110	251546	90	239007
9035	254820	95	240951
10010	257603	100	242238
10510	260215	102.5	244082
11110	265764	105.4	248110
11610	267584	107.7	249763
12110	268643	110	250054
13220	270340	115	250047

APPENDIX C - COMPUTER PROGRAMMES

Programme Notes for Sieve Potential Calculations - Run 63

Data Input This consists of the coordinates A(I), B(I), C(I) of the twelve oxygen ions and the single calcium ion in the (X, Y, Z) quadrant of the unit cell, in units of a_o. G0 to G12 are the dispersion constants B/a_o^6. H0 to H12 are the constants $\rho_e^6/2B$ such that H(I).G(I).G(I).Y(I) generates the repulsion constants where Y0 to Y12 are the correction terms 1 + C1 + C2. The temperature coefficient of the Y(I) is negligible and the value at 298°K is used throughout. $\pi 0$ to $\pi 12$ are the charges residing on the structural ions in units of the charge on an electron. Z(I) contains the remaining constants. Z0 to Z5 are the grid point reflection factors. Z6 to Z17 are the quadruple constants $e^2Q_b^2/20kTa_o^6$. Z18 to Z29 are the conversion factors $10^{-10}/kT$ for the twelve temperatures Z30 to Z41 used. Z42 is the polarisation constant $e^2\alpha b/2a_o^4$.

Organisation Potentials are calculated for a single CO_2 molecule using a tetrahedral grid with a gridline separation $b_o = a_o/20$. This gives a possible 284 points at which ϕ may be calculated, but only those with $\phi_{(T=173)} < 0.005 \times 10^{-10}$ ergs. are considered. The three cycles J, K and L select the next grid point, starting at the centre of the large cage. The CO_2 molecule's position is calculated from these, followed by the grid point reflection factor Z. The cycle I = 0(1)12 after label 17)

selects an ion from the data table and generates all the positions of ions obtainable by reflection and rotation of the data ion inside a cube, side $7a_o$ centred on the grid point (0, 0, 0). The cycles P, Q and R select in turn all these positions in the region $X \geq 0$. The separation distance squared from the gridpoint is calculated and if this distance is suitable the repulsion, dispersion, quadruple and polarisation contributions are calculated. If any of these potentials are calculated a test is made at label 29) to see if the ion position in $X < 0$, if this exists, has been considered. If not, the programme goes to label 27) and generates this ion position and calculates the relevant potentials before continuing with the calculations for the next generated ion position.

When all the data ions have been dealt with the polarisation potential is calculated from its resolved parts and the quadruple potential at various temperatures is calculated from the value at 298°K. The total potential is stored in V0 to V11 and the resulting exponential sums in X0 to X11. After obtaining the results for a grid point a decision is made as to the status of the last one or two grid points at which potentials were calculated. If $\phi_{173} > 0.005$ units at the last point only, the programme moves on to the next grid value of K, not L, and if the last two calculated were both greater than 0.005 units the programme moves to the next grid value of J, not K. This ensures that a minimum number of grid points with significantly positive

potentials are considered without missing any negative points.

Programme Output This includes the coordinates of all the grid points considered with a breakdown of the potential contributions and the numbers of ions involved in their calculation. Then follows the total potential, the quadruple potential, the partition exponential, and the continued sum of the partition exponential at each of the twelve temperatures programmed. The potentials are in units of 10^{-10}ergs. per CO_2 molecule. Finally the resolved components of the polarisation contribution are given.

Flow diagrams for this programme are given in Figures 3.8-10.

EXCHLF SIEVE POTENTIALS PROGRAMME

```
TITLE
CARBON DIOXIDE POTENTIALS IN LINDE MOLECULAR SIEVE 5A.

TITLE
PROGRAMME LJ,P,Q/20384  RMAX SQUARED = 12.25 MK5. OXYGEN AND CA ONLY.

TITLE
HIGH CO2 RADIUS, LOW OXYGEN POLARISABILITY.

TITLE
PARTIALLY IONISED STATES. 3/4 CA 1.5 +


CHAPTER 0
   A➤25
   B➤25
   C➤12
   G➤12
   H➤12
   π➤12
   Y➤12
   Z➤42
   U➤36
   F➤13
   W➤10
   D➤11
   E➤11
   V➤11
   X➤11
   I=0(1)12          | READ DATA IN
   READ(A(I))        | X COORDINATE OF ION(I)
   READ(B(I))        | Y COORDINATE OF ION(I)
   READ(C(I))        | Z COORDINATE OF ION(I)
   READ(G(I))        | DISPERSION CONSTANTS
   READ(H(I))        | PHI R1 CONSTANTS
   READ(π(I))        | CHARGE ON ION
   READ(Y(I))        | PHI R2 CONSTANTS
   READ(Z(I))        | REFLECTION FACTORS, QUADRUPOLE CONSTANTS
   REPEAT
   I=13(1)42
   READ(Z(I))        | QUADRUPOLE CONSTANTS CONTINUED, 1/kT CONSTANTS
                     | TEMPERATURES, POLARISATION CONSTANT
   REPEAT
```

```
>>LIMITS LARGE CAGE.
  NEWLINE 48
  CAPTION
  CO2 POTENTIALS AND PARTITION FUNCTIONS IN LARGE CAGE.
  NEWLINE 4
  I'=0
  J'=10
  K'=0
  M=0
  O=1                  |  CYCLE STEP LENGTH
  S'=0
  A18=3
  JUMP 2

>>LIMITS SMALL CAGE.
1)I=0(1)11
  XI=0                 |  CLEARS EXPONENTIAL SUM
  REPEAT
  NEWLINE 4
  CAPTION
  TOTAL NUMBER OF POINTS CALCULATED IN LARGE CAGE =
  PRINT(W',3,0)
  CHECK(A18,3,0.01,9)
  NEWLINE 18
  A18=3
  JUMP 10
9)NEWLINE 43
10)CAPTION
  CO2 POTENTIALS AND PARTITION FUNCTIONS IN SMALL CAGE.
  NEWLINE 4
  I'=10
  J'=7
  L'=0
  N=0
  O=-1                 |  CYCLE STEP LENGTH
  S'=1

>>SET TETRAHEDRAL GRID CYCLES.
2)W'=0
  J=I'(O)J'            |  START OF J GRID CYCLE
  X'=0.05J             |  X COORDINATE OF CO2 MOLECULE
  JUMP 3, S'=0
  JUMP 4, S'=1
3)L'=J
  JUMP 5
4)K'=J
5)K=K'(O)L'            |  START OF K GRID CYCLE
```

```
   Y'=0.05K            |  Y COORDINATE OF CO2 MOLECULE
   JUMP 6, S'=0
   JUMP 7, S'=1
 6)N=K
   JUMP 8
 7)M=K
 8)L=M(O)N             |  START OF L GRID CYCLE
   Z'=0.05L            |  Z COORDINATE OF CO2 MOLECULE
   W'=W'+1             |  COUNTS GRID POINTS
   JUMP 38, W'>100

 >>CALCULATE GRID POINT REFLECTION FACTOR.
   JUMP 15, J=0
   JUMP 11, J=K
   JUMP 14, K=L
   JUMP 13, L=0
   Z=Z5                |  REFLECTION FACTOR TYPE 8      48 VALUES
   JUMP 17
11)JUMP 12, L≠0
   Z=Z3                |  REFLECTION FACTOR TYPE 4      12 VALUES
   JUMP 17
12)JUMP 13,K≠L
   Z=Z2                |  REFLECTION FACTOR TYPE 3       8 VALUES
   JUMP 17
13)Z=Z4                |  REFLECTION FACTOR TYPE 5,6,7  24 VALUES
   JUMP 17
14)JUMP 16, K=0
   JUMP 13
15)Z=Z0                |  REFLECTION FACTOR TYPE 1       1 VALUE
   JUMP 17
16)Z=Z1                |  REFLECTION FACTOR TYPE 2       6 VALUES

 >>SELECT NEXT ION AND REFLECT.
17)V=0
   Y=0
   F'=0
   G'=0
   A21=0
   A22=0
   W8=0
   W0=0
   W10=0
   F13=0
   I=0(1)12            |  START OF REFLECTION CYCLE
   U0 = AI
   U1 = AI+1
   U2 = AI+2
   U3 = AI+3
```

```
    U4 =-AI+1
    U5 =-AI+2
    U6 =-AI+3
    M' = 0
    CHECK(AI,0,0.01,18)
    CHECK(AI,0.5,0.01,18)
    N' = 6
    JUMP 20
18)N' = 3
20)U7 = BI
    U8 = BI-1
    U9 = BI+1
    U10= BI-2
    U11= BI+2
    U12= BI-3
    U13= BI+3
    U14=-BI
    U15=-BI+1
    U16=-BI-1
    U17=-BI+2
    U18=-BI-2
    U19=-BI+3
    U20=-BI-3
    P' = 20
    CHECK(BI,0,0.01,21)
    CHECK(BI,0.5,0.01,22)
    O' = 7
    JUMP 23
21)O' = 14
    JUMP 23
22)O' = 13
23)U21= CI
    U22= CI-1
    U23= CI+1
    U24= CI-2
    U25= CI+2
    U26= CI-3
    U27= CI+3
    U28=-CI
    U29=-CI+1
    U30=-CI-1
    U31=-CI+2
    U32=-CI-2
    U33=-CI+3
    U34=-CI-3
    R' = 34
    CHECK(CI,0,0.01,24)
    CHECK(CI,0.5,0.01,25)
```

```
   Q' = 21
   JUMP 26
24)Q' = 28
   JUMP 26
25)Q' = 27

 >>CALCULATE RADIUS VECTOR SQUARED.
26)P=M'(1)N'          |  START OF P CYCLE
   A=UP-X'
   W2=A
   A13=AA
   A'=A-2UP
   W5=A'
   A14=A'A'
   Q=O'(1)P'          |  START OF Q CYCLE
   B=UQ-Y'
   W3=B
   B13=BB
   B'=B-2UQ
   W6=B'
   B14=B'B'
   R=O'(1)R'          |  START OF R CYCLE
   S=O
   C=UR-Z'
   W4=C
   D=CC+A13+B13
   JUMP 31, D>12.25   |  OMITS IF SEPARATION TOO LARGE
   G'=G'+1            |  COUNTS POSITIVE REFLECTION
   F'=O
   JUMP 28
27)S=3
   C'=C-2UR
   W7=C'
   D=C'C'+A14+B14     |  NEGATIVE REFLECTION
   F'=F'+1            |  COUNTS NEGATIVE REFLECTION
   E'=2

 >>CALCULATE 12-6 AND QUADRUPOLE CONTRIBUTION.
28)E=1/D
   JUMP 83, D>6.25    |  OMITS DISPERSION POTENTIAL IF SEPARATION TOO LARGE
   G=GIEEE            |  DISPERSION POTENTIAL
   JUMP 82, D>2.25    |  OMITS REPULSION POTENTIAL IF SEPARATION TOO LARGE
   H=HIGGYI           |  REPULSION POTENTIAL
   V=V+H
   A21=A21+1          |  SUMS NUMBER OF IONS CONTRIBUTING TO PHI R
82)Y=Y+G
   F12=πIπIEEE        |  QUADRUPOLE POTENTIAL
   F13=F13+F12
   A22=A22+1          |  SUMS NUMBER OF IONS CONTRIBUTING TO PHI D AND PHI Q
```

```
 >>CALCULATE POLARISATION CONTRIBUTION.
83)W0=*SQRT(E)
   W1=πIW0Σ
   W8=W8+W(S+2)W1      |  SUMS X COMPONENT
   W9=W9+W(S+3)W1      |  SUMS Y COMPONENT
   W10=W10+W(S+4)W1    |  SUMS Z COMPONENT
29)JUMP 30, I<2        |  JUMPS IF ON FIRST TWO LINES OF DATA
   JUMP 27, 1>E'       |  PICKS UP NEGATIVE REFLECTION IF NOT DONE
   JUMP 31
30)JUMP 31, P=0        |  CHECKS FOR X COORDINATE = ZERO
   JUMP 27, 1>E'       |  PICKS UP NEGATIVE REFLECTION IF NOT DONE
31)REPEAT              |  R CYCLE
   REPEAT              |  Q CYCLE
   REPEAT              |  P CYCLE
   REPEAT              |  REFLECTION CYCLE
   W=W8W8+W9W9+W10W10
   Γ=WZ↓2              |  POLARISATION POTENTIAL

 >>CALCULATE EXPONENTIALS.
   I=0(1)11
   F(I)=F13Z(I+6)      |  QUADRUPOLE AT VARIOUS TEMPERATURES
   VI=V-Y-F-F(I)       |  TOTAL POTENTIAL AT VARIOUS TEMPERATURES
   U=VI
   JUMP 32, U>0.005    |  JUMPS IF POTENTIAL SIGNIFICANTLY POSITIVE
   DI=Z(I+18)
   EI=*EXP(-VIDI)      |  SIMPLE PARTITION FUNCTION
   EI=EIZ
   XI=XI+EI            |  SUMS EXPONENTIALS
   JUMP 33
32)EI=0                |  EXPONENTIAL IS ZERO FOR POSITIVE POTENTIALS
33)REPEAT

 >>PRINT RESULTS.
   CAPTION
        GRID POINT    =
   PRINT(J,2,0)
   PRINT(K,2,0)
   PRINT(L,2,0)
   NEWLINE
   CAPTION
        REPULSION     =
   PRINT(V,0,3)
   CAPTION
     NUMBER OF IONS =
   PRINT(A21,5,0)
   NEWLINE
   CAPTION
        DISPERSION    =
   PRINT(-Y,0,3)
```

```
    CAPTION
      NUMBER OF IONS =
    PRINT(A22,5,0)
    NEWLINE
    CAPTION
         POLARISATION =
    PRINT(-F,0,3)
    CAPTION
      NUMBER OF IONS =
    PRINT(F'+G',5,0)
    NEWLINE
    CAPTION
         QUADRUPOLE   =
    PRINT(-F13Z12,0,3)
    CAPTION
      NUMBER OF IONS =
    PRINT(A22,5,0)
    CAPTION
   T=25 C
    NEWLINE 2
    CAPTION
                    POTENTIAL      QUADRUPOLE    EXPONENTIAL
    CAPTION
EXPONENTIAL SUM
    NEWLINE
    I=0(1)11
    NEWLINE
    CAPTION
         T =
    M'=30+I
    PRINT(ZM',3,0)
    PRINT(VI,0,5)
    SPACE
    PRINT(-FI,0,3)
    PRINT(EI,0,3)
    SPACE
    PRINT(XI,0,6)
    REPEAT
    NEWLINE 2
    CAPTION
         POLARISATION COMPONENTS          X DIRECTION  =
    PRINT(W8,0,0)
    NEWLINE
    CAPTION
                                          Y DIRECTION  =
    PRINT(W9,0,0)
    NEWLINE
    CAPTION
                                          Z DIRECTION  =
    PRINT(W10,0,0)
```

```
   CHECK(A18,2,0.01,40)|  ORGANISES OUTPUT SPACING
   A18=2
   JUMP 41
40)A18=3
41)NEWLINE 2
   CHECK(A18,2,0.01,42)
   NEWLINE
42)U=V11                  |  DECISION SECTION FOR GRID REPEAT CYCLES
   JUMP 34, U>0.005
   T=0
   JUMP 35
34)T=T+1
   JUMP 36, T=1
   JUMP 37, T=2
35)REPEAT                 |  GRID L CYCLE
36)REPEAT                 |  GRID K CYCLE
37)T=0
   REPEAT                 |  GRID J CYCLE
   A17=S'
   JUMP 1, 0.5>A17        | JUMPS TO SMALL CAGE IF NOT DONE
38)NEWLINE 4
   CAPTION
   TOTAL NUMBER OF POINTS CALCULATED IN SMALL CAGE =
   PRINT(W',3,0)
   END
   CLOSE
```

```
0        0.2720   0.5      2.32,-7   2384   -0.25   1.609   1
0        0.5      0.2720   2.32,-7   2384   -0.25   1.609   6
0.2720   0        0.5      2.32,-7   2384   -0.25   1.609   8
0.2720   0.5      0        2.32,-7   2384   -0.25   1.609   12
0.5      0        0.2720   2.32,-7   2384   -0.25   1.609   24
0.5      0.2720   0        2.32,-7   2384   -0.25   1.609   48
0.2122   0.2122   0.5      2.32,-7   2384   -0.25   1.609   7.030,-7
0.2122   0.5      0.2122   2.32,-7   2384   -0.25   1.609   8.510,-7
0.5      0.2122   0.2122   2.32,-7   2384   -0.25   1.609   0.520,-7
0.1518   0.3882   0.3882   2.32,-7   2384   -0.25   1.609   1.080,-6
0.3882   0.1518   0.3882   2.32,-7   2384   -0.25   1.609   1.158,-6
0.3882   0.3882   0.1518   2.32,-7   2384   -0.25   1.609   1.245,-6
0.3050   0.3050   0.3050   1.22,-7   2350    1.5    30.30   1.350,-6

1.473,-6      1.623,-6      1.804,-6      2.035,-6      2.325,-6

1265   1530   1710   1940   2080   2240
2430   2650   2918   3245   3655   4185

 573    473    423    373    348    323
 298    273    248    223    198    173

1.511,-5

***Z
```

Programme Notes for the Virial Programme - Run 74

Data Input This consists of the number of grid points P' to be processed, the reflection factors V0 to V5, the coordinates A(I), B(I), C(I) of the grid points with potential D(I) in units of 10^{-10}ergs/CO_2 molecule taken from run 63. The grid points are referred to a different origin from those in run 63. A', B', C' and D0 are the potential constants for the CO_2-CO_2 interaction and the temperature coefficient at 323°K. (See table A7).

Organisation The cycle P = 0(1)P' selects a grid point as the position of the first CO_2 molecule and the corresponding reflection factor for this point is calculated and stored in V. The second point is selected at Q = P(1)P' and a multiple V6 is set such that if the two molecule positions are coincident, V6 = 1/2 to prevent duplication of later inferred reflections. Otherwise V6 = 1. The second point coordinates are converted to integers J, K and L at label 81) and the properties of these integers are used to decide which of the positions given by labels 1) to 48) are the correct reflected and rotated positions of the second molecule within the sieve cage. When these have been selected in turn the separation between the first and second molecule positions is calculated at label 71) in units of b_o, and the resulting CO_2 - CO_2 interaction based on this distance is stored in G', omitting coincident molecules when they occur. The contributions to the double summation SIGMA 2 are divided into three parts determined by the value

of G'. These are the contributions from $F(I, J) > 0$, $-1 < F(I, J) \leq 0$ and $F(I, J) = -1$. These contributions are stored in H0 to H2 and the programme returns via the variable jump, JUMP(S) to the next reflected position of the second molecule. When all these have been done the next position for the first molecule is considered.

Output This includes the contributions to the double summation in the above ranges of F(I, J) together with the number of calculated interactions and inferred interactions for every first molecule considered. At the end of computation final results for all the summations considered together with the number of computed and inferred interactions is given.

A flow diagram for this programme is given in Figure 3.12.

EXCHLF CO2-CO2 INTERACTION AND CRYSTAL SECOND VIRIAL COEFFICIENT PROGRAMME

```
TITLE
C. J. WHITFORD, CHEM ENG, ICST.

TITLE
SECOND VIRIAL COEFFICIENT IN LINDE 5A-CO2 SYSTEM.

TITLE
POTENTIALS FROM RUN 63 AT 323 DEGREES ABSOLUTE.


CHAPTER 0
   A→90
   B→90
   C→90
   D→90
   E→3
   H→4
   U→9
   V→6
   π→2
   READ(P')              | NUMBER OF DATA POINTS
   P=0(1)5
   READ(V(P))            | REFLECTION FACTORS
   REPEAT
   P=0(1)P'
   READ(A(P))            | X COORDINATE OF CO2 MOLECULE
   READ(B(P))            | Y COORDINATE OF CO2 MOLECULE
   READ(C(P))            | Z COORDINATE OF CO2 MOLECULE
   READ(D(P))            | CO2 POTENTIAL AT (X,Y,Z)
   REPEAT
   READ(A')              | REPULSION CONSTANT
   READ(B')              | DISPERSION CONSTANT
   READ(C')              | QUADRUPOLE CONSTANT
   READ(E(0))            | TEMPERATURE COEFFICIENT
   H3=0
   H4=0
   U3=0
   U4=0
   U8=0
   U9=0
   NEWLINE
   CAPTION
 GP   , F(IJ)=-1     U0  0>F(IJ)>-1     U1     F(IJ)>0      U2
```

```
   CAPTION
      F(IJ)        U012     U567     F(IJ)>0        U2        U7
   NEWLINE 4

>>FIRST POINT CYCLE.
   P=0(1)P'          /    |  START OF P CYCLE
   NEWLINE
   X'=AP                  |  X COORDINATE OF FIRST CO2 MOLECULE
   Y'=BP                  |  Y COORDINATE OF FIRST CO2 MOLECULE
   Z'=CP                  |  Z COORDINATE OF FIRST CO2 MOLECULE

>>DETERMINE POINT MULTIPLE FOR FIRST POINT.
   JUMP 77, X'=10
   JUMP 73, X'=Y'
   JUMP 76, Y'=Z'
   JUMP 75, Z'=10
   V=V5                   |  REFLECTION TYPE 8      POINT MULTIPLE = 48
   JUMP 79
73)JUMP 74, Z'≠10
   V=V3                   |  REFLECTION TYPE 4      POINT MULTIPLE = 12
   JUMP 79
74)JUMP 75, Y'≠Z'
   V=V2                   |  REFLECTION TYPE 3      POINT MULTIPLE =  8
   JUMP 79
75)V=V4                   |  REFLECTION TYPE 5,6,7  POINT MULTIPLE = 24
   JUMP 79
76)JUMP 78, Y'=10
   JUMP 75
77)V=V0                   |  REFLECTION TYPE 1      POINT MULTIPLE =  1
   JUMP 79
78)V=V1                   |  REFLECTION TYPE 2      POINT MULTIPLE =  6

>>SECOND POINT CYCLE.
79)Q=P(1)P'               |  START OF Q CYCLE
   E2=DP-DQ
   π=*SIGN(E2)
   E3=E2π
   JUMP 80, 0.00000001>E3    |  CHECKS FOR COINCIDENCE OF MOLECULES
   V6=1                   |  FULL VALUE FOR FIRST POINT MULTIPLE
   JUMP 81
80)V6=0.5                 |  HALF VALUE FOR FIRST POINT MULTIPLE
81)J=*INTPT(AQ+0.01)
   K=*INTPT(BQ+0.01)
   L=*INTPT(CQ+0.01)

>>SELECT REFLECTION PROCEDURE FOR SECOND POINT.
   JUMP 69, J=10
   JUMP 51, J=K
   JUMP 61, K=L
   JUMP 63, L=10
```

```
   S=L50                  |  REFLECTION TYPE 8     48 VALUES
   I=1(1)48
   T)=I)
   JUMP(T)
50)REPEAT
   JUMP 72

51)JUMP 55, L≠10          |  REFLECTION TYPE 4     12 VALUES
   S=L52
   I=1(8)25
   T)=I)
   JUMP(T)
52)REPEAT
   S=L53
   I=4(8)28
   T)=I)
   JUMP(T)
53)REPEAT
   S=L54
   I=33(5)48
   T)=I)
   JUMP(T)
54)REPEAT
   JUMP 72

55)JUMP 58, K≠L           |  REFLECTION TYPE 3      8 VALUES
   S=L56
   I=1(1)4
   T)=I)
   JUMP(T)
56)REPEAT
   S=L57
   I=17(1)20
   T)=I)
   JUMP(T)
57)REPEAT
   JUMP 72

58)S=L59                  |  REFLECTION TYPE 6     24 VALUES
   I=1(16)17
   M=I+7
   N=I(1)M
   T)=N)
   JUMP(T)
59)REPEAT
   REPEAT
   S=L60
   I=33(8)41
   M=I+3
```

```
   N=I(1)M
   T)=N)
   JUMP(T)
60)REPEAT
   REPEAT
   JUMP 72

61)JUMP 66, K=10          |  REFLECTION TYPE 7     24 VALUES
   S=L62
   I=1(8)41
   M=I+3
   N=I(1)M
   T)=N)
   JUMP(T)
62)REPEAT
   REPEAT
   JUMP 72

63)S=L64                  |  REFLECTION TYPE 5     24 VALUES
   I=1(2)31
   T)=I)
   JUMP(T)
64)REPEAT
   S=L65
   I=33(1)40
   T)=I)
   JUMP(T)
65)REPEAT
   JUMP 72

66)S=L67                  |  REFLECTION TYPE 2      6 VALUES
   I=1(8)17
   T)=I)
   JUMP(T)
67)REPEAT
   S=L68
   I=27(8)43
   T)=I)
   JUMP(T)
68)REPEAT
   JUMP 72

69)S=L70                  |  REFLECTION TYPE 1      1 VALUE
   JUMP 1
70)JUMP 72
```

```
>>REFLECT SECOND POINT.
 1)X=J                    |  X COORDINATE OF SECOND CO2 MOLECULE
   Y=K                    |  Y COORDINATE OF SECOND CO2 MOLECULE
   Z=L                    |  Z COORDINATE OF SECOND CO2 MOLECULE
   JUMP 71
 2)Z=20-L
   JUMP 71
 3)Y=20-K
   Z=L
   JUMP 71
 4)X=J
   Y=20-K
   Z=20-L
   JUMP 71
 5)Y=L
   Z=K
   JUMP 71
 6)Y=20-L
   JUMP 71
 7)Y=L
   Z=20-K
   JUMP 71
 8)Y=20-L
   JUMP 71
 9)X=K
   Y=L
   Z=J
   JUMP 71
10)Y=20-L
   JUMP 71
11)Y=L
   Z=20-J
   JUMP 71
12)X=K
   Y=20-L
   Z=20-J
   JUMP 71
13)Y=J
   Z=L
   JUMP 71
14)Z=20-L
   JUMP 71
15)Y=20-J
   Z=L
   JUMP 71
16)Z=20-L
   JUMP 71
17)X=20-J
   Y=K
   Z=L
   JUMP 71
```

```
18)Z=20-L
   JUMP 71
19)Y=20-K
   Z=L
   JUMP 71
20)X=20-J
   Y=20-K
   Z=20-L
   JUMP 71
21)Y=L
   Z=K
   JUMP 71
22)Y=20-L
   JUMP 71
23)Y=L
   Z=20-K
   JUMP 71
24)Y=20-L
   JUMP 71
25)X=20-K
   Y=L
   Z=J
   JUMP 71
26)Y=20-L
   JUMP 71
27)X=20-K
   Y=L
   Z=20-J
   JUMP 71
28)X=20-K
   Y=20-L
   Z=20-J
   JUMP 71
29)Y=J
   Z=L
   JUMP 71
30)Z=20-L
   JUMP 71
31)Y=20-J
   Z=L
   JUMP 71
32)Z=20-L
   JUMP 71
33)X=L
   Y=J
   Z=K
   JUMP 71
34)Y=20-J
   JUMP 71
```

```
35)X=20-L
   Y=J
   Z=20-K
   JUMP 71
36)Y=20-J
   JUMP 71
37)X=L
   Y=K
   Z=J
   JUMP 71
38)X=20-L
   Y=K
   Z=20-J
   JUMP 71
39)X=L
   Y=20-K
   Z=J
   JUMP 71
40)X=20-L
   Z=20-J
   JUMP 71
41)X=20-L
   Y=J
   Z=K
   JUMP 71
42)X=L
   Z=20-K
   JUMP 71
43)X=20-L
   Y=20-J
   Z=K
   JUMP 71
44)X=L
   Z=20-K
   JUMP 71
45)X=20-L
   Y=K
   Z=J
   JUMP 71
46)X=L
   Z=20-J
   JUMP 71
47)X=20-L
   Y=20-K
   Z=J
   JUMP 71
48)X=L
   Y=20-K
   Z=20-J
```

```
>>CALCULATE EXPONENTIALS.
71)U'=X'-X              |  X SEPARATION BETWEEN CO2 MOLECULES
   V'=U'U'
   W=Y'-Y               |  Y SEPARATION BETWEEN CO2 MOLECULES
   W'=WW
   F'=Z'-Z              |  Z SEPARATION BETWEEN CO2 MOLECULES
   H'=F'F'+V'+W'
   JUMP 84, 0.5>H'      |  OMITS IF MOLECULES COINCIDENT
   E=1/H'
   D=EEE
   G'=A'DD-B'D-C'DEE    |  MOLECULE - MOLECULE INTERACTION
   JUMP 82, G'≠0.005    |  JUMPS IF POTENTIAL SIGNIFICANTLY POSITIVE
   F=*EXP(-G'EO)
   C=F-1
   E'=DPEO+DQEO         |  MOLECULE - ION INTERACTION
   G=*EXP(-E')
   JUMP 83, G'≠0
   U2=U2+1              |  SUMS NUMBER OF CALCULATIONS
   π2=GCVV6             |  CONTRIBUTION FROM F(I,J)>0
   H2=H2+π2             |  SUMS CONTRIBUTIONS
   U7=U7+VV6            |  SUMS NUMBER OF MOLECULES
   JUMP 85
82)C=-1
   UO=UO+1              |  SUMS NUMBER OF CALCULATIONS
   E'=DPEO+DQEO
   G=*EXP(-E')
   πO=GCVV6             |  CONTRIBUTION FROM F(I,J)=-1
   HO=HO+πO             |  SUMS CONTRIBUTIONS
   U5=U5+VV6            |  SUMS NUMBER OF MOLECULES
   JUMP 85
83)U1=U1+1              |  SUMS NUMBER OF CALCULATIONS
   π1=GCVV6             |  CONTRIBUTIONS FROM O≠F(I,J)>-1
   H1=H1+π1             |  SUMS CONTRIBUTIONS
   U6=U6+VV6            |  SUMS NUMBER OF MOLECULES
   JUMP 85
84)O=P
   O'=Q
85)JUMP(S)              |  JUMPS TO PRESET LABEL S
72)REPEAT               |  Q CYCLE

>>PRINT RESULTS.
   PRINT(O,2,O)         |  OUTPUT CHECK FOR COINCIDENCE
   SPACE
   H3=H3+HO+H1+H2       |  SUMS ALL CONTRIBUTIONS
   H4=H4+H2             |  SUMS ALL CONTRIBUTIONS FROM F(I,J)>O
```

```
U3=U3+U0+U1+U2          |  SUMS NUMBER OF ALL CALCULATIONS
U4=U4+U2                |  SUMS ALL CALCULATIONS FROM F(I,J)>0
U8=U8+U5+U6+U7          |  SUMS ALL MOLECULES
U9=U9+U7                |  SUMS ALL MOLECULES FROM F(I,J)>0
I=0(1)2
PRINT(H(I),0,4)         |  OUTPUTS CONTRIBUTIONS
PRINT(U(I),3,0)         |  OUTPUTS NUMBER OF CALCULATIONS
REPEAT
SPACE 2
PRINT(H3,0,4)           |  ALL CONTRIBUTIONS SUMMED TO DATE
PRINT(U0+U1+U2,4,0)     |  NUMBER OF CALCULATIONS IN LAST VALUE OF P DONE
PRINT(U5+U6+U7,5,0)     |  NUMBER OF MOLECULES IN LAST VALUE OF P DONE
PRINT(H4,0,4)           |  ALL CONTRIBUTIONS FROM F(I,J)>0 SUMMED TO DATE
PRINT(U2,4,0)           |  NUMBER OF CALCULATIONS FROM F(I,J)>0 IN
                        |  LAST VALUE OF P DONE
PRINT(U7,5,0)           |  NUMBER OF MOLECULES FROM F(I,J)>0 IN
                        |  LAST VALUE OF P DONE
I=0(1)2
UI=0                    |  CLEARS CONTRIBUTION AND CALCULATION COUNTERS
HI=0                    |  IN LAST VALUE OF P DONE
REPEAT
I=5(1)7
UI=0                    |  CLEARS MOLECULE COUNTERS
REPEAT
REPEAT                  |  P CYCLE
NEWLINE 6
CAPTION
FINAL RESULT FOR THE DOUBLE SUMMATION FOR ALL F(IJ) IS
PRINT(H3,0,9)
NEWLINE 2
CAPTION
NUMBER OF INTERACTING PAIRS OF CO2 MOLECULES =
PRINT(U8,7,0)
CAPTION
  NUMBER CALCULATED =
PRINT(U3,5,0)
NEWLINE 4
CAPTION
FINAL RESULT FOR THE DOUBLE SUMMATION FOR ALL F(IJ)>0 IS
PRINT(H4,0,8)
NEWLINE 2
CAPTION
NUMBER OF INTERACTING PAIRS OF CO2 MOLECULES =
PRINT(U9,7,0)
CAPTION
  NUMBER CALCULATED =
PRINT(U4,5,0)
END
CLOSE
```

61

1		6	8	12		24	48
10	10	10	-2.20201, -3	11	10	10	-2.27583, -3
11	11	10	-2.35675, -3	11	11	11	-2.44694, -3
12	10	10	-2.49358, -3	12	11	10	-2.59604, -3
12	11	11	-2.71346, -3	12	12	10	-2.89656, -3
12	12	11	-3.05847, -3	12	12	12	-3.50930, -3
13	10	10	-2.85313, -3	13	11	10	-2.98853, -3
13	11	11	-3.14868, -3	13	12	10	-3.37967, -3
13	12	11	-3.60073, -3	13	12	12	-4.15908, -3
13	13	10	-3.97524, -3	13	13	11	-4.25183, -3
13	13	12	-4.57201, -3	13	13	13	-1.98992, -3
14	10	10	-3.36552, -3	14	11	10	-3.53972, -3
14	11	11	-3.74809, -3	14	12	10	-4.02814, -3
14	12	11	-4.30127, -3	14	12	12	-4.77543, -3
14	13	10	-4.68121, -3	14	13	11	-4.89817, -3
14	13	12	-3.67721, -3	14	14	10	-5.20331, -3
14	14	11	-4.83638, -3	14	14	12	+4.31021, -3
15	10	10	-4.02948, -3	15	11	10	-4.22292, -3
15	11	11	-4.45735, -3	15	12	10	-4.71747, -3
15	12	11	-4.99738, -3	15	12	12	-5.03890, -3
15	13	10	-5.01543, -3	15	13	11	-5.01517, -3
15	13	12	-2.98148, -4	15	14	10	-3.99114, -3
15	14	11	-2.09698, -3	15	15	10	+2.75740, -3
16	10	10	-4.66914, -3	16	11	10	-4.76384, -3
16	11	11	-4.92581, -3	16	12	10	-4.41243, -3
16	12	11	-4.63781, -3	16	12	12	-3.31592, -3
16	13	10	-1.42514, -4	16	13	11	-5.62380, -4
17	10	10	-4.85669, -3	17	11	10	-4.31319, -3
17	11	11	-3.81599, -3	17	12	10	+2.81680, -3
17	12	11	+2.59574, -3	18	10	10	-4.15687, -3
18	11	10	-1.05069, -3	18	11	11	+1.80115, -3
19	10	10	-2.56568, -3	20	10	10	-1.64105, -3

6.200, +6 37 1418 2240

***Z

Programme Notes for the Diffusion Model

Input This consists of the parameters describing the model, finite difference increments and estimates of diffusivities, followed by practical breakthrough curves and the accuracy parameters for the desired degree of fit between the theoretical and practical curves.

Organisation The programme adjusts the pore and crystal diffusivities until the theoretical breakthrough curves generated by the algorithms in Section 2.7 best fit the practical curves. The information describing the two curves are stored in arrays Y1 and Y2 and comparison is made at the temperature specified on input.

Output This includes intermediate tabulated results for the theoretical breakthrough curves for the diffusivities currently set by the programme and a graphical plot of the final theoretical curve chosen compared with the practical curve.

Flow diagrams for this programme are given in Figures 3.13-15.

FORTRAN DIFFUSION MODEL PROGRAMME

```
C*************************************************************************
C****     MAIN PROGRAMME.
       INTEGER RUN
       DIMENSION A(3,10), C(10), D(10), G1(10), V1(10), W1(10,10)
       DIMENSION X2(200),Y2(200),X1(250),Y1(250),X(2),F(2),W(10)
       COMMON V1,W1,JMAX,KMAX /COMN1/ AJ,AK,Q,PHI,BETA,ITMAX
      1 /COMN2/ FRAC,PELPOR,ACCO,P /COMN3/ TIM,I /COMN4/ PSI,A
      2 /COMN5/ ITER,ERROR,ALPHA,G1,EQICON /COMN6/ C,D
      3 /COMN7/ X2,Y2,KGRAPH,XC1,YC1,X1,Y1,LGRAPH
      4 /COMN8/ TIME TIMAX,ALPELT,RADCRY,PELDIF

C****    READ AND PRINT DATA.
       READ(5,1000) PELDIF,CRYDIF,EQICON,TEMP,RUN,DIAM,ALPELT,RADCRY,
      1 PELPOR,JMAX,KMAX,ITMAX,BETA,ALPHA,TIME,TIMAX
 1000 FORMAT(F10.4,E15.4,2F10.1,I10,/
      2 F10.4,F10.2,E15.4,F10.4,/
      3 3I6,/
      4 F10.2,E15.4,/
      5 F10.4,F10.0)
       WRITE(6,2000) RUN,TEMP,EQICON,TEMP,DIAM,ALPELT,PELPOR,PELDIF,
      1 RADCRY,CRYDIF,TEMP,TIME,TIMAX
 2000 FORMAT (127H1 C O 2      A D S O R P T I O N      I N      A
      1O N E      D I M E N S I O N A L      5 A      S I E V E      P E
      2L L E T  /////
      32HOADSORPTION TRIAL NUMBER, I3,//
      437HOGAS TEMPERATURE                        =  F10.1, 7X,16H DEGREES CE
      4LSIUS ,/
      537H ISOTHERM EQUILIBRIUM CONSTANT      =  F10.1, 7X,3H AT,F7.1,16H
      5 DEGREES CELSIUS  /
      637HOPELLET DIAMETER                        =  F13.4, 4X,4H CMS      /
      737H PELLET LENGTH                          =  F11.2, 6X,4H CMS      /
      837H PELLET POROSITY                        =  F13.4,                /
      937H PELLET DIFFUSIVITY                     =  E17.4,    8H CM2/SEC /
      137HOMEAN CRYSTAL RADIUS                    =  E17.4,    4H CMS      /
      237H CRYSTAL DIFFUSIVITY                    =  E17.4,   11H CM2/SEC AT,
      2 F7.1,16H DEGREES CELSIUS /
      337HOREAL TIME INCREMENT                    =  F13.4, 1X,5H SECS     /
      437H TOTAL TIME FOR RUN                     =  F10.1, 7X,5H SECS     / )
       WRITE(6,2500) JMAX,KMAX,ALPHA,BETA,ITMAX
 2500 FORMAT(37H NUMBER OF PELLET INCREMENTS          =  I8     ,          /
      137H NUMBER OF CRYSTAL INCREMENTS       =  I8     ,                 /
      237H RELATIVE ERROR IN CONCENTRATION    =  E17.4,                   /
      337H RELAXATION PARAMETER               =  F11.2,                   /
      437HOMAX. NO. OF ITERATIONS PERMISSIBLE =  I8                ///// )
```

```
C****    COMPUTE DIMENSIONLESS PARAMETERS FOR OUTPUT.
      X(1) = PELDIF
      AJ   = JMAX
      AK   = KMAX
      DT   = TIME*X(1)/ALPELT**2
      DX   = 1. / AJ
      DR   = 1. / AK
      P = PELDIF*RADCRY**2 / (CRYDIF*ALPELT**2)
      X(2) = P
      Q    = X(2)*AJ**2/(3.*(1.-PELPOR))
      PHI  = 2.*X(2)/(AK**2*DT)
      PSI  = 2.*(PELPOR + (1. -PELPOR)*EQICON) / (AJ**2DT)
      ACCO = (PELPOR + (1. - PELPOR)*EQICON)
      IMAX = (TIMAX / TIME) + 0.5

C****    PRINT DIMENSIONLESS PARAMETERS.
      WRITE(6,3000) DT,DX,DR,P,Q,PHI,PSI,ACCO,IMAX
 3000 FORMAT(25H1DIMENSIONLESS PARAMETERS,/
     16HODT  =,E15.4,15X,6H DX  =,E15.4,15X,6H DR  =, E15.4, /
     26HOP   =,E15.4,15X,6H Q   =,E15.4,15X,6H PHI =,E15.4,15X,6H PSI =,
     3E15.4,/6HOACCO=,E15.4,/6HOIMAX=,I10//// )

C****    CALCULATE SIMPSONS RULE COEFFICIENTS FOR THE CRYSTAL.
C****    THESE ARE STORED IN ARRAY C(K).
      MAX=KMAX+1
      DO 1 K=1,MAX,2
      IF(K.EQ.MAX-2) GO TO 2
      BK=K
      C(K)      = 4.*(BK/AK)**2
      C(K+1)    = 2.*((BK+1.)/AK)**2
    1 CONTINUE
    2 BK=KMAX-1
      C(KMAX-1) = 4.*(BK/AK)**2
      C(KMAX)   = 1.

C****    CALCULATE SIMPSONS RULE COEFFICIENTS FOR THE PORES.
C****    THESE ARE STORED IN ARRAY D(J).
      MAX=JMAX+1
      DO 3 J=1,MAX,2
      IF(J.EQ.MAX-2) GO TO 4
      D(J)      = 4.
      D(J+1)    = 2.
    3 CONTINUE
    4 D(JMAX-1) = 4.
      D(JMAX)   = 1.
```

```
C****    VA04A PARAMETERS.
      N=2
      ICON=1
      IPRINT=1
      MAXIT=18
      MAXFUN=500
      READ(5,4000) E(1),E(2),ESCALE
 4000 FORMAT(2F10.6,F10.0)
      WRITE(6,5000) E(1),E(2),ESCALE
 5000 FORMAT(10H   E(1)  =,F10.6,10H   E(2)  =,F10.6,12H   ESCALE  =,
     1 F10.2)
      CALL PRACG
      N3N=N*(N+3)
      EXTERNAL CALCFX
      CALL VA04A(X,E,N,F,ESCALE,IPRINT,ICON,MAXIT,CALCFX,W,N3N,MAXFUN)
      WRITE(6,6000) X(1),X(2),F
 6000 FORMAT(10H   X(1)  =,F10.6,10H   X(2)  =,F10.2,7H   F  =,E15.8)
      CALL DRAWS
      STOP
      END


C*********************************************************************
      SUBROUTINE CALCFX(N,F,X)
      DIMENSION X(2)
      CALL MAIN(X,F)
      RETURN
      END


C*********************************************************************
      SUBROUTINE MAIN(X,F)
      INTEGER RUN
      DIMENSION A(3,10), C(10), D(10), G1(10), V1(10), W1(10,10)
      DIMENSION X2(200),Y2(200),X1(250),Y1(250),X(2),E(2)
      COMMON V1,W1,JMAX,KMAX /COMN1/ AJ,AE,Q,PHI,BETA,ITMAX
     1 /COMN2/ FRAC,PELPOR,ACCO,P /COMN3/ TIM,I /COMN4/ PSI,A
     2 /COMN5/ ITER,ERROR,ALPHA,G1,EQICON /COMN6/ C,D
     3 /COMN7/ X2,Y2,KGRAPH,XC1,YC1,X1,Y1,LGRAPH
     4 /COMN8/ TIME TIMAX,ALPFLT,RADCRY,PELDIF
      CRYDIF = X(1)*RADCRY**2/(X(2)*ALPELT**2)
      WRITE(6,9999) X(1),X(2),CRYDIF
 9999 FORMAT(6H  MAIN,10X,6HX(1) =,E18.8,10X,6HX(2) =,E18.8,
     1 ,6X,8HCRYDIF =,E18.8)

C****    SETS START VALUE FOR PRACTICAL RESULTS AT 0 CELSIUS.
      KGRAPH = 58
```

```
C****    OUTPUT COUNTERS.
      COUNT1 = 1.
      COUNT2 = 15.

C****    COMPUTE DIMENSIONLESS PARAMETERS.
  101 IF(COUNT1.LT.2.) GO TO 102
      I = 10
      TIME = 10.*TIME
      GO TO 103
  102 TIME = TIME/10.
  103 AJ   = JMAX
      AK   = KMAX
      DT   = TIME*X(1)/ALPELT**2
      DX   = 1./AJ
      DR   = 1./AK
      P    = X(2)
      Q    = P*AJ**2/(2.*(1.-PELPOR))
      PHI  = 2.*P/(AK**2*DT)
      PSI  = 2.*(PELPOR+(1.-PELPOR)*EQICON)/(AJ**2*DT)
      ACCO = (PELPOR+(1.-PELPOR)*EQICON)
      IMAX = (TIMAX/TIME)+0.5
      IF(COUNT1.GT.2.) GO TO 16

C****    SET INITIAL PELLET CONDITIONS.
      DO 9 K=1,KMAX
      DO 9 J=1,JMAX
      W1(J,K) = EQICON
    9 CONTINUE
      DO 13 J=1,JMAX
      G1(J) = 0.
      V1(J) = 1.
   13 CONTINUE
      ERROR = 0.
      TIM   = 0.
      FRAC  = 0.
      I     = 0
      ITER  = 0
      F     = 0.
   16 IF(ITER.LT.ITMAX) GO TO 20

C****    ITMAX EXCEEDED - ERROR MESSAGE AND STOP.
      WRITE(6,4000) P,I,ITER
 4000 FORMAT(54H1NUMBER OF ITERATIONS HAS EXCEEDED THE MAXIMUM ALLOWED,/
     1////5X,4HP  =,F10.2,10X,4HI  =,I10,10X,7HITER  =,I6)
      STOP
```

```
C****     START OF TIME ITERATION.
   20 I = I + 1
      IF(I.GT.IMAX) GO TO 96
      IF(P.EQ.0.) GO TO 25
      CALL COMP
      GO TO 49
   25 CALL POCOMP

C****     ALLOWS OUTPUT FOR EQUAL INCREMENTS OF SQUARE ROOT TIME ONLY.
   40 IF(TIME.GT.8.) GO TO 50
      KOUNT = COUNT1**2/TIME + 0.1
      IF(I.LT.KOUNT) GO TO 16
      COUNT1 = COUNT1 + 1.
      GO TO 60
   50 KOUNT = COUNT2**2/TIME + 0.5
      IF(I.LT.KOUNT) GO TO 16
      COUNT2 = COUNT2 + 5.
   60 CALL FRACT
      TIM = FLOAT(I)*TIME
      KGRAPH = KGRAPH + 1
      Y2(KGRAPH) = FRAC

C****      SUM OF SQUARES ERROR.
      IF(KGRAPH.GT.30) F=F+(Y2(KGRAPH)-Y1(KGRAPH))**2
      WRITE(6,5000) Y2(KGRAPH),Y1(KGRAPH),F,FRAC,TIM
 5000 FORMAT(6H       , F10.6,10X,F11.6,10X,E18.8,10X,F10.6,10X,F10.2)

C****     GO TO NEXT STEP IN TIME.
      IF(I.EQ.100.AND.KOUNT.EQ.1000) GO TO 101
      GO TO 16
   96 CONTINUE
      RETURN
      END


C*************************************************************************
C****     SUBROUTINE FOR P NOT EQUAL TO ZERO.
C****     COMPUTES ONE TIME STEP.
      SUBROUTINE COMP
      DIMENSION G1(10),G2(10),V1(10),V2(10),W1(10,10),W2(10,10),A3(10),
     1 B(10),V3(10)
      COMMON V1,W1,JMAX,KMAX /COMN1/ AJ,AK,Q,PHI,BETA,ITMAX
     1 /COMN3/ TIM,I /COMN4/ PSI,A /COMN5/ ITER,ERROR,ALPHA,G1,EQICON
      ITER  = 0
   10 ERROR = 0.
```

```
C****    COMPUTE ADSORPTION RATES USING THE MOST RECENT VALUE OF V1(J).
      DO 56 J=1,JMAX
      IF(J.EQ.1) GO TO 15
      IF(J.GT.1.AND.J.LT.JMAX) GO TO 16
      IF(J.EQ.JMAX) GO TO 17
   15 G2(J)=Q*(V1(J+1)-2.*V1(J))
      GO TO 20
   16 G2(J)=Q*(V1(J-1)+V1(J+1)-2.*V1(J))
      GO TO 20
   17 G2(J)=2.*Q*(V1(JMAX-1)-V1(JMAX))

C****    PUT RATES INTO ARRAY B(K) USING VALUES OF W1(J,K) AND
C****    G1(J) FROM THE PREVIOUS TIME STEP.
   20 B(1)     = 2.*(W1(J,2)-W1(J,1)) + PHI*W1(J,1)
      MAX = KMAX-1
      DO 21 K=2,MAX
      CK = K
      B(K)     = (CK-1.)*W1(J,K-1)/CK + (CK+1.)*W1(J,K+1)/CK
     1 - 2.W1(J,K) + PHI*W1(J,K)
   21 CONTINUE
      B(KMAX) = 2.*(W1(J,MAX)-W1(J,KMAX)) + PHI*W1(J,KMAX) + 2.*(AK+1.)*
     1 (G2(J)+G1(J))/AK**2

C****    FORM THE ARRAY A(I,K) FOR TLINEQ.
      S = PHI+2.
      A(1,1) =  0.
      A(2,1) =  S
      A(3,1) = -2.
      MAX    =  KMAX-1
      DO 22 K=2,MAX
      A(1,K) = -FLOAT(K-1)/FLOAT(K)
      A(2,K) =  S
      A(3,K) = -FLOAT(K+1)/FLOAT(K)
   22 CONTINUE
      A(1,K) = -2.
      A(2,K) =  S
      A(3,K) =  0.
      CALL TLINEQ(KMAX,A,B)

C****    PUT ARRAY B(K) INTO ARRAY W2(J,K).
      DO 50 K=1,KMAX
      W2(J,K)=B(K)
   50 CONTINUE

C****    NEW VALUE OF V2(J).
      V2(J) = B(KMAX)/EQICON
      IF(V2(J).GT.1.) V2(J) = 1.
```

```
C****    STORE THE MAXIMUM DIVERGENCE BETWEEN V2 AND V1 IN ERROR.
      IF(ABS(V1(J)-V2(J)).GT.ERROR) ERROR = ABS(V1(J)-V2(J))

C****    RELAXATION STEP GIVES THE NEW PORE CONCENTRATION, V3(J).
      V3(J) = BETA*V2(J) + (1.-BETA)*V1(J)
      IF(V3(J).GT.1.) V3(J) = 1.
   56 CONTINUE

C****    CHECK THE MAXIMUM ERROR AGAINST THE PERMITTED ERROR ALPHA.
      ITER = ITER + 1
      IF(ERROR.LT.ALPHA) GO TO 60
      DO 58 J=1,JMAX
      V1(J) = V3(J)
   58 CONTINUE

C****    CHECK ITMAX NOT EXCEEDED.
      IF(ITER.LT.ITMAX) GO TO 10

C****    STORE THE ARRAY W2(J,K) IN W1(J,K).
   60 DO 61 K=1,KMAX
      DO 61 J=1,JMAX
      W1(J,K) = W2(J,K)
      IF(W1(J,K).GT.EQICON) W1(J,K) = EQICON
   61 CONTINUE

C****    STORE THE ARRAY G2(J) IN G1(J) AND V3(J) IN V1(J).
      DO 70 J=1,JMAX
      G1(J) = G2(J)
      V1(J) = V3(J)
   70 CONTINUE
   99 RETURN
      END


C*************************************************************************
C****    SUBROUTINE FOR P EQUAL TO ZERO.
C****    COMPUTES ONE TIME STEP.
      SUBROUTINE POCOMP
      DIMENSION V1(10),A(3,10),B(10),W1(10,10)
      COMMON V1,W1,JMAX,KMAX /COMN3/ TIM,I /COMN4/ PSI,A

C****    COMPUTE THE ARRAY B(J) FOR TLINEQ USING V1(J).
      IF(I.EQ.1) GO TO 15
      B(1) = (PSI-2.)*V1(1)+V1(2)
      MAX = JMAX-1
      DO 10 J=2,MAX
      B(J) = V1(J-1)+(PSI-2.)*V1(J)+V1(J+1)
   10 CONTINUE
```

```
      B(JMAX) = 2.*V1(MAX)+(PSI-2.)*V1(JMAX)
      GO TO 25
   15 DO 20 J=1,JMAX
      B(J) = PSI
   20 CONTINUE

C****    FORM THE ARRAY A(I,J) FOR TLINEQ.
   25 S = PSI+2.
      A(1,1) =  0.
      A(2,1) =  S
      A(3,1) = -1
      MAX = JMAX-1
      DO 22 J=2,MAX
      A(1,J) = -1.
      A(2,J) =  S
      A(3,J) = -1.
   22 CONTINUE
      A(1,JMAX) = -2.
      A(2,JMAX) =  S
      A(3,JMAX) =  0.
      CALL TLINEQ(JMAX,A,B)
      DO 30 J=1,JMAX
      V1(J) = B(J)
   30 CONTINUE
      RETURN
      END

C*************************************************************************
C****    SOLVES SET OF LINEAR EQUATIONS WITH TRIDIAGONAL MATRIX.
      SUBROUTINE TLINEQ(N,A,B)
      DIMENSION A(3,10),B(10)
      DOUBLE PRECISION V1,V2
      A(1,1) = 0.
      A(3,N) = 0.

C****    ELIMINATION.
      DO 2 I=2,N
      V1 = A(2,I-1)
      IF(ABS(A(1,I)).GT.ABS(A(2,I-1))) GO TO 1
      IF(A(2,I-1).EQ.0.) GO TO 4
      V1 = A(1,I)/V1
      A(2,I) = A(2,I)-V1*A(3,I-1)
      B(I)   = B(I)  -V1*B(I-1)
      GO TO 2
```

```
C****    ELIMINATION WITH ROW INTERCHANGE.
    1 IF(A(1,I).EQ.0.) GO TO 4
      V1 = V1/A(1,I)
      V2 = A(3,I-1)
      A(1,I-1) = A(3,I)
      A(2,I-1) = A(1,I)
      A(3,I-1) = A(2,I)
      A(2,I)   = V2-V1*A(2,I)
      A(3,I)   = -V1*A(3,I)
      V2       = B(I-1)
      B(I-1)   = B(I)
      B(I)     = V2-V1*B(I)
    2 A(1,I)   = 0.
                          /
C****    BACK SUBSTITUTION.
      V1      = A(2,N)
      B(N)    = B(N)/V1
      V1      = B(N)
      B(N-1) = (B(N-1)-V1*A(3,N-1))/A(2,N-1)
      DO 3 I=1,N
      J  = N-I+1
      V1 = 0.
      V2 = 0.
      IF(J.EQ.N) GO TO 3
      V1 = B(J+1)
      V2 = B(J+2)
    3 B(J) = (B(J)-V1*A(3,J)-V2*A(1,J))/A(2,J)
      RETURN
    4 WRITE(6,1000) I
 1000 FORMAT(37HOSINGULAR MATRIX-ZERO PIVOT IN COLUMN.I3//)
      RETURN
      END


C*************************************************************************
C****    SUBROUTINE TO EVALUATE FRACTION DESORBED FROM THE PELLET.
      SUBROUTINE FRACT
      DIMENSION VS(10),V1(10),W1(10,10),T(10),C(10),D(10),G1(10)
      COMMON V1,W1,JMAX,KMAX /COMN2/ FRAC,PELPOR,ACCO,P
     2 /COMN5/ ITER,ERROR,ALPHA,G1,EQICON, /COMN6/ C,D

C****    INTEGRATE CRYSTAL CONCENTRATIONS USING SIMPSONS RULE.
      DO 24 J=1,JMAX
      DO 23 K=1,KMAX
      IF(P.EQ.0.) GO TO 22
      T(K) = W1(J,K)
      GO TO 23
   22 T(K) = V1(J)*EQICON
   23 CONTINUE
      SISUM = 0.
      CALL SIMPS(KMAX,C,T,SISUM)
      SIMSUM = SISUM*3.*(1.-PELPOR)
```

```
C****     VALUE FOR PORE ACCUMULATION.
      VS(J) = V1(J)*PELPOR + SIMSUM
   24 CONTINUE

C****     INTEGRATE PORE ACCUMULATION USING SIMPSONS RULE.
      SISUM = 0.
      CALL SIMPS(JMAX,D,VS,SISUM)

C****     CALCULATE FRACTION DESORBED FROM THE PELLET.
      FRAC = 1.-SISUM/ACCO
      RETURN
      END

C*************************************************************************
C****     SUBROUTINE TO INTEGRATE USING SIMPSONS RULE.
      SUBROUTINE SIMPS(M,A,B,SISUM)
      DIMENSION A(M),B(M)
      DO 10 I=1,M
      SUM = A(I)*B(I)/(3.*FLOAT(M))
      SISUM = SISUM+SUM
   10 CONTINUE
      RETURN
      END

C*************************************************************************
C****     SUBROUTINE TO CALCULATE PRACTICAL FRAC VALUES.
      SUBROUTINE PRACG
      DIMENSION X2(200),Y2(200),X1(250),Y1(250),Y3(200)
      COMMON /COMN7/ X2,Y2,KGRAPH,XC1,YC1,X1,Y1,LGRAPH
      READ(5,1000) (X1(I),I=1,29)
 1000 FORMAT(12F6.1)
      DO 10 I=1,29
      DO 10 J=1,50,20
      LGRAPH = I+J+28
      X1(LGRAPH) = X1(I)
   10 CONTINUE
      READ(5,2000) (Y3(I),I=1,180)
 2000 FORMAT(9F8.0)
      LGRAPH = 29
      DO 20 J=60,180,60
      KSET = J-60
      DO 20 K=1,29
      LGRAPH = LGRAPH+1
      KK = K+KSET
      Y1(LGRAPH) = (Y3(KK+30)-Y3(KK))/(Y3(KSET+60)-Y3(KSET+30))
   20 CONTINUE
```

```
      WRITE(6,3000)
 3000 FORMAT( 12H1 PRACTICAL RESULTS. FIRST SET IS DUMMY.  ///)
      DO 30 I=1,116
      WRITE(6,4000) X1(I),Y1(I),I
 4000 FORMAT(21H   SQUARE ROOT TIME =,F10.1,6X,6HFRAC =,F10.6,I10)
   30 CONTINUE
      RETURN
      END


C*********************************************************************
C****     CALLS PLOTTING ROUTINES.
      SUBROUTINE DRAWS
      DIMENSION X2(200),Y2(200),X1(250),Y1(250),Y3(300)
      COMMON /COMN7/ X2,Y2,KGRAPH,XC1,YC1,X1,Y1,LGRAPH
      IDRAW=2
      CALL START
      CALL PLOT(0.0,18.0,-3)
   64 IF(MOD(IDRAW,2).EQ.0) GO TO 65
      XC1 = -2.
      YC1 = 11.
      GO TO 66
   65 XC1 = 6.
      YC1 = -15.
   66 IDRAW = IDRAW + 1
      CALL AXES
      IF(IDRAW.LT.6) GO TO 64
      CALL ENPLOT(15.)
      RETURN
      END


C*********************************************************************
C****     DRAWS AXES, LABELS AND PLOTS GRAPHS.
      SUBROUTINE AXES
      DIMENSION X(200),Y(200),X1(250),Y1(250),X2(200),Y2(200)
      COMMON /COMN7/ X2,Y2,KGRAPH,XC1,YC1,X1,Y1,LGRAPH

C****     NEW PAGE ORIGIN.
      CALL PLOT(XC1,YC1,-3)

C****     RESET PLOT COUNTER FOR THEORETICAL RESULTS.
      KTOT = KGRAPH
      KGRAPH = 58
      KALCOM = 1
    1 KALCOM = KALCOM + 1
      DO 2 I=1,29
      KGRAPH = KGRAPH + 1
      X(I) = X1(KGRAPH)
      Y(I) = Y2(KGRAPH)
    2 CONTINUE
      IF(KALCOM.NE.2) GO TO 3
```

```
C****     AXES AND LABELS.
      CALL AXIS(2.0,2.0,1H ,-5.0,0.0,0.0,20.0)
      CALL SYMBOL(3.2,1.8,0.125,21H SQRT TIME (SECS 1/2),0.0,21)
      CALL AXIS(2.0,2.0,18H FRACTION DESORBED,18,4.0,90.0,0.0,0.25)
      CALL SYMBOL(1.46,0.60,0.20,38HTHEORETICAL SOLUTION FOR CO2 DIFFUSI
     1ON,0.0,38)
      CALL SYMBOL(2.23,0.30,0.20,20HIN A ONE DIMENSIONAL LINDE 5A,0.0,
     1 20)
      CALL SYMBOL(3.71,0.00,0.20,12HSIEVE PELLET,0.0,12)
      CALL SYMBOL(2.3,8.35,0.10,42HPRACTICAL RESULTS AT   0.0 DEGREES CE
     1LSIUS,0.0,42)
      CALL SYMBOL(2.3,8.05,0.10,44HTHEORETICAL RESULTS AT   0.0 DEGREES
     1CELSIUS,0.0,44)
      CALL SYMBOL(2.3,7.75,0.10,41HWITH PORE DIFFUSIVITY   = 0.0138 CM2/
     1SEC.,0.0,41)
      CALL SYMBOL(2.3,7.45,0.10,44HAND CRYSTAL DIFFUSIVITY = 0.306E-12 C
     1M2/SEC.,0.0,44)
      CALL PLOT(6.35,8.10,2)
      CALL PLOT(7.35,8.10,2)
      CALL SYMBOL(6.85,8.10,0.10,2,0.0,-1)

C****     NEW GRAPH ORIGIN.
      CALL PLOT(2.0,2.0,-3)

C****     PLOT THEORETICAL AS CONTINUOUS LINE.
    3 CALL PLOT(X(1)/20.,Y1(1)*4.,3)
      DO 4 KK=1,20
    4 CALL PLOT(X(KK)/20.,Y(KK)*4.,2)
      IF(KGRAPH.NE.KTOT) GO TO 1
      KTOT = LGRAPH

C****     RESET PLOT COUNTER FOR PRACTICAL.
      LGRAPH = 58
      KALCOM = 1
    5 KALCOM = KALCOM + 1
      DO 6 I=1,20
      LGRAPH = LGRAPH + 1
      X1(I) = X1(LGRAPH)
      Y1(I) = Y1(LGRAPH)
    6 CONTINUE

C****     PLOT PRACTICAL AS SYMBOLS.
      CALL SYMBOL(X1(1)/20.,Y1(1)*4.,0.10,2,0.0,-1)
      CALL SYMBOL(X1(6)/20.,Y1(6)*4.,0.10,2,0.0,-1)
      DO 8 I=11,20
      CALL SYMBOL(X1(I)/20.,Y1(I)*4.,0.10,2,0.0,-1)
    8 CONTINUE
      IF(LGRAPH.LT.87) GO TO 5
      RETURN
      END
```

Symbols Used in Text

Potential Theory

A	Repulsion constant
a_o	Sieve characteristic dimension
B, B_{ab}, B'	Dispersion constant
B	Potential function per molecule in sieve phase
B'	Potential function per mole in sieve phase
Bg	Potential function per molecule in gas phase
B'g	Potential function per mole in gas phase
b_o	Grid separation = $a_o/20$
C_a	Charge on ion (a) in units of e
C	Velocity of light
D	Polarisation constant
D'	Quadruple constant
E	Quadruple constant
E, E_M, E_{LT}	Total CO_2-CO_2 potential
E_D	Dispersion potential
E_P	Polarisation potential
E_Q	Quadruple potential
E_R	Repulsion potential

E/k	Depth of Lennard Jones potential well
e	Charge on the electron
F	Helmholtz free energy in sieve phase
Fg	Helmholtz free energy in gas phase
G	Transition probability per unit time
H	Heat of adsorption per mole
h	Planck's constant
k	Boltzmann constant
M	Molecular weight
m	Mass of the electron
N	Total number of molecules
$\bar{N}$	Avogadro number
n	Number of moles of CO_2 in sieve phase per cage
ng	Number of moles of CO_2 in gas phase
p	Bulk pressure
Q_b	Quadruple moment of CO_2 molecule
Q_N	Configuration Integral for N molecules
q	Grams of CO_2 per 100 grams of sieve
R	Dimensionless separation = r/a_o
R	Gas constant = $k\bar{N}$
R'	Dimensionless separation = r/b_o
S	Surface area of O 8 window
r, r_{ab}	Distance between CO_2 molecule and ion
$\underline{r}_i$	Position vector of species i

T	Absolute temperature
U	Internal energy in sieve phase
Ug	Internal energy in gas phase
V	Volume of sieve phase
Vg	Volume of gas in bulk phase
V_o	Potential function in sieve phase
Z_N	Partition function for N molecules
α, α_i	Polarisability of species i
γ	Frequency or Quantum Mechanical constant
χ, χ_i	Susceptibility of species i
ϕ_{ab}^{DIS}, ϕ_D	Dispersion potential
ϕ_{ab}^{REP}, ϕ_R	Repulsion potential
ϕ_{ab}^{IND}, ϕ_p	Polarisation potential
ϕ_{ab}^{ELEC}, ϕ_Q	Quadruple potential
ρ_e, ρ, ρ_e'	Equilibrium separation
ϕ	Total molecule ion potential
ϕ_T	Molecule-ion plus molecule-molecule potential
μ	Chemical potential in sieve phase
μg	Chemical potential in gas phase

Diffusion Model

C_o	Initial concentration
C_t	Concentration at time t
D_c	Crystal Diffusivity
D_p, D_e, D_T	Pore Diffusivities
Dg	Bulk gas diffusivity
Ep	Pellet porosity
G_{ij}	Concentration gradients in pellet
i	Finite difference subscripts - time
j	- space in pellet
k	- space in crystal
K	Equilibrium adsorption isotherm constant
L	Pellet length
Np	Mass flux in pellet
P, Q	Dimensionless groups
Q_c	Crystal accumulation
R	Crystal radius
r	Distance in crystal
r'	Dimensionless distance in crystal
T	Tortuosity
t	Time
t'	Dimensionless time
V	Volume of sieve
V_c	Volume of crystal

v	Gas concentration in pores
v'	Dimensionless gas concentration in pores
v_o	Initial gas concentration in pores
w	Gas concentration in crystal
w'	Dimensionless gas concentration in crystal
w_o	Initial gas concentration in crystal
x	Distance in pellet
x'	Dimensionless distance in pellet

REFERENCES

1. CHANDRASEKHARAN, K. Ph.D. Thesis, Imperial College, University of London (1962).

2. DWORJANYN, L.O. Ph.D. Thesis, Imperial College, University of London (1962).

3. WILSON, K.B. Ph.D. Thesis, Imperial College, University of London (1966).

4. BRECK, D.W., EVERSOLE, W.G., MILTON, R.M., REED, T.B. and THOMAS, T.L. Journal of the American Chemical Society, 78, 5963 (1956).

5. REED, T.B. and BRECK, D.W. Journal of the American Chemical Society, 78, 5972 (1956).

6. BARRER, R.M. and MEIER, W.M. Transactions of the Faraday Society, 54, 1074 (1958).

7. BROUSSARD, L. and SHOEMAKER, D.P. Journal of the American Chemical Society, 82, 1041 (1960).

8. BARRER, R.M. Lecture, Imperial College Chemistry Department, London, (1964).

9. BRECK, D.W. and SMITH, J.V. Scientific American (January 1959).

10. HIRSHFELDER, J.O., CURTISS, C.F. and BIRD, R.B. Molecular Theory of Gases and Liquids, Wiley and Sons. N.Y. (1954).

11. VINEYARD, G.H. Journal of the Physics and Chemistry of Solids, 3, 121 (1957).

12. FORSYTHE, G.E. and WASOW, W.R. Finite Difference Methods for the Solution of Partial Differential Equations, Wiley and Sons. N.Y. (1960).

13. POWELL, M.J.D. The Computer Journal, 7, 303 (1964).

14. CARLSLOW, H.S. and JAEGER, J.C. Conduction of Heat in Solids, Clarendon Press (1959).

REFERENCES (continued)

15. BARRER, R.M. and GIBBONS, R.M. Transactions of the Faraday Society, 59, 2575 (1963).

16. Ibid., 61, 948 (1965).

17. KISELEV, A.V. and LOPATKIN, A.A. Symposium on Molecular Sieves, Society of Chemical Industry (1968).

18. LINDE COMPANY. Adsorption Equilibrium Data Sheets No. 22 and 24. N.Y. (1959).

19. VERMEULEN, T. Advances in Chemical Engineering, Vol. 2, pp. 147-208, Academic Press, N.Y. (1958).

20. ROSEN, J.B. Journal of Chemical Physics, 20, 387 (1952) and Industrial Engineering Chemistry, 46, 1590 (1954).

21. SZYMANSKI, H.A., STAMIRES, D.N. and LYNCH, G.R. Journal of the Optical Society of America, 50, (12), 1323 (1960).

22. BARKER, J.A. and EVERETT, D.H. Transactions of the Faraday Society, 58, 1608 (1962).

23. BARRER, R.M. and COUGHLAN, B. Symposium on Molecular Sieves, Society of Chemical Industry (1968).

24. BARRER, R.M. and STUART, W.I. Proceedings of the Royal Society, 249, 464 (1959).

25. PAULING, L. The Nature of the Chemical Bond, Cornell University Press (1960).

26. BUCKHINGHAM, A.D. and DISCH, R.L. Proceedings of the Royal Society, 273, 275 (1963).

27. MEIER, W.M. Symposium on Molecular Sieves, Society of Chemical Industry (1968).